

Steering and Harvesting Technology for Minimally Invasive Biopsy



Filip Jelínek

Steering and Harvesting Technology for Minimally Invasive Biopsy

Filip Jelínek

Steering and Harvesting Technology for Minimally Invasive Biopsy

Proefschrift

ter verkrijging van de graad van doctor
aan de Technische Universiteit Delft,
op gezag van de Rector Magnificus prof. ir. K.C.A.M. Luyben,
voorzitter van het College voor Promoties,
in het openbaar te verdedigen op maandag 12 januari 2015 om 12:30 uur

door

Filip JELÍNEK

Master of Engineering in Mechanical and Medical Engineering
The University of Hull, Engeland, Verenigd Koninkrijk
geboren te Bratislava, Slowakije.

Dit proefschrift is goedgekeurd door de promotoren:

Prof.dr. J. Dankelman
Prof.dr.ir P. Breedveld

Samenstelling promotiecommissie:

Rector Magnificus,	voorzitter
Prof.dr. J. Dankelman,	Technische Universiteit Delft, promotor
Prof.dr.ir P. Breedveld,	Technische Universiteit Delft, promotor
Prof.dr.ir. S. Stramigioli,	Universiteit Twente
Prof.dr.ir. H.J.C.M. Sterenburg,	Academisch Medisch Centrum Amsterdam
Prof.dr. J.F. Lange,	Erasmus Universitair Medisch Centrum Rotterdam
Prof.dr.ir. J.L. Herder,	Technische Universiteit Delft
Dipl.-Ing. Dr. G. Kronreif,	Austrian Center for Medical Innovation and Technology
Prof.dr.ir. C.A. Grimbergen,	Academisch Medisch Centrum Amsterdam, reservelid



This research was performed within the framework of CTMM, the Center for Translational Molecular Medicine, project MUSIS (grant 030-202).

Title: Steering and Harvesting Technology for Minimally Invasive Biopsy
Author: Filip Jelínek (fjelinek@gmail.com)
Cover design: Martina Kubincová, Filip Jelínek, Bobo Jelínek
Printing: CPI Koninklijke Wöhrmann, The Netherlands

© Filip Jelínek 2015

All rights reserved. No part of the material protected by this copyright notice may be reproduced or utilised in any form or by any means, electronic or mechanical, including photocopying, recording or by any information storage and retrieval system, without written permission.

ISBN: 978-94-6203-742-7

Summary

Samenvatting

Summary

Contemporary medical imaging technologies, such as computed tomography or magnetic resonance imaging, play a pivotal role in medical diagnosis, allowing for a relatively fast and non-invasive examination of the human body. In the field of cancer surgery they allow for preoperative detection of tumorous tissue and aid the surgical planning. However, only recent developments in the imaging field have introduced the possibility for a real-time non-invasive intraoperative detection of tumorous tissue with sufficient margins for radical tumour resection. These imaging technologies are collectively called optical biopsy and besides providing the real-time visualisation of the tumorous tissue on a large scale, e.g. near-infrared fluorescence, they allow for an instant tumour detection and analysis on a small scale, e.g. differential pathlength spectroscopy, ultimately without the need for any pathological analysis.

While the optical biopsy provides an answer to the tumour detection, its subsequent accurate resection, or mechanical biopsy, remains a challenge. This challenge is further aggravated with more demanding applications, such as minimally invasive surgery, as compared to open surgery, and accurate resection of organ exterior as compared to organ interior. Yet, as challenges are here to be solved, the aim of this work is to provide an answer to combining the optical and the mechanical biopsies in an accurate manner with the aim to perform safe minimally invasive resection of small tumours at organ and tissue surfaces. Furthermore, as minimally invasive surgical applications pose various spatial restrictions on tissue manipulation, the second objective of this work is to present a reliable joint construction for the envisioned tissue resection instrument, allowing it to attain a proper orientation to the tissue of interest.

As the focus of this thesis is twofold, its chapters are grouped into two parts. The first part of this thesis treats the combination of the optical and the mechanical biopsies in a reliable and an effective manner, showing the development of a resection tip, the opto-mechanical biopsy harvester, for a minimally invasive surgical instrument (*Chapters 2-4*). The second part of this thesis addresses the issue of steerable joint constructions in the minimally invasive surgical instruments and their reliable controllability in order to provide both flexibility and stability for the accurate tumour detection and resection (*Chapters 5-8*).

With the vision to devise the design of the opto-mechanical biopsy harvester, a review of the state-of-the-art minimally invasive surgical instruments capable of performing the optical and the mechanical biopsies successively and accurately was performed and it is presented in *Chapter 2*. In addition, the review outlines any and all the minimally invasive surgical devices housing an accessory channel, thus mechanically capable of integrating a fibre optic cable for optical biopsy.

As the findings of the aforementioned literature review were rather limited, this gave an opportunity to conceive and develop a novel bio-inspired design of a frontally-acting opto-mechanical biopsy harvester. Its experimental design and prototype are presented in *Chapter 3* together with feasibility tests proving the concept. While the

instrument steerability was not yet incorporated, the experimental design was created with a great consideration of its ultimate functionality.

Chapter 4 concludes the first part of this thesis with a follow-up optimisation of the biopsy harvester's collapsible resection device, the crown-cutter, bio-inspired by the sea urchin's chewing organ Aristotle's lantern and shaped as a crown of numerous pointy teeth. The study researches the impact of tooth quantity and type of their bevel on the induced tissue deformation, penetration forces and proper tooth collapsibility.

Similarly to the first part of this thesis, the second part begins with a review article in *Chapter 5* of all the mechanical joint constructions used in the state-of-the-art steerable minimally invasive surgical instruments. By clear categorisation, the aim of this review is to help identify a reliably controllable steerable joint ensuring accurate operation of the envisioned instrument's tip. The fundamental joint classification can also serve as a design aid for other developments in this field.

With the vision to develop a stiff and reliably controllable joint for the envisioned biopsy instrument, a novel steerable laparoscopic instrument prototype DragonFlex was developed. As discussed in *Chapter 6*, its simple, repetitive and symmetrical design incorporates a rolling joint with a special tight cable guidance. Together they maximise the driving cable lifespan, equalise the forces in both cables and enable control of seven instrument degrees of freedom by only seven structural components. Not only is DragonFlex the world's first almost entirely additive manufactured steerable laparoscopic instrument prototype, but it also sheds new light on the potential of additive manufacturing in the surgical field.

The promisingly high bending stiffness of DragonFlex's rolling joint is evaluated in *Chapter 7*, which provides an empirical evidence that this joint construction is indeed superior to the state of the art in this respect. As clarified, the insight into achieving high bending stiffness of cable-driven joint constructions lies in the principle of full actuation of each degree of freedom, as opposed to underactuation.

In order to perfect DragonFlex's already stiff rolling joint *Chapter 8* illustrates a way to minimise the small degree of remaining cable slack in the original design. As opposed to the common design practice attempting to eliminate the cable slack by a cable tensioning mechanism, this chapter introduces a more fundamental solution applicable to rolling joints in general. On top of minimising the cable slack, this solution removes the need for a cable tensioning mechanism, hence simplifying the overall design and assembly even further.

The thesis is concluded with a discussion section in *Chapter 9* outlining the combination of the reliable steering and the accurate harvesting technology developed for the purpose of minimally invasive biopsy. This last chapter presents the envisioned design and the real-scale fully functional prototype of the steerable minimally invasive opto-mechanical biopsy harvester composed of a permanent and a disposable section. The fusion of all the presented insights and designs is addressed in a practical manner, especially with regard to the manufacturability and the proposed usage of the final envisioned instrument.

Samenvatting

Stuur en Harvest Technologie voor Minimaal Invasieve Biopsie

Huidige medische beeldvormende technologieën, zoals computed tomography (CT) en magnetic resonance imaging (MRI), spelen een centrale rol in de medische diagnostiek, waardoor het snel en non-invasief onderzoeken van het menselijk lichaam mogelijk wordt gemaakt. Op het gebied van oncologische chirurgie worden deze technieken gebruikt voor het preoperatief detecteren van tumoren en helpen ze bij de operatieplanning. Recentelijke ontwikkelingen hebben het mogelijk gemaakt om deze technieken ook in real-time toe te passen om op een non-invasieve, intra-operatieve manier tumoreus weefsel te detecteren met voldoende precisie voor een gehele tumorresectie. Gezamenlijk worden deze beeldvormende technieken optische biopsie genoemd. Naast de real-time visualisatie van tumoreus weefsel op grote schaal, zoals bijvoorbeeld met nabij-infrarood fluorescentie, zijn deze technieken ook in staat om direct tumoren te detecteren en te analyseren op een veel kleinere schaal, met bijvoorbeeld differential pathlength spectroscopie, opdat er uiteindelijk geen pathologische analyse nodig is.

Ondanks het feit dat optische biopsie een goede oplossing biedt voor tumor detectie, blijft de daaropvolgende accurate resectie, of mechanische biopsie, van deze tumor een uitdaging. Deze uitdaging wordt verder bemoeilijkt bij veeleisende toepassingen, zoals bij minimaal invasieve chirurgie, in tegenstelling tot open chirurgie, en accurate resectie van oppervlakkig orgaan weefsel, in tegenstelling tot intern orgaan weefsel. Omdat problemen er zijn om opgelost te worden, is het doel van dit onderzoek om optische en mechanische biopsieën op een accurate manier te combineren en daarmee minimaal invasieve resectie van kleine tumoren op orgaan- en weefseloppervlakken mogelijk te maken. Daarnaast is het tweede doel van dit onderzoek om een betrouwbare gewrichtsconstructie te ontwerpen voor het weefsel resectie instrument. Deze gewrichtsconstructie helpt bij het behouden van de juiste oriëntatie van het instrument ten opzichte van het weefsel in een minimaal invasieve operatie waar weefselmanipulatie beperkt is door de spatiale restricties.

Gezien de focus van deze thesis tweeledig is, zijn de hoofdstukken hierin onderverdeeld in twee delen. In het eerste deel van deze thesis wordt de combinatie van optische en mechanische biopsieën besproken (*Hoofdstukken 2-4*). Hierin wordt de ontwikkeling van een betrouwbare en effectieve minimaal invasieve resectie tip, de optisch-mechanische biopsie harvester, besproken. Het tweede deel van de thesis focust zich op de constructies van stuurbare gewrichten voor minimaal invasieve chirurgische instrumenten (*Hoofdstukken 5-8*). Een belangrijk aspect hierin betreft betrouwbare instrument controle om zo flexibiliteit en stabiliteit te verkrijgen voor accurate tumor detectie en resectie.

Met visie op het ontwerpen van een optisch-mechanische biopsie harvester is in *Hoofdstuk 2* een overzicht van alle huidige en gepatenteerde minimaal invasief chirurgische instrumenten gegeven, die in staat zijn om op een achtereenvolgende

accurate manier optische en mechanische biopsies te nemen. Daarnaast worden in dit overzicht ook minimaal invasieve instrumenten besproken die een aanvullend lumen bezitten waar, vanuit een mechanisch oogpunt, een optische fiber in geïntegreerd kan worden voor optische biopsie.

Omdat de uitkomsten van het literatuuronderzoek relatief beperkt waren, ontstond de mogelijkheid om een innovatief bio-geïnspireerd ontwerp te maken en te ontwikkelen tot een voorwaarts gerichte, optisch-mechanische biopsie harvester. Het experimentele ontwerp en het prototype worden gepresenteerd in *Hoofdstuk 3*, gezamenlijk met validatietesten die de werking van het prototype bewijzen. Ondanks het feit dat het instrument nog niet stuurbaar was gemaakt, werd er wel rekening mee gehouden om deze functionaliteit in het eindproduct te kunnen verwerken.

In *Hoofdstuk 4* worden conclusies getrokken over het eerste deel van de thesis en wordt ingegaan op de optimalisatie van het inklapbare resectie onderdeel van de biopsie harvester; de crown-cutter, dat bio-geïnspireerd is op het kauworgaan van de zee-egel, de lantaarn van Aristoteles, en is vormgegeven als een kroon met meerdere scherpe tanden. Onderzoek is gedaan naar de impact van het aantal tanden en de hoek van deze tanden op de weefseldeformatie, de penetratiekrachten en de juiste tand inklapbaarheid.

Het tweede deel van deze thesis begint op een soortgelijke manier als het eerste deel met een overzichtsartikel in *Hoofdstuk 5* over alle mechanische gewrichtsconstructies die gebruik worden in state-of-the-art stuurbare, minimaal invasieve chirurgische instrumenten. Met het opstellen van een duidelijke categorisatie, is het doel van dit artikel om een betrouwbaar controleerbaar en stuurbaar gewricht te identificeren dat met gepaste nauwkeurigheid de instrumenttip kan besturen. Bovendien kan deze fundamentele gewrichtsclassificatie dienen als hulpmiddel ter ondersteuning van het ontwerpproces voor andere ontwikkelingen op dit gebied.

Naar aanleiding van de categorisatie en met als doel om een stijf en betrouwbaar controleerbare gewrichtsconstructie te verkrijgen voor het biopsie instrument, is het innovatieve, stuurbare, en laparoscopische instrument de DragonFlex ontwikkeld. Zoals besproken in *Hoofdstuk 6*, heeft de DragonFlex een simpel, herhalend en symmetrisch ontwerp dat gebruik maakt van een rolgewricht met speciale kabelgeleiding. Het ontwerp maximaliseert de levensduur van de kabels, verdeelt de krachten evenredig in beiden kabels en stelt de gebruiker in staat om zeven graden van vrijheid te besturen met slechts zeven structurele componenten. De DragonFlex is niet alleen het enige stuurbare laparoscopische instrument prototype dat bijna volledig met behulp van een 3D printer is gefabriceerd, het biedt daarnaast ook nieuwe inzichten op de mogelijkheden om 3D printers te gebruiken in de medische wereld.

In *Hoofdstuk 7* wordt de veelbelovende hoge buigstijfheid van het rolgewricht van de DragonFlex geëvalueerd, en wordt empirisch bewezen dat dit ontwerp voor het rolgewricht inderdaad superieur is aan de state-of-the art als het gaat om buigstijfheid. Het inzicht in het bereiken van een hoge buigstijfheid van het kabel geactueerde

gewricht ligt, zoals beschreven, in het principe van volledige actuatie van elke graad van vrijheid in tegenstelling tot onder-actuatie.

Met doel het al stijve rolgewricht ontwerp van de DragonFlex verder te perfectioneren, wordt in *Hoofdstuk 8* een methode getoond om de speling in de actuatie kabels te minimaliseren. In tegenstelling tot het gebruik van een kabel spanmechanisme, wat de meest gebruikte manier voor het elimineren van slappe kabels is, wordt in dit hoofdstuk een fundamenteelere oplossing gegeven die toepasbaar is op rolgewrichten in het algemeen. Bovendien worden door het elimineren van een spanmechanisme het ontwerp en de assemblage van het prototype verder gesimplificeerd.

De thesis wordt afgesloten met een discussie in *Hoofdstuk 9* waarin de combinatie van een betrouwbaar stuurmechanisme en de harvesting technologie voor gebruik in minimaal invasieve biopsies wordt besproken. In dit laatste hoofdstuk wordt het voor ogen hebbende ontwerp en het op ware schaal volledig functionele prototype van het stuurbare, minimaal invasieve, optisch-mechanische biopsie harvester met een herbruikbare en wegwerpbaar sectie gepresenteerd. De samenvoeging van alle gepresenteerde inzichten en ontwerpen worden besproken op een praktische manier, vooral met betrekking tot de maakbaarheid en het gebruik van het uiteindelijke instrument.



Table of Contents



Chapter 1 – Introduction	I
1.1 Background.....	3
1.1.1 Minimally Invasive Surgery and Steerable Instruments	3
1.1.2 Biopsy	3
1.1.3 Radical Tumour Resection and Optical Biopsy	4
1.2 Problem Statement.....	7
1.3 Goal	7
1.4 Approach and Thesis Outline.....	8
Chapter 2 – Minimally Invasive Surgical Instruments with an Accessory Channel Capable of Integrating Fibre Optic Cable for Optical Biopsy.....	II
2.1 Introduction	13
2.1.1 Minimally Invasive Surgery	13
2.1.2 Biopsy	13
2.1.3 Optical Biopsy.....	14
2.1.4 Review Objectives.....	15
2.1.5 Literature Search Method	15
2.2 Classification Overview	16
2.3 Instruments with Fibreoptics	17
2.3.1 For Tissue Analysis – Optical Biopsy	17
2.3.2 For Tissue Observation or Illumination	19
2.3.3 For Tissue Treatment.....	20
2.4 Instruments with an Auxiliary Device.....	21
2.4.1 Device Independent from the Manipulator.....	21
2.4.2 Device Interconnected with the Manipulator	22
2.5 Discussion	23
2.5.1 Tissue Manipulator Limitations.....	23
2.5.2 Recent development.....	24
2.6 Conclusions.....	25
Chapter 3 – Bio-Inspired Spring-Loaded Biopsy Harvester.....	29
3.1 Introduction	31
3.1.1 Laparoscopy and Biopsy	31
3.1.2 Combining Optical and Mechanical Biopsy.....	31
3.1.3 Problem Statement – Need for a Novel Opto-Mechanical Biopsy Device	32
3.1.4 Minimal Tissue Deformation Approach towards Laparoscopic Biopsy.....	33
3.1.5 Objective – Design Requirements	34
3.2 Methods – Experimental Prototype Development.....	34
3.2.1 Design Inspiration and Cutting Principle.....	34
3.2.2 Cutting and Harvesting Mechanism	35
3.2.3 Propulsion – Pilot Cutter Experiments	35
3.2.4 Experimental Biopsy Harvester Design.....	37
3.2.5 Experimental Biopsy Harvester Prototype	37
3.2.6 Experimental Set-up for Feasibility Tests	38

3.3	Results.....	39
3.3.1	General Prototype Functionality	39
3.3.2	Prototype’s Cutting Performance and Feasibility Test	39
3.4	Discussion	40
3.4.1	Biopsy Harvester Highlights and Limitations.....	40
3.4.2	Future Work – Envisioned Instrument.....	41
3.5	Conclusions.....	41
Chapter 4 – Bio-Inspired Crown-Cutter		43
4.1	Introduction	45
4.1.2	Keyhole Surgery and Biopsy	45
4.1.3	Keyhole Biopsy Harvester.....	46
4.1.4	Biological Inspiration	47
4.1.5	Crown-Cutter	47
4.1.6	Problem Statement.....	48
4.2	Methods.....	49
4.2.1	Design Optimisation Variables.....	49
4.2.2	Tooth Quantity and Bevel Type Experiments.....	50
4.2.3	Tooth Collapsibility Calculations.....	51
4.3	Results.....	52
4.3.1	Impact of Tooth Quantity	52
4.3.2	Impact of Tooth Bevel Type.....	53
4.3.3	Ease of Tooth Collapsibility	53
4.4	Discussion	54
4.5	Conclusions.....	55
Chapter 5 – Classification of Joints Used in Steerable Instruments for Minimally Invasive Surgery.....		57
5.1	Introduction	59
5.1.1	Minimally Invasive Surgery	59
5.1.2	Steerable Instruments	59
5.1.3	Review Objectives.....	60
5.1.4	Literature Search Method	60
5.2	Classification of Steerable MIS Instrument Joints	61
5.2.1	Planar and Spatial Joints	61
5.3	Rolling Joint	64
5.3.1	Planar Rolling Joint	64
5.3.2	Perpendicular Rolling Joint.....	65
5.3.3	Revolved Rolling Joint.....	66
5.4	Sliding Joint.....	67
5.4.1	Planar Sliding Joint.....	67
5.4.2	Perpendicular Sliding Joint.....	69
5.4.3	Revolved Sliding Joint	69
5.5	Rolling Sliding Joint.....	70
5.5.1	Planar Rolling Sliding Joint.....	70
5.5.2	Perpendicular Rolling Sliding Joint.....	70
5.5.3	Revolved Rolling Sliding Joint	71

5.6	Bending Joint.....	71
5.6.1	Planar Bending Joint.....	71
5.6.2	Perpendicular Bending Joint.....	72
5.6.3	Revolved Bending Joint.....	73
5.7	Discussion	73
5.7.1	Design Suitability for Specific Purposes.....	73
5.7.2	Most Frequent Joint Types.....	74
5.7.3	New Joint Types and Joint Combinations	75
5.8	Conclusions.....	76
Chapter 6 – DragonFlex		81
6.1	Introduction	83
6.1.1	Laparoscopy and Steerable Instruments.....	83
6.1.2	Steerability at the Expense of Complexity and Vulnerability.....	83
6.1.3	Ideal Configuration Requirements	84
6.2	DragonFlex Design.....	85
6.2.1	Planar Joint Design.....	85
6.2.2	From Planar to Spatial, from Tip to Handle.....	89
6.2.3	Prototypes.....	91
6.2.4	Performance.....	93
6.3	Discussion	93
6.3.1	Instrument Highlights and Limitations	93
6.3.2	Opportunities for Further Research	94
6.4	Conclusions.....	95
Chapter 7 – Attaining High Bending Stiffness by Full Actuation in Steerable Minimally Invasive Surgical Instruments.....		97
7.1	Introduction	99
7.1.1	Minimally Invasive Surgery and Steerable Instruments.....	99
7.1.2	Steerability and Bending Stiffness.....	99
7.1.3	Bending Stiffness versus Actuation.....	100
7.1.4	Objective.....	102
7.2	Methods.....	102
7.2.1	Equipment.....	102
7.2.2	Experimental Procedure.....	103
7.3	Results.....	105
7.4	Discussion	106
7.5	Conclusions.....	108
Chapter 8 – Method for Minimising Rolling Joint Play in the Steerable Laparoscopic Instrument Prototype DragonFlex.....		109
8.1	Introduction	111
8.1.1	Laparoscopy and Steerable Instruments.....	111
8.1.2	Original DragonFlex Prototype	111
8.1.3	Objective.....	113

8.2	Methods.....	113
8.2.1	Rolling Joint Optimisation.....	113
8.2.2	Experimental Set-up.....	114
8.3	Results.....	116
8.3.1	Optimised Rolling Joint Evaluation.....	116
8.3.2	Improved DragonFlex Prototype.....	117
8.4	Discussion.....	118
8.5	Conclusions.....	119
Chapter 9 – Discussion.....		121
9.1	Envisioned Steerable Opto-Mechanical Biopsy Harvester.....	123
9.1.1	Biopsy Harvester Design.....	123
9.1.2	Joint Construction Design.....	126
9.1.3	Steerable Opto-Mechanical Biopsy Harvester Prototype.....	129
9.1.4	Envisioned Instrument Usage.....	130
9.2	Design Aspects and Issues for Further Consideration.....	132
9.2.1	Design and Manufacturing.....	132
9.2.2	Usage.....	134
9.3	Conclusions.....	137
Appendix.....		139
Acknowledgements.....		143
Curriculum Vitae.....		147
Publications.....		151



Chapter I

Introduction



1.1 Background

1.1.1 Minimally Invasive Surgery and Steerable Instruments

Conventional surgical procedures require open access to the operation site via a long incision, resulting in abundant postoperative scar tissue and relatively long recovery time. Minimally invasive surgery (MIS) was introduced to ameliorate these negative effects [1-5]. In particular, laparoscopy – minimally invasive surgery in the abdomen (Figure 1.1 left) [6] – involves making one or several small incisions in the abdominal wall in order to accommodate trocars. These serve as airtight seals used for the inflation of the abdominal cavity with carbon dioxide, creating a working space for the surgeon, as well as the portals for the instruments. Long and slender endoscopes and instruments provide either a visual feedback or tissue manipulation features.



Figure 1.1 Left – Schematic view of laparoscopy [6]. Middle – Rigid [7] & steerable [8] minimally invasive surgical instruments. Right – Rigid instrument DOF [9] and additional steerable tip DOF.

Laparoscopic instruments can be differentiated into rigid and steerable (Figure 1.1 middle) [4, 5, 7, 8]. The configuration of the rigid ones comprises a handle, rigid shaft and a tip, which equips them with four degrees of freedom (DOF), these being axial sliding, axial rotation and pivoting in two perpendicular planes around the incision point (Figure 1.1 right) [9]. This fulcrum effect greatly restricts the range of motion and limits the surgeon mainly to frontal or sideways approach to the tissue [5, 8]. In contrast, steerable instruments have additional degrees of freedom due to one or more joints in the tip, enabling the surgeon to reach behind or over obstacles [5, 8, 10, 11].

1.1.2 Biopsy

Biopsy is a minimally invasive medical test in the field of pathology, whose objective is to research and comprehend the nature and the properties of diseased tissue. Tissue samples that are resected from the patient's body using specialised biopsy instruments are sent to pathologists for tissue analysis. The contemporary biopsy techniques include fine-needle aspiration (Figure 1.2 left), core needle biopsy (Figure 1.2 middle) and punch biopsy (Figure 1.2 right) [12].

The fine needle aspiration technique utilises a syringe, which quickly and often automatically samples a limited amount of tissue on a cellular level from deep within the organs. Another deep tissue biopsy technique, the core needle biopsy, employs a core needle with a wide bore that can resect larger tissue samples even from much stiffer tissues, such as a bone. The punch biopsy, which is slightly more invasive and ungainly, uses punches for sampling superficial easily accessible tissue, such as skin, and longer trephines for sampling the surface of deep and stiff tissues, such as bones. Once sectioning is performed, the punch biopsy, however, usually requires the assistance of auxiliary devices or features for tissue retrieval.

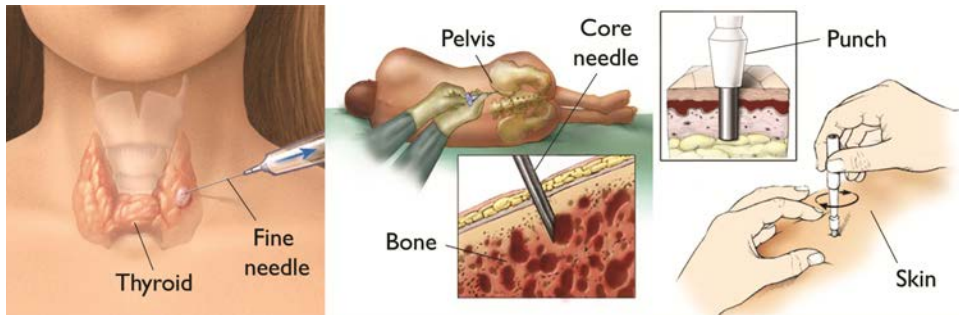


Figure 1.2 Contemporary biopsy techniques including fine-needle aspiration (left), core needle biopsy (middle) and punch biopsy (right) [12].

On the whole, despite being used in the minimally invasive context, the contemporary biopsy devices suffer from geometrical and operational limitations, undermining their usage versatility [13, 14]. Namely, the deep tissue biopsy needles employing suction require full needle tip immersion into the tissue for proper functioning. Hence, they cannot be used for peripheral tissue sampling. Likewise, since the punches and trephines require fully manual and often forceful and lengthy operation [15, 16], unlike fine-needle aspiration, they cannot be used in the minimally invasive context with regard to accuracy at high speed. In addition, the use of conventional minimally invasive forceps or scissors for the purpose of tissue resection can easily lead to tissue slip and thus inaccurate sampling with accompanying hazards [17].

1.1.3 Radical Tumour Resection and Optical Biopsy

Safe tissue sampling is of utmost importance particularly in the field of cancer surgery, where the diseased tumorous tissue has to be detected and removed in its entirety. This so-called radical tumour resection has always been one of the most difficult issues in the field as its insufficient execution potentially leads to a high number of revision surgeries and an increased risk of cancer spread in between or during treatments [18]. The fact that, historically, surgeons had to rely solely on palpation and visual cues in order to identify the tumorous tissue did not make the treatment any easy or reliable [19].

With the introduction of non-invasive medical imaging technologies, such as computed tomography (CT), magnetic resonance imaging (MRI), or positron emission tomography (PET), the tumorous tissue could be detected at earlier stages preoperatively, aiding the surgical planning and the subsequent resection. Nevertheless, only recent developments in the medical imaging field have provided for a real-time intraoperative means of detecting tumorous tissue with sufficient margins for radical tumour resection [19, 20]. The newly emerging non-invasive real-time imaging technologies are collectively referred to as optical biopsy and provide instant tissue analysis, ultimately without the need for a subsequent pathological analysis [18, 21-23].

One of the optical biopsy techniques called near-infrared (NIR) fluorescence incorporates the use of NIR light. In comparison with visible light and hence human sight, the NIR light is capable of penetrating a couple of millimetres or even centimetres into tissue [24]. Aside from high tissue penetration, the NIR light is invisible to the human eye and hence does not alter surgeon's perception [19]. However, the main ingredient in the NIR fluorescence technique is the use of a fluorescent dye, capable of binding to tissues of specific oxygenation status. Once visualised by the NIR light (Figure 1.3) [25], the fluorescent dye can reveal relatively deep structures, such as nerves and vessels. More importantly, it can differentiate the tumorous and the normal tissue [19, 24], since the tumours have higher levels of oxygen saturation accelerating their growth. With appropriate imaging devices, such as Quest's multispectral medical camera Artemis (Figure 1.3 bottom), one can show a real-time image overlay (Figure 1.3 top left) of a distant surgical field viewed under the visible light (Figure 1.3 middle) and the tumorous structures highlighted by the fluorescent dye and captured under the NIR light (Figure 1.3 right), thus considerably enhancing open or minimally invasive cancer



Figure 1.3 Top – Image overlay of the surgical field viewed under visible light and the tumours highlighted by the fluorescent dye and visible under near-infrared light. Bottom – Multispectral medical camera Artemis by Quest for open and minimally invasive surgical applications [25].

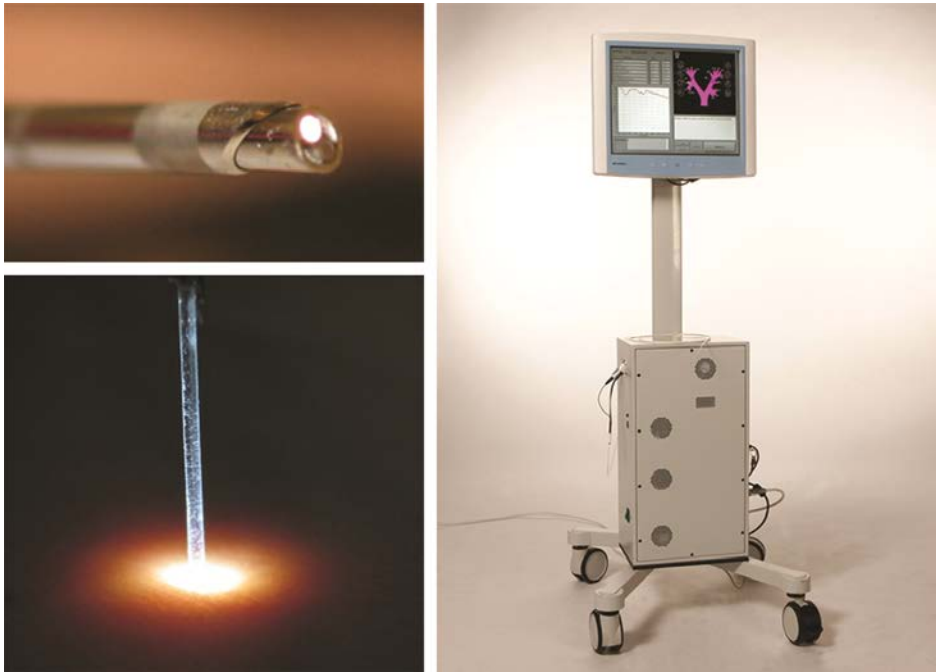


Figure 1.4 Fibre optic cable bundle used in differential pathlength spectroscopy (left) implemented in the diagnostic device DPS-Research system by Luminostix (right) [27].

surgery [20, 25]. Nevertheless, the NIR light is still scattered by the surrounding living tissue, making the visualisation of the deep structures more cumbersome [24]. Furthermore, the large penetration depth of the NIR light can make the differentiation between the superficial and the deep tissues, and thus the precise localisation, difficult. However, if used as a global visualisation and tumour detection technique together with a more localised optical biopsy technique with a limited penetration depth, one could achieve greater accuracy, reliability and efficiency of the overall procedure.

A promising optical biopsy technique enabling localised tissue analysis remotely is differential pathlength spectroscopy (DPS). Contrary to the NIR fluorescence, the DPS, similarly to other spectroscopic techniques [21], uses only the visible light and its subsequent spectral analysis to perform the optical biopsy. Whereas the NIR light penetrates up to a few centimetres into the tissue, the visible light used during the DPS penetrates only a few hundred micrometres below the surface of the analysed tissue [24]. However, the identification of the precancerous tissue depends on its structural changes occurring within or at a close vicinity of a superficial tissue layer no thicker than a couple of hundred micrometres. Hence, the DPS technique is capable of measuring blood oxygen saturation and thus of cancer detection within the most superficial layers of the analysed tissue [22, 26]. With appropriate diagnostic tool, such as DPS-Research system by Luminostix (Figure 1.4 right), one can readily use the DPS technology by means of a fibre optic cable as a signal carrier (Figure 1.4 left) and probe the local tissue of interest *in situ* and in real time [22, 27].

1.2 Problem Statement

Once analysed and identified as hazardous, the tissue can be readily resected by means of a tissue removal instrument. Standard surgical instruments or biopsy devices could be used to some extent for tissue extraction in conjunction with the NIR fluorescence in either open or minimally invasive surgery. Nonetheless, the optical biopsy techniques, such as the DPS, that are applied locally on a finer scale by means of a fibre optic cable lack a reliable surgical resection tool, especially in the minimally invasive context, that would enable an accurate mechanical biopsy co-registered with the optical biopsy.

As outlined earlier, the state-of-the-art minimally invasive surgical instruments and biopsy devices are rather limited in application, not to mention that attempting to resect the previously analysed tissue using a separate tool or in a separate operation can quickly prove challenging and inaccurate [23]. Hence, there is a need for a MIS instrument capable of accommodating a fibre optic cable for the DPS technology with the possibility of subsequently and immediately providing an accurate tumour resection. Even though the ultimate goal of the optical biopsy is to reduce the need for the pathological analysis to minimum, hence reducing procedural risks and costs, there is still a need for accurate validation of these techniques, which could be provided by such an opto-mechanical biopsy instrument [21].

Furthermore, the DPS technology requires complete, unobstructed and gentle tissue contact in order to minimise the bias of the blood oxygen saturation readings. Nevertheless, the fibre optic cable guiding the light signal is polished under a certain non-zero angle in order to prevent excessive backscatter of the emitted light, possibly degrading the readout quality and reliability [26]. The resulting implications and ramifications might not be serious in the context of open surgery. However, due to the restricting site access and difficult instrument manipulation during MIS procedures, there would be a need to adjust the orientation of the instrument's tip under such limiting conditions, thus enhancing its usability. Hence, the tip of such an opto-mechanical biopsy instrument would benefit from featuring a reliably controllable steerable construction providing articulation towards complete fibre-tissue contact.

1.3 Goal

The aim of this thesis is to present a practical approach towards development and evaluation of an envisioned steerable minimally invasive opto-mechanical biopsy harvester that would serve as a resection and a validation tool for the newly emerging optical biopsy technology based on the differential pathlength spectroscopy. The design of the MIS instrument would feature an unimpeded hollow channel for the fibre optic cable for non-invasive tissue analysis *in situ*, a cutting device for subsequent accurate mechanical biopsy of the analysed tissue and a disposable container for sample storage and transport. The instrument's tip would be mounted on top of a reliably controllable

steerable construction enabling fibre articulation and its proper orientation with respect to the tissue of interest.

1.4 Approach and Thesis Outline

As indicated, the purpose of this thesis is twofold and thus its chapters, each representing a published peer-reviewed journal article, can be grouped into two parts. The first part of this thesis is dealing with the issue of combining the optical and the mechanical biopsies in a reliable and an effective manner, illustrating the development of the opto-mechanical biopsy harvester (*Chapters 2-4*); and the second part is treating the issue of steerable joint constructions in MIS instruments and their reliable controllability with the vision of providing a stable platform for the tumour detection and resection (*Chapters 5-8*). As common in the research and design practice, the work was initiated by investigating the state of the art in both areas, identifying their strengths and weaknesses, and thus helping to devise an instrument design most fit for purpose, whose performance was evaluated empirically. The outline of this thesis is illustrated below.

With the objective to initiate the design of the opto-mechanical biopsy harvester, *Chapter 2* presents a state of the art review of all the MIS instruments capable of performing the optical and the mechanical biopsies in an accurate and successive fashion. The review also considers any and all the MIS devices housing an accessory channel and capable of integrating fibre optic cable for optical biopsy after relevant design modifications.

With regard to the limited findings of the aforementioned literature review, *Chapter 3* presents an experimental prototype design of the envisioned MIS instrument's tip and its feasibility tests proving the concept. Although the question of steerability has not yet been accounted for, the novel bio-inspired spring-loaded biopsy harvester was already designed with a great consideration of the ultimate functionality of the final instrument.

The first part of this thesis is concluded with *Chapter 4* presenting a follow-up optimisation study of the biopsy harvester's collapsible frontally acting resection device, bio-inspired by the sea urchin's chewing organ Aristotle's lantern, thus shaped as a crown featuring numerous pointy teeth. In particular, the research focus is on the impact of tooth quantity and type of their bevel on tissue deformation, penetration forces and tooth collapsibility.

The second part of this thesis is also initiated with a review article in *Chapter 5*, contemplating the development of a reliably controllable steerable joint ensuring accurate operation of the envisioned instrument's tip. Here the focus is on identifying and categorising all the mechanical joint constructions used in the state-of-the-art steerable MIS instruments with the aim of discovering a promising design for the vision of this work. Being on the fundamental design level, the joint classification can also serve as a design aid for other developments in this field.

The goal of developing a stiff and reliable joint for the use in a steerable MIS instrument led to the creation of a novel steerable laparoscopic instrument prototype DragonFlex presented in *Chapter 6*. Its simple, repetitive and symmetrical design incorporates a rolling joint with a special tight cable guidance, together maximising the cable lifespan, equalising the forces in both cables and enabling control of seven DOF by only seven structural components. Being the world's first almost entirely additive manufactured steerable MIS instrument prototype, DragonFlex further sheds new light on the possibilities of additive manufacturing in the surgical field.

Chapter 7 provides an empirical evidence that the promisingly high bending stiffness of the rolling joint used in DragonFlex is indeed superior to the state of the art. The chapter implies and verifies that the insight into attaining high bending stiffness of cable-driven joint constructions lies in the principle of full actuation, as opposed to underactuation.

With the vision to perfect DragonFlex's stiff rolling joint, *Chapter 8* presents a method for minimising the small degree of cable slack and thus joint play in the original design. Contrary to the common practice of reducing cable slack by a cable tensioning mechanism, this chapter introduces a more fundamental solution applicable to rolling joints in general. Furthermore, by minimising the joint play, this solution removes the need for a cable tensioning mechanism, thus simplifying the overall design and assembly even further.

Discussion in *Chapter 9* combines the topics of accurate tissue resection and steerability, presenting the envisioned design of the steerable minimally invasive opto-mechanical biopsy harvester. Naturally, this concluding section of the thesis addresses the fusion of the presented insights and designs in a practical manner with regard to manufacturability and usage of the final instrument.

References

- [1] Khoorjestan, S. M., Najarian, S., Simforoosh, N., and Farkoush, S. H., 2010, "Design and Modeling of a Novel Flexible Surgical Instrument Applicable in Minimally Invasive Surgery," *Int J Nat Eng Sci*, 4(1), pp. 53-60.
- [2] Braga, M., Vignali, A., Gianotti, L., Zuliani, W., Radaelli, G., Gruarin, P., Dellabona, P., and Carlo, V. D., 2002, "Laparoscopic Versus Open Colorectal Surgery: A Randomized Trial on Short-Term Outcome," *Ann Surg*, 236(6), pp. 759-767.
- [3] Velanovich, V., 2000, "Laparoscopic vs open surgery," *Surg Endosc*, 14(1), pp. 16-21.
- [4] Minor, M., and Mukherjee, R., 1999, "A Mechanism for Dexterous End-Effector Placement During Minimally Invasive Surgery," *J Mech Des*, 121(4), pp. 472-479.
- [5] Breedveld, P., Stassen, H. G., Meijer, D. W., and Jakimowicz, J. J., 1999, "Manipulation in laparoscopic surgery: Overview of impeding effects and supporting aids," *J Laparoendosc Adv Surg Tech A*, 9(6), pp. 469-480.
- [6] Disability Guidelines, 2014, "Laparoscopy," <https://www.mdguidelines.com/laparoscopy>.
- [7] Arrow Medical, 2012, "Bruder 5mm \emptyset Laparoscopic Instruments," <http://www.arrowmedical.com/sites/default/files/5MM%20LAP%20DISSECTOR,%20GRASPER,%20BIOPSY%20FORCEPS%20%26%20SCISSORS.pdf>.
- [8] Breedveld, P., 2010, "Steerable Laparoscopic Cable-Ring Forceps," *J Med Device*, 4(2), p. 027518.
- [9] Breedveld, P., Stassen, H. G., Meijer, D. W., and Stassen, L. P. S., 1999, "Theoretical background and conceptual solution for depth perception and eye-hand coordination problems in laparoscopic surgery," *Minim Invasive Ther Allied Technol*, 8(4), pp. 227-234.
- [10] Breedveld, P., Scheltes, J. S., Blom, E. M., and Verheij, J. E. I., 2005, "A new, easily miniaturized steerable endoscope," *IEEE Eng Med Biol Mag*, 24(6), pp. 40-47.
- [11] Jelínek, F., Pessers, R., and Breedveld, P., 2014, "DragonFlex Smart Steerable Laparoscopic Instrument," *J Med Device*, 8(1), p. 015001.
- [12] Mayo Clinic, 2013, "Mayo Clinic medical information and tools for healthy living," <http://www.mayoclinic.com/health/medical/>.
- [13] Cerwenka, H., Hoff, M., Rosanelli, G., Hauser, H., Thalhammer, M., Smola, M. G., and Klimpfinger, M., 1997, "Experience with a high speed biopsy gun in breast cancer diagnosis," *Eur J Surg Oncol*, 23(3), pp. 206-207.
- [14] Layfield, L. J., 1995, "Fine needle aspiration of the breast: review of the technique and a comparison with excisional biopsy," *Curr Diagn Pathol*, 2(3), pp. 138-145.
- [15] Miller, L. J., Philbeck, T. E., Montez, D. F., Puga, T. A., Brodie, K. E., Cohen, S. C., Spadaccini, C., Swords, R., and Brenner, A. J., 2011, "Powered bone marrow biopsy procedures produce larger core specimens, with less pain, in less time than with standard manual devices," *Hematol Rep*, 3:e8.
- [16] Weiner, D., Wainwright, M., Tacvorian, E., Hall, D., Gaudette, G., and Dunn, R., "Design of a novel elliptical skin biopsy punch device," Proc. IEEE 35th Annual Northeast Bioengineering Conference, 2009, pp. 1-2.
- [17] Heijnsdijk, E. A. M., Visser, H., Dankelman, J., and Gouma, D. J., 2004, "Slip and damage properties of jaws of laparoscopic graspers," *Surg Endosc*, 18(6), pp. 974-979.
- [18] Volpe, A., Kachura, J. R., Geddie, W. R., Evans, A. J., Gharajeh, A., Saravanan, A., and Jewett, M. A. S., 2007, "Techniques, Safety and Accuracy of Sampling of Renal Tumors by Fine Needle Aspiration and Core Biopsy," *J Urol*, 178(2), pp. 379-386.
- [19] Verbeek, F. P. R., van der Vorst, J. R., Tummers, Q. R. J. G., Boonstra, M. C., de Rooij, K. E., Löwik, C. W. G. M., Valentijn, A. R. P. M., van de Velde, C. J. H., Choi, H. S., Frangioni, J. V., and Vahrmeijer, A. L., 2014, "Near-Infrared Fluorescence Imaging of Both Colorectal Cancer and Ureters Using a Low-Dose Integrin Targeted Probe," *Ann Surg Oncol*, pp. 1-10.
- [20] van Melick, R. G. M., Bakker, D., Meester, R. J. C., Cilia, G., and Löwik, C. W. G. M., "DLP technology's pivotal role in O2view's versatile medical projection/illumination device," Proc. SPIE, 2010, p. 759603.
- [21] Wang, T. D., and Van Dam, J., 2004, "Optical biopsy: a new frontier in endoscopic detection and diagnosis," *Clin Gastroenterol Hepatol*, 2(9), pp. 744-753.
- [22] Amelink, A., Kok, D. J., Sterenberg, H. J. C. M., and Scheepe, J. R., 2011, "In vivo measurement of bladder wall oxygen saturation using optical spectroscopy," *J Biophotonics*, 4(10), pp. 715-720.
- [23] Rodriguez-Diaz, E., Bigio, I. J., and Singh, S. K., 2011, "Integrated optical tools for minimally invasive diagnosis and treatment at gastrointestinal endoscopy," *Robot Comput Integr Manuf*, 27(2), pp. 249-256.
- [24] Vahrmeijer, A. L., and Frangioni, J. V., 2011, "Seeing the invisible during surgery," *Br J Surg*, 98(6), pp. 749-750.
- [25] Quest Medical Imaging, 2014, "Artemis Handheld System," <http://www.quest-mi.com/products/artemis-features-benefits/artemis-overview.html>.
- [26] Amelink, A., Sterenberg, H. J. C. M., Bard, M. P. L., and Burgers, S. A., 2004, "In vivo measurement of the local optical properties of tissue by use of differential path-length spectroscopy," *Opt Lett*, 29(10), pp. 1087-1089.
- [27] Luminostix, 2014, "DPS-Research System," <http://www.luminostix.com/>.

Chapter 2

Minimally Invasive Surgical Instruments with an Accessory Channel Capable of Integrating Fibre Optic Cable for Optical Biopsy

A Review of the State of the Art

Filip Jelínek, Ewout A Arkenbout, Aimée Sakes and Paul Breedveld

*Published in Proceedings of the Institution of Mechanical Engineers,
Part H: Journal of Engineering in Medicine, 228(8), 2014.*

Abstract

Introduction | This review article provides a comprehensive overview and classification of minimally invasive surgical instruments with an accessory channel incorporating fibreoptics or another auxiliary device for various purposes. More specifically, the review was performed with the focus on the newly emerging field of optical biopsy, its objective being to discuss primarily the instruments capable of carrying out the optical biopsy and subsequent tissue resection. Instruments housing the fibreoptics for other uses, as well as instruments with an accessory channel capable of housing the fibreoptics instead of their original auxiliary device after relevant design modifications, supplement the review.

Methods | The entire Espacenet and Scopus databases were searched, yielding numerous patents and articles on conceptual and existing instruments satisfying the criteria. The instruments were categorised based on the function the fibreoptics or the auxiliary device serves. On the basis of their geometrical placement with respect to the tissue resector or manipulator, the subcategories were further defined. This subdivision was used to identify the feasibility of performing the optical biopsy and the tissue resection in an accurate and successive fashion.

Results and Conclusions | In general, the existing concepts or instruments are regarded as limited with regard to such a functionality, either due to the placement of their accessory channel with or without the fibreoptics, or due to the operational restrictions of their tissue manipulators. A novel opto-mechanical biopsy harvester, currently under development at Delft University of Technology, is suggested as a promising alternative ensuring a fast and accurate succession of the optical and the mechanical biopsies of a flat superficial tissue.

2.1 Introduction

2.1.1 Minimally Invasive Surgery

Minimally invasive surgery (MIS) is an increasingly popular trend within the field of surgery as it requires only small incisions or none at all, as in the case of natural orifice transluminal endoscopic surgery (NOTES). Compared to conventional open surgery, MIS leads to considerable patient benefits, such as a shorter hospital stay and recovery time, as well as less postoperative scar tissue [1-5]. Nevertheless, the limited operation site access does not enable the use of traditional instruments designed for and used in the open surgery. Consequently, long and slender MIS instruments have been developed, which provide the surgeon with visual feedback and tissue manipulation features.

2.1.2 Biopsy

Biopsy is a minimally invasive medical test in the field of pathology, whose objective is to research and comprehend the nature and the properties of diseased tissues. Tissue samples that are resected from the patient's body using specialised biopsy instruments are sent to pathologists for tissue analysis. The contemporary biopsy techniques include fine-needle aspiration (Fig. 2.1(a)), core needle biopsy (Fig. 2.1(b)) and punch biopsy (Fig. 2.1(c)) [6].

The fine needle aspiration technique utilises a syringe, which quickly and often automatically samples a limited amount of tissue on a cellular level from deep within the organs. Another deep tissue biopsy technique, the core needle biopsy, employs a core needle with a wide bore that can resect larger tissue samples even from much stiffer tissues, such as a bone. The punch biopsy, which is slightly more invasive and ungainly, uses punches for sampling an easily accessible superficial tissue, such as skin, and longer trephines for sampling the surface of deep and stiff tissues, such as bones. Once sectioning is performed, the punch biopsy, however, usually requires the assistance of auxiliary devices or features for tissue retrieval.

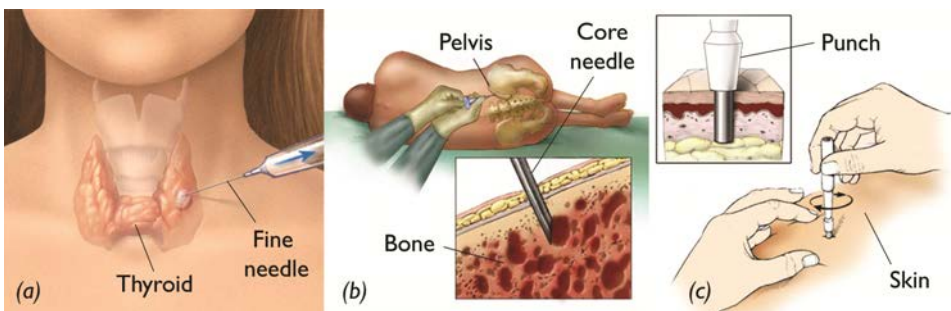


Figure 2.1 Contemporary biopsy techniques including (a) fine-needle aspiration, (b) core needle biopsy and (c) punch biopsy. Adopted from Jelínek et al. [6] (Courtesy of ASME).

2

On the whole, despite being used in the minimally invasive context, the contemporary biopsy devices suffer from geometrical and operational limitations, undermining their usage versatility [7, 8]. Namely, the deep tissue biopsy needles employing suction require full needle tip immersion into the tissue for proper functioning. Hence, they cannot be used for peripheral tissue sampling. Likewise, since the punches and trephines require fully manual and often forceful and lengthy operation [9, 10], unlike fine-needle aspiration, they cannot be used in the minimally invasive context with regard to accuracy at high speed. In addition, the use of a conventional minimally invasive forceps or scissors for the purpose of a tissue resection can easily lead to a tissue slip and thus an inaccurate sampling with accompanying hazards [11]. In particular, these include a potential cancer spread when treating a tumorous tissue [12], which can arise in the event of an accidental tumour perforation. This is especially relevant in the minimally invasive context, as the tumour boundary identification is performed not only through computed tomography or magnetic resonance imaging, but also with the considerable aid of visual cues and force feedback. Hence, tissue perforation and subsequent contamination may easily occur, since the surgeon's senses are greatly limited during the minimally invasive procedures.

2.1.3 Optical Biopsy

In order to ameliorate the minimally invasive handling and identification of unhealthy or hazardous tissues, the new field of optical biopsy is under worldwide research and development [12-15]. The optical biopsy techniques incorporate various types of spectroscopic analyses, employing the fibre optic cable as a signal carrier, and aim to deliver an instant automated non-invasive tissue analysis remotely, without the need for an actual a priori tissue resection. By this means the surgeon could, for instance, easily map the tumour boundaries in real time without the need for any educated estimation or the risk of contamination.

Once analysed and identified as hazardous, the tissue has to be resected by means of a minimally invasive tissue removal instrument. As outlined earlier, the state-of-the-art biopsy devices are rather limited in application, not to mention that attempting to resect the previously analysed tissue using a separate tool or in a separate operation can quickly prove challenging and inaccurate [15]. For that reason, specialised MIS instruments have been conceptualised or are currently being developed into marketable products, which combine the fibre optic cable for the optical biopsy with some sort of a tissue manipulator or a resector for the subsequent mechanical biopsy. Hence, such a functionality integration into a single device would enable executing certain pathological procedures without the need for separate devices or operations and thus more promptly and likely at reduced costs [15].

2.1.4 Review Objectives

The paper by Wang et al. [13] provides a clear overview of the state-of-the-art optical biopsy technologies. In addition to a detailed coverage of several diagnostic methods, the papers by Rodriguez-Diaz et al. [15] and Wong Kee Song et al. [16] outline and demonstrate the implementation of the optical biopsy from a clinical viewpoint, while sharing their experience and results leading to the future development of biopsy instrument prototypes integrating the optical and the mechanical biopsies.

Nevertheless, this newly emerging field of optical biopsy still remains to be explored in terms of the MIS instruments suitable for such an application. In other words, rather than presenting another take on this subject from either clinical or biomedical optics point of view, the aim of this review article is to cover the scope of mechanical engineering and design applicable to this area. Therefore, the primary objective is to collectively outline the state-of-the-art MIS instruments developed specifically for the purpose of the optical biopsy. However, as the fibreoptics can have various uses, this review also discusses any and all the other MIS instruments housing a glass fibre for other purposes, yet capable of carrying out the spectroscopic analysis after relevant design modifications. Moreover, since from the design point of view the incorporation of the fibreoptics basically requires only an unimpeded hollow channel, instruments incorporating such an accessory channel are also outlined with respect to the auxiliary devices embedded in this channel, as well as with regard to their use, design or geometrical configuration.

2.1.5 Literature Search Method

For the purpose of covering the broadest range of ideas, concepts, inventions and existing devices pertaining to this field, both the patent and the paper databases were thoroughly searched. Namely, the Espacenet patent database was searched using the following terms in title or abstract:

Field: *endoscop** or *laparoscop** or *biopsy*

Tissue manipulator: *forceps* or *grasp** or *grip** or *jaw** or *cut** or *resect**

Feature: *channel* or *optic** or *fib**

The reviewed patents were supplemented with a search for review and research articles in Scopus database using the same search string. This was, however, supplemented with the following terms in order to refine the search focus: *device* or *prototyp** or *instrument**.

For the purpose of a general understanding of the researched inventions, the patent search was limited to world (WO), United States (US) and European (EP) patents only, thus yielding more than 450 results – only 56 of which were determined as relevant based on scrutinising the inventions' designs and the intended application. The

paper search resulted in more than 800 hits, of which only 21 proved pertinent to this review due to the broad scope of this search (valid as of 9 January 2014).

2.2 Classification Overview

In general, the MIS instruments capable of incorporating the fibreoptics can be categorised as shown in Fig. 2.2.

On the fundamental level they differentiate into the instruments with the fibreoptics and those with a different auxiliary device in their accessory channel. The instruments with the fibreoptics can be split into subcategories based on the intended use of the fibreoptics – be it tissue analysis, tissue observation or illumination, or tissue treatment. When analysing the geometrical arrangement of the fibre optic cable with respect to the tissue manipulator, the tissue analysis devices always have the fibre

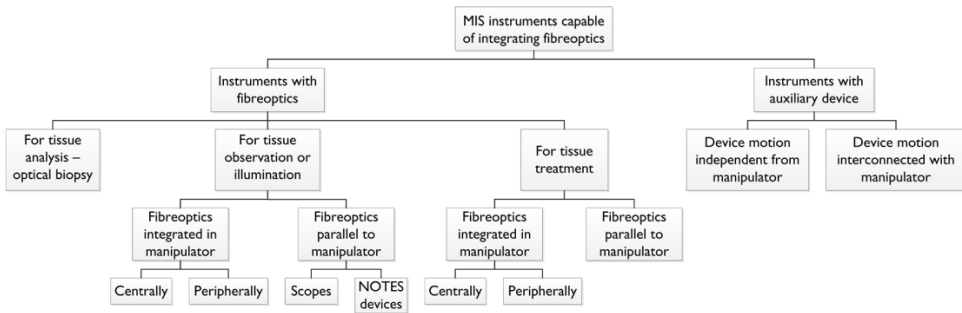


Figure 2.2 Classification overview of the minimally invasive surgical instruments with an accessory channel capable of integrating fibre optic cable for optical biopsy.

integrated centrally. The tissue observation or illumination and the tissue treatment devices have the fibre either integrated into or parallel to the tissue manipulator. When integrated into the tissue manipulator, the fibre can be positioned either centrally or peripherally. On the other hand, the category of the devices intended for tissue observation or illumination with the fibre parallel to the manipulator can be subdivided into scopes in general, with one tissue manipulator, or NOTES devices, with two or more tissue manipulators capable of reaching a common point in space.

The second fundamental category comprises the instruments with an auxiliary device instead of the fibreoptics and can be split into a category where the auxiliary device motion is independent from the tissue manipulator and a category where the two are interconnected. The specific types of the auxiliary devices used are discussed in the following sections.

2.3 Instruments with Fiberoptics

2.3.1 For Tissue Analysis – Optical Biopsy

As outlined earlier, the purpose of the MIS opto-mechanical biopsy instruments, combining the fiberoptics and a tissue manipulation device, is to perform an instant *in situ* tissue diagnosis with the possibility for an accurate tissue resection exactly at the analysed site for the purposes of either plain elimination or further pathological analysis. Since these instruments present the primary focus of this review article, they are discussed in greater detail, both with respect to the proposed imaging or spectroscopic technology and the feasibility of performing both the optical and the mechanical biopsies in an accurate and successive manner.

The patent by Boppart et al. [17] schematically outlines the incorporation of the two biopsy actions in a generic endoscopic device, which can serve as a simple probe or provide a tissue manipulation function in the form of scissors or a forceps. The proposed optical imaging techniques include optical coherence tomography and spectroscopic techniques, such as fluorescence or Raman spectroscopy. A MIS device equipped with such imaging technologies could be used for diagnostic purposes as in screening of oesophagus for adenocarcinoma, or in image guided procedures, such as atherectomy, enhancing the procedural safety.

The patents by Lacombe et al. [18] (Fig. 2.3(a)) and Lind [19] present a more concrete embodiment of such a device, incorporating the fiberoptics centrally, with respect to the biopsy forceps, which could be alternatively replaced or supplemented by a snare for handling protruding tissue during polypectomy, for instance.

Similarly, the patent by Sharon et al. [20] (Fig. 2.3(b)) presents an invention, also suggested in the paper by Rodriguez-Diaz et al. [15], describing a regular endoscopic biopsy forceps with a central channel either for the fiberoptics or other functionalities. These include an irrigation channel, a snare for cauterisation, a spike for collection of multiple biopsy samples or for tissue stabilisation, or vacuum possibly for tissue collection. On top of the aforementioned optical technologies, they propose elastic

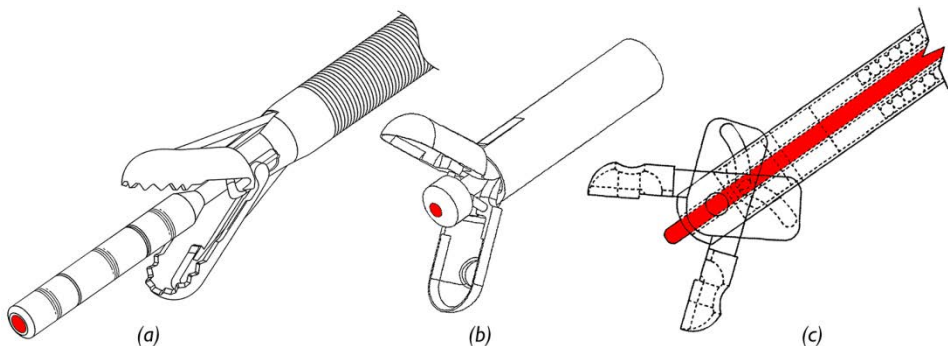


Figure 2.3 Minimally invasive instruments integrating fiberoptics (highlighted) for optical biopsy. Patents by (a) Lacombe et al., (b) Sharon et al. and (c) Sievert et al.

scattering spectroscopy and fluorescent or confocal microscopy. The envisioned application areas include almost any hollow viscus or tissue cavity as follows: the gastrointestinal and hepatobiliary tracts, the genitourinary tract, the airways, the oral cavity and oropharyngeal structures, the mediastinum, the peritoneum, the joint spaces, the cervicovaginal region and the cranium. More specifically, the possibility of the image guided biopsy would be especially beneficial in the case of Barrett's oesophagus, colonic and gastric polyps, flat dysplasia in chronic inflammatory bowel disease, as well as in cervical and bladder dysplasia.

The patent by Sievert et al. [21] (Fig. 2.3(c)) presents an existing device, WavSTAT optical biopsy forceps (SpectraScience, San Diego, CA, USA), also used in the paper by Wong Kee Song et al. [16]. Apart from the discussed optical technologies, they propose laser or photo dynamic therapy. Similar to the invention by Sharon et al. [20], the proposed applications include diagnostics or image guidance of the therapeutic device with the goal of detecting early cancer and lesions with high-grade dysplasia in gastrointestinal endoscopy, bronchoscopy, or other endoscopic fields, such as urology, cardiovascular, neurology, orthopaedics, laparoscopy, obstetrics and gynaecology.

As far as the biopsy forceps are concerned, the patents by Sutton et al. [22] and Whitehead et al. [23] also support the integration of the fiberoptics in such a tissue manipulator. Aside from the general application areas, the patent by Sutton et al. [22] envisions the use of such an opto-mechanical biopsy device for diagnosis and removal of vascular obstructions, such as atherosclerotic lesions and thrombi. The patent by Whitehead et al. [23] recognises the need for such a diagnostic device in evaluating the acceptance of heart transplants which is normally performed via a rather invasive, lengthy and potentially hazardous percutaneous transvenous endomyocardial biopsy. On the other hand, besides the forceps, the patent by Seibel et al. [24] suggests the incorporation of the optical fibre bundle in a cannula. This embodiment would enable performing the optical and the mechanical biopsies in previously inaccessible regions, such as more peripheral airways. Other application areas include for instance urinary tracts, pancreatic and biliary ducts, sinus cavities, or ear canals. Similar use is also proposed in the patent by Ramanujam et al. [25] where the fibre is integrated in a needle or a cannula and serves as an optical probe for ultraviolet-visible reflectance or near infrared optical spectroscopy for detection of breast cancer, for instance.

As identified from the extensive search within patent and paper databases, despite the vast range of potential applications, the scope of the existing opto-mechanical biopsy concepts or instruments is rather limited. Moreover, the proposed tissue manipulators that should perform the subsequent mechanical biopsy in an accurate manner, with respect to the preceding optical biopsy, most often represent simply a traditional biopsy forceps or occasionally a snare or a cannula. For now it suffices to say that such tissue manipulators are very limited both in terms of the geometry of the sampled tissue as well as the accuracy to an extent, as outlined earlier. This is analysed in further detail in section the '2.5 Discussion', where a promising alternative by Jelínek et al. [6] is proposed in the form of a novel opto-mechanical biopsy

harvester featuring a rapid tissue resector ensuring mutual accuracy of the optical and the mechanical biopsies of a flat superficial tissue.

2.3.2 For Tissue Observation or Illumination

Another category of MIS instruments incorporating fibreoptics defines tissue observation or illumination as their intended use. Since the range of such devices is rather broad, they are subdivided into more subcategories based on the geometrical arrangement or placement of the optic fibre with respect to the tissue manipulator.

Fibreoptics integrated into the manipulator. The instruments integrating the optical fibre centrally into the tissue manipulator include a regular forceps or a grasper with the fibreoptics for tissue observation, illumination or both. The central integration of the fibre optic cable would be especially beneficial if used as an opto-mechanical biopsy device due to the relative proximity of the optic fibre and the tissue manipulator. Such instruments are illustrated in the patents by Hildebrandt [26], Simpson et al. [27] and Zeitels et al. [28] (Fig. 2.4(a)). Other inventions include an epidural catheter by Bleich et al. [29] with a central fibre optic cable for observation, an endoscope by Kortenbach et al. [30] surrounded by a ring of detachable jaws at its tip for cauterisation or a MIS instrument by Worcel [31] with a side-firing cutting device and a central fibre.

The instruments that integrate the fibre optic cable peripherally within their lumens include a grasper by InBae [32] (Fig. 2.4(b)) with an illuminating fibre on the side, an existing bronchoscopic optical grasper (Karl Storz, Tuttlingen, Germany), also discussed in the paper by Ponsky et al. [33] and a resection cap by Smith et al. [34] similar to a punch.

Fibreoptics parallel to the manipulator. Most of the instruments incorporating the fibreoptics side by side to the tissue manipulator and other features or devices comprise any type of MIS scopes in general, such as endoscopes, colonoscopes, urethrosopes, cystoscopes, etc. Naturally, covering the entire range of MIS scopes would be excessive without much added value for the purposes of this review. Thus only a few examples are listed below. For instance, the patent by Correa [35] presents a subcutaneous endoscope. An echoendoscope GF-UCT180 (Olympus Medical, Tokyo, Japan) is presented in the paper

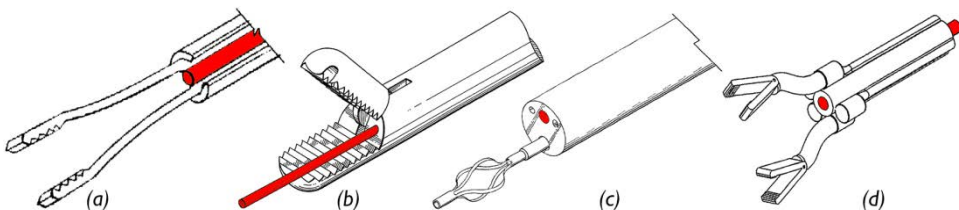


Figure 2.4 Minimally invasive instruments integrating fibreoptics (highlighted) for tissue observation or illumination. Patents by (a) Zeitels et al. – central fibre, (b) InBae – peripheral fibre, (c) Foster – scope device and (d) Heimberger – NOTES device.

by De Lusong et al. [36] and the patent by Masatoshi [37]. Gilkey et al. [38] outline an endoscope with a suturing device. Other embodiments of the endoscopes or the forcipex for use in the endoscopes are described in the patents by Hasson [39], Karpel et al. [40], Kortenbach et al. [41], Kostylev et al. [42], Okada [43], Ouchi [44], Shelton et al. [45], Sonnenschein et al. [46] and Takasaki [47] as well as in the paper by Reavis et al. [48] describing SpyGlass (Boston Scientific, Natick, MA, USA). Furthermore, the paper by Miller et al. [49] introduces a cystoscope. Last but not least, the paper by Bach et al. [50] mentions several urethroscopes or renoscopes such as Viper (Richard Wolf, Vernon Hills, IL, USA), Flex-X 2 (Karl Storz, Tuttlingen, Germany), DUR series scopes (Gyrus ACMI, Southborough, MA, USA) or URF-P5 (Olympus Medical, Tokyo, Japan) used in combination with various biopsy micro-forcipex, listed in the paper by Ritter et al. [51], or with a basket as the one presented by Foster [52] (Fig. 2.4(c)).

The other group of devices where the fibre optic cable is placed parallel to more than one tissue manipulation device is represented by the MIS instruments intended for NOTES procedures. A complete overview of NOTES devices is provided by Arkenbout et al. [53]. Several examples include 160R prototype, later named R-scope (Olympus Optical, Tokyo, Japan), presented in the papers by Astudillo et al. [54], Moyer et al. [55] and Reavis et al. [48]; Direct Drive Endoscopy System (Boston Scientific, Natick, MA, USA) described in the papers by Ikeda et al. [56] and Thompson et al. [57]; Anubis scope or IsisScope [58] (Karl Storz, Tuttlingen, Germany); TransPort [59] (USGI Medical, San Clemente, CA, USA); EndoSAMURAI [56] (Olympus Medical, Tokyo, Japan); Flexible Endoscopic Surgical System [60] (Pentax, Tokyo, Japan) or the invention by Heimberger et al. [61] (Fig. 2.4(d)).

In contrast to the instruments with integrated fibreoptics, the scopes and the NOTES devices with the fibre optic cable parallel to the tissue manipulator would likely suffer from an undermined accuracy or an increased execution complexity if used as opto-mechanical biopsy devices. This is due to the mutual device spacing which would require separate tool alignment for both the optical biopsy and the subsequent resection.

2.3.3 For Tissue Treatment

A few of the MIS devices incorporating fibreoptics suggest tissue treatment as their intended use. Here, the phrase tissue treatment is interpreted as any form of tissue interaction through light, such as laser resection, ablation, coagulation, etc. Thus, the fibre optic cable is also referred to as the laser fibre in this context. From the mechanical design point of view, these devices are virtually identical to those using the fibreoptics for tissue observation or illumination.

Fibreoptics integrated into the manipulator. The patent by Ash et al. [62] envisions a hybrid device combining a tissue grasper and a retractor with a centrally positioned fibre optic cable for tissue coagulation. Similarly, the paper by Khoder et al. [63] presents a custom-made MIS optical grasper featuring the fibreoptics for tissue resection. Last but not

least, the patent by Wilk et al. [64] also discusses a generic grasper, possibly with telescopic jaws, using the fibre optic cable for tissue resection or coagulation.

The patent by Knoepfler [65] illustrates a MIS grasping device with a laser fibre integrated peripherally, more specifically in one of the grasper jaws, and serving for tissue resection or coagulation. An analogous custom-made optical grasper prototype, shown in the paper by Theisen-Kunde et al. [66], uses the laser fibre instead of one grasper jaw, hence serving for both mechanical handling and optical resection.

Fibreoptics parallel to the manipulator. Once again, the design configuration of the devices incorporating the fibreoptics parallel to the tissue manipulator, yet for the purpose of tissue treatment, is analogous to any MIS scope. As a matter of fact, only one patent by Adair [67] proposes the combination of a laser fibre for tissue ablation with a snare or a suture loop.

2.4 Instruments with an Auxiliary Device

As outlined earlier, an opto-mechanical biopsy function could be provided by any MIS device with a tissue manipulator and an accessory channel serving an auxiliary function or housing an auxiliary device. Such a channel is normally integrated centrally into the instrument's lumen. The range of auxiliary functions or devices is rather broad, yet on the basic level they can be subdivided into two categories, in which the motion of the inner device is either independent from or interconnected with the tissue manipulator.

2.4.1 Device Independent from the Manipulator

Functions that could be performed through an accessory channel independently from the tissue manipulator's motion include suction, aspiration, irrigation and storage, among others. The papers by Bhatti [68] and Hucke et al. [69] describe a powered soft-tissue shaver (Stryker, Kalamazoo, MI, USA) with such auxiliary functions, whereas the patent by Clements et al. [70] introduces a biopsy tool for use in an endoscope with a scoop-like frontal resector. The patents by InBae [71] and Treat [72] show MIS graspers with a suction or irrigation channel and similarly the patent by Shibata [73] (Fig. 2.5(a)) discusses an endoscopic biopsy forceps with such an accessory channel. Finally, the patent by Wieser et al. [74] illustrates a trephine with a central channel for sample storage.

Other instruments introduce an auxiliary device operated or supplied through an accessory channel. One of the devices can be a cutter inside a biopsy forceps, as shown in the patent by Landman et al. [75], or incorporated in a bipolar forceps, such as LigaSure (Covidien, Mansfield, MA, USA) described in the patents by Dycus et al. [76] and Olson et al. [77], serving as a vessel sealer and divider (Fig. 2.5(b)).

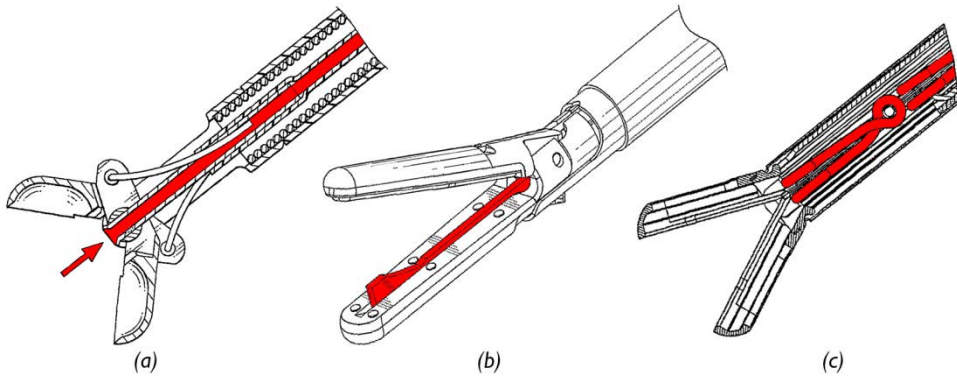


Figure 2.5 Minimally invasive instruments integrating an auxiliary device or a function (highlighted) independent from the tissue manipulator motion. Patents by (a) Shibata – suction channel, (b) Olson et al. – cutter and (c) Shipp et al. – clip.

Another auxiliary device is a ligation clip inside a MIS grasper, such as SpringLock (Surgicon, Stratford, CT, USA) as shown in the patent by Shipp et al. [78] (Fig. 2.5(c)). Similarly, staples can be supplied through an accessory channel as seen in the patent by Shelton et al. [79], showing a surgical stapler ENDOPATH (Ethicon Endo, Cincinnati, OH, USA) or in the patent by Nakao et al. [80]. Furthermore, the patent by Farascioni et al. [81] describes a curved surgical stapler Endo GIA Radial Reload (Covidien, Mansfield, MA, USA).

Last but not least, the patent by Exconde et al. [82] envisions a modification of a laparoscopic grasper where one of the jaws is replaced by a retractable cannula.

2.4.2 Device Interconnected with the Manipulator

The devices whose motion is interconnected with the opening and closing of the grasper jaws comprise needles, spikes and drivers. The needles are usually incorporated in the endoscopic biopsy forceps, such as the one shown in the patent by Freeman [83]. Such devices are also used in the paper by Abudayyeh et al. [84] mentioning Radial Jaw (Boston Scientific, Natick, MA, USA), Alligator Cup (ConMed, Utica, NY, USA) and EndoJaw (Olympus Medical, Tokyo, Japan), the last being described in the patent by Yamamoto [85] as well (Fig. 2.6(a)).

Another device which is usually operated in conjunction with the tissue manipulator is a spike for tissue stabilisation, retraction or collection, as shown in the patent by Kolozsi [86]. Similarly, the paper and the patents by Taylor [87-89] show a cup-like biopsy forceps with one or more spikes in series for a single or multiple tissue samples (Fig. 2.6(b)). Furthermore, the patent by Satake et al. [90] demonstrates a ligation clip applicator that closes with the retraction of the clip.

Finally, the patents by Peters [91] (Fig. 2.6(c)) and Sabin et al. [92] introduce MIS forceps whose jaws are operated by an inner rod with either a driving rack or a ball joint respectively.

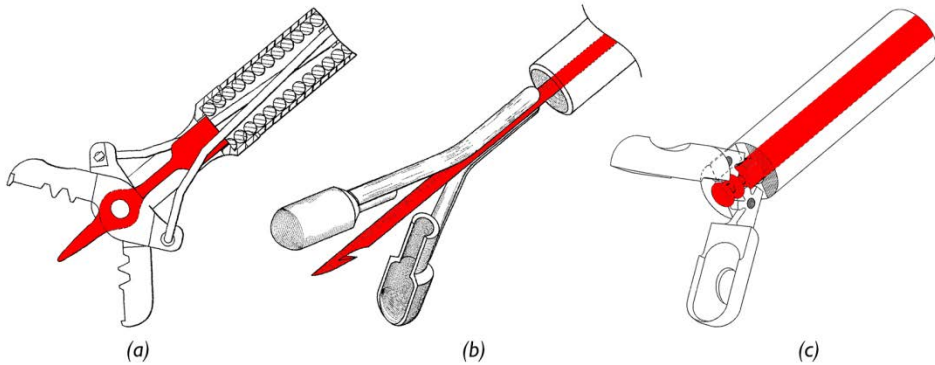


Figure 2.6 Minimally invasive instruments integrating an auxiliary device (highlighted) interconnected with the tissue manipulator motion. Patents by (a) Yamamoto - needle, (b) Taylor - spike and (c) Peters - driver.

2.5 Discussion

2.5.1 Tissue Manipulator Limitations

The review of MIS instruments with an accessory channel for either fibreoptics or other auxiliary devices clearly indicates a general preference towards the use of a biopsy forceps or a grasper; very occasionally this is replaced by a different tissue manipulator, such as a snare. In either case it is evident that such tissue manipulators are well suited for the handling of any protruding tissue, such as polyps. Therefore, for the purposes of applying the optical and the mechanical biopsies on a protruding tissue, the use of an optical grasper becomes an obvious and effective choice [15].

However, once the tissue configuration changes the handling may become more troublesome, requiring the use of other auxiliary devices. To illustrate, as the forceps is easily susceptible to a tissue slip, it may often require the aid of another separate instrument or an embedded feature for tissue stabilisation, as previously shown by numerous designs incorporating needles or spikes. This is especially relevant when handling or resecting larger tissue surfaces, which, compared to the limited MIS instrument tip dimensions, appear as flat. In essence, when attempting to sample flat superficial tissue with sufficient accuracy, one would aim for its minimal deformation in order to prevent its mislocation. As illustrated in Figure 2.7, this can be achieved by various means of tissue fixation, which, however, imply the incorporation of an auxiliary feature providing adequate tissue traction or countertraction. As seen in this review article, no MIS instrument has been identified to contain a tissue resector acting accurately at the same place as the optic cable and supplemented with an auxiliary device for tissue stabilisation or fixation. It stands to reason that the incorporation of such a multitude of features into the limiting geometry of a slender MIS device easily becomes geometrically complex. Despite achievable to some extent, as in the case of endoscopes or NOTES devices, it is at the expense of much greater instrument

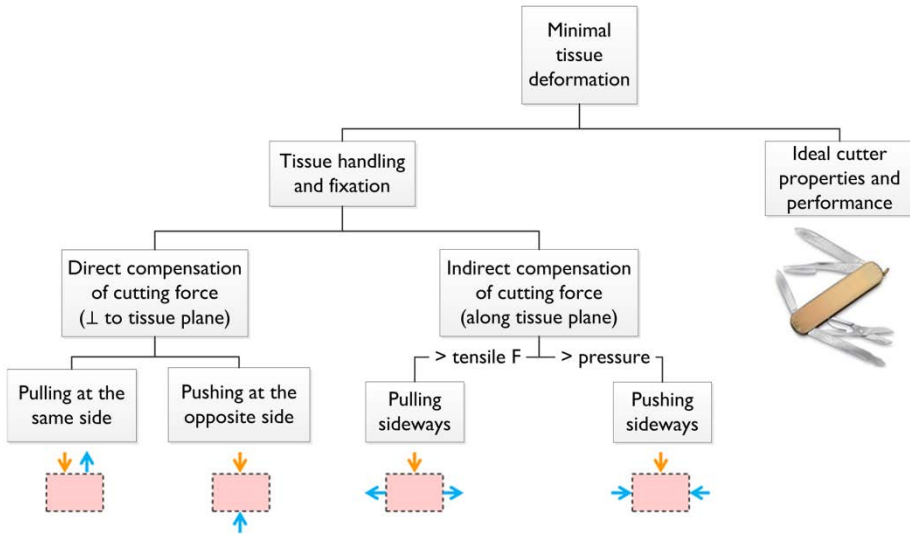


Figure 2.7 The methods for minimal tissue deformation facilitating the superficial tissue sampling (fixation force vector – upward & sideways arrows – in relation to the cutting force vector – downward arrows). Adopted from Jelínek et al. [6] (Courtesy of ASME).

dimensions, cumbersome manipulation and parallel arrangement of the fiberoptics and the tissue manipulator introducing mutual spacing.

On the other hand, the minimal tissue deformation could be attained by devising a smart cutting tool, which would enable effortless or even fast tissue penetration and containment, in order to reduce the chance of mislocation due to the device limitations or a human error. Furthermore, for the purposes of accurate successiveness of the optical and the mechanical biopsies and enhanced ease of use, the optic cable should be integrated centrally and coaxially with the tissue resector.

2.5.2 Recent development

A novel MIS opto-mechanical biopsy instrument of 5mm outer diameter featuring the aforementioned geometrical configuration is currently under development at Delft University of Technology. It will contain a minimally invasive modification of a frontally acting spring-loaded biopsy harvester [6] at its tip (Figure 2.8) integrating the fibre optic cable centrally and enabling the execution of the optical and the mechanical biopsies in a fast and accurate succession. Contrary to the fully manual operation of the biopsy forceps, a single compliant resector – the bio-inspired crown-cutter – enables an automatic simultaneous tissue resection and containment in less than 1ms. As seen in Figure 2.8 and presented in the paper by Jelínek et al. [6], the crown-cutter is capable of rapidly resecting a uniform conical liver biopsy, leaving a clean round cut. It is envisioned that the opto-mechanical biopsy instrument will fill the missing gap among the biopsy devices developed specifically for the purpose of the minimally invasive

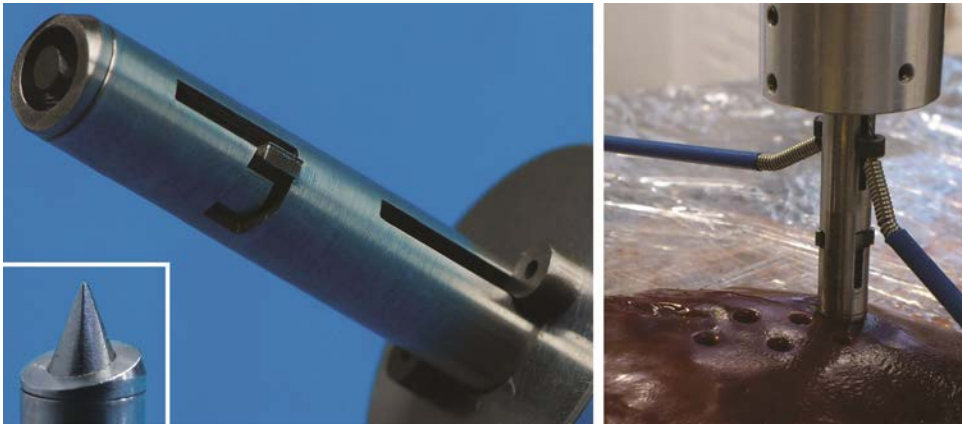


Figure 2.8 *Opto-mechanical biopsy harvester prototype capable of rapidly sampling a flat superficial tissue, such as a liver. Adopted from Jelínek et al. [6] (Courtesy of ASME).*

optical analysis and the resection of a flat superficial tissue. Aside from the aforementioned application areas, other uses would also include the diagnosis and sampling of a liver or an inner surface of the abdominal wall. The envisioned use would be limited to the identification and the removal of small tumours due to the particular geometry of the instrument's cutting device.

2.6 Conclusions

A comprehensive overview of the minimally invasive instruments developed for, or capable of carrying out, the optical biopsy and the tissue resection is provided. The modest category of the minimally invasive devices intended specially for the optical and the mechanical biopsies favours the use of a biopsy forceps or a grasper with a centrally integrated fibre optic cable. As recognised in the literature, such tissue manipulators are well developed and applicable to the sampling of a protruding tissue. Furthermore, with the recent development at Delft University of Technology, the scope of the minimally invasive applications can be broadened to taking small samples of a flat superficial tissue as well, with an enhanced operational simplicity, speed and accuracy. Last but not least, the vast scope of the discussed MIS devices shows that with relevant design modifications these devices can easily house a fibre optic cable and thus provide the optical biopsy functionality. The question then remains how accurate each of these devices can be with regard to the optical and the subsequent mechanical biopsy and what application they would be suitable for.

Acknowledgements

The research of Filip Jelínek was performed within the framework of CTMM, the Center for Translational Molecular Medicine, project MUSIS (grant 030-202). The research of Ewout A Arkenbout and Aimée Sakes was supported by Technology Foundation STW.

References

- [1] Braga, M., Vignali, A., Gianotti, L., Zuliani, W., Radaelli, G., Gruarin, P., Dellabona, P., and Carlo, V. D., 2002, "Laparoscopic Versus Open Colorectal Surgery: A Randomized Trial on Short-Term Outcome," *Ann Surg*, 236(6), pp. 759–767.
- [2] Breedveld, P., Stassen, H. G., Meijer, D. W., and Jakimowicz, J. J., 1999, "Manipulation in laparoscopic surgery: Overview of impeding effects and supporting aids," *J Laparoendosc Adv Surg Tech A*, 9(6), pp. 469–480.
- [3] Khorjastan, S. M., Najarian, S., Simforoosh, N., and Farkoush, S. H., 2010, "Design and Modeling of a Novel Flexible Surgical Instrument Applicable in Minimally Invasive Surgery," *Int J Nat Eng Sci*, 4(1), pp. 53–60.
- [4] Minor, M., and Mukherjee, R., 1999, "A Mechanism for Dexterous End-Effector Placement During Minimally Invasive Surgery," *J Mech Des*, 121(4), pp. 472–479.
- [5] Velanovich, V., 2000, "Laparoscopic vs open surgery," *Surg Endosc*, 14(1), pp. 16–21.
- [6] Jelínek, F., Smit, G., and Breedveld, P., 2014, "Bioinspired Spring-Loaded Biopsy Harvester—Experimental Prototype Design and Feasibility Tests," *J Med Device*, 8(1), p. 015002.
- [7] Cerwenka, H., Hoff, M., Rosanelli, G., Hauser, H., Thalhammer, M., Smola, M. G., and Klimpfinger, M., 1997, "Experience with a high speed biopsy gun in breast cancer diagnosis," *Eur J Surg Oncol*, 23(3), pp. 206–207.
- [8] Layfield, L. J., 1995, "Fine needle aspiration of the breast: review of the technique and a comparison with excisional biopsy," *Curr Diagn Pathol*, 2(3), pp. 138–145.
- [9] Miller, L. J., Philbeck, T. E., Montez, D. F., Puga, T. A., Brodie, K. E., Cohen, S. C., Spadaccini, C., Swords, R., and Brenner, A. J., 2011, "Powered bone marrow biopsy procedures produce larger core specimens, with less pain, in less time than with standard manual devices," *Hematol Rep*, 3:e8.
- [10] Weiner, D., Wainwright, M., Tacvorian, E., Hall, D., Gaudette, G., and Dunn, R., "Design of a novel elliptical skin biopsy punch device," Proc. IEEE 35th Annual Northeast Bioengineering Conference, 2009, pp. 1–2.
- [11] Heijnsdijk, E. A. M., Visser, H., Dankelman, J., and Gouma, D. J., 2004, "Slip and damage properties of jaws of laparoscopic graspers," *Surg Endosc*, 18(6), pp. 974–979.
- [12] Volpe, A., Kachura, J. R., Geddie, W. R., Evans, A. J., Gharajeh, A., Saravanan, A., and Jewett, M. A. S., 2007, "Techniques, Safety and Accuracy of Sampling of Renal Tumors by Fine Needle Aspiration and Core Biopsy," *J Urol*, 178(2), pp. 379–386.
- [13] Wang, T. D., and Van Dam, J., 2004, "Optical biopsy: a new frontier in endoscopic detection and diagnosis," *Clin Gastroenterol Hepatol*, 2(9), pp. 744–753.
- [14] Amelink, A., Kok, D. J., Sterenberg, H. J. C. M., and Scheepe, J. R., 2011, "In vivo measurement of bladder wall oxygen saturation using optical spectroscopy," *J Biophotonics*, 4(10), pp. 715–720.
- [15] Rodriguez-Diaz, E., Bigio, I. J., and Singh, S. K., 2011, "Integrated optical tools for minimally invasive diagnosis and treatment at gastrointestinal endoscopy," *Robot Comput Integr Manuf*, 27(2), pp. 249–256.
- [16] Wong Kee Song, L. M., and Wilson, B. C., 2005, "Endoscopic detection of early upper GI cancers," *Best Pract Res Clin Gastroenterol*, 19(6), pp. 833–856.
- [17] Boppart, S. A., Tearney, G. J., Bouma, B. E., Brezinski, M. E., Fujimoto, J. G., and Swanson, E. A., "Instrument for Optically Scanning of Living Tissue," Massachusetts Institute of Technology, WO Patent 98/38907, 11 September 1998.
- [18] Lacombe, F., Hughett, D., Tihansky, C., and Genet, M., "Multi-Purpose Biopsy Forceps," Mauna Kea Technologies, US Patent 2010/0168610, 1 July 2010.
- [19] Lind, S. J., "Medical Forceps Jaw Assembly," Annex Medical, Inc., US Patent 5,820,630, 13 October 1998.
- [20] Sharon, A., Singh, S., Bigio, I., Atladottir, S., Foss, D., and Vogtel, P., "Low Cost Disposable Medical Forceps to Enable a Hollow Central Channel for Various Functionalities," Trustees of Boston University et al., WO Patent 2009/111717, 11 September 2009.
- [21] Sievert, C. E., Wilson, S. R., Townsend, G. L., Pokorney, J. L., and McMahon, B. T., "Optical Forceps System and Method of Diagnosing and Treating Tissue," SpectraScience, Inc., US Patent 6,394,964, 28 May 2002.
- [22] Sutton, G. S., and McMahon, B. T., "Optical Biopsy Forceps," SpectraScience, Inc., US Patent 6,129,683, 10 October 2000.
- [23] Whitehead, P. D., MacAulay, C. E., MacKinnon, N. B., and Zeng, H., "Catheters and Endoscopes Comprising Optical Probes and Bioptomes and Methods of Using the Same," Biomax Technologies, Inc., WO Patent 98/40015, 17 September 1998.
- [24] Seibel, E. J., Johnson, R. S., and Melville, C. D., "Catheter with Imaging Capability Acts as Guidewire for Cannula Tools," University of Washington, WO Patent 2008/121143, 9 October 2008.
- [25] Ramanujam, N., Zhu, C., and Lubawy, C., "Side-Firing Probe for Performing Optical Spectroscopy during Core Needle Biopsy," Wisconsin Alumni Research Foundation, WO Patent 2005/087092, 22 September 2005.
- [26] Hildebrandt, S., "Forceps," US Patent 4,027,510, 7 June 1977.
- [27] Simpson, P. J., Matsuura, D. G., and Kilcoyne, J., "Articulated Medical Device," Endonetics, Inc., US Patent 6,139,508, 31 October 2000.
- [28] Zeitels, J. R., and Grewe, D. D., "Endoscopic Retriever," US Patent 5,746,770, 5 May 1998.
- [29] Bleich, J. L., Spisak, S. A., Hlavka, E. J., Saadat, V., Miller, D. R., and Yurchenko, J., "Devices and Methods for Tissue Removal," Baxano, Inc., WO Patent 2006/044727, 27 April 2006.
- [30] Kortenbach, J. A., and McBrayer, M. S., "Methods and Apparatus for the Treatment of Gastric Ulcers," Syntheon, LLC, US Patent 2003/0233092, 18 December 2003.
- [31] Worcel, A., "Endoscopic Cutting Surgical Device," WO Patent 2010/106299, 23 September 2010.
- [32] InBae, Y., "Penetrating Endoscope and Endoscopic Surgical Instrument with CMOS Image Sensor and Display," WO Patent 01/01847, 11 January 2001.

- [33] Ponsky, T. A., and Lukish, J. R., 2008, "Single site laparoscopic gastrostomy with a 4-mm bronchoscopic optical grasper," *J Pediatr Surg*, 43(2), pp. 412-414.
- [34] Smith, P., and Carrillo, O., "Tissue Resection Bander and Related Methods of Use," Boston Scientific Scimed, Inc., US Patent 2013/0172918, 4 July 2013.
- [35] Correa, M. A. M. d. F., "Surgical Instrument to Perform Subcutaneous Endoscopic Surgery," WO Patent 95/10982, 27 April 1995.
- [36] De Lusong, M. A., Shah, J. N., Soetikno, R., and Binmoeller, K. F., 2008, "Treatment of a completely obstructed colonic anastomotic stricture by using a prototype forward-array echoendoscope and facilitated by SpyGlass (with videos)," *Gastrointest Endosc*, 68(5), pp. 988-992.
- [37] Masatoshi, S., "Puncture Needle for Ultrasound," Olympus Medical Systems Corp., EP Patent 2 662 036, 13 November 2013.
- [38] Gilkey, L. J., Nagreiter, B. E., Kratsch, P. K., Jones, D. K., and Mittelberg, V., "Method of Endoscopic Suturing," Apollo Endosurgery, Inc., US Patent 2013/0096581, 18 April 2013.
- [39] Hasson, H. M., "Multi-Pronged Laparoscopy Forceps," US Patent 4,174,715, 20 November 1979.
- [40] Karpel, J. A., and Ducharme, R. W., "Endoscopic Sheet Delivery," Wilson-Cook Medical, Inc., WO Patent 2010/053737, 14 May 2010.
- [41] Kortenbach, J. A., Sixto, R., Smith, K. W., Slater, C. R., and Gottlieb, S., "Apparatus for the Endoluminal Treatment of Gastroesophageal Reflux Disease (GERD)," US Patent 2002/0068946, 6 June 2002.
- [42] Kostylev, A. N., Novikov, C. V., and Pesotchinsky, L. L., "Biopsy Apparatus," LSVP International, Inc., US Patent 6,273,860, 14 August 2001.
- [43] Okada, T., "Treatment Tool for Endoscope," Olympus Corporation, US Patent 2006/0149222, 6 July 2006.
- [44] Ouchi, T., "Treatment Accessories for an Endoscope," Asahi Optical Co., Ltd., EP Patent 0 835 637, 15 April 1998.
- [45] Shelton, F. E., and Ortiz, M. S., "Articulatable Surgical Device with Rotary Driven Cutting Member," Ethicon Endo-Surgery, Inc., US Patent 2013/0197556, 1 August 2013.
- [46] Sonnenschein, E., Govrin, A., and Sonnenschein, M., "Transgastric Method for Carrying out a Partial Fundoplication," Medigus Ltd., US Patent 2007/0282356, 6 December 2007.
- [47] Takasaki, K., "Image Pickup Device and Endoscope," Fujifilm Corporation, US Patent 2011/0074941, 31 March 2011.
- [48] Reavis, K. M., and Melvin, W. S., 2008, "Advanced endoscopic technologies," *Surg Endosc*, 22(6), pp. 1533-1546.
- [49] Miller, R. A., Parry, J., Creighton, S., Coptcoat, M., and Wickham, J. E. A., 1989, "Integrated cystoscope: First rigid multipurpose operating cystoscope for local anesthetic endoscopy," *Urology*, 33(3), pp. 193-197.
- [50] Bach, T., Geavlete, B., Herrmann, T. R. W., and Gross, A. J., 2008, "Working tools in flexible ureterorenoscopy - Influence on flow and deflection: What does matter?," *J Endourol*, 22(8), pp. 1639-1643.
- [51] Ritter, M., Bolenz, C., Bach, T., Ströbel, P., and Häcker, A., 2013, "Standardized ex vivo comparison of different upper urinary tract biopsy devices: Impact on ureterorenoscopes and tissue quality," *World J Urol*, 31(4), pp. 907-912.
- [52] Foster, T. L., "Minimally-Invasive Medical Retrieval Device," Hunt, J. B., US Patent 2001/0041899, 15 November 2001.
- [53] Arkenbout, E. A., Henselmans, P. W. J., Jelinek, F., and Breedveld, P., 2014, "A state of the art review and categorization of multi-branched instruments for NOTES and SILS," *Surg Endosc*, in press.
- [54] Astudillo, J. A., Sporn, E., Bachman, S., Miedema, B., and Thaler, K., 2009, "Transgastric cholecystectomy using a prototype endoscope with 2 deflecting working channels (with video)," *Gastrointest Endosc*, 69(2), pp. 297-302.
- [55] Moyer, M. T., Haluck, R. S., Gopal, J., Pauli, E. M., and Mathew, A., 2010, "Transgastric organ resection solely with the prototype R-scope and the self-approximating transluminal access technique," *Gastrointest Endosc*, 72(1), pp. 170-176.
- [56] Ikeda, K., Sumiyama, K., Tajiri, H., Yasuda, K., and Kitano, S., 2011, "Evaluation of a new multitasking platform for endoscopic full-thickness resection," *Gastrointest Endosc*, 73(1), pp. 117-122.
- [57] Thompson, C. C., Ryou, M., Soper, N. J., Hungess, E. S., Rothstein, R. I., and Swanstrom, L. L., 2009, "Evaluation of a manually driven, multitasking platform for complex endoluminal and natural orifice transluminal endoscopic surgery applications (with video)," *Gastrointest Endosc*, 70(1), pp. 121-125.
- [58] Leroy, J., Diana, M., Barry, B., Mutter, D., Melani, A. G. F., Wu, H. S., and Marescaux, J., 2012, "Perirectal oncologic gateway to retroperitoneal endoscopic single-site surgery (PROGRESS): A feasibility study for a new notes approach in a swine model," *Surg Innov*, 19(4), pp. 345-352.
- [59] Clayman, R. V., Box, G. N., Abraham, J. B. A., Lee, H. J., Deane, L. A., Sargent, E. R., Nguyen, N. T., Chang, K., Tan, A. K., Ponsky, L. E., and McDougall, E. M., 2007, "Transvaginal single-port NOTES nephrectomy: Initial laboratory experience," *J Endourol*, 21(6), pp. 640-644.
- [60] Kobayashi, T., Lemoine, S., Sugawara, A., Tsuchida, T., Gotoda, T., Oda, I., Ueda, H., and Kakizoe, T., 2005, "A flexible endoscopic surgical system: First report on a conceptual design of the system validated by experiments," *Jpn J Clin Oncol*, 35(11), pp. 667-671.
- [61] Heimberger, R., and Lambertz, M., "Endoscopic Instrument," Richard Wolf GmbH, EP Patent 2 340 759, 6 July 2011.
- [62] Ash, S. R., and Loeb, M. P., "Surgical Device for Internal Operations," Laserscope, Inc., WO Patent 83/03189, 29 September 1983.
- [63] Khoder, W. Y., and Sroka, R., 2011, "Concept of a fiber guidance instrument for laser-assisted laparoscopic partial nephrectomy," *Med Laser Appl*, 26(4), pp. 176-182.
- [64] Wilk, P. J., and Pirak, L., "Laparoscopic Instrument Assembly and Associated Method," US Patent 5,578,031, 26 November 1999.
- [65] Knoepfler, D. J., "Multiple Purpose Forceps," US Patent 5,300,087, 5 April 1994.
- [66] Theisen-Kunde, D., Ott, V., Brinkmann, R., and Keller, R., 2007, "Potential of a new cw 2 μ m laser scalpel for laparoscopic surgery," *Med Laser Appl*, 22(2), pp. 139-145.

- [67] Adair, E. L., "Laparoscopic Surgical Ligation and Electrosurgical Coagulation and Cutting Device," US Patent 5,290,284, 1 March 1994.
- [68] Bhatti, M. T., 2007, "Neuro-ophthalmic complications of endoscopic sinus surgery," *Curr Opin Ophthalmol*, 18(6), pp. 450-458.
- [69] Hucke, J., and Füllers, U., 2005, "New developments in gynaecological endoscopy," *Innov Gynäkol Endosk*, 38(11), pp. 952-958.
- [70] Clements, R. M., and Face, A. R., "Device and System for Multiple Core Biopsy," WO Patent 2011/066470, 3 June 2011.
- [71] InBae, Y., "Multifunctional Grasping Instrument with Cutting Member and Operating Channel for Use in Endoscopic and Non-Endoscopic Procedures," US Patent 5,984,939, 16 November 1999.
- [72] Treat, M. R., "Multiple Bit, Multiple Specimen Endoscopic Biopsy Forceps," The Trustees of Columbia University in the City of New York, US Patent 6,632,182, 14 October 2003.
- [73] Shibata, H., "Forceps Unit for Endoscope," Pentax Corporation, US Patent 2005/0261735, 24 November 2005.
- [74] Wieser, M., and Stocker, P., "Bone Biopsy Cutter," WO Patent 2011/135070, 3 November 2011.
- [75] Landman, J. L., Wingler, T. W., Foster, T. L., and Ryan, W. N., "Back Loading Endoscopic Instruments," Cook Urological, Inc., WO Patent 2005/063127, 14 July 2005.
- [76] Dycus, S. T., Buysse, S. P., and Brown, D. D., "Vessel Sealer and Divider with Non-Conductive Stop Members," Sherwood Services AG, EP Patent 1 685 806, 2 August 2006.
- [77] Olson, J. E., and Unger, J. R., "Vessel Sealer and Divider," Tyco Healthcare Group LP, US Patent 2012/0310240, 6 December 2012.
- [78] Shipp, J. I., Shepard, S. Y., and Satterfield, J. A., "Ligation Clip and Clip Applier," Surgicon, Inc., US Patent 2004/0106936, 3 June 2004.
- [79] Shelton, F. E., and Uth, J., "Surgical Cutting and Stapling Instrument with Self Adjusting Anvil," Ethicon Endo-Surgery, Inc., US Patent 2012/0234897, 20 September 2012.
- [80] Nakao, N., and Wilk, P. J., "Endoscopic Stapling Device and Method," WO Patent 92/19144, 12 November 1992.
- [81] Farascioni, D., and Beardsley, J. W., "Surgical Instrument and Loading Unit for Use Therewith," Covidien LP, EP Patent 2 647 342, 9 October 2013.
- [82] Exconde, P. D., and Thomas, J. S., "Endoscopic Cholangiogram Guide Instrument and Method of Use," US Patent 5,496,310, 5 March 1996.
- [83] Freeman, K. V., "Modular Medical Instrument and Method of Using Same," US Patent 6,074,408, 13 June 2000.
- [84] Abudayyeh, S., Hoffman, J., El-Zimaity, H. T., and Graham, D. Y., 2009, "Prospective, randomized, pathologist-blinded study of disposable alligator-jaw biopsy forceps for gastric mucosal biopsy," *Dig Liver Dis*, 41(5), pp. 340-344.
- [85] Yamamoto, T., "Endoscopic Instrument," Olympus Optical Co., Ltd., US Patent 2001/0047124, 29 November 2001.
- [86] Kolozsi, W. Z., "Biopsy Apparatus for Use in Endoscopy," US Patent 5,373,854, 20 December 1994.
- [87] Taylor, T. V., "Multiple-Specimen, Endoscopic Biopsy Forceps," US Patent 6,419,640, 16 July 2002.
- [88] Taylor, T. V., "Multiple Biopsy Device," WO Patent 98/06336, 19 February 1998.
- [89] Taylor, T. V., 2004, "A system of multiple biopsy forceps," *Curr Surg*, 61(6), pp. 594-596.
- [90] Satake, M., Ban, A., Kaneko, Y., Kimura, K., Sato, K., and Kogiso, J., "Ligation Apparatus and a Ligation Member," Olympus Medical Systems Corp., US Patent 2008/0255427, 16 October 2008.
- [91] Peters, J.-B., "Device for Taking Samples, for Example for a Biopsy, and Rack System Fitted to Such a Device," Nivarox-FAR S.A., US Patent 6,155,988, 5 December 2000.
- [92] Sabin, P. J.-C., Sabin, J.-L., and Hugueny, J.-M., "Clamping Device, Particularly a Biopsy Forceps," Warnier, A. et al., WO Patent 98/03116, 29 January 1998.

Chapter 3

Bio-Inspired Spring-Loaded Biopsy Harvester

Experimental Prototype Design and Feasibility Tests

Filip Jelínek, Gerwin Smit and Paul Breedveld

Published in Journal of Medical Devices 8(1), 2014.

Abstract

Introduction | Current minimally invasive laparoscopic tissue harvesting techniques for pathological purposes involve taking multiple imprecise and inaccurate biopsies, usually using a laparoscopic forceps or other assistive devices. Potential hazards, e.g. cancer spread when dealing with tumorous tissue, call for a more reliable alternative in the form of a single laparoscopic instrument capable of repeatedly taking a precise biopsy at a desired location. Therefore, the aim of this project was to design a disposable laparoscopic instrument tip, incorporating a centrally positioned glass fibre for tissue diagnostics; a cutting device for fast, accurate and reliable biopsy of a precisely defined volume and a container suitable for sample storage.

Methods | Inspired by the sea urchin's chewing organ, Aristotle's lantern, and its capability of rapid and simultaneous tissue incision and enclosure by axial translation, we designed a crown-shaped collapsible cutter operating on a similar basis. Based on a series of *in vitro* experiments indicating that tissue deformation decreases with increasing penetration speed leading to a more precise biopsy, we decided on the cutter's forward propulsion via a spring. Apart from the embedded spring-loaded cutter, the biopsy harvester comprises a smart mechanism for cutter preloading, locking and actuation, as well as a sample container.

Results and Conclusions | A real-sized biopsy harvester prototype was developed and tested in a universal tensile testing machine at TU Delft. In terms of mechanical functionality, the preloading, locking and actuation mechanism as well as the cutter's rapid incising and collapsing capabilities proved to work successfully *in vitro*. Further division of the tip into a permanent and a disposable segment will enable taking of multiple biopsies, mutually separated in individual containers. We believe the envisioned laparoscopic opto-mechanical biopsy device will be a solution ameliorating time demanding, inaccurate and potentially unsafe laparoscopic biopsy procedures.

3.1 Introduction

3.1.1 Laparoscopy and Biopsy

Laparoscopy, minimally invasive surgery in the abdomen, is becoming increasingly more popular due to its capability to considerably minimise incision size, postoperative tissue trauma and patient recovery time [1-5]. Yet, the advantages come at the expense of a limited site access and restricted tissue manipulation [2, 6].

The state-of-the-art minimally invasive biopsy methods [7] mainly involve needle biopsy, usually used for sampling thyroid, breast and prostate tissue, and punch biopsy used for sampling skin and bone tissue (Fig. 3.1) [8]. However, these biopsy techniques generally lack application versatility mainly due to the limitations of the existing biopsy devices [9, 10]. To illustrate, the biopsy needles have been designed and used for deep tissue biopsy, thus rendering them inappropriate for peripheral intra-abdominal tissue sampling. Similarly, punches used for peripheral tissue biopsy would be very limited in terms of use within the laparoscopic context with regard to speed or accuracy at a smaller scale, for instance. Furthermore, using a regular laparoscopic forceps or scissors for biopsy can likely result in tissue slip and hence insufficiently accurate tissue sampling with associated risks [11].

The need for greater accuracy, procedure reliability, time- and cost-efficiency as well as minimising potential handling hazards [9, 12-14], e.g. cancer spread when dealing with tumorous tissue [15], calls for an alternative, more robust biopsy technique combining a real-time tissue diagnosing technology with a precise, easily operable laparoscopic biopsy harvester. For clarification, the terms robust and robustness are used throughout this paper in the context of enhanced device capabilities and fitness for purpose while satisfying the aforementioned needs.

3.1.2 Combining Optical and Mechanical Biopsy

When it comes to endoscopic tissue diagnosis, there are various emerging technologies that could ameliorate lengthy pathological procedures by providing instant real-time *in situ* tissue analysis. Hence, pathology could be performed without the need for

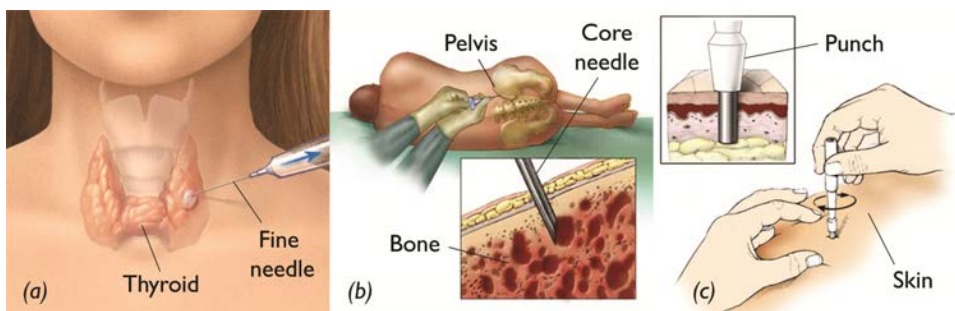


Figure 3.1 Examples of contemporary biopsy techniques including (a) fine-needle aspiration, (b) core needle biopsy and (c) punch biopsy. Adopted from [8].

multiple discrete and lengthy operations – in other words much more readily and thus supposedly at reduced costs. These diagnostic technologies incorporate a range of differing tissue imaging techniques, usually using fibre optics as a signal carrier, and they are collectively designated as ‘optical biopsy’ [14, 16].

By incorporating the optical biopsy technology within a laparoscopic instrument and combining it with a mechanical tissue removal device – a biopsy harvester – one could achieve greater robustness and time-efficiency compared to the current standard. Normally, the retrieved biopsies (usually of indefinite volume and tissue properties) are sent to a lengthy pathological analysis and may require subsequent treatment of the patient after a couple of days or even weeks, either for more biopsy samples or for tumour resection. Naturally, apart from the obvious time delays, such a segmented and usually repetitive process can increase the risk of cancer spread. Instead, with an opto-mechanical biopsy harvester one would be capable of an instant optical analysis *in situ* with the possibility of a precise tissue removal exactly at the analysed site and all within a matter of seconds.

3.1.3 Problem Statement – Need for a Novel Opto-Mechanical Biopsy Device

Current patented concepts of laparoscopic instruments combining glass fibres for optical measurements with tissue manipulation devices (Fig. 3.2) [17-19] lack accuracy and practicality, mainly due to insufficiencies of their end-effectors and their inappropriateness for accurate targeting and delicate tissue handling at smaller scale. As a consequence, such devices would be inadequate for performing the optical and mechanical biopsy operations in a reliable, accurate and fast succession at the same location, or in a single procedure. Hence, such device concepts were not considered for the envisioned laparoscopic application of optically analysing and sampling the diseased internal abdominal organ and tissue surfaces.

Therefore, in order to enhance the contemporary laparoscopic biopsy procedures with robustness, accuracy and efficiency, there is a need for a novel dexterous opto-mechanical biopsy device that would compensate for the aforementioned weaknesses of the state-of-the-art biopsy techniques, devices and concepts.

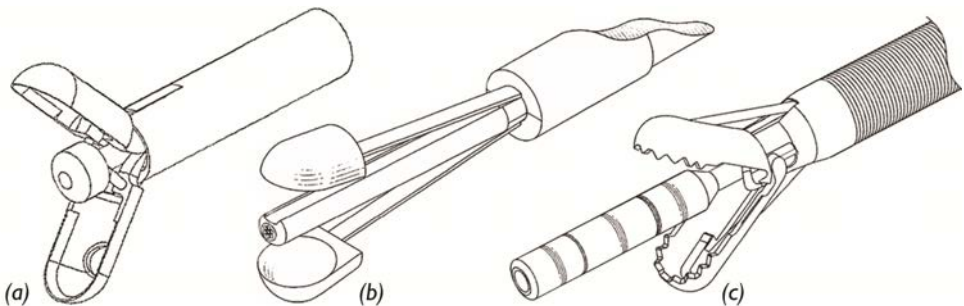


Figure 3.2 Examples of laparoscopic opto-mechanical biopsy tip concepts patented by (a) Sharon et al. [18], (b) Whitehead et al. [19] and (c) Lacombe et al. [17].

3.1.4 Minimal Tissue Deformation Approach towards Laparoscopic Biopsy

To outline the combination and incorporation of optical and mechanical biopsy in laparoscopy, one has to look at the fusion of these two technologies in a practical manner – from the perspective of reaching the targeted site and the means of tissue handling.

With a laparoscopic instrument, a surgeon can approach the targeted peripheral tissue either frontally or laterally [2]. Since tissue analysis and its subsequent accurate extraction are required, one has to reconsider the ideal approach to the tissue based on the design constraints of both the laparoscope and the imaging technology. Once a thick glass-fibre bundle of a large bending radius [20] is integrated into a long slender tubular geometry of a laparoscope's shaft, the only possible way the fibres can then guide the signal is frontally and coaxially with the instrument itself. Furthermore, in order to ensure an accurate and rapid succession of actions at reduced complexity, the mechanical biopsy should follow the direction of the preceding optical measurements. Therefore, rather than analysing and handling the targeted tissue separately or from different angles, a reasonable decision was made to enable performing both the optical and mechanical biopsy frontally and in a close succession.

One could successfully perform the mechanical biopsy at a high level of accuracy by ensuring a minimal deformation of the targeted tissue caused by the cutting device. As described in Fig. 3.3, this could be in theory achieved by compensating for the frontal cutting force either directly or indirectly. Direct compensation would involve either pulling or pushing action perpendicular to the tissue surface and parallel to the applied cutting force vector. Indirect compensation would comprise a pulling action along the

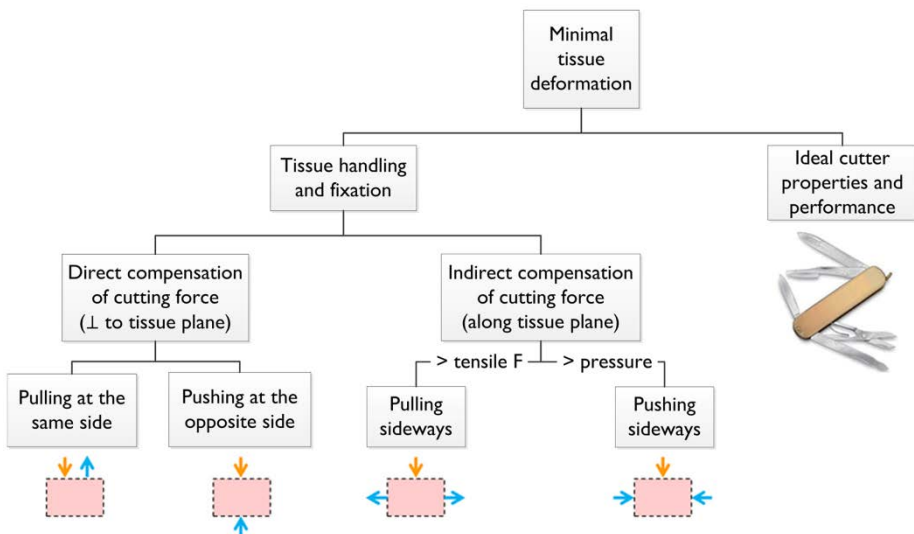


Figure 3.3 The means of achieving minimal tissue deformation during frontal tissue penetration (compensation force, upward & sideways arrows, is described relative to the cutting force vector, downward arrows).

tissue surface, thus increasing the tissue's surface tension, which would ameliorate the cutting process. Alternatively, indirect compensation could also involve a pushing action parallel to the tissue surface, thus increasing the tissue's inner pressure, helping to make it more stable for the cutter penetration.

Nevertheless, from the design point of view, such tissue handling and fixation would most likely require auxiliary features in the laparoscope's tip, such as hooks or adhesives. On the other hand, the invasive tissue-tip interaction prior to the actual cutting operation could result in an undesired bias in the diagnostic readings – due to an impeded blood flow for instance. Such additional auxiliary features would also result in higher design complexity or even design infeasibility, given the limited dimensions.

In order to simplify the method of achieving minimal tissue deformation as well as the laparoscope's tip design, a different approach would be required. Such approach would be to devise an idealised cutter capable of an effortless penetration at a minimal tissue deformation, solely thanks to its clever design with no use of auxiliary features. Thus, design simplicity and robustness could be achieved while preventing any biasing tissue manipulation prior to the optical biopsy.

3.1.5 Objective – Design Requirements

The aim of this project was to design a simple novel laparoscopic instrument tip of dimensions typical of a regular laparoscopic forceps, i.e. \varnothing 5mm and 20-40mm length [21]. Such a tip has to provide a central unimpeded \varnothing 2mm lumen for a glass-fibre bundle for the optical analysis of superficial tissue properties. The optical analysis feature has to be supplemented with a compact frontally acting cutting device for fast, accurate and reliably controlled mechanical biopsy of the analysed superficial tissue. The biopsy sample of a precisely defined tissue volume will also be kept and transported in an embedded sample storage container for further pathological analysis.

3.2 Methods – Experimental Prototype Development

3.2.1 Design Inspiration and Cutting Principle

In pursuit of developing an ideal biopsy device, one might wonder how to combine a perfect tissue incision with biopsy retrieval in a single tool or procedure. Since accurate laparoscopic frontally-acting biopsy harvesters of peripheral tissue do not yet exist, at TU Delft we decided to search for an inspiration in similar approaches in nature. Therefore, we took a closer look at the sea urchin's clever chewing organ, Aristotle's lantern (Fig. 3.4 left) [22].

Aristotle's lantern is a relatively large and featureful structure, around 15mm in height and diameter, consisting of five larger bones ending in a beak with five small pointy teeth and it is actuated by a complex network of muscle tendons located within the sea urchin's bulky exoskeleton. The beak bites through and encompasses even a very tough material, e.g. corals, by pressing the mutually fitting teeth together by axial

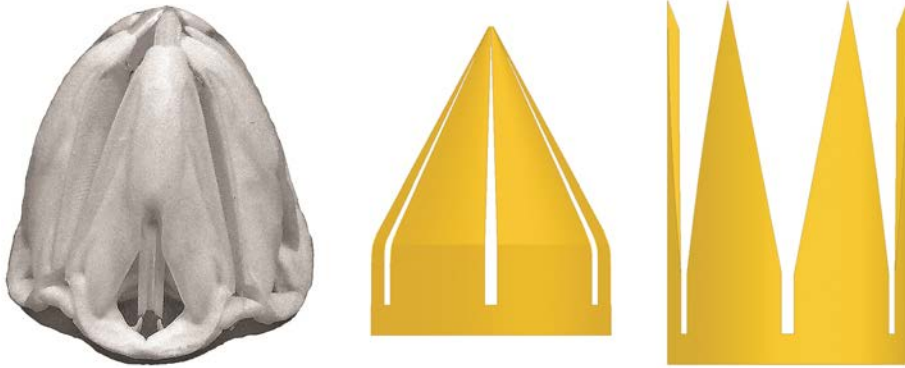


Figure 3.4 Sea urchin's chewing organ, Aristotle's lantern – left, providing an inspiration to the biopsy harvester's crown-shaped collapsible cutter (collapsed – centre, at rest – right).

translation, due to the basal attachment of the muscle tendons [22, 23]. More specifically, Aristotle's lantern is open when protruding outwards and closed when retracted inwards. As demonstrated by Giorgio Scarpa's bionic model of Aristotle's lantern [24, 25], by this means, the sea urchin can simultaneously cut off and enclose its food in a seemingly unified and continuous motion. The capability of the simultaneous tissue incision and enclosure by axial translation exactly fits the envisioned biopsy harvester's functionality needs. This is due to the fact that the arising opportunity for a close succession of the optical and the mechanical biopsies could lead to an enhanced accuracy of the analysed and sampled tissue.

3.2.2 Cutting and Harvesting Mechanism

Building on this principle, yet restrained by the limited laparoscopic tip dimensions, a round crown-shaped collapsible cutter was designed (Fig. 3.4 right) physically resembling Aristotle's lantern and enabling simultaneous tissue incision and enclosure. Since any hinged features would likely lack sturdiness at this scale, not to mention their manufacturing feasibility, the cutter had to be designed thin enough as to allow the collapsibility of the blades and thus the enclosure of the sampled tissue. Six symmetrical blades were chosen as optimal both for manufacturing feasibility and for creating a seemingly straight blade cross-section for easy inward bending, while keeping the blade profiles wide and strong enough to prevent outward bending when retracted.

3.2.3 Propulsion – Pilot Cutter Experiments

The sea urchin's beak geometry and working principle were recognised as essential for the envisioned biopsy harvester, combining frontal cutting with tissue encompassing. However, together with its muscle and tendon actuators, it is difficult to replicate in a miniature and simple form. Therefore, it has been decided to modify the crown-cutter's operation such that it would close automatically by forward propulsion. Furthermore, to

gain further insight and inspiration on the means of the cutter actuation, an *in vitro* experiment was performed in the Tensile Testing Lab of our department. Its goal was to find out what forces such a cutter encounters during tissue penetration and to test its cutting capabilities. The crown-cutter was mounted in a clamp (Fig. 3.5 left) attached to a 1kN load cell of a tensile tester Zwick/Roell Z005 (TÜV Nord AG, Hanover, Germany) and pushed vertically downwards into a single piece of chicken liver placed freely on a platform. This test was performed repeatedly at different locations on the liver. During the push-in tests, the forces exerted on the cutter were plotted against the increasing penetration depth at a sampling rate of 10Hz and at push-in speeds: 6, 12, 24 and 48mm/s. The same protocol was followed with the cutting experiments performed on a single piece of chicken breast. The collapsing motion of the cutter blades was not yet taken into account in this experiment, i.e. the cutter stayed open.

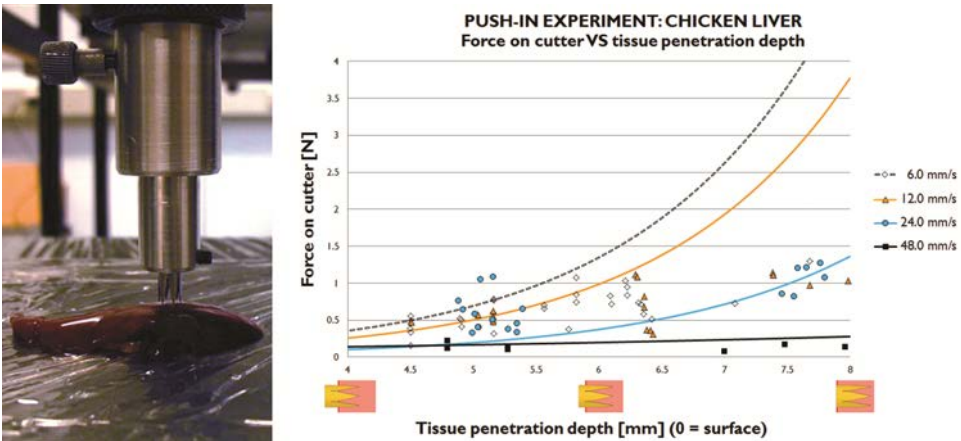


Figure 3.5 Close-up of the pilot test set-up, left, and the results of the *in vitro* push-in tests, right, performed with the crown-cutter on a chicken liver at push-in speeds 6, 12, 24 and 48mm/s. For clarity, the data is presented from the penetration depth of 4mm onwards and they are fitted with exponential curves for easy comparison.

The data from numerous push-in trials on chicken liver is plotted at every speed (10 trials per speed) and fitted with exponential curves for clear comparison (Fig. 3.5 right). Based on these force measurements it was determined that the higher the push-in speed was, the lower the forces on the cutter or tissue were. It was also observed that at higher speeds the cutter penetrated the tissue effortlessly and with less visible tissue deformation, thus presumably leading to a more accurate biopsy. Compared to the chicken liver trials, the experiments with the chicken breast showed only a slight increase in the exerted forces on the tissue/cutter, yet the push-in speed increase showed the same trend (hence not shown). It was therefore concluded that a plausible approach to a precise and accurate biopsy is high-speed cutting. Hence, we decided on the cutter's forward propulsion via a fast and strong compression spring.

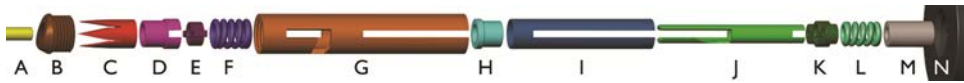


Figure 3.6 Exploded view of the spring-loaded biopsy harvester design with its 14 components (A-N), showing their mutual axial alignment.

3.2.4 Experimental Biopsy Harvester Design

The concept of a crown-shaped collapsible cutter propelled by a compression spring with an embedded glass-fibre bundle was determined. The next challenge was to incorporate these founding features into a laparoscope's tip design, which would also comprise a smart mechanism for cutter preloading, locking and actuation. As the purpose of this prototype design was to test the cutter's functionality and feasibility, the biopsy harvester was initially designed without a removable container for sample transport.

The finalised prototype design, illustrated in Fig. 3.6, contains a collapsible crown-cutter (C, D, E) that sits on a compression spring (F), with a tubular, \varnothing 6mm and 30mm long outer shell (G) positioned around them. The tip accommodates an internally tapered screw-on cap (B) which serves to collapse the cutter blades into a cone-shaped sample storage container when pushed forwards through the tissue. Thus, a maximum biopsy volume and penetration depth are maintained, as they are defined solely by the angle of the internal taper and the cutter's geometry. The design furthermore features a central \varnothing 2mm inner channel, suited for accommodating a glass-fibre bundle (A) and a smart mechanism for cutter preloading, locking and actuation. Due to the small working space confined in between the \varnothing 2mm central channel and the \varnothing 4.5mm inner diameter of the outer shell, the tip comprises a compact sandwich construction of several tubular parts that slide over each other and operate the crown-cutter. A short-pinned sleeve (E) runs in a slot in the outer shell (G) which is shaped as a letter "J" in order to enable fast and easy cutter loading and locking. The compression spring is released by pulling a long inner sleeve (J) with a specially angled guiding slot. The angled slot translates the sleeve's pulling motion into a rotational motion of the pinned sleeve (E), turning the pins into the straight part of the J-shaped slot and rapidly releasing the spring from the compressed state.

The long inner sleeve (J) is fused with a short sleeve (K) featuring two round protrusions with holes. Bowden cables run through these holes with their outer coils pushing at the short sleeve (K) protrusions and their inner wires anchored in the base (N) (Fig. 3.9 left). By this means, the cutter can be actuated remotely by pulling the components (J) and (K) towards the base (N).

3.2.5 Experimental Biopsy Harvester Prototype

The experimental biopsy harvester prototype (Fig. 3.7) was manufactured from stainless steel and mounted to an aluminium base suited for clamping in a tensile testing machine. The axisymmetric six-blade crown-cutter was electric discharge

machined (EDM) from a thin extruded steel tube \varnothing 4.3x0.15mm and equipped with a 20° inner bevel. All other components were machined via regular means of milling and turning, with the exception of several symmetrical slots and protrusions that had to be machined by the EDM as well. Components (J) and (K) were fused by the means of a heat treated permanent metal glue.

3.2.6 Experimental Set-up for Feasibility Tests

The experimental biopsy harvester prototype was firstly trialed and observed in free space in order to investigate the mechanism functionality in general. This was supplemented by a footage of the cutter closure in free space taken by a high-speed camera Fastcam Ultima APX-RS (Photron USA Inc., San Diego, CA) at 30,000fps.

For the purposes of the *in vitro* feasibility tests, the biopsy harvester was mounted on a 1kN load cell of the tensile tester Zwick/Roell Z005 (TÜV Nord AG, Hanover, Germany) and tested on a single piece of chicken liver placed freely on a platform. The biopsy harvester was firstly brought as close to the tissue as possible, making a gentle tissue contact with its tip. This was followed by the rapid incision operation remotely actuated by the Bowden cables and performed repeatedly at 20 different locations on the liver. The cutting process was recorded at a sampling rate of 100kHz with respect to the measured force on tissue/cutter over time.

Last but not least, to verify the cutting consistency, the 20 biopsy samples were weighed on Scaltec analytical balance SBC 33 (Denver Instrument GmbH, Göttingen, Germany).



Figure 3.7 Assembled biopsy harvester prototype manufactured nearly at real-scale, \varnothing 6mm, (top) also showing a fully closed crown-cutter (inset). Intermediate assembly (bottom) shows the outer shell, the assembled inner working mechanism and the glass-fibre dummy.

3.3 Results

3.3.1 General Prototype Functionality

The cutter preloading, locking and actuation mechanism proved to work successfully and continues to function even after daily demonstrations, with no visible signs of plastic deformation or material fatigue. As shown by inset in Fig. 3.7, the crown-cutter closes seamlessly, hence capable of extracting an almost perfectly conical biopsy volume of about 9mm^3 at most (estimated from geometry); this equates to $9.8\mu\text{g}$ of liver tissue at the liver density of approximately 1090kg/m^3 [26]. As observed from a sequence of snapshots (Fig. 3.8) the spring shoots the crown-cutter from open to closed position in 0.8ms. At the cutter's axial travel of 4.4mm, this equates to the cutting speed of 5.5m/s.

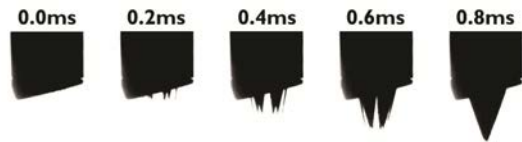


Figure 3.8 High-speed camera snapshots of the rapid cutting process performed in 0.8ms.

3.3.2 Prototype's Cutting Performance and Feasibility Test

Using the experimental set-up for feasibility tests (Fig. 3.9 left) discussed previously, a plot of force on cutter against the cutting time was generated (Fig. 3.9 right). The readings indicate that only during the first 0.5ms of the cutting operation measurable forces can be registered – their maxima being in the range of just 0.23 – 0.37N. As demonstrated in Fig. 3.10, the cutter managed to perform successful biopsies, rapidly sampling and storing conical tissue volumes while leaving clean round cuts as desired. Based on a pure observation, the 20 extracted liver samples were roughly consistent in terms of geometry and volume. Their further weighing revealed an average sample mass of $3.1 \pm 0.4\mu\text{g}$.

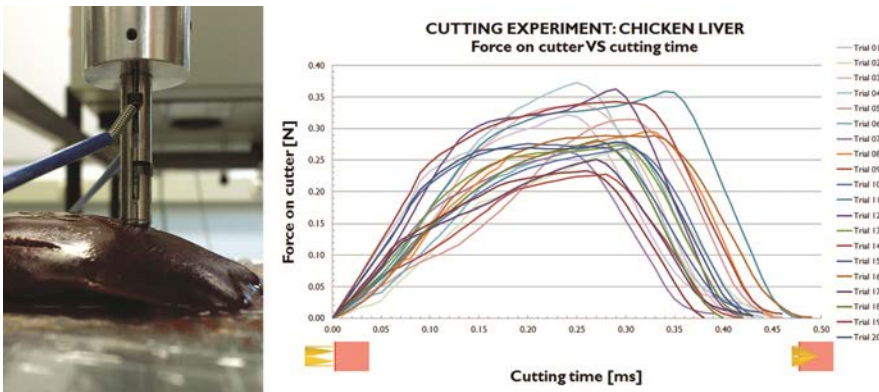


Figure 3.9 Close-up of the Bowden cable driven biopsy harvester testing set-up, left, and the results of the in vitro cutting tests on a chicken liver, right, illustrating the forces exerted on the cutter during the rapid cutting process.

3.4 Discussion

3.4.1 Biopsy Harvester Highlights and Limitations

The experimental prototype of our novel bio-inspired opto-mechanical biopsy harvester proved to work successfully. The success was demonstrated by the cutter's incising and collapsing capabilities enabling rapid sampling of chicken liver tissue of conical volume *in vitro*, while operating at low friction. The experimental prototype tests also showed repeatable flawless mechanical operation of the preloading, locking and actuation mechanism. The desired functionality was achieved despite the amount of numerous miniature components – many of them on the verge of manufacturability.

The crown-cutter design proved to exert minimal forces on tissue during the rapid cutting process, barely reaching 0.4N at the speed of 5.5m/s. For the sake of comparison, a generic core needle biopsy gun operates at 30m/s [9]. At the same time the cutting process managed to deliver roughly constant results, both in terms of tissue sample shapes and sizes, with a standard deviation of the sample mass of only $\pm 13\%$. As revealed from the high-speed footage, the cutter takes 0.8ms to fully close, even though the force plots indicate measurable forces only during the first 0.5ms. A plausible explanation is that as the cutter closes and becomes a pointy cone, the surrounding tissue is no longer pushed away along the cutter's motion vector, but rather sideways as it is ripped apart. Hence, no measurable force is registered during the last 0.3ms of the cutting process, during which the cutter closes completely, sealing off the biopsy sample from the rest of the tissue.

Despite the successful sample retrieval and a visually seamless closure of the cutter blades, the liver tissue did not appear to be perfectly separated just by the cutting process itself. However, the full sample separation was effortlessly achieved immediately upon retracting the biopsy harvester from the site, thus breaking off the miniscule remaining connecting tissue. It was in fact observed that, since the EDM process easily melts very thin metal features, it caused the blades' tips to be mutually slightly unequal, introducing a modest clearance at the very tip of a closed conical cutter. Hence, sharpening would have to be performed separately, by turning for instance. This could explain the relatively smaller average sample size of approximately 32% of the maximum theoretically extracted biopsy volume of 9mm³. Nevertheless, both the perfect tissue separation and the sample volume maximisation could be supposedly achieved by optimising the cutter's blade bevel.

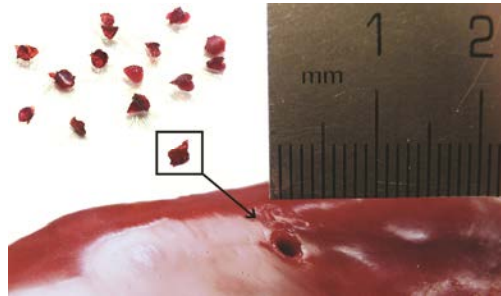


Figure 3.10 Clean-cut conical biopsies of a chicken liver made with the bio-inspired biopsy harvester.

3.4.2 Future Work – Envisioned Instrument

As suggested, the next step would be a series of *in vitro* evaluations carried out on animal tissues with the objective of optimising the cutter's incising and retrieving capabilities. More specifically, the research goals will involve optimising the crown-cutter's blade bevel with regard to further minimising the tissue deformation, maximising the retrieved tissue volume as well as achieving a perfect separation of the sampled volume from the tissue site just by the cutting process itself.

Further design modifications and division of the tip into a permanent and a disposable segment will enable taking of multiple biopsies, mutually separated in individual storage containers, suited for accurate and efficient pathological analysis. For surgical purposes, the individual segments will further have to be enclosed or sealed, so that no potential tissue entrapment could occur due to the slots or the protrusions.

The real-scale criterion of \emptyset 5mm was not yet fulfilled due to the removability feature of the screw-on cap requiring a thicker outer shell for thread. The cap in the final instrument would be permanently glued, soldered or spot-welded to the outer shell, hence allowing it to be much thinner. In the end, the final real-scale \emptyset 5mm partitioned device will be evaluated *in vivo* on small and large animals.

3.5 Conclusions

A \emptyset 6mm bio-inspired opto-mechanical biopsy harvester prototype was developed and tested *in vitro* on chicken liver using a universal tensile testing machine. In terms of mechanical functionality, the preloading, locking and actuation mechanism as well as the cutter's rapid incising and collapsing capabilities proved to work successfully. The embedded crown-cutter enables rapid tissue incision and enclosure, highly accurate with regard to the preceding optical biopsy. The biopsy harvester features a \emptyset 2mm lumen either for the purposes of the optical tissue analysis or for expanding its capabilities, e.g. flushing/suction channel or micro-grasper. Further division of the tip into a permanent and a disposable segment will enable sampling multiple biopsies, mutually separated in individual containers. Once mounted on top of a laparoscopic instrument, the envisioned opto-mechanical biopsy harvester would provide an accurate, efficient and comfortable solution towards ameliorating time demanding, inaccurate and potentially unsafe laparoscopic biopsy procedures with regard to peripheral tissue sampling.

Acknowledgements

This research was performed within the framework of CTMM, the Center for Translational Molecular Medicine, project MUSIS (grant 030-202). Many thanks to TU Delft's fine mechanical workshop DEMO for their support and elaborate work on the biopsy harvester prototype.

References

- [1] Braga, M., Vignali, A., Gianotti, L., Zuliani, W., Radaelli, G., Gruarin, P., Dellabona, P., and Carlo, V. D., 2002, "Laparoscopic Versus Open Colorectal Surgery: A Randomized Trial on Short-Term Outcome," *Ann Surg*, 236(6), pp. 759–767.
- [2] Breedveld, P., Stassen, H. G., Meijer, D. W., and Jakimowicz, J. J., 1999, "Manipulation in laparoscopic surgery: Overview of impeding effects and supporting aids," *J Laparoendosc Adv Surg Tech A*, 9(6), pp. 469–480.
- [3] Khorjastan, S. M., Najarian, S., Simforoosh, N., and Farkoush, S. H., 2010, "Design and Modeling of a Novel Flexible Surgical Instrument Applicable in Minimally Invasive Surgery," *Int J Nat Eng Sci*, 4(1), pp. 53–60.
- [4] Minor, M., and Mukherjee, R., 1999, "A Mechanism for Dexterous End-Effector Placement During Minimally Invasive Surgery," *J Mech Des*, 121(4), pp. 472–479.
- [5] Velanovich, V., 2000, "Laparoscopic vs open surgery," *Surg Endosc*, 14(1), pp. 16–21.
- [6] Breedveld, P., 2010, "Steerable Laparoscopic Cable-Ring Forceps," *J Med Device*, 4(2), p. 027518.
- [7] Mayhew, P., 2009, "Surgical views: techniques for laparoscopic and laparoscopic assisted biopsy of abdominal organs," *Compend Contin Educ Vet*, 31(4), pp. 170–176.
- [8] MayoClinic.com, 2013, "Mayo Clinic medical information and tools for healthy living," <http://www.mayoclinic.com/health/medical/>.
- [9] Cerwenka, H., Hoff, M., Rosanelli, G., Hauser, H., Thalhammer, M., Smola, M. G., and Klimpfinger, M., 1997, "Experience with a high speed biopsy gun in breast cancer diagnosis," *Eur J Surg Oncol*, 23(3), pp. 206–207.
- [10] Layfield, L. J., 1995, "Fine needle aspiration of the breast: review of the technique and a comparison with excisional biopsy," *Curr Diagn Pathol*, 2(3), pp. 138–145.
- [11] Heijnsdijk, E. A. M., Visser, H., Dankelman, J., and Gouma, D. J., 2004, "Slip and damage properties of jaws of laparoscopic graspers," *Surg Endosc*, 18(6), pp. 974–979.
- [12] Provenzale, D., and Onken, J., 2001, "Surveillance issues in inflammatory bowel disease: ulcerative colitis," *J Clin Gastroenterol*, 32(2), pp. 99–105.
- [13] Wallace, J. E., Saylor, C., McDowell, N. G., and Stephens Moseley, H., 1996, "The role of stereotactic biopsy in assessment of nonpalpable breast lesions," *Am J Surg*, 171(5), pp. 471–473.
- [14] Wang, T. D., and Van Dam, J., 2004, "Optical biopsy: a new frontier in endoscopic detection and diagnosis," *Clin Gastroenterol Hepatol*, 2(9), pp. 744–753.
- [15] Volpe, A., Kachura, J. R., Geddie, W. R., Evans, A. J., Gharajeh, A., Saravanan, A., and Jewett, M. A. S., 2007, "Techniques, Safety and Accuracy of Sampling of Renal Tumors by Fine Needle Aspiration and Core Biopsy," *J Urol*, 178(2), pp. 379–386.
- [16] Amelink, A., Kok, D. J., Sterenborg, H. J. C. M., and Scheepe, J. R., 2011, "In vivo measurement of bladder wall oxygen saturation using optical spectroscopy," *J Biophotonics*, 4(10), pp. 715–720.
- [17] Lacombe, F., Hughett, D., Tihansky, C., and Genet, M., "Multi-Purpose Biopsy Forceps," Mauna Kea Technologies, US Patent 2010/0168610, July 1, 2010.
- [18] Sharon, A., Singh, S., Bigio, I., Atladottir, S., Foss, D., and Vogtel, P., "Low Cost Disposable Medical Forceps to Enable a Hollow Central Channel for Various Functionalities," Trustees of Boston University, Boston Medical Center Corp., Fraunhofer USA, Inc., WO Patent 2009/111717, September 11, 2009.
- [19] Whitehead, P. D., MacAulay, C. E., MacKinnon, N. B., and Zeng, H., "Catheters and Endoscopes Comprising Optical Probes and Bioptomes and Methods of Using the Same," Biomax Technologies, Inc., WO Patent 98/40015, September 17, 1998.
- [20] Komachiya, M., Fumino, T., Sakaguchi, T., and Watanabe, S., 1999, "Design of a sensing glass fiber with specific refractive-index composition for a system with 1.3 μm wavelength light source," *Sens Actuators A Phys*, 78(2–3), pp. 172–179.
- [21] Aesculap, 2010, "Laparoscopic Instruments - Product Catalog," http://www.aesculapusa.com/assets/base/doc/DOC465_REV_F_Laparoscopic_Catalog.pdf.
- [22] Candia Carnevali, M. D., Wilkie, I. C., Lucca, E., Andrietti, F., and Melone, G., 1993, "The Aristotle's lantern of the sea-urchin *Stylocidaris affinis* (Echinoida, Cidaridae): functional morphology of the musculo-skeletal system," *Zoomorphology*, 113(3), pp. 173–189.
- [23] Dolmatov, I., Mashanov, V., and Zueva, O., 2007, "Derivation of muscles of the Aristotle's lantern from coelomic epithelia," *Cell Tissue Res*, 327(2), pp. 371–384.
- [24] Scarpa, G., 1985, *Modelli di bionica. Capire la natura attraverso i modelli*, V. Rossi, ed., Nicola Zanichelli Editore S.p.A., Bologna, pp. 13–74.
- [25] Trogu, P., 2013, "Giorgio Scarpa - Bionic Models and Rotational Geometry Models," San Francisco State University, San Francisco, CA, http://online.sfsu.edu/trogu/scarpa/movies/scarpa_bionics.mov.
- [26] Sturesson, C., and Andersson-Engels, S., 1995, "A mathematical model for predicting the temperature distribution in laser-induced hyperthermia. Experimental evaluation and applications," *Phys Med Biol*, 40(12), p. 2037.

Chapter 4

Bio-Inspired Crown-Cutter

The Impact of Tooth Quantity and Bevel Type
on Tissue Deformation, Penetration Forces
and Tooth Collapsibility

Filip Jelínek, Jeffrey Goderie, Alice van Rixel, Daan Stam, Johan Zenhorst
and Paul Breedveld

Published in Journal of Medical Devices 8(4), 2014.

Abstract

Introduction | Current keyhole biopsy devices are rather ungainly, inaccurate and limited in application. A keyhole biopsy harvester was designed to facilitate peripheral cancerous tissue detection and resection at high speed and accuracy. The harvester's cutting tool, the crown-cutter, was bio-inspired by the sea urchin's chewing organ – Aristotle's lantern. This paper focuses on the optimisation of the crown-cutter with regard to the impact of different tooth quantity and bevel type on tissue deformation, penetration forces and tooth collapsibility.

Methods | Two sets of crown-cutter designs were manufactured and tested in push-in experiments using gelatine – the first set having no bevel and differing tooth quantity (4, 6, 8, 10 teeth) and the second set of constant tooth quantity and differing bevel type (no, inner, outer and inner & outer bevel). The gelatine surface deformation and the penetration forces were evaluated utilising a high-speed camera and a universal testing machine respectively.

Results and Conclusions | The experimental results on the crown-cutters of different tooth quantity (no bevel) showed a steady increase in the tissue deformation with the increasing amount of teeth. Unlike the bevel type, the different tooth quantity revealed significant differences with regard to the tissue deformation in between 4 versus 6-teeth and 10 versus 6-teeth cutters. As for the penetration forces, the significant difference was found only between 10 and 6-teeth cutters. In conclusion, reducing the cutter's tooth quantity resulted in lower tissue deformation, whereas differing the bevel type was found to have a negligible influence. Ultimately, a high ratio of outward to inward tooth collapsibility and a relatively low inner moment of inertia proved the 6-teeth cutter to be the most optimal.

4.1 Introduction

4.1.2 Keyhole Surgery and Biopsy

Keyhole surgery, also called minimally invasive surgery, is a modern trend within the surgical domain requiring only small incisions in the patient's skin. This leads to considerable benefits for the patients, which include shorter hospital stay, shorter recovery time and less postoperative scar tissue in comparison with regular open surgery [1-5]. Yet, due to the limited site access, the traditional surgical instruments for the open surgery cannot be used. Hence, specialised long and slender, usually \varnothing 5mm, keyhole instruments have been developed. The keyhole endoscopes and instruments provide the surgeon with either a visual feedback or tissue manipulation features.

Related to the minimally invasive context, biopsy is a medical test used within the field of pathology, whose aim is to study and better understand the nature and the properties of diseased tissue. During biopsy, tissue samples are removed from the patient's body with the aid of minimally invasive biopsy instruments and they are subsequently sent to pathologists for analysis. The most common biopsy techniques include fine-needle aspiration (Fig. 4.1(a)) [6, 7] that employs a syringe with a very thin needle that can quickly sample a limited amount of tissue on a cellular level from deep within the body and organs. Further techniques include core needle biopsy (Fig. 4.1(b)) [6, 7], which is capable of extracting a much larger cylindrical tissue sample using a so-called core needle, even from much tougher tissues, such as a bone. Lastly, a third biopsy technique, which is slightly more invasive and cumbersome, is a so-called punch biopsy (Fig. 4.1(c)) [6, 7]. This technique uses sharp tubular knives named punches or much longer trephines for sampling the surface of skin or bones, respectively. Yet, once cutting is complete, the task sometimes needs some assistance in the form of a grasping device, such as tweezers or a keyhole forceps, in order to help retrieve the sampled tissue.

Although most of these biopsy techniques can be used in the keyhole surgery, they generally suffer from geometrical and operational limitations, impeding their usage versatility [8, 9]. To illustrate, the biopsy needles used for deep tissue biopsy are inappropriate for peripheral tissue sampling. This is due to the fact that needles rely on

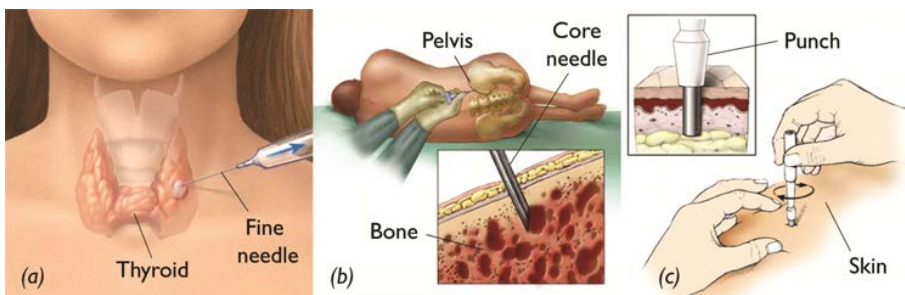


Figure 4.1 Contemporary biopsy techniques including (a) fine-needle aspiration, (b) core needle biopsy and (c) punch biopsy. Adopted from [6, 7].

suction, thus requiring their tips to be fully inserted into and embraced by the tissue to ensure perfect contact. Similarly, the punches or trephines used for peripheral tissue biopsy cannot be used in the keyhole surgery with regard to accuracy and speed. While the operation of biopsy needles is usually fast and automatic, the punches or trephines are required to be manually pressed and spun towards the tissue with considerable force. Thereby, the surgeon can achieve partial sample separation, yet at the expense of elevated time demands and a risk of mislocation. Furthermore, using a regular keyhole forceps or scissors for biopsy can likely result in tissue slip and hence insufficiently accurate tissue sampling with associated risks [10]. The most serious potential hazards include cancer spread when dealing with tumorous tissue [11], which can occur if, for instance, a tumour is accidentally perforated. As a matter of fact, such contamination can easily happen, since, apart from computed tomography or magnetic resonance imaging scans, the surgeon greatly relies on visual cues and palpation when trying to identify the tumour boundaries. This becomes even more critical in the context of the keyhole surgery, as the surgeon's senses are greatly limited.

4 For that reason, so-called optical biopsy techniques [11-13] are under development worldwide, whose aim is to provide the surgeon with non-invasive diagnostic readings identifying the nature of the analysed tissue remotely and in real time without the need for the actual *a priori* physical extraction. Thus, tumour boundaries could be easily identified without the need to resect the tissue and risk the spread of contamination. These tissue imaging techniques usually incorporate an optical fibre bundle as a signal carrier. Nevertheless, once the tissue is identified as tumorous, i.e. likely to be resected, the optical fibre bundle cannot serve as a tissue removal tool and thus the state-of-the-art biopsy devices are used in the attempt to extract the tissue at the analysed site. As outlined before, this may prove rather ungainly and inaccurate, as multiple devices that would be required and exchanged during such a procedure have not been, in simple terms, designed to cooperate. Hence, there is a need for a more reliable alternative in the form of a single keyhole instrument capable of both analysing the tissue optically and taking a precise biopsy at the same desired location.

4.1.3 Keyhole Biopsy Harvester

A \emptyset 5mm keyhole biopsy device incorporating the aforementioned technologies is currently under development at TU Delft and it is named bio-inspired spring-loaded biopsy harvester (Fig. 4.2) [6]. It combines a central lumen for a \emptyset 2mm glass-fibre bundle (for non-invasive optical biopsy) with a compact frontally acting cutting device (for fast, accurate and reliable mechanical biopsy). Such an opto-mechanical biopsy harvester is capable of an instant optical analysis of tissue *in situ* with the opportunity for a precise tissue resection exactly at the analysed site within a matter of seconds. Hence, pathological procedures could be performed without the need for multiple discrete and lengthy operations, i.e. more time effectively and thus supposedly at reduced costs [12]. In addition, the benefit of a \emptyset 2mm central lumen opens the opportunity for a suction channel for the extraction of liquids or solid samples, or for

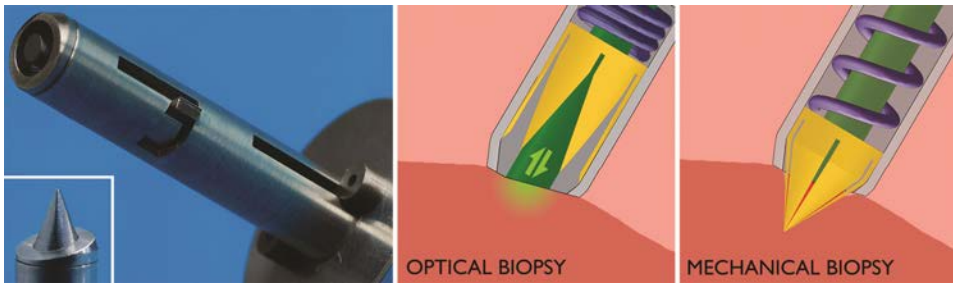


Figure 4.2 Keyhole biopsy harvester [6] and its working principle combining optical and mechanical biopsy.

other auxiliary functions or accessories such as a flushing channel or an articulatable micro-grasper for enhanced tissue manipulation.

4.1.4 Biological Inspiration

Due to the need for an unimpeded \varnothing 2mm central lumen, the harvester's frontally acting cutting device for the extraction of solid samples had to be cleverly designed in order to fit and operate in the limiting tubular geometry of a \varnothing 5mm keyhole instrument. At TU Delft we decided to search for an inspiration for such a design challenge in nature. In particular, we took a closer look at the sea urchin's ingenious chewing organ, Aristotle's lantern (Fig. 4.3(a)) [6, 14-17].

Aristotle's lantern is a relatively large and featureful structure, around 15mm in height and diameter. It is composed of five larger calcareous jaws ending in a beak of small pointy teeth mutually fitting together. The jaws are actuated by a highly complex network of muscle bundles [15] attached to the inner wall of the sea urchin's bulky exoskeleton. The beak bites through and encompasses even a very tough material, e.g. corals and rocks. As clearly demonstrated by the work of Giorgio Scarpa on the bionic model of Aristotle's lantern [15, 16], the chewing organ can simultaneously cut off and enclose its food by axial translation, thus pressing the mutually fitting teeth together. In particular, the lantern is fully open when pushed outwards and closed when retracted into the exoskeleton.

Thanks to its simple unified operation and the arising opportunity for a close succession of the optical and the mechanical biopsies, Aristotle's lantern served as a biological inspiration for the biopsy harvester's cutting device from both the design and the functional point of view.

4.1.5 Crown-Cutter

As far as the design is concerned, the biopsy harvester's cutting device – the crown-cutter (Fig. 4.3(b)) – was devised round and crown-shaped featuring numerous triangular teeth. Since any hinged features would likely lack sturdiness at this scale, not

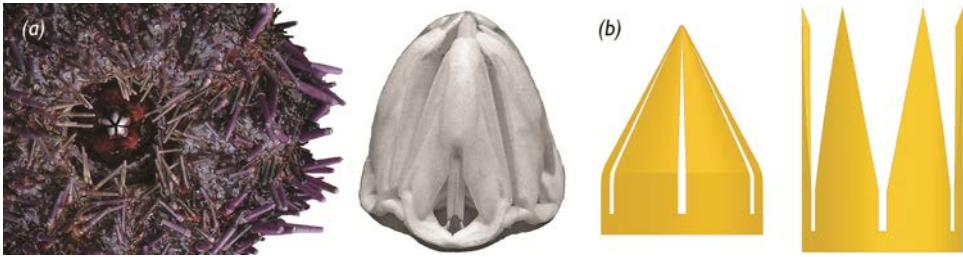


Figure 4.3 Close-up of (a) sea urchin *Echinus esculentus*, adopted from [6, 17], and its chewing organ Aristotle's lantern that served as a biological inspiration for (b) the biopsy harvester's crown-cutter [6].

to mention their manufacturing feasibility, the teeth had to be designed thin enough as to allow their inward collapsibility and thus the enclosure of the sampled tissue.

From the operational viewpoint, similarly to Aristotle's lantern, the crown-cutter combines the axial translation with the inward tooth collapsibility. However, due to the space limitations and complexity of the lantern's anatomy, the crown-cutter's teeth and the surrounding mechanism [6] were designed such that they close automatically by forward propulsion. The closure is achieved by forcing the crown-cutter towards an inner taper of the biopsy harvester's cap and the forward propulsion is provided by a strong compression spring situated behind the crown-cutter (Fig. 4.2).

The development of the crown-cutter's design was guided not only by its operational requirements, but also by the manufacturing limitations. In order to ensure effortless tissue penetration and proper cutter closure, the original cutter was made from the thinnest acquirable stainless steel tube. The number of teeth was chosen as even in order to achieve symmetry as required by the manufacturing method, the electric discharge machining (EDM). Initially, six symmetrical teeth were selected as ideal for creating a seemingly straight tooth cross-section for easy inward bending, while keeping the tooth profiles wide and strong enough to prevent outward bending when retracted. The tooth tips were sharpened by giving them an inner bevel of 20° . The inner bevel would supposedly enable both easier tissue penetration and tighter mutual fit of the teeth when collapsed inwards.

4.1.6 Problem Statement

Despite being fully functional, as demonstrated in inset of Fig. 4.2, the crown-cutter's design has not been optimised with regard to its interaction with tissue and tooth collapsibility. Therefore, with the vision of achieving and justifying the best performing crown-cutter, the aim of this project was to optimise its design, so that it requires minimal penetration forces, induces minimal tissue deformation and ensures proper tooth collapsibility.

4.2 Methods

4.2.1 Design Optimisation Variables

The crown-cutter design optimisation was approached by varying the number of cutting teeth (with constant inter-tooth gap) and the bevel type of their very tips, as detailed in Fig. 4.4.

As indicated before, the EDM process has its limits that also include melting of very thin features, e.g. sharpened blade bevel. Hence, for the sake of design integrity and objective performance comparison, the crown-cutters of different designs were manufactured at twice the original scale, i.e. from a $\varnothing 9 \times 0.5$ mm stainless steel tube, assuming that the relative cutter performance would be similar at both scales.

It was also assumed, based on common sense, that the deformation of the tissue and the penetration forces would reduce by increasing the amount of contact points, i.e. the number of teeth. The reasoning being that more contact points could build up surface tension faster, thus speeding up the penetration. Hence, the first set of

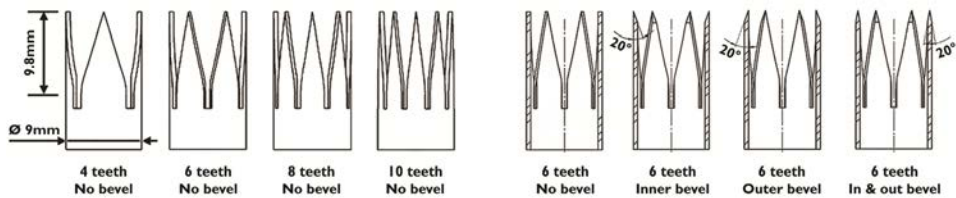


Figure 4.4 Cutter designs of different tooth quantity (4, 6, 8 and 10 teeth with no bevel) and different bevel type (no, inner, outer and inner & outer bevel on cutters with 6 teeth).

experiments was used to compare the crown-cutters of different tooth quantity as described before. The cutters of 4, 6, 8 and 10 teeth (no bevel) were used (Fig. 4.4). Once again, the even number of teeth was chosen to achieve symmetry, needed for the EDM process.

Furthermore, it was expected that an outside cutting bevel should lead to lower tissue deformation and lower penetration forces. A study on knife cutting performance by Marsot et al. revealed that it is preferred to use bevelled blades for reducing the cutting force [18]. Furthermore, Cao et al. claimed that a rotating core cutter with an outside bevel yields the lowest penetration force [19]. However, it should be noted that during this crown-cutter study the cutters did not rotate.

Therefore, the second set of experiments was used to compare the crown-cutters of different bevel type, yet of a constant bevel angle of 20° each. For simplicity, the tooth quantity was also kept constant at 6 teeth. An unsharpened 6-teeth cutter (no bevel) was used as a reference for the evaluation of the 6-teeth cutters with bevels on the inside, outside and both sides (Fig. 4.4).

4.2.2 Tooth Quantity and Bevel Type Experiments

The crown-cutters of different tooth quantity and bevel type were evaluated separately in simple push-in tests using the experimental set-up shown in Fig. 4.5, left. For all the experiments, a Zwick/Roell Z005 (TÜV Nord AG, Hanover, Germany) universal testing machine (4) was used. An aluminium base plate (1) was bolted to the tensile tester, featuring a slot for Perspex containers (3) of perfectly straight and uniform walls.

The containers were half-filled with gelatine (5wt% gelatine powder, 95wt% water) that was prepared according to a widely used freezing and thawing formula for creating ballistic gelatine. The 5wt% gelatine concentration was used to roughly simulate the properties of a stiff human liver [20]. Nevertheless, rather than mimicking the exact behaviour of the liver tissue, the goal was to provide a reliable experimental medium of relatively constant material properties, thereby attaining objectivity. In total, four containers were used to provide enough experimental material for the scope of these experiments. The gelatine was assumed to be isotropic within one as well as among all the containers, since it was made by the same preparation procedure every time.

The crown-cutters (5) were secured in a mount (6) on top of a 1kN tensile tester load cell and initially positioned 3mm above the gelatine surface (Fig. 4.5, middle). After positioning the crown-cutters, they were set up to travel vertically downwards at 30mm/s, penetrating the gelatine and stopping at 15mm from their initial position (Fig. 4.5, right). This way it was ensured that the cutters' teeth penetrated the gelatine fully. The actual biopsy harvester operates at a much higher speed of 5.5m/s; however, due to the limitations of the tensile tester, the speed had to be lowered to 30mm/s. Similarly, even though the original crown-cutter collapses into a cone while moving forwards (Fig. 4.2, inset), the collapsing motion of the upscaled crown-cutters was not introduced or tested. Hence, the tested crown-cutters performed downward translation only, in order to easily visualise and compare their interaction with the gelatine.

While penetrating the gelatine with the crown-cutter, the tensile tester measured the force on tissue/cutter [N] and the travel of the machine head [mm] at a sample rate of 100Hz. In each of the four containers, four push-in tests of each crown-cutter type were performed. The testing order was randomised to account for any possible temperature fluctuation influence.

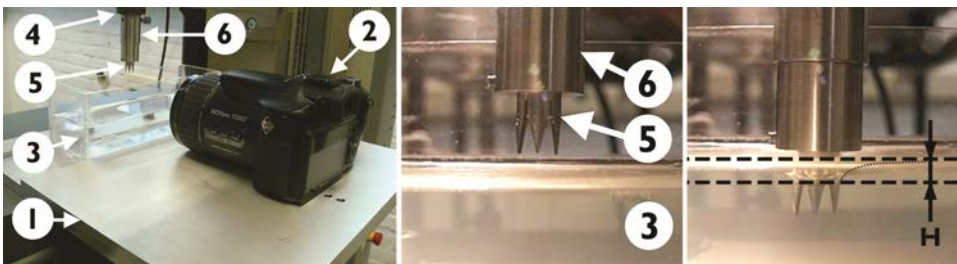


Figure 4.5 Experimental set-up and the cutter's initial and final positions indicating the maximum gelatine deformation H .

In addition, a Casio EX-F1 high-speed camera (2) was used to film the deformation of the gelatine at 300fps. The camera was mounted on top of the base plate and placed parallel to the container wall (50mm apart) with the focal point on the intersection of the gelatine surface and the location of cutter penetration. The maximum gelatine deformation values (H in Fig. 4.5, right) were measured from the high-speed footage for all the cutters. As indicated by the curved dotted line in Fig. 4.5, right, the gelatine deformation was measured from the point where it started to detach from the cutter's outer surface, up to the point where the gelatine's surface turned completely horizontal.

4.2.3 Tooth Collapsibility Calculations

The tooth collapsibility of various crown-cutter designs was not evaluated empirically due to the relatively straightforward nature of the tooth geometry. Instead, numerical analysis was performed to approximate the ease of inward and outward tooth collapsibility with respect to the tooth quantity. Since bending motion is involved, the ease of tooth collapsibility can be numerically expressed as a moment of inertia of a maximum tooth cross-section

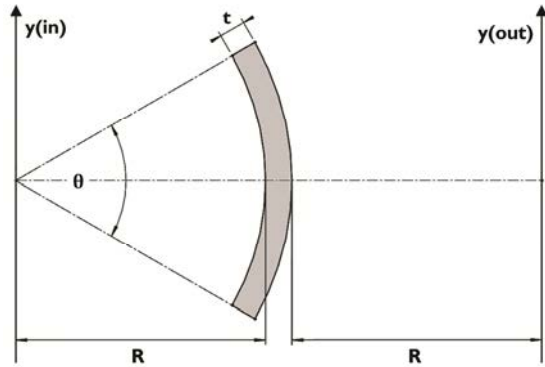


Figure 4.6 Generic tooth cross-section of radius R , shell thickness t and central angle θ . Moment of inertia of the tooth cross-section is evaluated about axes $y(in)$ and $y(out)$ for inward and outward bend respectively.

about an inner or an outer axis (Fig. 4.6). In other words, the lower the moment of inertia, the easier the tooth collapsibility and vice versa.

For evaluating the inward tooth collapsibility, the moment of inertia $I_{y(in)}$ of an annular sector ($R = 4\text{mm}$, $\theta = 2\pi/n$, $t = 0.5\text{mm}$) about an inner axis $y(in)$ can be calculated using Eq. (4.1) [21], where n is the number of teeth of a given crown-cutter configuration. For the outer tooth collapsibility, the moment of inertia $I_{y(out)}$ was determined about an outer axis $y(out)$, displaced equally from the tooth cross-section as $y(in)$ by the distance R . Yet, for the sake of effortless evaluation the moment of inertia about $y(out)$ was determined with the aid of SolidWorks.

$$I_{y(in)} = \frac{1}{8} \times (\theta + \sin \theta) \times [(R + t)^4 - R^4] \quad (4.1)$$

4.3 Results

4.3.1 Impact of Tooth Quantity

The maximum tissue deformation values for the \emptyset 9mm crown-cutters of different tooth quantity are presented in Fig. 4.7(a). The deformation values were determined at the point when the cutter penetrated to 9.8mm depth, as that would theoretically be the maximum penetration depth if used in an upscaled biopsy harvester (for reference, see Fig. 4.4).

The results show an increasing tissue deformation with the increasing tooth quantity, contrary to the expectations. Analysis of variance (ANOVA) test combined with post-hoc Tukey HSD test revealed that the difference between the majority of the cutters is significant ($p < 0.05$), except for the 6 versus 8-teeth cutter.

The mean penetration forces (and standard deviations) of the crown-cutters of different tooth quantity are plotted in Fig. 4.7(b), up to 9.6mm penetration depth (due to incompleteness of data at penetration depth >9.6 mm).

The mean penetration force differences, when the cutter penetrated (travelled) 9.6mm, of the 4, 8 and 10-teeth cutters versus the 6-teeth cutter are -0.002 N, 0.062 N and 0.196 N, respectively. This is equal to -0.144% , 4.454% and 14.080% difference from the mean penetration force of 1.392 N of the 6-teeth cutter (no bevel) when travelled 9.6mm in this first set of experiments.

A combination of an ANOVA test and a Dunnett test revealed that the force difference, when penetrated 9.6mm, between the 10 and 6-teeth cutter is significant ($p < 0.05$). Nevertheless, the force differences of 4 and 8-teeth cutters compared to the 6-teeth cutter are negligible.

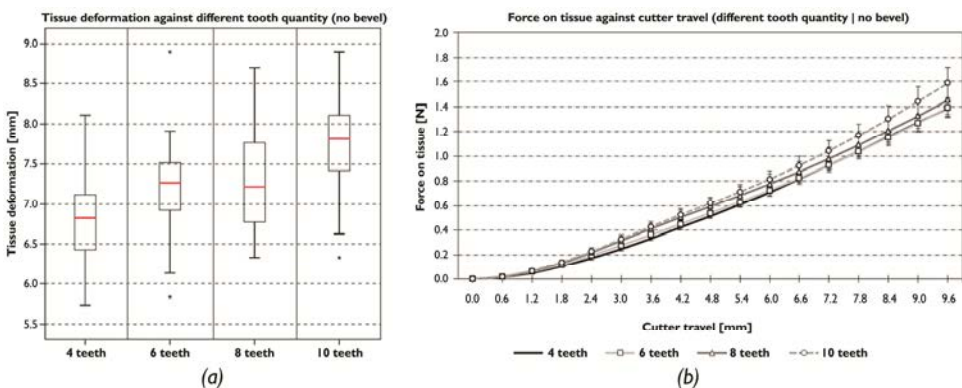


Figure 4.7 (a) Maximum tissue deformation results of the \emptyset 9mm unsharpened crown-cutters of different tooth quantity when penetrated 9.8mm. (b) Plot of force on tissue against cutter travel of the \emptyset 9mm unsharpened crown-cutters of different tooth quantity.

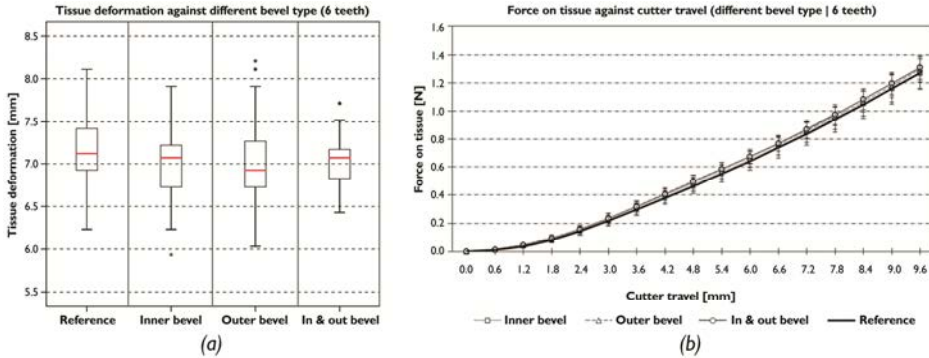


Figure 4.8 (a) Maximum tissue deformation results of the $\emptyset 9\text{mm}$ 6-teeth crown-cutters of different bevel type when penetrated 9.8mm. (b) Plot of force on tissue against cutter travel of the $\emptyset 9\text{mm}$ 6-teeth crown-cutters of different bevel type.

4.3.2 Impact of Tooth Bevel Type

The maximum tissue deformation values for the $\emptyset 9\text{mm}$ 6-teeth crown-cutters of different bevel type are presented in Fig. 4.8(a). Once again, the deformation values were determined at the point when the cutter penetrated to 9.8mm depth.

The mean penetration forces (and standard deviations) of the 6-teeth crown-cutters of different bevel type are plotted in Fig. 4.8(b), up to 9.6mm penetration depth (due to incompleteness of data at penetration depth $>9.6\text{mm}$).

The mean penetration force differences, when the cutter penetrated (travelled) 9.6mm, comparing the 6-teeth cutters of inner, outer and both-sided bevel type to the reference cutter (no bevel) are -0.008N , 0.024N and 0.036N , respectively. This is equal to -0.629% , 1.887% and 2.830% difference from the mean penetration force of 1.272N of the 6-teeth cutter (no bevel) when travelled 9.6mm in this second set of experiments.

The experimental results on the impact of 6-teeth crown-cutters of different bevel type on tissue deformation and penetration forces show no significant differences at all.

4.3.3 Ease of Tooth Collapsibility

The calculations of the inward and outward tooth collapsibility, expressed as a moment of inertia of a maximum tooth cross-section about the inner and outer axes, are summarised in Fig. 4.9. It can be seen that the moment of inertia decreases with the increasing tooth quantity, thus leading to an easier tooth collapsibility. As common sense tells, given the particular tooth cross-section, the moment of inertia values for an outer bend are generally higher than those for an inner bend.

As indicated before, an effortless inward bending is essential for the cutter's complete closure, whereas the outward bending should be prevented upon cutter's backward retraction, so that the cutter retains the sampled tissue. Hence, for the sake

ideal crown-cutter functionality, the moment of inertia about an inner axis should be minimised, whereas the moment of inertia about an outer axis should be maximised. Thus, for an easier comparison of the cutter configurations, ratios of outward to inward tooth collapsibility were determined based on the moment of inertia values (Table 4.1). As observed, the ratio $I_{y(out)}/I_{y(in)}$ decreases with increasing tooth quantity.

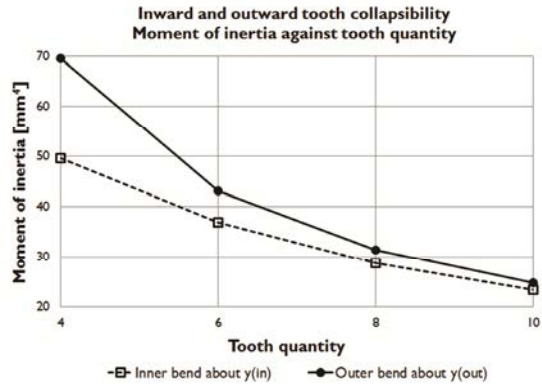


Figure 4.9 Plot of inward and outward tooth collapsibility expressed as a moment of inertia of a maximum tooth cross-section with respect to axes $y(in)$ and $y(out)$ against increasing tooth quantity.

4.4 Discussion

The experimental results on crown-cutters of different tooth quantity (no bevel) show a steady increase in the tissue deformation with the increasing amount of teeth. Even though this is conflicting with the initial expectations, during the experiments it became clear that the major part of the deformation does not start with the onset of the cutter penetration, but with its further insertion into the gelatine. As determined later from the cutter geometry, with fewer teeth the tissue-cutter contact area towards the base of the cutter is smaller than that of the cutters with more teeth. Therefore, a reasonable explanation for the obtained results is that as the contact area decreases, so do the frictional forces, hence resulting in the lower tissue deformation. The initial assumption that the higher number of contact points would build up the surface tension faster, thus leading to faster penetration, would be more probably valid either on larger scale or with a presumably tougher tissue, where the deformations would be minimal.

Contrary to the literature on core cutters, the experiments with 6-teeth crown-cutters of different bevel type yielded no significant differences. Yet, the expected behaviour might have only been applicable to large-scale rotating core cutters that do not have teeth *per se*, but instead feature a solid tubular design with only a sharpened cutting edge.

Table 4.1 Ratios of outward to inward tooth collapsibility at varying tooth quantity.

Tooth quantity	$I_{y(out)}/I_{y(in)}$
4	1.40
6	1.17
8	1.09
10	1.06

Furthermore, while only the tips of the teeth had a bevel, the majority of the tissue deformation occurred at a greater cutter penetration depth. This would imply that the cutter-tissue contact area is more critical to the tissue deformation than the tip's bevel. Of course, this finding might only be specific to this particular cutter design and the use of gelatine, as compared to another medium.

Throughout all the experiments, the gelatine temperature might have slightly influenced the results. However, by randomising the testing order of the cutters this influence has been largely filtered out, possibly causing just a larger spread of measured data.

4.5 Conclusions

In conclusion, based on the significant differences within the tissue deformation results, it can be said that a crown-cutter with a higher number of teeth causes a significantly greater maximum tissue deformation. However, this does not hold for the comparison of the 8 and 6-teeth cutters. Similarly, the analysis of the force differences shows that the cutters with a greater amount of teeth tend to induce a slightly higher force when penetrating the tissue. This force difference is only significant for the 10 versus 6-teeth cutter comparison. As for the bevel type results, one can only conclude that there are no significant differences in either the penetration forces or the tissue deformation. Hence, the bevel's effect is considered negligible. As for the tooth collapsibility calculations, it was clearly shown that both the outer, inner moments of inertia and their ratios decrease with increasing tooth quantity.

Based on the experimental results, a crown-cutter of either 4 or 6 teeth and an arbitrary bevel type is considered the best. Yet, only the tooth collapsibility calculations revealed that the 4-teeth cutter has an excessively high moment of inertia for both the inner and the outer bend. Therefore, a 6-teeth crown-cutter was concluded as the most optimal, due to lower moments of inertia and their ratio still being relatively high compared to 8 and 10-teeth cutters.

Since the cutter's bevel does not seem of significant influence at a smaller scale in terms of the penetration forces, the cutter's original bevel can remain at the inner 20° for a tight inter-tooth fit when collapsed inwards. Last but not least, in order to decrease the tissue deformation by decreasing the cutter-tissue contact area, open features could be introduced to the tooth profiles. Yet, these would have to be optimised to prevent any eventual release of the retrieved biopsy sample.

Acknowledgements

This research was performed within the framework of CTMM, the Center for Translational Molecular Medicine, project MUSIS (grant 030-202).

References

- [1] Braga, M., Vignali, A., Gianotti, L., Zuliani, W., Radaelli, G., Gruarin, P., Dellabona, P., and Carlo, V. D., 2002, "Laparoscopic Versus Open Colorectal Surgery: A Randomized Trial on Short-Term Outcome," *Ann Surg*, 236(6), pp. 759–767.
- [2] Breedveld, P., Stassen, H. G., Meijer, D. W., and Jakimowicz, J. J., 1999, "Manipulation in laparoscopic surgery: Overview of impeding effects and supporting aids," *J Laparoendosc Adv Surg Tech A*, 9(6), pp. 469-480.
- [3] Khorjastan, S. M., Najarian, S., Simforoosh, N., and Farkoush, S. H., 2010, "Design and Modeling of a Novel Flexible Surgical Instrument Applicable in Minimally Invasive Surgery," *Int J Nat Eng Sci*, 4(1), pp. 53-60.
- [4] Minor, M., and Mukherjee, R., 1999, "A Mechanism for Dexterous End-Effector Placement During Minimally Invasive Surgery," *J Mech Des*, 121(4), pp. 472-479.
- [5] Velanovich, V., 2000, "Laparoscopic vs open surgery," *Surg Endosc*, 14(1), pp. 16-21.
- [6] Jelinek, F., Smit, G., and Breedveld, P., 2014, "Bioinspired Spring-Loaded Biopsy Harvester—Experimental Prototype Design and Feasibility Tests," *J Med Device*, 8(1), p. 015002.
- [7] MayoClinic.com, 2013, "Mayo Clinic medical information and tools for healthy living," <http://www.mayoclinic.com/health/medical/>.
- [8] Layfield, L. J., 1995, "Fine needle aspiration of the breast: review of the technique and a comparison with excisional biopsy," *Curr Diagn Pathol*, 2(3), pp. 138-145.
- [9] Cerwenka, H., Hoff, M., Rosanelli, G., Hauser, H., Thalhammer, M., Smola, M. G., and Klimpinger, M., 1997, "Experience with a high speed biopsy gun in breast cancer diagnosis," *Eur J Surg Oncol*, 23(3), pp. 206-207.
- [10] Heijnsdijk, E. A. M., Visser, H., Dankelman, J., and Gouma, D. J., 2004, "Slip and damage properties of jaws of laparoscopic graspers," *Surg Endosc*, 18(6), pp. 974-979.
- [11] Volpe, A., Kachura, J. R., Geddie, W. R., Evans, A. J., Gharajeh, A., Saravanan, A., and Jewett, M. A. S., 2007, "Techniques, Safety and Accuracy of Sampling of Renal Tumors by Fine Needle Aspiration and Core Biopsy," *J Urol*, 178(2), pp. 379-386.
- [12] Wang, T. D., and Van Dam, J., 2004, "Optical biopsy: a new frontier in endoscopic detection and diagnosis," *Clin Gastroenterol Hepatol*, 2(9), pp. 744-753.
- [13] Amelink, A., Kok, D. J., Sterenborg, H. J. C. M., and Scheepe, J. R., 2011, "In vivo measurement of bladder wall oxygen saturation using optical spectroscopy," *J Biophotonics*, 4(10), pp. 715-720.
- [14] Candia Carnevali, M. D., Wilkie, I. C., Lucca, E., Andrietti, F., and Melone, G., 1993, "The Aristotle's lantern of the sea-urchin *Stylocidaris affinis* (Echinoidea, Cidaridae): functional morphology of the musculo-skeletal system," *Zoomorphology*, 113(3), pp. 173-189.
- [15] Trogu, P., 2013, "Giorgio Scarpa - Bionic Models and Rotational Geometry Models," San Francisco State University, San Francisco, CA, http://online.sfsu.edu/trogu/scarpa/movies/scarpa_bionics.mov.
- [16] Scarpa, G., 1985, *Modelli di bionica. Capire la natura attraverso i modelli*, V. Rossi, ed., Nicola Zanichelli Editore S.p.A., Bologna, pp. 13-74.
- [17] Choi, C. Q., 2010, "Rock-Chewing Sea Urchins Have Self-Sharpening Teeth," National Geographic News, <http://news.nationalgeographic.com/news/2010/12/101228-sea-urchin-teeth-self-sharpening-tools-science-animals/>.
- [18] Marsot, J., Claudon, L., and Jacqmin, M., 2007, "Assessment of knife sharpness by means of a cutting force measuring system," *Appl Ergon*, 38(1), pp. 83-89.
- [19] Cao, P.-L., Yin, K., Peng, J.-m., and Liu, J.-l., 2007, "Optimization Design and Finite Element Analysis of Core Cutter," *J China Univ Min Tech*, 17(3), pp. 399-402.
- [20] Houwink, R., and Decker, H. K. d., 2009, *Elasticity, Plasticity and Structure of Matter*, Cambridge University Press, Cambridge, UK.
- [21] Carpinteri, A., 2013, *Structural Mechanics Fundamentals*, Taylor & Francis Group, Boca Raton, p. 17.

Chapter 5

5

Classification of Joints Used in Steerable Instruments for Minimally Invasive Surgery

A Review of the State of the Art

Filip Jelínek, Ewout A. Arkenbout, Paul W. J. Henselmans, Rob Pessers
and Paul Breedveld

Published in Journal of Medical Devices 9(1), 2015.

Abstract

Introduction | This review article provides a comprehensive overview and classification of the joint types used in the steerable tips of minimally invasive surgical instruments. The review was carried out with the objective to pinpoint the essence of the joints' fundamental mechanical design and to provide a qualitative comparison of their strengths and weaknesses with respect to a number of straightforward criteria.

Methods | Besides researching the ASME scientific literature, the entire Espacenet patent database was searched using the keywords *endo** or *lapar** or *surg** in title and *steer** or *articu** or *deflect** in title or abstract. The extensive scope of the patent results was further limited to WO, US and EP patents only as well as to the period of the last decade, 2003-2013, with a few exceptions predating this period. Overall, more than 840 patents were reviewed and categorised on the basis of the joints' mechanical design and supplemented with the scientific papers.

Results and Conclusions | A number of joint categories and subcategories were identified. At the fundamental level the joints can be differentiated as planar and spatial, where the spatial are further split as perpendicular mirrored and revolved. Based on the means of establishing rotational motion, the joint types can be discriminated as rolling, sliding, the combination of rolling and sliding, and bending. Lastly, the rolling and sliding categories can be further split with regard to the phenomenon or feature used for transferring the rotational motion, i.e. friction, teeth, belts, curved features and hinges. In general, the most favoured joint types were identified as the sliding and the bending joint categories overall. Nevertheless, it was recognised that no single fundamental joint type can be considered as ideal and that novel and preferably more superior joint configurations can be generated by combining several fundamental categories together.

5.1 Introduction

5.1.1 Minimally Invasive Surgery

Conventional surgical procedures require open access to the operation site via a long incision, resulting in abundant postoperative scar tissue and relatively long recovery time. Minimally invasive surgery (MIS) was introduced to ameliorate these negative effects [1-5]. For instance, laparoscopy – MIS in the abdomen – involves making one or several small incisions in the abdominal wall in order to accommodate trocars. These serve as airtight seals, allowing for the inflation of the abdominal cavity with carbon dioxide, thereby creating a working space for the surgeon, as well as the portals for the surgical instruments. Long and slender endoscopes and instruments provide the surgeon with visual feedback and tissue manipulation features.

5.1.2 Steerable Instruments

Minimally invasive surgical instruments can be differentiated into rigid [6] and steerable [7] categories (Fig. 5.1(a)) [2, 4]. The configuration of rigid instruments comprises a handle, rigid shaft and a tip, which equips them with four degrees of freedom (DOF), these being axial sliding, axial rotation and pivoting in two perpendicular planes around the incision point (Fig. 5.1(b)) [8]. This fulcrum effect greatly restricts the range of motion and limits the surgeon mainly to frontal or sideways approach to tissue [2, 7]. In contrast, steerable instruments have additional DOF due to one or more joints in the tip, enabling the surgeon to reach behind or over obstacles (Fig. 5.1(c)) [2, 7, 9, 10].

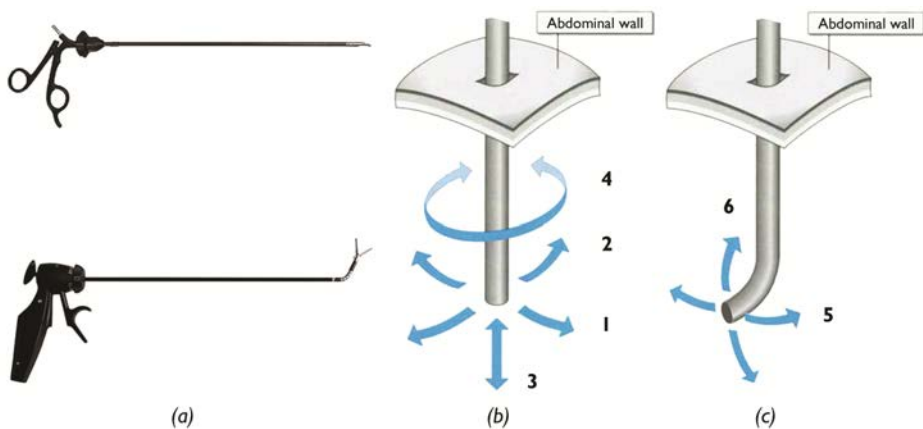


Figure 5.1 (a) Rigid [6] & steerable [7] laparoscopic instruments; (b) Rigid instrument DOF [8]; (c) Additional steerable tip DOF. Adopted from [10].

5.1.3 Review Objectives

The tips of steerable MIS instruments come in numerous configurations when it comes to the joints used for enabling and transferring rotational motion. Even though previous reviews of steerable MIS instruments were carried out, their focus is mainly on actuation, Catherine et al. [11], and control principles of such instruments, Fan et al. [12], or they concentrate on the robotics and micro-electro-mechanical systems, Cepolina et al. [13]. However, the primary objective of this literature review is to provide a clear classification of the steerable MIS instruments with respect to the fundamental mechanical design and working principles of their tip articulations. Such a classification would not only serve for a better understanding of the essence of the state-of-the-art steerable constructions, but also outline their strengths and weaknesses, helping to establish a set of design guidelines for the next generations of steerable MIS instruments. Besides investigating the joints of the existing inventions, new joints types were determined by filling out the gaps in the classification.

5.1.4 Literature Search Method

For simplicity and clear focus of this review, the literature search was based purely on mechanical steerable constructions, excluding pneumatics, hydraulics, electronics, magnetics or shape memory alloy solutions. The ASME scientific literature was supplemented with the aforementioned review articles and used as a starting point, yet it was soon determined that the discussed scope of the fundamental articulation principles and the added value were rather limited and thus insufficient for the purposes of this review. Therefore, for the sake of creative solutions and broadness of this overview, the classification is not restricted solely to the existing steerable MIS instruments or scientific papers, however, it also reviews the entire Espacenet patent database.

The following keywords were used to perform the patent (Espacenet) and paper searches (Web of Knowledge and ASME Digital Collection): *endo** or *lapar** or *surg** in title and *steer** or *articu** or *deflect** in title or abstract. Due to the extensiveness of the patent search query, the results were cropped down to include world (WO), United States (US) and European (EP) patents only. In particular, the patents shown in this classification were further limited to the period of the last decade, 2003-2013, with a few exceptions that predated this period, yet helped to fill missing gaps in the classification. In the end, more than 840 patents were reviewed and categorised on the basis of the joints' articulation principles and supplemented with the scientific papers.

For coherence, the patent search results constitute the most recent up-to-date patents (valid as of 31 October 2013) by a given patent assignee. In other words, if a certain patent assignee has more patents featuring the same joint type, only the most recent one is mentioned in the joint type categorisation.

5.2 Classification of Steerable MIS Instrument Joints

The results of the extensive patent and paper searches on steerable MIS instruments revealed the use of two basic joint types – planar (2D) and spatial (3D); here the spatial joints are further categorised as perpendicular mirrored and revolved. Each of these joint types is further split into more subcategories depending on the means of the joint articulation, as outlined in the following sections. Figure 5.2 presents a graphical summary of the joint type classification, listing all the relevant up-to-date patents for each joint type category over the period 2003-2013, including a few exceptions predating this period. This classification is further supported by Table 5.1, which provides a comprehensive overview of all the reviewed patents listed according to the joint type and the patent assignees, whose count indicate the most frequently applied joint types. Despite being discussed in the paper, the supplementary scientific literature merely expands the list of several joint categories and thus it is not included in the pictorial material, for the sake of its conciseness and uniformity.

5.2.1 Planar and Spatial Joints

The working principle of a planar joint is two dimensional and allows for one rotational DOF, whereas a spatial joint is simply a geometrical extension of the planar joint allowing for more DOF. The spatial joint category comprises a perpendicular mirrored configuration and a revolved configuration. In comparison with the planar joint, the perpendicular mirrored configuration uses an additional plane of motion placed orthogonally to the first one in order to increase the number of DOF to two, thus generating three-dimensional motion. In other words, the perpendicular mirrored configuration features two one-DOF joints closely stacked on top of each other, together allowing for two-DOF motion. From a design point of view, the second joint working along the perpendicular plane is not only turned axially 90° , but it is also mirrored about a horizontal plane with respect to the first one – yet this configuration will be simply referred to as a perpendicular joint for short.

Similarly to the perpendicular joint, the revolved configuration is a modification of the planar joint. Here the planar joint, or its two-dimensional cross-section, is revolved around its vertical central axis, hence translating planar into a spatial joint. Such a revolved joint allows not only for sideways rotation in two perpendicular planes, like the perpendicular joint, but in principle also for rotation along its vertical axis, thus featuring all three rotational DOF in a single joint. However, certain planar joint configurations, i.e. rolling belted joint and sliding hinged joint, cannot be revolved into a spatial three-DOF joint, either due to the theoretical infeasibility or the elimination of DOF due to such a construction.

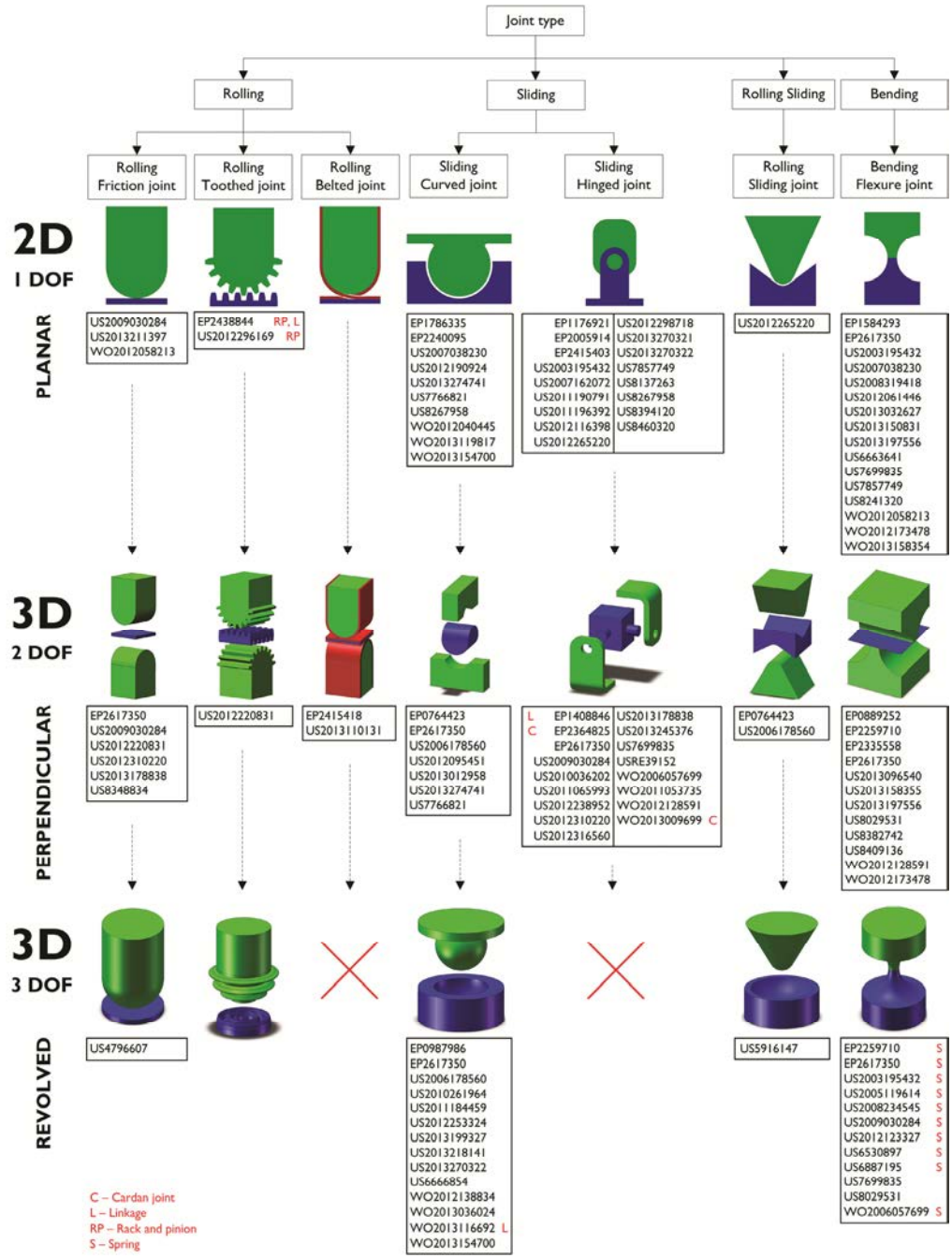


Figure 5.2 Graphical summary of the joint type classification, listing all the relevant up-to-date patents for each joint type category. Additional descriptors (C, L, RP, S) highlight various differing joint configurations within several joint type categories.

The rotational motion of all of these joints is established by either rolling, sliding, the combination of rolling and sliding, or bending. These four basic principles are used for the categorisation of the relevant existing patents. The rolling and sliding categories are further split into more subcategories based on the phenomenon or feature used for transferring the rotational motion. In the following paragraphs, the four aforementioned principles of transferring rotational motion are each outlined separately in their planar, perpendicular and revolved configurations, supported by the relevant reviewed patents. Aside from the working principle, they are also discussed on the basis of torsional stiffness and general joint stability and reliability.

5.3 Rolling Joint

5.3.1 Planar Rolling Joint

A generic planar rolling joint consists of two interfacing halves which, during rolling, both rotate and translate with respect to each other along a trajectory defined by their curvature – thus sharing a moving point of contact. Since the contact area in between such joint halves is relatively small, the motion transfer relies on sufficiently large friction between the contacting surfaces. Alternatively, physical features such as gears or belts can be used to prevent slip and transfer the rotation. Therefore, the basic rolling joint types can be defined as: rolling friction joint, rolling toothed joint and rolling belted joint.

A tip featuring a series of simple planar rolling friction joints is presented by Cole et al. [14], Parihar et al. [15] and Parrott et al. [16] (Fig. 5.3(a)). All the joints work within a single plane, allowing for sideways rotation only in that plane. As the individual joint segments have a certain thickness they interface along a contact line, yet still depend on sufficient friction to prevent slip. Likewise, without any additional constraints, e.g. stops or driving cables, the rolling joint segments are susceptible to transverse and axial split or disconnection (with respect to the instrument shaft) as well as do not provide torsional stiffness by the joint design itself.

In its planar configuration, the rolling toothed joint was identified in the paper by Minor et al. [4] as a set of planar gears in series transferring the rotational motion. On the other hand, such a basic planar joint in the form of two identical mirrored halves rolling against each other was not found amongst the patents. Instead, Blase [17] (Fig. 5.3(b)) and Kleyman et al. [18] present the toothed modification as a rack and pinion mechanism. Here an inner driving rod features a rack that meshes with a pinion mounted to the distal part of the tip joint, hence translating the rod's axial motion into rotation of the joint. Moreover, although unconventional, Blase [17] uses a special linkage in between two joint segments enabling compact joint articulation, yet at the expense of obstructing the instrument's lumen. Naturally, stability of the rack and pinion configuration relies on tight gear tolerances and pins holding the components in place, the strength of which can be considerably compromised at such a small scale.

The last rolling joint type is the rolling belted joint, which uses crossed belts or cables running from one side of the joint's half to the opposite side of the other half. These belts function as constraints for the prevention not only of slip, but also of transverse and axial split, as well as they ensure torsional stiffness. However, these advantages come at the expense of greater design complexity, i.e. the incorporation of belts. Considering a simple planar joint where the pair of belts works antagonistically in two parallel planes, the joint's thickness and width are then determined by the belt geometry and sufficient mutual spacing. A simple one-DOF rolling belted joint is only presented in the paper by Nai et al. [19], who use thin flexures, instead of cables, that are smartly embedded in the rolling joint design, thereby reducing the number of parts.

5.3.2 Perpendicular Rolling Joint

As outlined before, the perpendicular rolling joint incorporates two horizontally mirrored planar rolling joints in series aligned perpendicularly to each other, thus providing two DOF in three dimensions. This joint usually incorporates driving cables running through all the joints, which in case of the rolling friction joint help prevent transverse split and joint slip to an extent. Furthermore, depending on the cable diameter, the cables also increase the joint's torsional stiffness. Perpendicular rolling friction joints are presented in the patents by Bakos [20], Banik et al. [21] (Fig. 5.3(c)), Cole

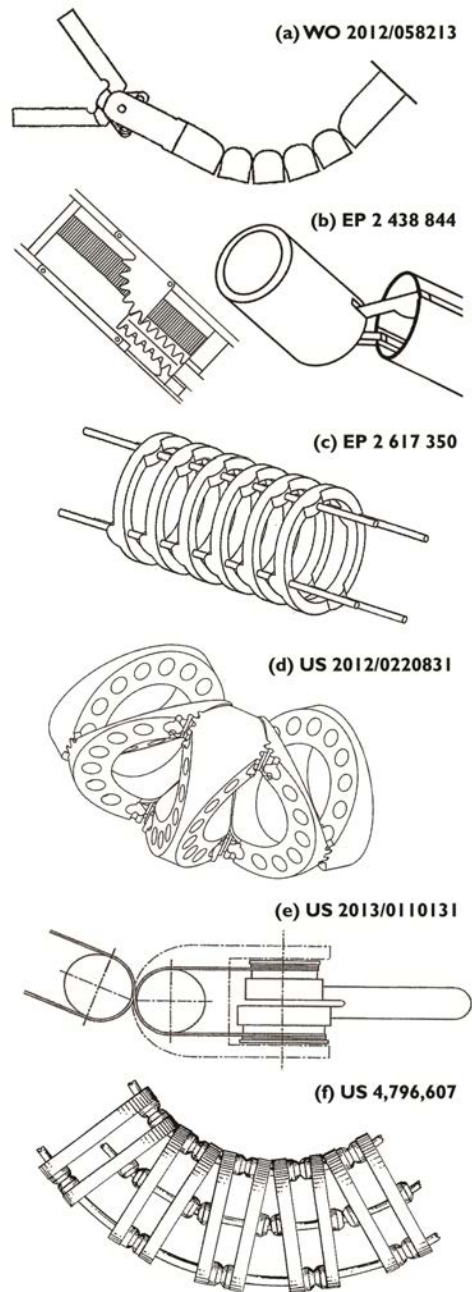


Figure 5.3 Overview of the rolling joint types adopted from the patents by (a) Parrott et al. [16], (b) Blase [17], (c) Banik et al. [21], (d) Cooper et al. [22], (e) Madhani et al. [26] and (f) Allred et al. [27].

et al. [14], Cooper et al. [22], Malkowski [23] and Malkowski et al. [24].

The perpendicular rolling toothed joint presented in the patent by Cooper et al. [22] (Fig. 5.3(d)) resembles the basic perpendicular rolling friction joint modification. However, instead of relying on high enough friction it uses teeth or gears to prevent slip and to transfer the joint's rotation. Yet, even if fitted with cables, this configuration still lacks features preventing axial split. Similarly, Jelínek et al. [10] use a perpendicular rolling toothed joint in their DragonFlex design with a special embedded cable guidance supporting the cables at all times, maximising their bending radius and equalising their moment arms.

The perpendicular rolling belted joint is shown in the patents by Fiorini et al. [25] and Madhani et al. [26] (da Vinci's EndoWrist by Intuitive Surgical, Sunnyvale, CA, USA, Fig. 5.3(e)). It features a set of pulleys that support the driving cables through the first planar joint. The pulleys can roll on top of each other and their rolling motion is secured by the intercrossing cables at the pulley-pulley interface, which therefore function as belts as well. Similarly, the second orthogonally placed planar joint also features a pulley, which operates the tip's grasper. As a matter of fact, instead of forming a rolling joint construction, the pulley is already incorporated in the grasper itself. Therefore, the perpendicular joints found in these two patents feature essentially a combination of the rolling belted joint with a moving point of rotation and the cable-driven pulley with a fixed point of rotation.

5.3.3 Revolved Rolling Joint

The revolved rolling friction joint consists of two mirrored dome- or hemisphere-shaped halves, capable of rolling on top of each other both axially and sideways in two perpendicular planes. In spite of being rather agile and space efficient, this friction joint is very susceptible to slip, since the two joint halves always interface at a single moving point only. Hence, the joint has almost no torsional stiffness, which is again mainly dependent on the driving cable diameter. Similarly, the joint itself cannot prevent axial or transverse split of the two interfacing halves. Possibly for these reasons, this particular joint type has not been very popular over the discussed period 2003-2013 and the latest patent using it is by Allred et al. [27] (Fig. 5.3(f)) from 1989.

A new fundamental joint type was identified via a systematic design procedure (ACRREx method educated at TU Delft) [28], which employs the knowledge categorisation within the researched domain with the aim to identify the missing gaps in that domain. Here, a theoretically interesting, yet likely difficult to achieve construction-wise, would be a revolved rolling toothed joint. Such a joint would feature teeth revolved into rings that would prevent slip during sideways rotation and provide larger contact surface than that of a revolved rolling friction joint. Nevertheless, the axial split and the torsional stiffness of this joint type would still remain an issue. As indicated, no patents were found to utilise this joint modification, however, it might be interesting to investigate such a concept, at least for the sake of design feasibility.

5.4 Sliding Joint

5.4.1 Planar Sliding Joint

Sliding is another principle used in steerable MIS instruments. Whereas the rolling friction joint relies on high enough friction to transfer the rotational motion, an excessively high friction in the sliding joint could impede its rotation. The sliding joint thus depends on smooth and rather precise geometry of the joint halves. Furthermore, contrary to the rolling joint, the two interfacing halves of a sliding joint rotate about a fixed axis. For that reason, this type of joint is generally resistant to transverse split, and may further be modified to be torsion-stiff and resistant to axial split. The fixed axis can be provided by a protrusion on one joint half, or by a separate component, such as a pin or a rivet. Hence, the sliding joints can be further categorised as sliding curved and sliding hinged joints.

The joint halves of the sliding curved joint are always shaped as two mutually fitting jigsaw puzzle pieces. The range of motion of such a single joint is therefore rather limited as it depends on the joint's clearance, whose increase can only lead to greater joint backlash and even increased vulnerability. On the one hand, the connecting parts can be designed to feature a slight curvature running over

$\leq 180^\circ$, allowing for resistance only to transverse split. A series of such joints, all working in a single plane, is used by Braun [29] or Frede et al. [30] (Radius Surgical System by Tuebingen Scientific, Tuebingen, Germany), Kerver et al. [31], Marczyk et al. [32], Padget et al. [33], Stone et al. [34], Stroup et al. [35] (Fig. 5.4(a)) and Worrell et al. [36]. On the other hand, the connecting parts of the joint halves can feature a curvature of more than 180° . This enables the connecting part of one joint half to embrace the connecting part of the opposite half, essentially making the joint virtually torsion-stiff (considering an

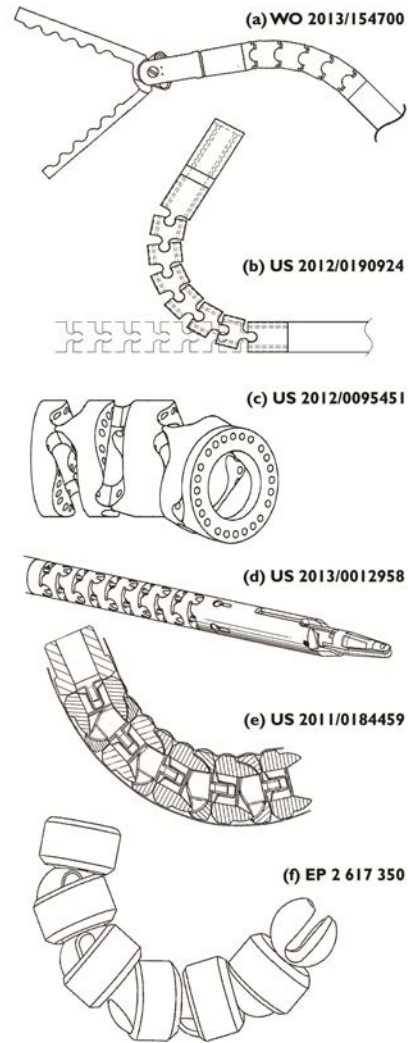


Figure 5.4 Overview of the sliding curved joint types adopted from the patents by (a) Stroup et al. [35], (b) Tseng [39], (c) Hegeman et al. [56], (d) Marczyk et al. [32], (e) Malkowski et al. [80] and (f) Banik et al. [21].

extruded cross-section) and resistant to axial split as well. This type of connector is demonstrated by Brunnen et al. [37], Dawoodjee [38] and Tseng [39] (Fig. 5.4(b)).

As the nomenclature reveals, the fixed axis of the sliding hinged joint is formed by a hinge – this being simply a pin, a rivet or an axle-like protrusion on one of the joint halves. Unlike in the sliding curved joint, the two halves of the sliding hinged joint do not interface along the same plane. Instead, they are aligned parallel to each other, accommodating concentric holes for the hinge. Therefore, despite being torsion-stiff and resistant to transverse and axial split, the limiting factor for the joint robustness is the strength and stiffness of the relatively small hinge. Nevertheless, due to its geometry, the sliding hinged joint can provide a large range of motion of almost 360° in theory. Despite the increased design complexity, the patent group using this joint type is the largest.

Designs incorporating only a single sliding hinged joint in the tip are presented in the work of Agarwal et al. [40], Braun [29], Brock et al. [41] (Fig. 5.5(a)), Doyle et al. [42], Hirzel [43], Jacobs et al. [44], Kortenbach et al. [45], Krzyzanowski [46], Marczyk [47], Nicholas et al. [48], Ouchi [49] and Scheib et al. [50]. Naturally, using only a single joint enabling a sharp bend renders the instrument lumen nearly unusable for any additional tasks or accessories that would require a smooth and gradual inner instrument environment when bent. For that reason, certain inventions feature a series of sliding hinged joints, thus having a potential for creating a smooth gradual bend, rather than one local pivoting point; these include patents by Goldfarb et al. [51], Joshi et al. [52], Marescaux et al. [53], Menn [54] and Saadat et al. [55] (Fig. 5.5(b)).

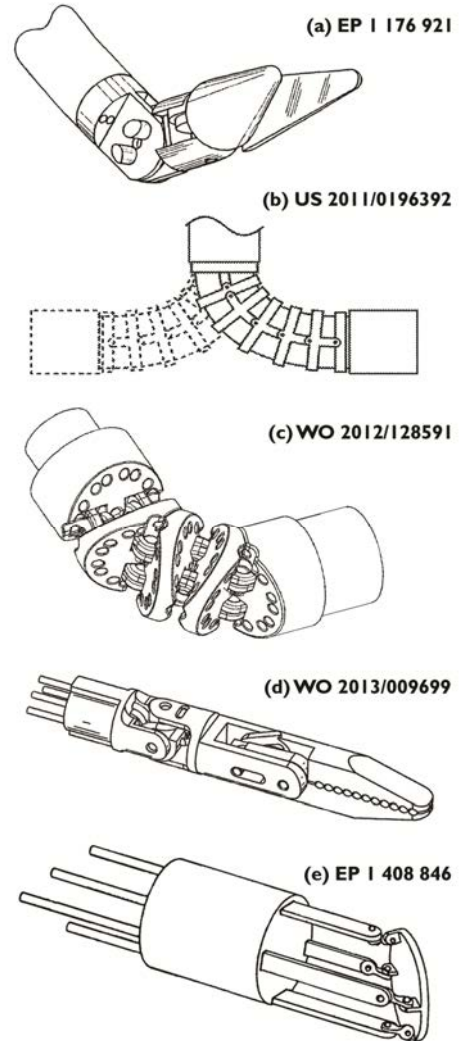


Figure 5.5 Overview of the sliding hinged joint types adopted from the patents by (a) Brock et al. [41], (b) Saadat et al. [55], (c) Jeong et al. [65], (d) Steege [71] and (e) Wallace et al. [73].

5.4.2 Perpendicular Sliding Joint

The two-DOF perpendicular sliding joint closely resembles the perpendicular rolling joint, yet operates on the sliding principle. The perpendicular sliding curved joint featuring connecting parts whose curvature runs over $\leq 180^\circ$ is used in the patents by Banik et al. [21], Hegeman et al. [56] (Fig. 5.4(c)) and Saadat et al. [57]. The perpendicular sliding curved joint whose connecting part curvature runs over $> 180^\circ$, thereby preventing axial joint split, is demonstrated in the work of Breedveld [7] (Miflex by DEAM, Amsterdam, The Netherlands), Brunnen et al. [37], Heimberger [58] and Marczyk et al. [32] (SILS Hand by Covidien, Mansfield, MA, USA, Fig. 5.4(d)).

Designs featuring perpendicular sliding hinged joints are presented in the work of Ananthanarayanan et al. [59], Aust et al. [60], Banik et al. [21], Belson et al. [61], Cole et al. [14], Danitz [62], Harris et al. [63], Hassoun [64], Jeong et al. [65] (Fig. 5.5(c)), Lee et al. [66], Lin et al. [67], Malkowski [23], Malkowski et al. [24], Mitchell et al. [68] and Oku [69]. Unlike the planar modification, the perpendicular hinged joints most often come in series of multiple stacked joints, thereby helping to create smooth bends along two planes in three dimensions.

Nevertheless, the paper by Awtar et al. [70] and the patent by Steege [71] (Fig. 5.5(d)) present a Cardan, or universal, joint that enables localised two-DOF pivoting, thus being more space efficient. However, this is at the expense of obstructing the instrument's lumen that could otherwise house auxiliary devices. Milani et al. [72] demonstrate a tooth-driven modification of the Cardan joint.

Last but not least, the hinged configuration also features a relatively space efficient rod-driven platform. As shown in the patent by Wallace et al. [73] (Fig. 5.5(e)), there are four miniscule hinges that work in pairs, thereby enabling two-DOF rotation of this platform. However, the torsional stiffness of such a construction depends on the stiffness as well as the stability of the four driving rods. Moreover, due to the relatively small hinge sizes, the hinged platform could be rather vulnerable to the external forces.

5.4.3 Revolved Sliding Joint

As mentioned previously, the revolved sliding joint is only constructionally feasible for the sliding curved variant. The revolved sliding curved joint, also called simply a ball joint, features all three rotational DOF acting around the same point. Hence, the joint is easily controllable, yet at the same time easily susceptible to spin. Similarly to the planar and the perpendicular version, here the two types of joint connectors either allow or prevent the axial split. The connectors of cross-sectional curvature running over $\leq 180^\circ$, allowing the axial split, are used in the work of Castro et al. [74], Danitz et al. [75] (RealHand by Novare, Cupertino, CA, USA), Hinman et al. [76], Jeong et al. [77], Lange [78], Lee et al. [79], Malkowski et al. [80] (Fig. 5.4(e)), Park et al. [81], Saadat et al. [57], Seow et al. [82] and Zirps et al. [83]. On the contrary, Banik et al. [21] (Fig. 5.4(f)), Scheib et al. [50] and Stroup et al. [35] use click-on connectors of cross-sectional curvature greater than 180° , thus preventing the axial split.

Similarly to the hinged platform by Wallace et al. [73], the patent by Hallbeck et al. [84] also presents a set of four links or rods connected to a distal platform accommodating the instrument's tip. The rods connect to the tip with ball-joint ends. First of all, the overall construction of multiple ball joints connected to a platform represents a relatively torsion-stiff modification to a regular revolved sliding joint. Furthermore, similarly to a single ball joint, the rod-driven platform is in fact more space efficient than a perpendicular joint. Here the platform essentially pivots about its centroid, unlike the stacked construction of two or more displaced planar joints in the perpendicular arrangement. However, this complex construction is, similarly to the hinged platform, challenging in terms of minimisation at the expense of robustness.

5.5 Rolling Sliding Joint

5.5.1 Planar Rolling Sliding Joint

As indicated by its name, the rolling sliding principle is used in joints that combine the rolling motion with the sliding motion. The patent by Menn [54] (Fig. 5.6(a)) presents a series of rolling sliding joints that work essentially as sliding curved joints with looser constraints. To be more specific, the joint motion can involve the combination of partial rolling and sliding at the same time, or firstly rolling then sliding, or just sliding itself. Obviously, the mode of operation of such a joint depends on the tolerances in between the two joint halves and the tightness of their interface, or in other words on friction. A simple planar rolling sliding joint could be easily susceptible to axial and transverse split as well as axial spin, unless it is constrained by a tight cable connection.

5.5.2 Perpendicular Rolling Sliding Joint

The perpendicular rolling sliding joint, also called a saddle joint, is presented in the paper by Breedveld [7] and the patent by Saadat et al. [57] (Fig. 5.6(b)). Here the one joint half features alternating concave and convex borders, or surfaces, which fit into their reversed counterparts in the opposite joint half. Due to the wave-like outline the two joint halves fit tightly together, resulting in an enhanced torsional stiffness as well as resistance to a transverse and axial split if a tight cable connection is ensured. However, such a joint usually has a rather limited deflection range, meaning that a multitude of such joints is needed in series for a given bending angle compared to, for instance, a single Cardan joint.

Similarly to the jigsaw protrusions in the sliding curved joint, the design by Heimberger [58] (Fig. 5.6(c)) uses interlocking components at the joint interface, yet with a large clearance. This clearance enables the joint halves to become mutually more displaced, while their curved endpoint expansions enable the sliding and/or rolling motion when moved sideways. Such a configuration provides torsional stiffness as well as prevents axial and transverse split to an extent, yet the driving cables are still inevitable for ensuring the joint's integrity.

5.5.3 Revolved Rolling Sliding Joint

Similarly to the ball joint, the revolved rolling sliding joint makes use of the hemisphere-shaped components, yet with a looser fit. The most recent patent using this joint type is the one by Boury [85] (Fig. 5.6(d)) from 1999. The demonstrated cup-like geometry does not limit the motion just to sliding, but allows for rolling as well. Therefore, the revolved rolling sliding joint type might appear more adaptable than a simple ball joint, especially if the central instrument channel was utilised for housing fiberoptics or a micro-grasper. To illustrate, instead of jamming the inner auxiliary device shortly after the initiation of bending, the revolved rolling sliding joint could simply roll further apart, thus creating a more continuous obstructionless passage. However, naturally, the rolling out motion would require the opportunity for axial displacement of joint parts, which might be difficult to achieve unless, for example, the driving cables were elastic to an extent. Nevertheless, even though the axial split would be desirable for this particular configuration, the transverse split and axial spin would still have to be prevented by additional features such as cables.

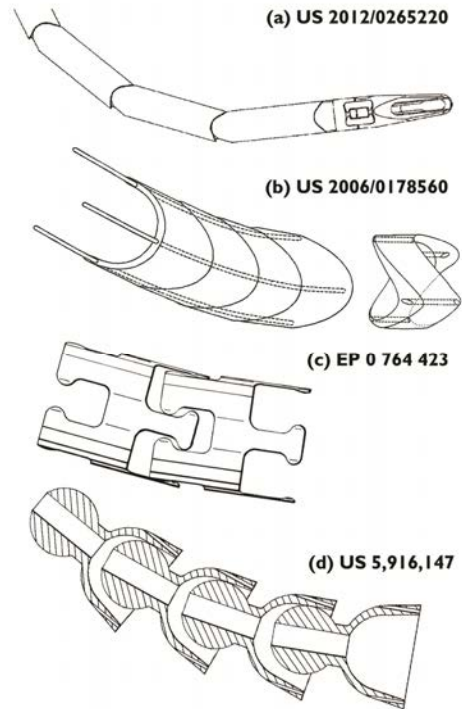


Figure 5.6 Overview of the rolling sliding joint types adopted from the patents by (a) Menn [54], (b) Saadat et al. [57], (c) Heimberger [58] and (d) Boury [85].

5.6 Bending Joint

5.6.1 Planar Bending Joint

The rolling and sliding principles discussed so far both revolve around friction in between the joint halves – whether sufficiently high or negligibly small, respectively. In contrast, the principle of bending, used in compliant flexure joints, depends purely on the dimensions of the flexural part enabling the bending as well as the joint's material properties, such as stiffness or yield strength. These geometrical and material properties also determine how torsion-stiff the joint is as well as how well it can resist axial and transverse forces. Since the joint is formed of a single piece and operates within the range of the material's elastic deformation, it essentially acts as a spring. Such

a spring requires a continuous force in order to remain in a bent state, as it always tries to return to its neutral state that ideally represents a straight joint. Incidentally, if allowed, the joint may overstretch thus introducing plastic deformation, after which the spring finds a new position for its neutral state.

Designs incorporating a series of planar flexure joints enabling only a single bend at a time are demonstrated in the patents by Banik et al. [21], Chong [86], Erhard [87], Griffiths [88], Knodel et al. [89], Kortenbach et al. [45], Kovac et al. [90], Lee et al. [66], Lenker et al. [91], Lyons et al. [92], Ouchi [49], Parrott et al. [16], Verbeek [93] and Viola [94]. The patent by Stone et al. [34] (Fig. 5.7(a)) is an example showing how the flexural parts can be simply embedded in the thin instrument's shell by cutting out unnecessary material, thus creating clearance for the bend. In addition, Shelton et al. [95] (Fig. 5.7(b)) present two flexure joint clusters working coplanarly in series, hence enabling two simultaneous bends in either direction within one plane.

5.6.2 Perpendicular Bending Joint

Similarly to the planar configuration, the individual joints of the perpendicular bending flexure are all fused together, essentially carved from a single piece of material with thin intermediate flexural parts. The two-DOF joint structure is resistant to both axial and transverse split and is as torsion-stiff as the flexural part's geometry and material properties allow. This joint is used in the work of Banik et al. [21], Breedveld et al. [96], Cooper et al. [97] (Fig. 5.7(c)), Danitz et al. [98], Harder et al. [99], Hermann et al. [100], Jeong et al. [65], Lee et al. [101] (Autonomy Laparo-Angle by Cambridge Endo, Framingham, MA, USA), Lin [102], Shelton et al. [95], Verbeek [93] and Wallace et al. [103]. The perpendicular flexure joint usually features a thick-shelled bulk of compliant material with embedded

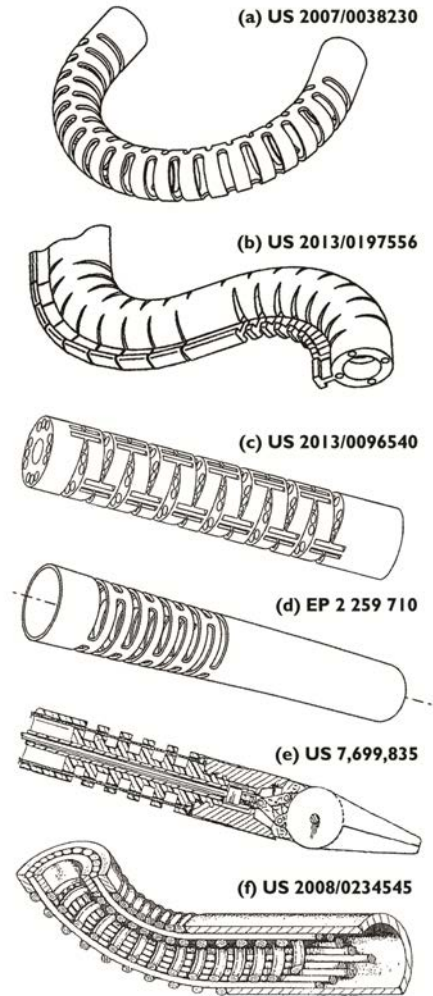


Figure 5.7 Overview of the bending flexure joint types adopted from the patents by (a) Stone et al. [34], (b) Shelton [95], (c) Cooper et al. [97], (d) Dewaele et al. [104], (e) Lee et al. [66] and (f) Breedveld et al. [109].

driving cables, however, the patent by Dewaele et al. [104] (Fig. 5.7(d)) shows the thin-shelled alternative with cut-outs.

5.6.3 Revolved Bending Joint

In its basic configuration the two-DOF revolved bending joint resembles a simple tubular construction, sometimes enriched by alternating narrow and wide sections for localised bending. Here the narrow sections serve as flexural parts and the wide sections are used to guide the cables. The revolved bending joint is demonstrated in the work of Burgner et al. [105], Hendrick et al. [106], Lee et al. [66] (Fig. 5.7(e)), Lee et al. [101], Yen et al. [107] and Zhang et al. [108]. The driving force required to bend the revolved flexure and the joint's torsional stiffness are both directly proportional to the flexural part's diameter. Therefore, there is a trade-off between the ease of controllability of such a joint and its resistance to axial spin.

Nevertheless, a more preferred compliant configuration arises from revolving an eccentric circular or polygonal cross-section along a helical trajectory, hence creating a coil spring. Such a flexure may be popular due to the ease of design or availability. Nevertheless, since the coil spring represents an assembly of infinite number of flexural points, it is difficult to control fully and reliably. Hence, a certain supporting construction is needed to limit the number of DOF and considerable fine-tuning is required with respect to the spring's axial and torsional stiffness. The coil spring is used in the patents by Banik et al. [21], Breedveld et al. [7, 109] (Fig. 5.7(f)), Cole et al. [14], Danitz [62], Dewaele et al. [104], Kortenbach et al. [45], Melsky [110], Miller [111], Nardeo [112] and Pilvisto [113]. Here the patent by Breedveld et al. [109] uses a pair of concentric coil springs, mutually spaced out by driving and supporting cables, thereby stiffening the overall construction.

5.7 Discussion

5.7.1 Design Suitability for Specific Purposes

With the aid of Table 5.2 this section aims to summarise the outlined advantages and disadvantages of the reviewed designs in relation to their space efficiency and their inherent capabilities for preventing the joint slip, spin, the transverse and axial split, enabling the creation of the inner lumen and the ease of miniaturisation related to the design simplicity in general.

The most space efficient designs, i.e. concentrating three rotational DOF around a single pivoting point, consist primarily of all the revolved joints, such as the ball joint. Further space efficient solutions also include the Cardan joint and the rod-driven platform, which are in addition torsion-stiff, yet provide only two rotational DOF by design.

With regard to the joint's inherent capabilities for preventing slip, spin and transverse and axial split, the most suitable joint types ensuring the joint's stability and

Table 5.2 Qualitative evaluation of the joint types with regard to their performance in several merits related to the joint geometry and motion. Performance is evaluated as good (+), neutral (0) or weak (-).

Joint type		Merit	Preventing axial split	Preventing transverse split	Preventing slip	Torsional stiffness	Space efficiency (Size vs. DOF)	Providing inner lumen	Overall design complexity	TOTAL
Rolling	Friction	Planar	-	-	-	-	-	+	+	-3
		Perpendicular	-	-	-	-	0	+	+	-2
		Revolved	-	-	-	-	+	0	+	-2
	Toothed	Planar	-	+	+	+	-	0	-	0
		Perpendicular	-	+	+	+	0	0	-	1
		Revolved	-	+	+	-	+	-	-	-1
	Belted	Planar	+	+	+	+	-	-	-	1
		Perpendicular	+	+	+	+	0	-	-	2
	Sliding	Curved	Planar	0	+	+	+	-	+	0
Perpendicular			0	+	+	+	0	+	0	4
Revolved			0	+	+	0	+	+	0	4
Hinged		Planar	+	+	+	+	-	0	-	2
		Perpendicular	+	+	+	+	+	0	-	4
		Revolved	-	0	0	0	-	+	+	0
Rolling Sliding	Perpendicular	-	0	0	0	0	+	+	1	
	Revolved	-	-	0	-	+	+	+	0	
	Planar	+	+	+	+	-	+	+	5	
Bending Flexure	Perpendicular	+	+	+	+	0	+	+	6	
	Revolved	+	+	+	0	+	+	+	6	

reliability are the rolling belted joints, majority of the sliding joints except certain ball joint configurations, the perpendicular rolling sliding joint and the bending joints in general, yet the bending joints can be questionable in terms of torsional stiffness.

Naturally, outside the scope of the fundamental joint design, there are other means of providing the abovementioned joint capabilities. For instance, the axial split can be easily prevented in all the joints by pre-tensioning the cables that hold the entire construction together. Taking this into account, the rolling toothed joint would then also fulfil the criteria for axial and transverse split as well as the torsional stiffness. Furthermore, the transverse split and the torsional stiffness can also be provided by introducing a set of protrusions and cut-outs in the joint itself [7, 10]. By the same token, enclosing any joint into a sleeve can prevent the transverse split to an extent, just as a braided sleeve [114] can enhance the joint's torsional stiffness. Yet, such enhancements always elevate not only the number of components, but the overall complexity of the design and assembly.

Considering the feasibility of the internal lumen, all the joint types can be in essence designed hollow, yet some joints are less suitable for this than the others; these include the planar rolling toothed joint, the rolling belted joint category as well as the sliding hinged joints in certain configurations.

As for the overall design simplicity and the ease of miniaturisation, the following designs should be suitable for such a purpose: the rolling friction joints, the rolling sliding revolved joint, the bending joints and the sliding curved joints, especially the ball joint, yet its manufacture might pose a challenge.

5.7.2 Most Frequent Joint Types

Once looking at the distribution of the inventions across Fig. 5.2 and Table 5.1, it becomes apparent that certain joint types are generally more frequently applied than

the others; these include the sliding and the bending joint categories overall. One could speculate that the preference for these joints is due to their capabilities for performing the best in the majority of the criteria discussed previously and summarised in Table 5.2. Yet, in all the joints, the advantages come hand in hand with one or more striking disadvantages.

The sliding hinged joints can easily prevent both axial and transverse joint split, they are torsion-stiff and can be easily made space efficient and feature an inner lumen, however, all this comes at the expense of considerable complexity with respect to miniaturisation, manufacturing and assembly.

The ball joints or alike can easily prevent axial and transverse split, be very space efficient and relatively simple in design, as well as they can accommodate an inner lumen to an extent. Nevertheless, without additional features they have no torsional stiffness whatsoever and thus rely on the driving cables or some kind of overlaying torsion-stiff construction.

Last but not least, the bending joint category can prevent axial and transverse split by default, it can easily have an inner lumen and be relatively simple in terms of manufacture, yet its torsional stiffness greatly depends on the choice of material and flexure geometry. Unfortunately, the increase in torsional stiffness by expanding the cross-sectional area decreases the joint's bending compliance; hence, such a design cannot compete with, for instance, the Cardan joint in this regard.

5.7.3 New Joint Types and Joint Combinations

As far as new joint designs are concerned, one unexplored, yet theoretically feasible joint type was identified – the revolved rolling toothed joint. Nonetheless, the geometrical feasibility and practicality of this particular joint remain to be investigated.

With respect to new innovative designs, their novelty might not necessarily lie outside the boundaries of the provided joint classification. Instead, new joints could be created using combinations of the identified fundamental categories. Such joints include, for instance, the design by Banik et al. [21] showing a perpendicular rolling joint with springs (revolved bending joints) as interconnecting features increasing the overall constructional integrity. The patent by Madhani et al. [26] demonstrates a sort of a perpendicular rolling belted joint, where the first planar joint is an actual rolling belted joint and the second planar joint is a hinged pulley. Lastly, Milani et al. [72] demonstrate a modification to the Cardan joint which is driven by teeth or gears.

Naturally, further design combinations are always possible and welcome as no single joint can be regarded as ideal in its basic configuration. Yet, care has to be taken with respect to a possibly elevated design complexity and hence reduced ease of manufacturability.

5.8 Conclusions

This review article provides a comprehensive overview and classification of the joint types used in the steerable tips of the minimally invasive surgical instruments, with the intention of better understanding the essence of their fundamental mechanical design, their strengths and weaknesses. The entire Espacenet patent database was reviewed, yet for comprehensiveness only the most up-to-date patents over the last decade, 2003-2013, are discussed together with a few exceptions predating this period.

During the review process, several categories and subcategories of joint types were identified. At the fundamental level the joints can be differentiated as planar (2D) and spatial (3D), where the spatial are further split as perpendicular mirrored and revolved. Based on the means of establishing the rotational motion, the joint types can be discriminated as rolling, sliding, the combination of rolling and sliding, and bending. Finally, the rolling and sliding categories can be further split with regard to the phenomenon or feature used for transferring the rotational motion, i.e. friction, teeth, belts, curved features and hinges.

Despite lacking perfection, the most preferred joint types in general were identified as the sliding hinged joints, the sliding curved revolved joints and the bending joint category overall. Aside from recognising a new fundamental joint type, it was suggested and shown that novel joint configurations can be generated by combining several fundamental categories together.

Acknowledgements

The research of Filip Jelínek was performed within the framework of CTMM, the Center for Translational Molecular Medicine, project MUSIS (grant 030-202). The research of Ewout A. Arkenbout and Paul W. J. Henselmans was supported by Technology Foundation STW.

References

- [1] Braga, M., Vignali, A., Gianotti, L., Zuliani, W., Radaelli, G., Gruarin, P., Dellabona, P., and Carlo, V. D., 2002, "Laparoscopic Versus Open Colorectal Surgery: A Randomized Trial on Short-Term Outcome," *Ann Surg*, 236(6), pp. 759–767.
- [2] Breedveld, P., Stassen, H. G., Meijer, D. W., and Jakimowicz, J. J., 1999, "Manipulation in laparoscopic surgery: Overview of impeding effects and supporting aids," *J Laparoendosc Adv Surg Tech A*, 9(6), pp. 469-480.
- [3] Khorjastan, S. M., Najarian, S., Simforoosh, N., and Farkoush, S. H., 2010, "Design and Modeling of a Novel Flexible Surgical Instrument Applicable in Minimally Invasive Surgery," *Int J Nat Eng Sci*, 4(1), pp. 53-60.
- [4] Minor, M., and Mukherjee, R., 1999, "A Mechanism for Dexterous End-Effector Placement During Minimally Invasive Surgery," *J Mech Des*, 121(4), pp. 472-479.
- [5] Velanovich, V., 2000, "Laparoscopic vs open surgery," *Surg Endosc*, 14(1), pp. 16-21.
- [6] Arrow Medical, 2012, "Bruder 5mm Ø Laparoscopic Instruments," <http://www.arrowmedical.com/sites/default/files/5MM%20LAP%20DISSECTOR,%20GRASPER,%20BIOPSY%20FORCEPS%20%26%20SCISSORS.pdf>.
- [7] Breedveld, P., 2010, "Steerable Laparoscopic Cable-Ring Forceps," *J Med Device*, 4(2), p. 027518.
- [8] Breedveld, P., Stassen, H. G., Meijer, D. W., and Stassen, L. P. S., 1999, "Theoretical background and conceptual solution for depth perception and eye-hand coordination problems in laparoscopic surgery," *Min Invas Ther Allied Technol*, 8(4), pp. 227-234.
- [9] Breedveld, P., Scheltes, J. S., Blom, E. M., and Verheij, J. E. I., 2005, "A new, easily miniaturized steerable endoscope," *IEEE Eng Med Biol Mag*, 24(6), pp. 40-47.
- [10] Jelinek, F., Pessers, R., and Breedveld, P., 2014, "DragonFlex Smart Steerable Laparoscopic Instrument," *J Med Device*, 8(1), pp. 015001-015009.
- [11] Catherine, J., Rotinat-Libersa, C., and Micaelli, A., 2011, "Comparative review of endoscopic devices articulations technologies developed for minimally invasive medical procedures," *Appl Bionics Biomech*, 8(2), pp. 151-171.
- [12] Fan, C., Dodou, D., and Breedveld, P., 2013, "Review of manual control methods for handheld maneuverable instruments," *Minim Invasive Ther Allied Technol*, 22(3), pp. 127-135.
- [13] Cepolina, F., and Michelini, R. C., 2004, "Review of robotic fixtures for minimally invasive surgery," *Int J Med Robot*, 1(1), pp. 43-63.
- [14] Cole, D., Harris, M. L., Castro, C. E., Stewart, J. S., Crews, S. T., and Balbierz, D. J., "Overtube Introducer for use in Endoscopic Bariatric Surgery," Barosense, Inc., US Patent 2009/0030284, January 29, 2009.
- [15] Parihar, S. K., Miller, M. C., and Worrell, B. C., "Robotically Controlled Surgical Instrument," Ethicon Endo-Surgery, Inc., US Patent 2013/0211397, August 15, 2013.
- [16] Parrott, D. A., Krupp, B. T., Gillum, C. L., Matice, C. J., and Mingione, L. P., "Articulating Laparoscopic Surgical Instruments," Carefusion 207, Inc., WO Patent 2012/058213, May 3, 2012.
- [17] Blase, B., "Articulated Section of a Shaft for an Endoscopic Instrument," Karl Storz GmbH & Co. KG, EP Patent 2 438 844, April 11, 2012.
- [18] Kleymann, G., and Taylor, E., "Articulating Laparoscopic Surgical Access Instrument," Tyco Healthcare Group LP, US Patent 2012/0296169, November 22, 2012.
- [19] Nai, T. Y., Herder, J. L., and Tuijthof, G. J. M., 2011, "Steerable Mechanical Joint for High Load Transmission in Minimally Invasive Instruments," *J Med Device*, 5(3), p. 034503.
- [20] Bakos, G. J., "Steerable Surgical Access Devices and Methods," Ethicon Endo-Surgery, Inc., US Patent 8,348,834, January 8, 2013.
- [21] Banik, M. S., Boulais, D. R., Couvillon, L. A., Chin, A. C. C., Anderson, F. J., Macnamara, F. T., Fantone, S. D., Braunstein, D. J., Orband, D. G., Saber, M., Hunter, I. W., Coppola, P. A., Kirouac, A. P., Clark, R. J., Wiesman, R. M., Mason, T. J., Mehta, N. R., and Greaves, A. E. R., "Articulation Joint," Boston Scientific Ltd., EP Patent 2 617 350, July 24, 2013.
- [22] Cooper, T. G., Wallace, D. T., Chang, S., Anderson, S. C., Williams, D., and Manzo, S., "Surgical Tool Having Positively Positionable Tendon-Actuated Multi-Disk Wrist Joint," Intuitive Surgical Operations, Inc., US Patent 2012/0220831, August 30, 2012.
- [23] Malkowski, J. T., "Surgical Articulation Assembly," Covidien LP, US Patent 2013/0178838, July 11, 2013.
- [24] Malkowski, J. T., and Hathaway, P., "Surgical Articulation Assembly," Tyco Healthcare Group LP, US Patent 2012/0310220, December 6, 2012.
- [25] Fiorini, P., Reppele, L., and Morselli, M., "Robotic Surgical Utensil," Surgica Robotica Sp.A., EP Patent 2 415 418, February 8, 2012.
- [26] Madhani, A. J., and Salisbury, J. K., "Articulated Surgical Instrument for Performing Minimally Invasive Surgery with Enhanced Dexterity and Sensitivity," Intuitive Surgical Operations, Inc., US Patent 2013/0110131, May 2, 2013.
- [27] Allred, J. B., and Bingham, R., "Endoscope Steering Section," Welch Allyn, Inc., US Patent 4,796,607, January 10, 1989.
- [28] Breedveld, P., Herder, J. L., and Tomiyama, T., "Teaching creativity in mechanical design," *Proc. IASDR2011. Diversity and Unity*, pp. 1-10.
- [29] Braun, M., "Surgical Instrument Comprising an Instrument Handle and Zero Point Adjustment," Tuebingen Scientific Surgical Product GmbH, US Patent 8,267,958, September 18, 2012.
- [30] Frede, T., Hammady, A., Klein, J., Teber, D., Inaki, N., Waseda, M., Buess, G., and Rassweiler, J., 2007, "The radius surgical system - a new device for complex minimally invasive procedures in urology?," *Eur Urol*, 51(4), pp. 1015-1022.
- [31] Kerver, L., Tang, B., Ho, F., and Nordell, B., "Method and Apparatus for Articulating the Wrist of a Laparoscopic Grasping Instrument," Aesculap Werke AG, EP Patent 2 240 095, November 7, 2012.

- [32] Marczyk, S., Pribanic, R., Farascioni, D., Taylor, E. J., and Hathaway, P., "Endoscopic Vessel Sealer and Divider Having a Flexible Articulating Shaft," Covidien LP, US Patent 2013/0274741, October 17, 2013.
- [33] Padgett, M., Skinlo, D., Weisel, T., and Chu, L., "Medical Device with Articulating Shaft," Surgical Solutions, LLC, EP Patent 1 786 335, July 24, 2013.
- [34] Stone, K. T., Walters, T. M., and Kaiser, R. A., "Steerable Suture Passing Device," Arthrotek, Inc., US Patent 2007/0038230, February 15, 2007.
- [35] Stroup, D. K., and Deptala, A., "Wrist Assembly for Articulating Laparoscopic Surgical Instruments," Carefusion 207, Inc., WO Patent 2013/154700, October 17, 2013.
- [36] Worrell, B. C., Bourdeaux, C. P., Conlon, S. P., Knight, G., Miller, M. C., Schieb, C. J., Shelton, F. E., Strobl, G. S., Swayze, J. S., Trees, G. A., Voegelé, A. C., Black, C. S., and Avimukta, K. B., "Articulation Joint Features for Articulating Surgical Device," Ethicon Endo-Surgery, Inc., WO Patent 2012/040445, March 29, 2012.
- [37] Brunnen, R. D., and Simon, T. J., "Flexible Section of an Insertion Tube of an Endoscope and Method of Manufacturing thereof," Henke-Sass, Wolf GmbH, US Patent 7,766,821, August 3, 2010.
- [38] Dawoodjee, A. E., "Flexible Laparoscopic Device," National Advanced Endoscopy Devices, Inc., WO Patent 2013/119817, August 15, 2013.
- [39] Tseng, H. T., "Flexible Tubular Interlocking Structure for a Handheld Endoscope," US Patent 2012/0190924, July 26, 2012.
- [40] Agarwal, S. K., Chatzigeorgiou, D., Petrzela, J. E., Menon, M. C., Lustrino, M., Slocum, A. H., and Stefanov-Wagner, C. J., 2011, "An Articulating Tool for Endoscopic Screw Delivery," *J Med Device*, 5(1), p. 011004.
- [41] Brock, D. L., and Lee, W., "Surgical Instrument," Hansen Medical, Inc., EP Patent 1 176 921, February 23, 2011.
- [42] Doyle, M. C., and Caputo, J., "Hand-actuated Articulating Surgical Tool," Carefusion 2200, Inc., EP Patent 2 005 914, April 4, 2012.
- [43] Hirzel, D. L., "Urethrovessical Anastomosis Suturing Method Using Articulating Laparoscopic Device," Terumo Corp., US Patent 8,460,320, June 11, 2013.
- [44] Jacobs, M., Armenteros, J. R., Barker, G., and French, C. K., "Surgical Clamp and Surgical Clamp Installation Tool," Advanced Bariatric Technology, LLC, US Patent 2011/0190791, August 4, 2011.
- [45] Kortenbach, J. A., Gottlieb, S., Smith, K. W., Slater, C. R., and Bales, T. O., "Rotatable and Deflectable Biopsy Forceps," Syntheon, LLC, US Patent 2003/0195432, October 16, 2003.
- [46] Krzyzanowski, J., "End Effector Assembly with Increased Clamping Force for a Surgical Instrument," US Patent 8,394,120, March 12, 2013.
- [47] Marczyk, S., "Surgical Stapling Apparatus with Powered Articulation," Tyco Healthcare Group LP, US Patent 2012/0298718, November 29, 2012.
- [48] Nicholas, D. A., Aranyi, E., Zvenyatsky, B., Matula, P. A., Remiszewski, S. H., Green, D. T., and Bolanos, H., "Articulating Endoscopic Surgical Apparatus," United States Surgical Corp., US Patent 2007/0162072, July 12, 2007.
- [49] Ouchi, T., "Treatment Tools for Endoscope," Hoya Corp., US Patent 7,857,749, December 28, 2010.
- [50] Scheib, C. J., Jaworek, G. S., and Hall, S. G., "Articulatable Surgical Instrument Comprising a Firing Drive," Ethicon Endo-Surgery, Inc., US Patent 2013/0270322, October 17, 2013.
- [51] Goldfarb, M. A., and Goldfarb, E., "Articulated Surgical Probe and Method for Use," Dynamic Surgical Inventions, LLC, US Patent 2012/0116398, May 10, 2012.
- [52] Joshi, S., Boulnois, J.-L., Woolfson, S. B., LePage, A. A., and Delvin, C., "Articulable Surgical Instrument," Microline Surgical, Inc., EP Patent 2 415 403, February 8, 2012.
- [53] Marescaux, J. F. B., Melanson, J. S., Dallemagne, B., Leroy, J., Mutter, D. R. D., Barry, J. P., Storz, S., and Leonhard, M., "Articulating Endoscope Instrument," Karl Storz Endovision, Inc., US Patent 8,137,263, March 20, 2012.
- [54] Menn, P., "Articulating Steerable Clip Applier for Laparoscopic Procedures," US Patent 2012/0265220, October 18, 2012.
- [55] Saadat, V., and Peh, R.-F., "Apparatus and Methods for Performing Transluminal Gastrointestinal Procedures," USGI Medical, Inc., US Patent 2011/0196392, August 11, 2011.
- [56] Hegeman, D. E., Danitz, D. J., Hinman, C. D., and Alvord, L. J., "Tool with Articulation Lock," Intuitive Surgical Operations, Inc., US Patent 2012/0095451, April 19, 2012.
- [57] Saadat, V., Rothe, C. A., Ewers, R. C., Maahs, T. D., and Michlitsch, K. J., "Endoluminal Tool Deployment System," USGI Medical, Inc., US Patent 2006/0178560, August 10, 2006.
- [58] Heimberger, R., "Bendable Tube and Method for its Manufacture," Richard Wolf GmbH, EP Patent 0 764 423, March 3, 2010.
- [59] Ananthanarayanan, A., Gupta, S. K., Ehrlich, L., and Desai, J. P., 2011, "Design of Revolute Joints for In-Mold Assembly Using Insert Molding," *J Mech Des*, 133(12), p. 121010.
- [60] Aust, G. M., and Taylor, T. E., "Surgical Instrument," Endius, Inc., US Patent RE39,152, June 27, 2006.
- [61] Belson, A., Frey, P. D., McElhaney, C. W. H., Milroy, J. C., Ohline, R. M., and Tartaglia, J. M., "Steerable Segmented Endoscope and Method of Insertion," Neoguide Systems, Inc., US Patent 2011/0065993, March 17, 2011.
- [62] Danitz, D. J., "Articulating Mechanism Comprising Pairs of Link Components Connected by Cables and which can be Easily Assembled," Novare Surgical Systems, Inc., WO Patent 2006/057699, June 1, 2006.
- [63] Harris, A. N., Thompson, J. R., and Rone, R. J., "Articulating Surgical Hand Tool," The Curators of the University of Missouri, WO Patent 2011/053735, May 5, 2011.
- [64] Hassoun, B., "Surgical Instrument," US Patent 2012/0316560, December 13, 2012.
- [65] Jeong, C. W., and Kim, H. T., "Minimally Invasive Surgical Instrument Having a Bent Shaft," WO Patent 2012/128591, September 27, 2012.

- [66] Lee, W., Chamorro, A., Ailinger, R., and Meglan, D., "Robotically Controlled Surgical Instruments," Hansen Medical, Inc., US Patent 7,699,835, April 20, 2010.
- [67] Lin, W.-T., and Chan, C.-C., "Four-dimensional Tip Deflection Device for Endoscope," Medical Intubation Technology Corp., US Patent 2010/0036202, February 11, 2010.
- [68] Mitchell, S., Ewers, R. C., and Maahs, T. D., "Endoluminal Surgical Tool with Small Bend Radius Steering Section," USGI Medical, Inc., US Patent 2012/0238952, September 20, 2012.
- [69] Oku, M., "Tube Assembly For Endoscope and Attaching Method," Fujifilm Corp., US Patent 2013/0245376, September 19, 2013.
- [70] Awtar, S., Geiger, J., Trutna, T. T., Nielsen, J. M., and Abani, R., 2010, "FlexDex™: A Minimally Invasive Surgical Tool With Enhanced Dexterity and Intuitive Control," *J Med Device*, 4(3), p. 035003.
- [71] Steege, A. T. C., "Surgical Tool," Agile Endosurgery, Inc., WO Patent 2013/009699, January 17, 2013.
- [72] Milani, M., Fiorini, P., and Reppele, L., "Instrument for Robotic Surgery," Surgica Robotica S.p.A., EP Patent 2 364 825, September 14, 2011.
- [73] Wallace, D. T., Anderson, C. S., and Manzo, S., "Platform Link Wrist Mechanism," Intuitive Surgical Operations, Inc., EP Patent 1 408 846, March 7, 2012.
- [74] Castro, M. S., and Flaherty, J. C., "Articulating Surgical Tools and Tool Sheaths, and Methods of Deploying the Same," Medrobotics Corp., WO Patent 2012/138834, October 11, 2012.
- [75] Danitz, D. J., and Gold, A., "Articulating Endoscopes," Novare Surgical Systems, Inc., US Patent 2010/0261964, October 14, 2010.
- [76] Hinman, C. D., and Danitz, D. J., "Link Systems and Articulation Mechanisms for Remote Manipulation of Surgical or Diagnostic Tools," Intuitive Surgical Operations, Inc., US Patent 2013/0218141, August 22, 2013.
- [77] Jeong, C. W., Sin, C. C., Kim, S. R., and Kim, H. T., "Minimally Invasive Surgical Instrument Having Detachable End Effector," Movasu, Inc., WO Patent 2013/036024, March 14, 2013.
- [78] Lange, G., "Endoscopic Surgical Instrument for Rotational Manipulation," La Precision, US Patent 6,666,854, December 23, 2003.
- [79] Lee, W., Chamorro, A., Fortier, R. C., and Cerier, J. C., "Surgical Instrument," Cambridge Endoscopic Devices, Inc., US Patent 2012/0253324, October 4, 2012.
- [80] Malkowski, J. T., Cabrera, R., Fortier, R., Ziegler, A., Cruz, A., Stellon, G. A., and Evans, S., "Articulating Surgical Device," Tyco Healthcare Group LP, US Patent 2011/0184459, July 28, 2011.
- [81] Park, H. Y., Kim, Y. J., Kim, J. H., and Lee, Y. B., "Link Unit, Arm Module, and Surgical Apparatus Including the Same," Samsung Electronics Co., Ltd., US Patent 2013/0199327, August 8, 2013.
- [82] Seow, C. M., Jian Chin, W., Nelson, C. A., Nakamura, A., Farritor, S. M., and Oleynikov, D., 2013, "Articulated Manipulator With Multiple Instruments for Natural Orifice Transluminal Endoscopic Surgery," *J Med Device*, 7(4), p. 041004.
- [83] Zirps, C. T., and Rebh, W. R., "Surgical Instrument," Endius, Inc., EP Patent 0 987 986, December 26, 2012.
- [84] Hallbeck, S. M., Riggle, J., Laveaga, A. D., and Kaufman, J., "Laparoscopic Devices and Methods of Using," Board of Regents of the University of Nebraska, WO Patent 2013/116692, August 8, 2013.
- [85] Boury, H. N., "Selectively Manipulable Catheter," US Patent 5,916,147, June 29, 1999.
- [86] Chong, E., "A Catheter Steering Device," CathRx Pty Ltd., US Patent 2008/0319418, December 25, 2008.
- [87] Erhard, M., "Laparoscopic Instrument," AMI Agency for Medical Innovations GmbH, EP Patent 1 584 293, October 12, 2005.
- [88] Griffiths, J. R., "System and Method for an Articulating Distal End of an Endoscopic Medical Device," Symmetry Medical New Bedford, Inc., US Patent 2013/0150831, June 13, 2013.
- [89] Knodel, B. D., Thompson, B., Manoux, P. R., and White, N. H., "Method for Treating Tissue With an Articulated Surgical Instrument," Cardica, Inc., US Patent 2012/0061446, March 15, 2012.
- [90] Kovac, T. J., and Wei, M. F., "Endoscopic Surgical Instrument for Rotational Manipulation," Origin Medsystems, Inc., US Patent 6,663 641, December 16, 2003.
- [91] Lenker, J. A., and Pool, S. L., "Steerable Endoluminal Punch," Indian Wells Medical, Inc., WO Patent 2013/158354, October 24, 2013.
- [92] Lyons, E., Rose-Innes, D. J., and Brewer, R. J., "Surgical Instrument," Gyrus Medical Ltd., US Patent 8,241,320, August 14, 2012.
- [93] Verbeek, M. A. E., "Steerable Tube, Endoscopic Instrument and Endoscope Comprising Such a Tube, and an Assembly," Fortimedix B.V., WO Patent 2012/173478, December 20, 2012.
- [94] Viola, F. J., "Surgical Stapler Having an Articulation Mechanism," Covidien LP, US Patent 2013/0032627, February 7, 2013.
- [95] Shelton, F. E., and Ortiz, M. S., "Articulatable Surgical Device with Rotary Driven Cutting Member," Ethicon EndoSurgery, Inc., US Patent 2013/0197556, August 1, 2013.
- [96] Breedveld, P., and Hirose, S., 2004, "Design of Steerable Endoscopes to Improve the Visual Perception of Depth During Laparoscopic Surgery," *J Mech Des*, 126(1), pp. 2-5.
- [97] Cooper, T. G., and Anderson, S. C., "Flexible Wrist for Surgical Tool," Intuitive Surgical Operations, Inc., US Patent 2013/0096540, April 18, 2013.
- [98] Danitz, D. J., and Hinman, C. D., "Articulating Sheath for Flexible Instruments," Novare Surgical Systems, Inc., EP Patent 2 335 558, June 22, 2011.
- [99] Harder, H. E., Jensen, H.-I., and Speitling, A. W., "An Elongate Element for Transmitting Forces," Howmedica GmbH, EP Patent 0 889 252, April 2, 2003.
- [100] Hermann, R., Hegemann, O., and Lutze, T., "Surgical Instrument," Aesculap AG, US Patent 8,382,742, February 26, 2013.

- [101] Lee, W., Chamorro, A., and Lee, W., "Surgical Instrument," Cambridge Endoscopic Devices, Inc., US Patent 8,029,531, October 4, 2011.
- [102] Lin, W.-T., "Two-way Endoscope Steering Mechanism and Four-way Endoscope Steering Mechanism," Pioneer Medical Instrument Co., Ltd., US Patent 2013/0158355, June 20, 2013.
- [103] Wallace, D. T., Moll, F. H., Younge, R. G., Martin, K. M., Stahler, G. J., Moore, D. F., Adams, D. T., Zinn, M. R., and Niemeyer, G. D., "Robotic Catheter System," Hansen Medical, Inc., US Patent 8,409,136, April 2, 2013.
- [104] Dewaele, F., Mabilde, C., and Blanckaert, B., "Steerable Tube," Steerable Instruments B.V.B.A., EP Patent 2 259 710, May 15, 2013.
- [105] Burgner, J., Swaney, P. J., Bruns, T. L., Clark, M. S., Rucker, D. C., Burdette, E. C., and Webster, R. J., 2012, "An Autoclavable Steerable Cannula Manual Deployment Device: Design and Accuracy Analysis," *J Med Device*, 6(4), p. 041007.
- [106] Hendrick, R. J., Lathrop, R. A., Schneider, J. S., and Webster, I. I. R. J., 2013, "Design of an Endonasal Graft Placement Tool for Repair of Skull Base Defects," *J Med Device*, 7(2), p. 020916.
- [107] Yen, P.-L., Chu, Y.-J., Hu, R.-H., Yeh, C.-C., and Luo, R. C., 2013, "An Automatic Object Tracking Steerable Endoscope," *J Med Device*, 7(3), p. 030921.
- [108] Zhang, J., and Simaan, N., 2013, "Design of Underactuated Steerable Electrode Arrays for Optimal Insertions," *J Mech Robot*, 5(1), p. 011008.
- [109] Breedveld, P., and Scheltes, J. S., "Instrument for Fine-Mechanical or Surgical Applications," Technische Universiteit Delft, US Patent 2008/0234545, September 25, 2008.
- [110] Melsky, G., "Irrigation and Aspiration Device," Scope Medical, Inc., US Patent 2005/0119614, June 2, 2005.
- [111] Miller, A. J., "Steerable Endoluminal Devices and Methods," BioCardia, Inc., US Patent 2012/0123327, May 17, 2012.
- [112] Nardeo, M., "Steerable Medical Catheter with Bendable Encapsulated Metal Spring Tip Fused to Polymeric Shaft," US Patent 6,530,897, March 11, 2003.
- [113] Pilvisto, T., "Endoscope-type Device, Especially for Emergency Intubation," Karl Storz GmbH & Co. KG, US Patent 6,887,195, May 3, 2005.
- [114] Stefanchik, D., and Ghabrial, R. M., "Methods for Stabilizing and Positioning an Endoscope and Surgical Procedures," Ethicon Endo-Surgery, Inc., US Patent 2008/0021277, January 24, 2008.

Chapter 6

DragonFlex

Smart Steerable Laparoscopic Instrument

Filip Jelínek, Rob Pessers and Paul Breedveld

Published in Journal of Medical Devices 8(1), 2014.

Abstract

Introduction | Despite its success, e.g. in prostatectomy, da Vinci's steerable grasper EndoWrist from Intuitive Surgical has a complex design prone to steel cable fatigue, potential sterilisation issues and high associated costs, all of which insinuate a need for an alternative. The aim of this paper is to demonstrate a design of a structurally simple handheld steerable laparoscopic grasping forceps free from cable fatigue, while attaining sufficient bending stiffness for surgery and improving on EndoWrist's manoeuvrability and dimensions.

Methods | Having equal joint functionality to EndoWrist, DragonFlex's instrument tip contains only four parts, driven and bound by two cables mechanically fixed in the handle. Two orthogonal planar joints feature an innovative rolling link mechanism allowing the cables to follow circular arc profiles of a diameter 1.5 times larger than the width of the instrument shaft. Besides maximising the cable lifespan, the rolling link was designed to equalise the force requirements on both cables throughout joint rotation, making the handling fluid and effortless. The smart joint design and stacked instrument construction enable control of seven degrees of freedom by only two cables and seven instrument components in tip, shaft and handgrip altogether.

Results and Conclusions | Two DragonFlex prototypes were developed by means of additive manufacturing technology, allowing grasping and omnidirectional steering over $\pm 90^\circ$, exhibiting promisingly high bending stiffness and featuring extreme simplicity at 5mm dimensions. DragonFlex concept sheds new light on the possibilities of additive manufacturing of surgical instruments, allowing for a feature-packed design, simple assembly, suitability for a disposable use and potential MRI compatibility.

6.1 Introduction

6.1.1 Laparoscopy and Steerable Instruments

Conventional surgical procedures require open access to the operation site via a long incision, resulting in abundant postoperative scar tissue and relatively long recovery time. Minimally invasive surgery (MIS) was introduced to ameliorate these negative effects [1-5]. In particular, laparoscopy – minimally invasive surgery in the abdomen – involves making one or several small incisions in the abdominal wall in order to accommodate trocars. These serve as airtight seals used for the inflation of the abdominal cavity with carbon dioxide, creating a working space for the surgeon, as well as the portals for the instruments. Long and slender endoscopes and instruments provide either a visual feedback or tissue manipulation features.

Laparoscopic instruments can be differentiated into rigid [6] and steerable [7] (Fig. 6.1(a)) [4, 5]. The configuration of the rigid ones comprises a handle, a rigid shaft and a tip, which equips them with four degrees of freedom (DOF), these being axial sliding, axial rotation and pivoting in two perpendicular planes around the incision point (Fig. 6.1(b)) [8]. This fulcrum effect greatly restricts the range of motion and limits the surgeon mainly to frontal or sideways approach to the tissue [5, 7]. In contrast, steerable instruments have additional degrees of freedom due to one or more joints in the tip, enabling the surgeon to reach behind or over obstacles (Fig. 6.1(c)) [5, 7, 9].

6.1.2 Steerability at the Expense of Complexity and Vulnerability

A state-of-the-art example of a steerable instrument is Intuitive Surgical's EndoWrist (Fig. 6.2(a)) [10, 11] made for the da Vinci master-slave system and favourably used in prostatectomy procedures [12, 13]. In its basic design, EndoWrist has two rotational DOF acting in two perpendicular planes in a form of pulleys, each individually controlled

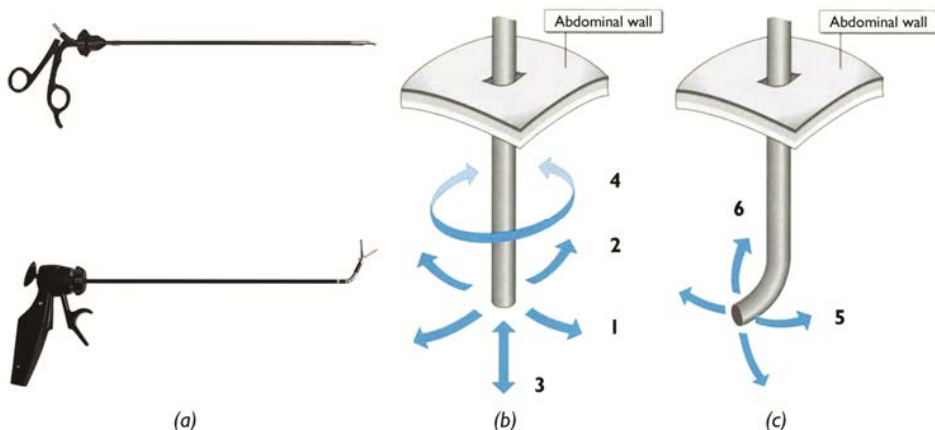


Figure 6.1 (a) Rigid [6] & steerable [7] laparoscopic instruments; (b) Rigid instrument DOF [8]; (c) Additional steerable tip DOF.

by a looped cable (Fig. 6.2(b)) [5, 11]. In ideal conditions, once the cables are fully tensioned, there should be no room for backlash in the joints. The stiffness of the tip is therefore mainly dependent on the tensile strength of the cables and stiffness of the rigid bodies within the tip. Since both the steel cables and the rigid bodies are highly stiff, EndoWrist can be considered stiff as well.

Despite its high stiffness, EndoWrist's lifespan is limited to only ten procedures [7, 10, 14, 15]. From a purely mechanical perspective, i.e. disregarding possible failure synergists such as sterilisation, the main limiting factor here is the fatigue resistance of the steel cables, which are guided over pulleys whose diameter is smaller than half of the tip's width. By taking a closer look at the EndoWrist's design [16], it can be observed that the pulley-to-cable diameter (D/d) ratio is within a range of 6 to 8. According to a safe engineering practice, the recommended minimum D/d ratio ranges from 18 to 42, thus helping to prevent or postpone cable fatigue due to high bending stresses arising from excessively small bending radii [17-20]. Hence, after repeatedly bending and rolling over a very small radius, the steel cables in EndoWrist inevitably fail resulting in expensive replacement and maintenance costs [5, 15]. Moreover, the tip features a complex design of numerous miniature elements, including pulleys and rivets, leading to high manufacturing and assembly costs as well as potential sterilisation issues [5, 7, 15].

6.1.3 Ideal Configuration Requirements

Taking into consideration the scope of the potential improvements, one would desirably aim for a design of a structurally simple steerable laparoscopic instrument tip free from cable fatigue, while attaining sufficient bending stiffness for the surgical environment

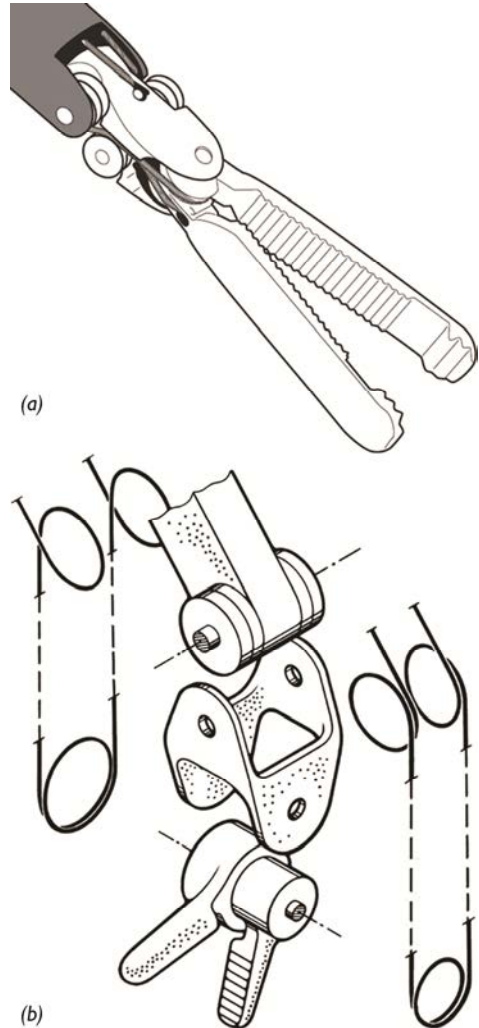


Figure 6.2 (a) Close-up of one of the EndoWrist's tips, Pericardial Dissector [10]; (b) Impression of the EndoWrist's exploded view showing pulleys and driving cables [5], based on the original patent by Madhani et al. [11].

and possibly even improving on EndoWrist's manoeuvrability and dimensions. Considering all these requirements, at TU Delft we designed a smart steerable laparoscopic instrument prototype named DragonFlex.

6.2 DragonFlex Design

6.2.1 Planar Joint Design

As already mentioned, one of the major limitations of EndoWrist is the small bending radius of the steel cables. One conceivable solution to address this issue could involve an adequate choice of sterilisable material that would be more fatigue resistant, e.g. a steel cable of more braids better suited for bending. However, even if this proved to increase the cable lifespan, a fundamentally stronger solution would be eliminating one of the fatigue causes, rather than just treating its symptoms. Therefore, in order to improve both the reliability and the lifespan of cable-driven joints, a solution pursued in this paper involves maximising the cable bending radius to its theoretical limits.

One straightforward approach for increasing the cable bending radius is widely implemented in conventional flexible endoscopes such as gastroscopes, or colonoscopes, as well as in a number of steerable laparoscopic instruments. These involve state-of-the-art instruments such as Cambridge Endo's Laparo-Angle [21], Covidien's SILS Hand Instrument [22], the cable-ring forceps developed at TU Delft [7, 23] (Fig. 6.1(a)) and many others, developed for either handheld or robotic applications and discussed in detail in the review articles by Fan et al. [23] and Catherine et al. [24]. In all these instruments, instead of guiding the cables sharply over one hinge, the cables are smoothly guided along a series of hinged elements that together form a flexible shaft section with a bending radius sufficiently large as to avoid fatigue [5, 7, 9]. A drawback of a majority of such mechanisms is the rise in complexity and a strong reduction of stiffness due to introducing underactuated DOF.

The problem of underactuated DOF may be resolved by aiming to control each joint individually, as achieved by Breedveld et al. [25] with their Ø5mm fully actuated Multi-Flex prototype (Fig. 6.3) [7, 23, 25]. However, despite the individual joint actuation and high resultant stiffness, such mechanisms also suffer from elevated design complexity and associated issues.

While building on the full actuation principle, the opposite approach,



Figure 6.3 Cable-ring mechanism-based Multi-Flex prototype [7, 23, 25] featuring a fully actuated ten DOF tip (excluding tip function), developed within the BITE-group of BioMechanical Engineering Dept., TU Delft.

implemented in EndoWrist and in our DragonFlex design, is decreasing the number of steerable elements to the bare minimum, which is two mutually rotatable elements per one planar rotational DOF.

Logically, without any further design modifications, once a 90° bend is made with only two elements, the cable bending radius at the inner bend gets critically small, as observed in Fig. 6.4(a). Combined with the tensile forces exerted on the cables during manipulation, the immediate critical consequences i.e. cable kinking, breakage, unbraiding and ultimate failure would be inevitable. However, once the cables are leaning over pulleys of sufficient bending radius, the fatigue problem could be overcome easily.

While EndoWrist implements the use of pulleys in its design, it is their diameter that is problematic as explained earlier. The question is then how to maximise the diameter of a pulley preferably even beyond the instrument diameter. A solution for this seemingly unsolvable design challenge can be found once one reaches beyond the concept of a regular perfectly circular pulley.

Let us imagine a simple planar scenario featuring two generic mutually rotatable elements with two driving cables running along them on both sides (Fig. 6.4(a)). Once a turn is made towards either side, the cables actually need to bend and slide only over a small section of a round profile on either side of the joint and not necessarily over a fully circular profile like a pulley that fits within the instrument diameter (Fig. 6.4(b)). Therefore, one can split a fixed circular profile along the instrument's longitudinal axis into two equal axisymmetric non-tangential arcs (Fig. 6.4(c)). By this means, the arcs' individual diameters can be increased beyond the instrument's diameter as much as the lengths of the tip elements allow, creating a leaf or drop like shape, yet confined within the instrument's width.

Furthermore, once the rotation is made to either side, both the inner and outer cables need such arced guiding profiles on both their sides to avoid sharp bends.

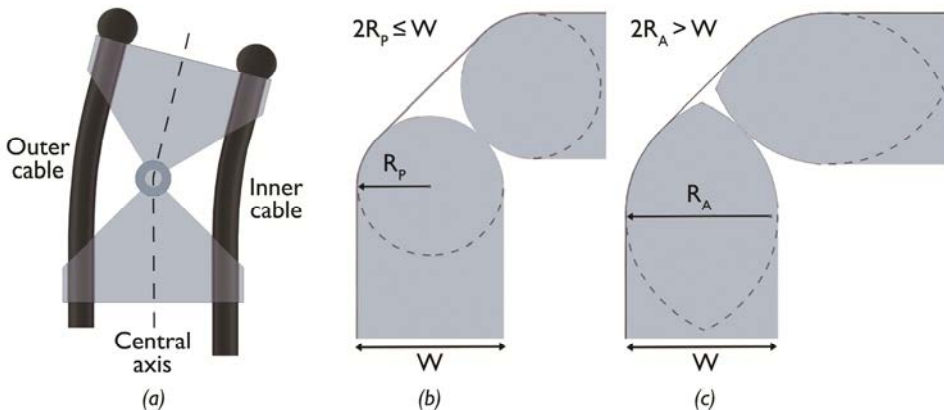


Figure 6.4 (a) Two generic cable driven joint elements with no cable support; Once axisymmetric arced guides (c) are implemented, the cable bending radius R_A is far superior to the pulley's radius R_p (b) at a given element width W .

Therefore, maintaining the design compact, the cables need to be guided along the instrument's central axis, rather than along the outside of the joint, with enough material on both their sides to accommodate the arced guides. Therefore, each tip element should feature four arced guides, two inner and two outer, in order to support both cables during the rotation to either side (Fig. 6.5(a)).

In order to determine a theoretically maximal guide radius for both cables at any turn, the arcs' radii have to be equal and the cables are assumed to be infinitely thin, i.e. as curved lines. A smooth cable trajectory along the inner and outer guides can be then achieved by maintaining tangency between the inner guides themselves; the outer guides and the inner guides; as well as the outer guides and the outer boundaries of the elements at their width (Fig. 6.5(b)). In order to achieve smooth cable transfer from one element to another at $\pm 90^\circ$ joint rotation, the inner guides' arc lengths have to run over 45° each. Hence, setting the inner guide arc angle α to 45° , the maximum allowable arc radius R_B can be determined as shown in Eq. (6.1), where $\cos \alpha = 1/\sqrt{2}$ and W is the element width:

$$R_B = \frac{W}{2} + R_B \cos \alpha = \frac{W}{2(1-\cos \alpha)} = \frac{W}{2-\sqrt{2}} = 1.7 W \quad (6.1)$$

The result shows that the arc radius is only dependent on the element width with a theoretical maximum of 1.7 times the element width, whereas in EndoWrist the bending radius of the steel cables is at maximum only 0.25 times the instrument width.

Despite this enthusiastic finding, the current joint configuration is still imperfect due to the following reason. The joint elements, pictured in Fig. 6.5(a), feature a common

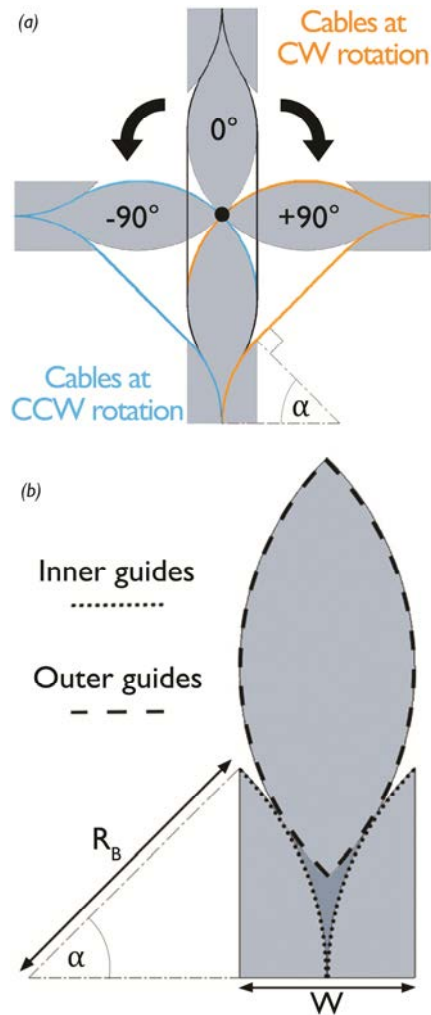


Figure 6.5 (a) Hinge concept showing cables supported by inner and outer guides at CW and CCW bends; (b) Hinge element, of width W , featuring four guides, of equal radius R_B , with inner guides running along arc angle α .

connection point, which is essentially a hinge (the black dot in the figure). Once the joint is fully bent, the outer cable will run exactly through this point of rotation, which leads to a zero moment arm, disabling the straightening of the elements. Evidently, rather than a fixed hinge, the joint needs a moving point of rotation that would provide a moment arm for both cables anywhere within $\pm 90^\circ$. An articulation having this property is a rolling joint, featuring two arc-shaped surfaces rolling over each other, resulting in a varying point of contact [5, 26, 27]. In Fig. 6.6, the rolling

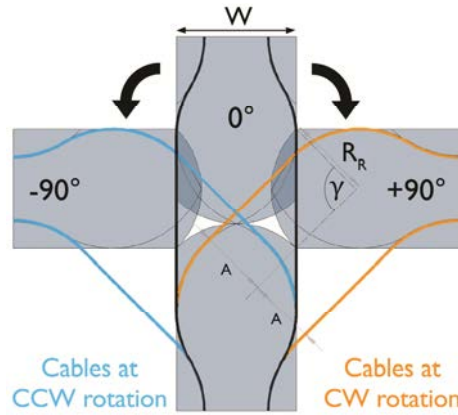


Figure 6.6 Improved rolling joint concept, of radius R_R and angle γ , with cable moment arms A mutually equal at 0° and $\pm 90^\circ$.

surface is integrated on top of the existing geometry presented previously in Fig. 6.5. In order to maintain tangency during the full joint rotation of $\pm 90^\circ$ the rolling joint arcs have to run over 90° each; ending at $\pm 45^\circ$ at the left and the right side of the shaft. The radius of the rolling joint arc R_R is only dependent on the element width W in the following fashion, Eq. (6.2), where γ is the rolling arc angle of 90° :

$$R_R = \frac{W/2}{\sin(\gamma/2)} = 0.7 W \tag{6.2}$$

However, maximising the radii of either the arced guides or the rolling surfaces, may not necessarily be advantageous at all times. Various configurations of guide arc lengths and rolling joint arc lengths showed that, at full bends, the inner and outer cables get unequally eccentric from the central axis and can, therefore, have noticeably differing moment arms (Fig. 6.7). For that reason, not only should the moment arms of both cables be equal at a straight position, they also have to be the same at the extremes of $\pm 90^\circ$. Upon inputting these boundary conditions and relations into a complex 2D geometrical SolidWorks model, it was revealed that in this fully constrained scenario, the

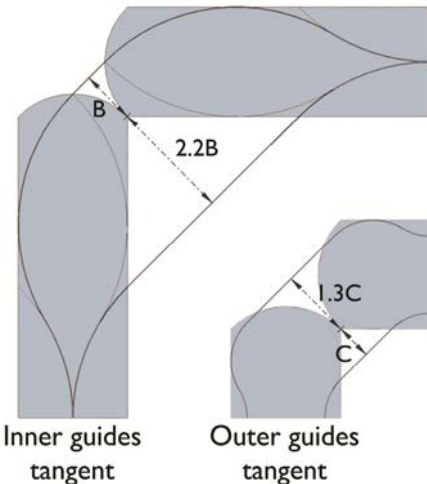


Figure 6.7 Unless the cable moments arms are equalised, they may differ considerably depending on the cable guide constraints; at the extremes defined by inner and outer guide tangency, the moment arms B & C can differ by factors 2.2 & 1.3, respectively.

maximum realisable arced guide radius R_B is now approximately 0.8 times the width of the element. The mutual difference of the moment arm means between the inner and outer cables during rotation is in that case less than 0.1mm at the element width of 5mm, which can be considered negligible (Fig. 6.8). Hence, the tensile forces acting on both cables at any point of rotation to either side can be regarded as equal. Once cables of non-zero thickness t are introduced to the element design, the original maximum arced guide radius ($R_B = 0.8W$) decreases by the radius of the cable cross-section to ($R_B' = R_B - 0.5t$). At 5mm element width and $\varnothing 0.4$ mm cable channels, the maximum guide radius R_B decreases from 0.8 to 0.75 times the width of the element – still being much larger than the 0.25 factor in EndoWrist’s pulley design.

In terms of functionality, a simple planar rolling joint relies solely on friction between its two surfaces, when resisting sideways slip. For that reason, involute gear profiles were implemented in the rolling joint (Fig. 6.9) with their pitch diameter exactly following the arced rolling surfaces. This leads to a strong, reliable joint structure resistant to tangent forces.

6.2.2 From Planar to Spatial, from Tip to Handle

The 2D joint construction can be easily translated into the third dimension by giving it a depth, for instance equal to the element width, hence creating a square cross-section. In the planar scenario, the joint needed to be resistant only to two translational DOF (along x & y axes) (Fig. 6.10(a)). The undesired joint translation along x and y axes is prevented by gears and tight cable

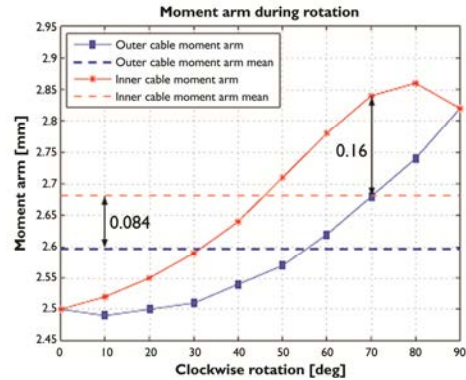


Figure 6.8 In the optimised 5mm wide joint design, the inner and outer cable moment arms change slightly during rotation, by 0.35mm, nevertheless their mutual length difference is negligibly small: on average 0.084mm and 0.16mm at its maximum.

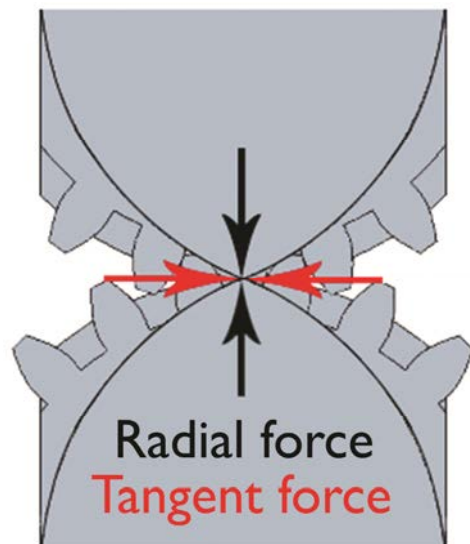


Figure 6.9 Gears were incorporated in the rolling joint design to resist tangent forces and prevent slippage. Their pitch diameter exactly follows the arced rolling surfaces to prevent tooth jamming once radial forces are applied.

connection respectively. However, introducing another dimension requires further measures preventing the joint motion in two additional rotational DOF (x - z & y - z planes) and one translational DOF (z axis). In order to eliminate the new DOF, a protrusion was added to one element, combined with a cut-out in the opposite element (Fig. 6.10(b)). This way the geared rolling joint is allowed only one rotational DOF (x - y plane) as required. As the joint design is essentially planar in both 2D and 3D, allowing only for one rotational DOF, the second joint in the tip is duplicated and turned axially 90° , in order to allow pivoting in the perpendicular plane and hence full two DOF motion in 3D space.

Apart from the two orthogonal planar joints, the tip features a novel grasper design which is also hinge-free. In the grasper, the forceps copies the basic element design consisting of a rolling joint, gears and protrusions, yet split axially in the middle, as to enable independent motion of the two jaws. Furthermore, they feature additional outer flaps preventing them from splitting transversely while opening the grasper (Fig. 6.11).

In the grasper, the cables are looped and fixed thus enabling jaw opening and closing. This looping of the two driving cables doubles the number of their ends one can pull at. These four ends work in pairs. For instance, to pivot the proximal tip joint to the side, both side cable ends are pulled. If only one of these two ends is pulled, the motion is transmitted further to either the distal joint or the jaw. The same working principle applies to the distal joint, where only pulling of both cable ends in a pair results in its pivoting. If only one cable end is pulled again, this results either in jaw opening or closing. For analogy, one can refer to EndoWrist (Fig. 6.2(b)). Figure 6.12 illustrates how the driving cables are guided over the proximal joints in the tip and the handle. Here one can clearly see

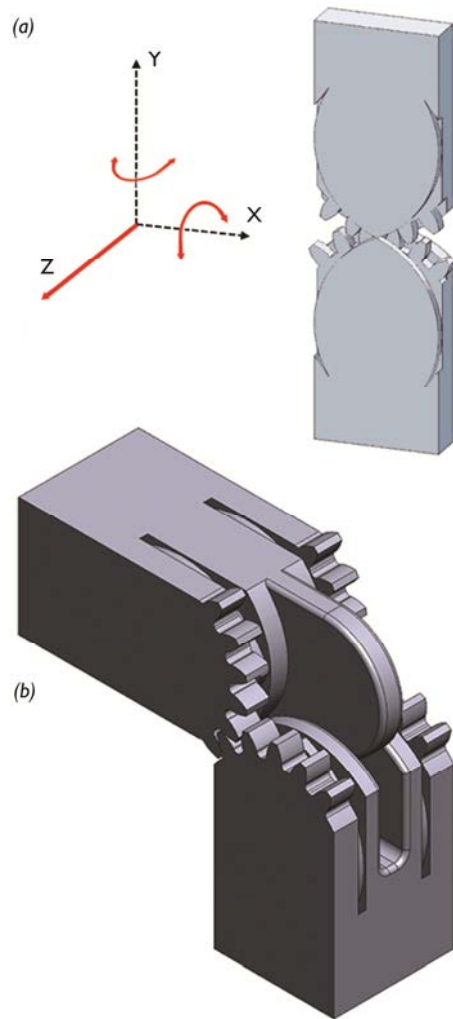


Figure 6.10 (a) Apart from translation along x & y axes, the rolling joint needs to resist two additional rotational DOF (x - z & y - z planes) and one translational DOF (z axis); (b) A protrusion was added to help allow only one required rotational DOF (x - y plane).

the intuitively controllable parallelogram motion [9] of the whole construction, where a clockwise rotation of the handle results in a clockwise rotation of the tip and vice versa, which is then repeated in the distal joints.

Being the tip's almost identical counter-copy, the handle utilises the basic element design featuring two individually controllable orthogonal planar joints (wrist controlled) ending with an openable scissor-like handgrip (finger controlled) connected to them via the identical rolling link mechanism. The handle joint elements are further equipped with angled protrusions on their sides that stop the individual joint/jaw rotation at both the handle and the tip at the maximum of $\pm 90^\circ$ (Fig. 6.12).

6.2.3 Prototypes

Despite its novel design, the question of materialising the DragonFlex prototype might seem unsolvable in terms of conventional manufacturing methods. Besides the miniature features on each joint element, such as the gear teeth or the protrusions, the most difficult design aspect to machine would be the embedded curved cable holes in all the elements. Nevertheless, additive manufacturing technology [28-33] easily helped resolve these issues by generating fast and relatively inexpensive prototypes.

In order to evaluate the mechanical principle and the design feasibility from a merely geometrical point of view, an upscaled DragonFlex prototype of 15mm shaft width was first made by additive manufacturing from a resin-like Objet VeroBlue™ RGD840 material (Fig. 6.13). The prototype was printed at TU Delft at 0.1mm voxel



Figure 6.11 Three DOF grasper design showing the jaw flaps and the looped driving cables.

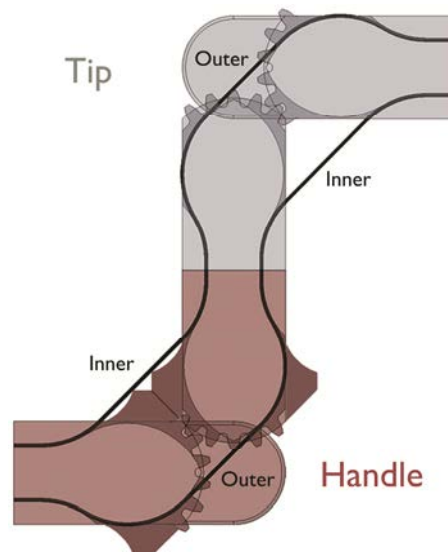


Figure 6.12 Cables are smoothly guided along the instrument and enable parallelogram motion.

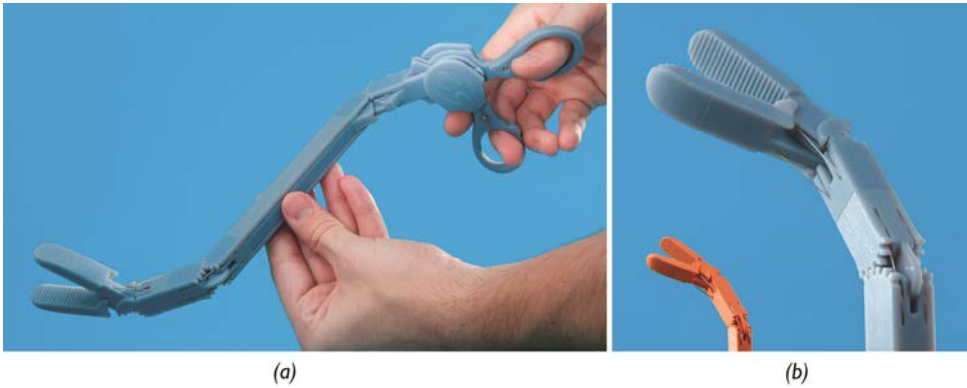


Figure 6.13 (a) Upscaled plastic DragonFlex prototype demonstrating tip opening and pivoting in two DOF; (b) Close-up picture highlighting the striking size difference between the 5mm & 15mm thick prototype tips.

resolution, using Objet Eden260V™ 3D printer, and later assembled and fitted with $\varnothing 0.3\text{mm}$ steel cables (D/d ratio of 75).

After a successful functionality test, a real-scale DragonFlex prototype of 5mm shaft width was manufactured in a close collaboration with the Dutch Organisation for Applied Scientific Research (TNO) in Eindhoven, which is highly specialised in the development of state-of-the-art additive manufacturing machines. The real-scale prototype was made by micro-stereo lithography [33], Digital Light Processing™ (DLP) method [29], from a ceramic-filled epoxy resin, EnvisionTEC® NanoCure RCP 30, and printed by Perfactory® SXGA+ Mini Multi Lens rapid prototype manufacturing system at $30\mu\text{m}$ resolution and $50\mu\text{m}$ layer thickness. Figure 6.14 illustrates the printing process and separate manufactured elements. The real-scale DragonFlex prototype (Fig. 6.15) was fitted with $\varnothing 0.2\text{mm}$ Dyneema cables (D/d ratio of 37.5) for the sake of easier handling during assembly. For future surgical applications Dyneema could be replaced by much stiffer steel cables whose bending radius is a significant issue, as elaborated in this paper.

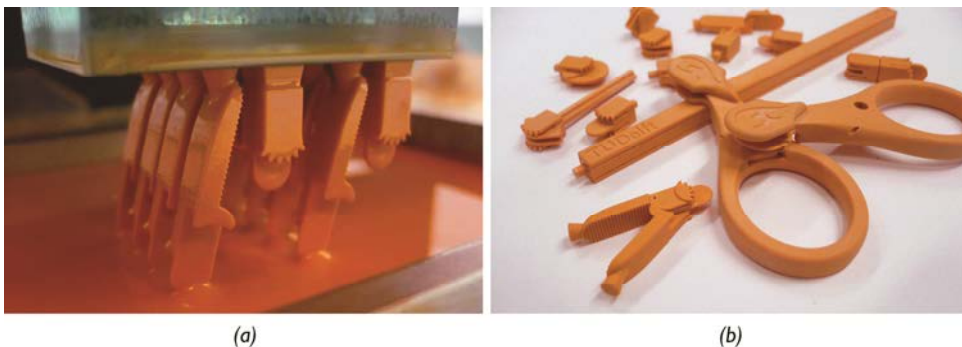


Figure 6.14 (a) Real-scale DragonFlex prototype components 3D-printed from a ceramic-filled epoxy resin; (b) Individual solidified components after the printing process (courtesy of TNO).

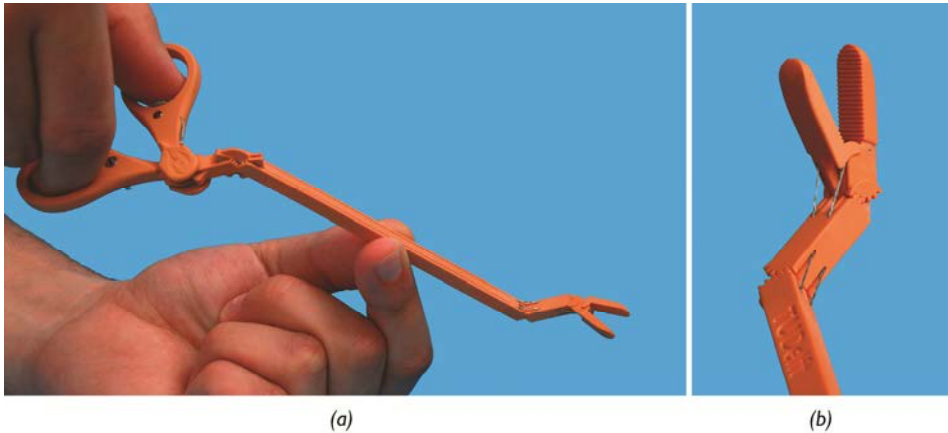


Figure 6.15 (a) Real-scale ceramic DragonFlex prototype allowing seven DOF control by only seven structural components; (b) Close-up on the tip showing joint and jaw actuation by Dyneema cables.

6.2.4 Performance

Simple functionality tests in a form of everyday manipulation revealed no cable fatigue or any other structural failure, visible to the naked eye, in either prototype to this day. Grasping and omnidirectional steering over $\pm 90^\circ$ proved to work successfully with a very large maximum grasper opening angle of 180° . Thanks to the novel cable guide design, the prototypes' joints exhibited a promisingly high bending stiffness, i.e. bending resistance to external forces, which will be evaluated quantitatively with respect to the state of the art in further experiments. The upscaled prototype experienced a little wear, due to the use of the steel cables interfacing with a relatively soft plastic. In the real-scale prototype, Dyneema cables proved to minimise the material wear at low friction. Yet, the shaft of the real-scale ceramic prototype turned out to be much more flexible than a standard laparoscopic instrument shaft, which would insinuate a need for an additive manufacturable material of superior mechanical properties. Nevertheless, none of the material drawbacks had any detrimental effect on the prototypes' performance in free space and they continue to function flawlessly during daily demonstrations.

6.3 Discussion

6.3.1 Instrument Highlights and Limitations

DragonFlex's minimalistic design shows that steerable MIS instruments can be designed stacked, without axles or hinges. This essentially simplifies the design, manufacture and assembly while minimising the number of instrument parts per controlled DOF. Referring back to Fig. 6.2(b), the ability to steer and manipulate the grasper over $\pm 90^\circ$ in three DOF by only two looped cables, or four cable ends, is analogous to EndoWrist [7]. Nevertheless, the three DOF tip of DragonFlex consists of only four parts, which is the

theoretical minimum, compared to more than ten parts in EndoWrist. As a matter of fact, the entire instrument enables controlling seven instrument DOF by only two cables and seven structural instrument components; the seven DOF comprising the conventional four rigid instrument DOF (Fig. 6.1(b)), the two steerable tip DOF (Fig. 6.1(c)) and the opening/closing DOF of the grasper.

Nonetheless, DragonFlex comes with a drawback of sticking-out cables and joint protrusions. During rotation, the inner cables tend to be more displaced from the instrument centreline with the increasing angle of the bend. Combined with the small gears, slots, grooves and long narrow curved cable channels, the instrument would be hardly cleanable and sterilisable in its current shape. This issue could be solved by a flexible seal that would encompass each planar joint allowing for reusability. However, this seal would have to be flexible enough to allow variable cable eccentricity while resisting the harsh treatment of steam sterilisation. On the other hand, since the instrument could be manufactured relatively inexpensively, it would be highly suited for a disposable use, providing it was additive manufactured from a biocompatible material. Depending on the choice of material and the force requirements of the surgical environment, the gears might eventually prove prone to fatigue. In such circumstances, a belted rolling joint could be utilised instead, incorporating flexures for higher load transmission [34]. Nevertheless, this could in turn introduce complexity to the current DragonFlex design.

6.3.2 Opportunities for Further Research

In the context of surgical workspace, the real-scale fully actuated segmented DragonFlex tip might reveal new steering techniques for tissue approach, different from a single two DOF joint assembly used in most of the state-of-the-art instruments. Nevertheless, the displacement of the two planar joints in the DragonFlex tip is about threefold in comparison with EndoWrist. Hence, solutions regarding joint element shortening or development of a single two DOF joint of comparable performance would be researched further.

Besides ameliorating the listed issues and considerably lengthening the instrument shaft, the opportunities for future research could include introducing a circular cross-section to the design or investigating the possibilities of mass production by additive manufacturing.

Layer-building additive manufacturing processes are very fast and much more affordable than the conventional manufacturing methods [30-33], as well as allow for a feature-packed design that would be normally extremely hard to achieve [28]. Furthermore, contrary to injection moulding, there are no set-up costs involved, due to no need for a metal die, the manufacture of which is the main reason why injection moulding is only economical for mass production [30-32]. Yet, for surgical purposes, suitable biocompatible materials would have to be used, such as EnvisionTEC® E-Dent 100 – a strong non-metallic material used in the dental industry, thus being a promising candidate also with regard to its superior mechanical properties.

The micro-stereo lithography process, used in the making of the real-scale prototype, not only features a minimum resolution of approximately $30\mu\text{m}$, but also enables printing in metal or even a simultaneous combination of materials [29-31, 33]. Such a striking advantage could open far-reaching opportunities in the MIS instrument manufacture. For instance, apart from a fast and relatively inexpensive production, printing plastics, ceramics and metals together could enable fusion of complex mechanical functionality with electronic circuits, e.g. in steerable bipolar forceps, which are conventionally very problematic in terms of sealing. Furthermore, similar materials as those used in the current real-scale DragonFlex prototype, i.e. ceramics and Dyneema, could help enable the development of MRI compatible MIS instruments.

6.4 Conclusions

To summarise, in addition to steering the tip in $\pm 90^\circ$ and operating its grasper, as in the EndoWrist design, DragonFlex's tip contains only four parts, driven and bound by two cables mechanically fixed in the handle. Two orthogonal planar joints feature an innovative rolling link mechanism allowing the cables to follow circular arc profiles of a diameter 1.5 times larger than the width of the instrument shaft; whereas EndoWrist uses simple pulleys of barely half of the instrument shaft diameter. Besides maximising the cable lifespan, the rolling joint was designed to equalise the length of and forces on both cables throughout the joint rotation, making the handling fluid and effortless. The smart joint design and stacked instrument construction enable control of seven DOF by only seven structural instrument components. DragonFlex concept sheds a new light on the possibilities of additive manufacture of the surgical instruments, allowing for a feature-packed design, simple assembly, suitability for a disposable use and even potential MRI compatibility.

Acknowledgements

This research was performed within the framework of CTMM, the Center for Translational Molecular Medicine, project MUSIS (grant 030-202). The authors would like to thank the Dutch Organisation for Applied Scientific Research (TNO) for their collaboration.

References

- [1] Khorjastan, S. M., Najarian, S., Simforoosh, N., and Farkoush, S. H., 2010, "Design and Modeling of a Novel Flexible Surgical Instrument Applicable in Minimally Invasive Surgery," *Int J Nat Eng Sci*, 4(1), pp. 53-60.
- [2] Braga, M., Vignali, A., Gianotti, L., Zuliani, V., Radaelli, G., Gruarin, P., Dellabona, P., and Carlo, V. D., 2002, "Laparoscopic Versus Open Colorectal Surgery: A Randomized Trial on Short-Term Outcome," *Ann Surg*, 236(6), pp. 759-767.
- [3] Velanovich, V., 2000, "Laparoscopic vs open surgery," *Surg Endosc*, 14(1), pp. 16-21.
- [4] Minor, M., and Mukherjee, R., 1999, "A Mechanism for Dexterous End-Effector Placement During Minimally Invasive Surgery," *J Mech Des*, 121(4), pp. 472-479.
- [5] Breedveld, P., Stassen, H. G., Meijer, D. W., and Jakimowicz, J. J., 1999, "Manipulation in laparoscopic surgery: Overview of impeding effects and supporting aids," *J Laparoendosc Adv Surg Tech A*, 9(6), pp. 469-480.
- [6] Arrow Medical, 2012, "Bruder 5mm \emptyset Laparoscopic Instruments," <http://www.arrowmedical.com/sites/default/files/5MM%20LAP%20DISSECTOR,%20GRASPER,%20BIOPSY%20FORCEPS%20%26%20SCISSORS.pdf>.
- [7] Breedveld, P., 2010, "Steerable Laparoscopic Cable-Ring Forceps," *J Med Device*, 4(2), p. 027518.
- [8] Breedveld, P., Stassen, H. G., Meijer, D. W., and Stassen, L. P. S., 1999, "Theoretical background and conceptual solution for depth perception and eye-hand coordination problems in laparoscopic surgery," *Minim Invasive Ther Allied Technol*, 8(4), pp. 227-234.
- [9] Breedveld, P., Scheltes, J. S., Blom, E. M., and Verheij, J. E. I., 2005, "A new, easily miniaturized steerable endoscope," *IEEE Eng Med Biol Mag*, 24(6), pp. 40-47.
- [10] Intuitive Surgical, 2013, "EndoWrist - Instrument and Accessory Catalog," http://www.intuitivesurgical.com/products/871145_Instrument_Accessory_%20Catalog.pdf.
- [11] Madhani, A. J., and Salisbury, J. K., "Wrist mechanism for surgical instrument for performing minimally invasive surgery with enhanced dexterity and sensitivity," Intuitive Surgical, Inc., US Patent 5,797,900, August 25, 1998.
- [12] Sotelo, R., Clavijo, R., Carmona, O., Garcia, A., Banda, E., Miranda, M., and Fagin, R., 2008, "Robotic Simple Prostatectomy," *J Urol*, 179(2), pp. 513-515.
- [13] Ficarra, V., Cavalleri, S., Novara, G., Aragona, M., and Artibani, W., 2007, "Evidence from Robot-Assisted Laparoscopic Radical Prostatectomy: A Systematic Review," *Eur Urol*, 51(1), pp. 45-56.
- [14] Palep, J. H., 2009, "Robotic assisted minimally invasive surgery," *J Minim Access Surg*, 5(1), pp. 1-7.
- [15] Cepolina, F., and Michelini, R. C., 2004, "Review of robotic fixtures for minimally invasive surgery," *Int J Med Robot*, 1(1), pp. 43-63.
- [16] Senapati, S., and Advincula, A., 2007, "Surgical techniques: robot-assisted laparoscopic myomectomy with the da Vinci surgical system," *J Robotic Surg*, 1(1), pp. 69-74.
- [17] Chaplin, C. R., and Potts, A. E., 1991, "Wire Rope Offshore - a Critical Review of Wire Rope Endurance Research Affecting Offshore Applications," HSMO BOOKS, London, p. 157.
- [18] Childs, P. R. N., 2014, "Chapter 17 - Wire Rope," *Mechanical Design Engineering Handbook*, Butterworth-Heinemann, Oxford, pp. 721-733.
- [19] Miller, B. A., 2004, "Wire Ropes," *Encyclopedia of Materials: Science and Technology (Second Edition)*, K. H. J. Buschow, W. C. Robert, C. F. Merton, I. Bernard, J. K. Edward, M. Subhash, and V. Patrick, eds., Elsevier, Oxford, pp. 1-10.
- [20] Nabijou, S., and Hobbs, R. E., 1994, "Fatigue of wire ropes bent over small sheaves," *Int J Fatigue*, 16(7), pp. 453-460.
- [21] Lee, W., "Surgical instrument guide device," Cambridge Endoscopic Devices, Inc., WO Patent 2007/018898, February 15, 2007.
- [22] Marczyk, S., Farascioni, D., Taylor, E. J., and Hathaway, P., "Endoscopic Vessel Sealer and Divider Having a Flexible Articulating Shaft," Tyco Healthcare Group LP, WO Patent 2008/045350, April 17, 2008.
- [23] Fan, C., Dodou, D., and Breedveld, P., 2013, "Review of manual control methods for handheld maneuverable instruments," *Minim Invasive Ther Allied Technol*, 22(3), pp. 127-135.
- [24] Catherine, J., Rotinat-Libersa, C., and Micaelli, A., 2011, "Comparative review of endoscopic devices articulations technologies developed for minimally invasive medical procedures," *Appl Bionics Biomech*, 8(2), pp. 151-171.
- [25] Breedveld, P., and Hoeven, F. H. v. d., "Skull base surgery with multi-steerable instruments," Proc. 3rd Dutch Bio-Medical Engineering Conference, 2011.
- [26] Jobin, J.-P., Buddenberg, H. S., and Herder, J. L., "An Underactuated Prosthesis Finger Mechanism With Rolling Joints," Proc. 28th Biennial Mechanisms and Robotics Conference, Parts A and B, 2004, ASME, pp. 549-559.
- [27] Jeanneau, A., Herder, J., Laliberte, T., and Gosselin, C., "A Compliant Rolling Contact Joint and Its Application in a 3-DOF Planar Parallel Mechanism With Kinematic Analysis," Proc. 28th Biennial Mechanisms and Robotics Conference, Parts A and B, 2004, ASME, pp. 689-698.
- [28] Vayre, B., Vignat, F., and Villeneuve, F., 2012, "Designing for Additive Manufacturing," *Procedia CIRP*, 3(2012), pp. 632-637.
- [29] Janssen, R., 2011, "3D Printing Now With Ceramics Too," TNO Time, TNO, Delft, pp. 18-19.
- [30] Kruf, W., Vorst, B. v. d., Maalderink, H., and Kamperman, N., 2006, "Design for Rapid Manufacturing functional SLS parts," *Intelligent Production Machines and Systems*, D.T. Pham, E. E. Eldukhri, and A. J. Soroka, eds., Elsevier, Oxford, pp. 389-394.
- [31] Kruth, J. P., Leu, M. C., and Nakagawa, T., 1998, "Progress in Additive Manufacturing and Rapid Prototyping," *CIRP Ann - Manuf Technol*, 47(2), pp. 525-540.
- [32] Yan, X., and Gu, P., 1996, "A review of rapid prototyping technologies and systems," *Comput Aided Des*, 28(4), pp. 307-318.
- [33] Taylor, C. S., Cherkas, P., Hampton, H., Frantzen, J. J., Shah, B. O., Tiffany, W. B., Nanis, L., Booker, P., Salahieh, A., and Hansen, R., "Spatial forming - a three dimensional printing process," Proc. IEEE MEMS, 1995, p. 203.
- [34] Nai, T. Y., Herder, J. L., and Tuijthof, G. J. M., 2011, "Steerable Mechanical Joint for High Load Transmission in Minimally Invasive Instruments," *J Med Device*, 5(3), p. 034503.

Chapter 7

Attaining High Bending Stiffness by Full Actuation in Steerable Minimally Invasive Surgical Instruments

**Filip Jelínek, Giada Gerboni, Paul W. J. Henselmans, Rob Pessers
and Paul Breedveld**

Published early online in Minimally Invasive Therapy and Allied Technologies.

Abstract

Introduction | Steerable instruments are a promising trend in minimally invasive surgery (MIS), due to their manoeuvring capabilities enabling reaching over obstacles. Despite the great number of steerable joint designs, currently available steerable tips tend to be vulnerable to external loading, thus featuring low bending stiffness. This work aims to provide empirical evidence that the bending stiffness can be considerably increased by using fully actuated joint constructions, enabling left/right and up/down tip rotations with the minimum of two degrees of freedom (DOF), rather than conventional underactuated constructions enabling these rotations with more than two DOF.

Methods | A steerable MIS instrument prototype with a fully actuated joint construction was compared to state-of-the-art underactuated steerable instruments in a number of tip deflection experiments. The tip deflections due to loading were measured by means of a universal testing machine in four bending scenarios: straight and bent over 20°, 40° and 60°.

Results and Conclusions | The experimental results support the claim that a fully actuated joint construction exhibits a significantly larger bending stiffness than an underactuated joint construction. Furthermore, it was shown that the underactuated instrument tips show a considerable difference between their neutral positions before and after loading, which could also be greatly minimised by full actuation.

7.1 Introduction

7.1.1 Minimally Invasive Surgery and Steerable Instruments

Minimally invasive surgery (MIS) is gaining on popularity due to considerable patient benefits including shorter recovery time and less postoperative scar tissue compared to open surgery [1-4]. Nevertheless, the drawback of a limited site access during MIS procedures has led to the inevitable development of long, slender instruments providing surgeons with visual feedback or tissue manipulation features.

Conventionally used rigid MIS instruments (Fig. 7.1(a)) [5] are limited to only four degrees of freedom (DOF) (Fig. 7.1(b)) [2, 3, 6], thus binding the surgeon to frontal or lateral approach to the tissue and limiting the surgical possibilities [2, 7]. Hence, steerable MIS instruments (Fig. 7.1(a)) [7] have been developed to ameliorate this drawback by providing additional DOF through one or more joints in their flexible tips, thus enabling the surgeon to redirect the approach to the tissue and even manoeuvre around obstacles (Fig. 7.1(c)) [2, 7-9].

7.1.2 Steerability and Bending Stiffness

The tips of steerable MIS instruments come in numerous mechanical joint configurations as seen in the review papers by Jelínek et al. [10], Catherine et al. [11], Cepolina et al. [12] and Fan et al. [13]. Despite being mutually different from the design point of view, all these joint constructions aim at delivering sufficient manoeuvrability, or a range of motion, but more importantly a reliable tip controllability for safe and predictable operation in a surgical setting. Reliable controllability of the tip (slave) can be interpreted as its ability to exactly execute the desired action, or follow the desired motion, that is transferred from the handle (master). In layman's terms, while disregarding any amplification mechanism, when the handle joint of a handheld MIS

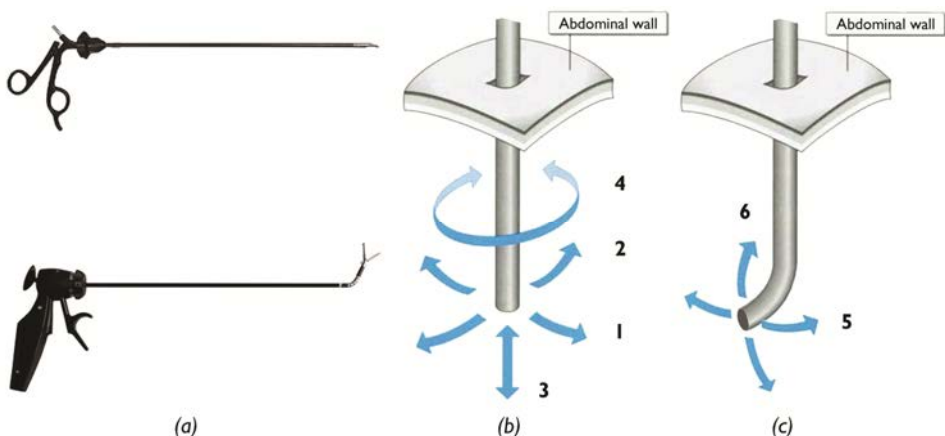


Figure 7.1 (a) Rigid [5] & steerable [7] minimally invasive surgical instruments; (b) Rigid instrument DOF [6]; (c) Additional steerable tip DOF. Adopted from [9] (Courtesy of ASME).

instrument is bent over X° , the tip joint should follow, bend and stay bent at X° . This may appear straightforward and easily achievable from a design perspective, nevertheless, one has to realise that in a surgical setting there are omnipresent external forces acting on the tip, which can easily result in its unpredictable behaviour. To avoid this, the joint constructions in the steerable instrument tips should be, yet rarely are, designed to be stiff when bent. Here the bending stiffness is defined as the joint's motion resistance to an external bending moment, preferably at any bending angle. In other words, the less the joint deflects due to the external forces the stiffer it is.

At present, there are no data available in the literature about the required bending stiffness of a steering section, whose determination would be a vast research question on its own. However, there is a general consensus that the tip should be manually controlled with ease while being bent, yet exhibit maximum bending stiffness once bent as desired and exposed to external forces. The question of maximising joint's bending stiffness can be more challenging than it appears. One might say that a simple stiffening of individual components, such as cables or joint segments, would be a satisfactory option. However, such a solution would easily result in a construction too stiff to control manually. Instead of searching for a compromise between ease of control and bending stiffness, a better answer lies in designing a joint construction that exhibits these properties already on a geometrical level.

7.1.3 Bending Stiffness versus Actuation

As suggested in the paper by Jelínek et al. [9] the trick behind achieving high bending stiffness lies in the actuation of the joints. Almost all mechanical joints used in MIS instruments nowadays are actuated by cables or rods due to their ease of control and miniaturisation. Their configuration and place of attachment determine the bending stiffness and hence the reliable controllability of a given joint construction.

Examples of state-of-the-art steerable MIS instruments for handheld applications include Autonomy Laparo-Angle (Cambridge Endo, Framingham, MA, USA) [14], Miflex (DEAM, Amsterdam, The Netherlands) [7, 13], RealHand (Novare, Cupertino, CA, USA) [15] and SILS Hand (Covidien, Mansfield, MA, USA) [16]. In all these instruments, the steering cables are guided smoothly along a stacked series of joint segments, which altogether form a flexible shaft section of a relatively large bending radius, beneficial for preventing steel cable fatigue [9]. However, the drawback of these instruments is that while featuring multiple steerable segments, the steering cables are attached only to the most distal tip segment and merely run through the more proximal ones. This results in the phenomenon of underactuation. For example, the joint construction of Miflex features eight one-DOF joints in series arranged perpendicularly in an alternating fashion as illustrated in Fig. 7.2(c) [7], thereby enabling 3D motion. However, only the most distal two DOF are actuated by the cables, leaving the remaining six DOF unactuated. The underactuation leads to a compliant behaviour of the tip when exposed to external tip forces, leading to a flexible change in its configuration and a user experience of low bending stiffness, which is undesired. Such an unpredictable

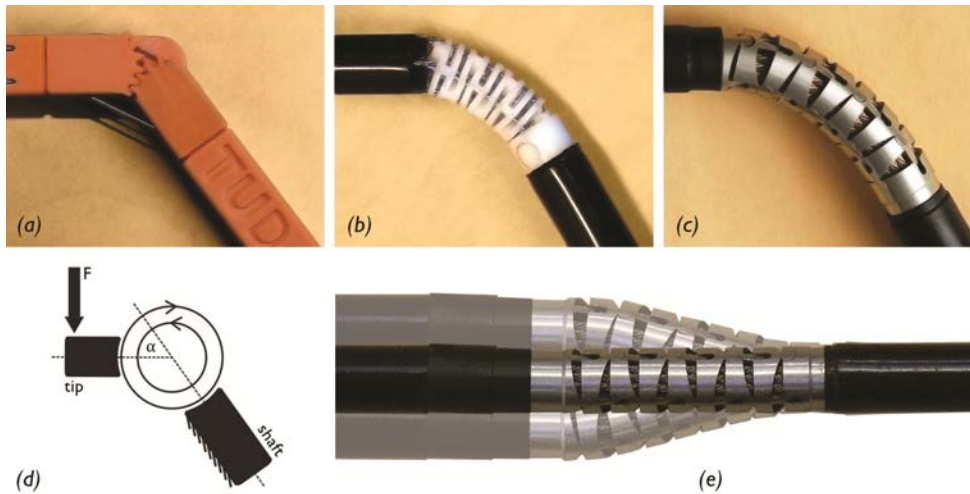


Figure 7.2 Steerable tip joint constructions of (a) DragonFlex; (b) Laparo-Angle; (c) Miflex [7]. (d) Free body diagram of the bending scenarios showing a vertically downward force F and an angle of bend α . (e) While maintaining its orientation (angle), an underactuated joint construction can change its shape uncontrollably when loaded.

behaviour is illustrated in Fig.7.2(e) by the phenomenon of snaking, where the instrument handle is fixed in the straight orientation and the underactuated tip is subjected to the external forces. Here, its joint construction shifts uncontrollably, despite keeping the tip's original straight orientation.

One of the solutions to the problem of underactuation is to control each joint segment individually by increasing the number of actuators to the number of controllable DOF. This was achieved by Breedveld et al. [17] with their handheld fully mechanically actuated Multi-Flex prototype [7, 9, 13, 17]. Yet, in such cases, the individual joint actuation results in a strongly increased design complexity. Alternatively, instead of controlling each tip joint segment by a corresponding handle joint segment, a coupling mechanism can be devised, linking the motion of a single joint segment to the remaining segments in the steerable tip [18, 19]. However, this solution increases the design complexity even further.

On the other hand, a better solution towards full actuation is to minimise the number of joint segments to the number of actuators. Yet, minimising the number of joint segments introduces a challenge of sharp bends, where the steel cables may soon fail due to fatigue elicited by the small bending radius, as in the case of da Vinci's EndoWrist (Intuitive Surgical, Sunnyvale, CA, USA) [7, 9, 12, 20, 21]. For that reason, a fully actuated handheld DragonFlex prototype [9] was devised at TU Delft and produced by additive manufacturing. DragonFlex not only maximises the cable bending radius to the theoretical limits thanks to the use of a special cable guidance and rolling joints, but also reduces the number of components in its steerable tip to the theoretical minimum [9].

7.1.4 Objective

Despite the strong benefit of full actuation, almost all steerable MIS instruments have been and still are being developed with the inherent disadvantage of underactuation, with only a few exceptions. Hence, it is the aim of this work to provide empirical evidence that fully actuated joint constructions have considerably higher bending stiffness than underactuated joint constructions. This knowledge can serve as a design guideline either for improving the existing steerable constructions or for the future development of fully actuated steerable MIS instruments providing high bending stiffness.

7.2 Methods

7.2.1 Equipment

Three available steerable MIS instruments, featuring either the fully actuated or the underactuated joint constructions were used in a series of tip deflection experiments. These included DragonFlex with two planar fully actuated rolling joints (Fig. 7.2(a)), Laparo-Angle with a compliant underactuated flexure joint construction (Fig. 7.2(b)) and Miflex with an underactuated sliding joint construction resembling jigsaw puzzle pieces (Fig. 7.2(c)).

All of these instruments are capable of manoeuvring in two perpendicular planes, yet for simplicity in our experiments only their downward tip deflections were trialled in a single vertical plane (Fig. 7.2(d)). The vertical tip deflections were measured at four different scenarios, in which the instrument tips were either locked in a straight horizontal configuration or in a bend of 20°, 40° and 60°. In all cases their closed graspers were pointing horizontally with the angle between the instrument shaft and the horizontal plane being 0°, 20°, 40° or 60°. This ensured that all the tips were capable of being loaded perpendicularly downwards.

The tips were either locked by means of a shape-locking mechanism in the handle, featured in both Laparo-Angle and Miflex, or by specially designed rapid prototyped handle clamps in the case of DragonFlex that does not possess a locking mechanism. The building material for all the rapid prototyped set-up components (Fig. 7.3) was a stiff and strong resin-like Objet VeroBlue™ RGD840 printed at TU Delft using Objet Eden260V™ 3D printer.

As seen in Fig. 7.3, the positioning of all the instruments was achieved by two universal rapid prototyped shaft clamps. The first shaft clamp was used for the straight configuration and secured the instruments horizontally along 10cm of their shafts. The second angle-adjustable shaft clamp was used for the scenarios in which the instrument tips were bent over 20°, 40° or 60°, also securing the shafts along 10cm.

Both the shaft clamps and DragonFlex's handle clamps were designed strongly over-dimensioned, thus preventing any contribution to the measured tip deflections. Also the shafts were regarded as non-deflectable in the minor loading conditions used in

this experiment, as they were made either from strong stainless steel tubes in the case of Laparo-Angle and Miflex, or from a stiff ceramic-filled epoxy resin [9] in the case of DragonFlex.

7.2.2 Experimental Procedure

In all the bending scenarios, an increasing vertical force with a maximum of 1N was applied on the instrument tips at a constant horizontal distance of 30mm from the proximal end of the jointed section, thus achieving a uniform maximum moment of 0.03Nm. The maximal load of 1N was an arbitrary choice well within the safe limits from any induced damage or deformation of the set-up.

The individual shaft clamp components were bolted firmly together and to an aluminium base, which secured everything to the universal testing machine Zwick/Roell Z005 (TÜV Nord AG, Hanover, Germany). The instruments were positioned and fixed in a

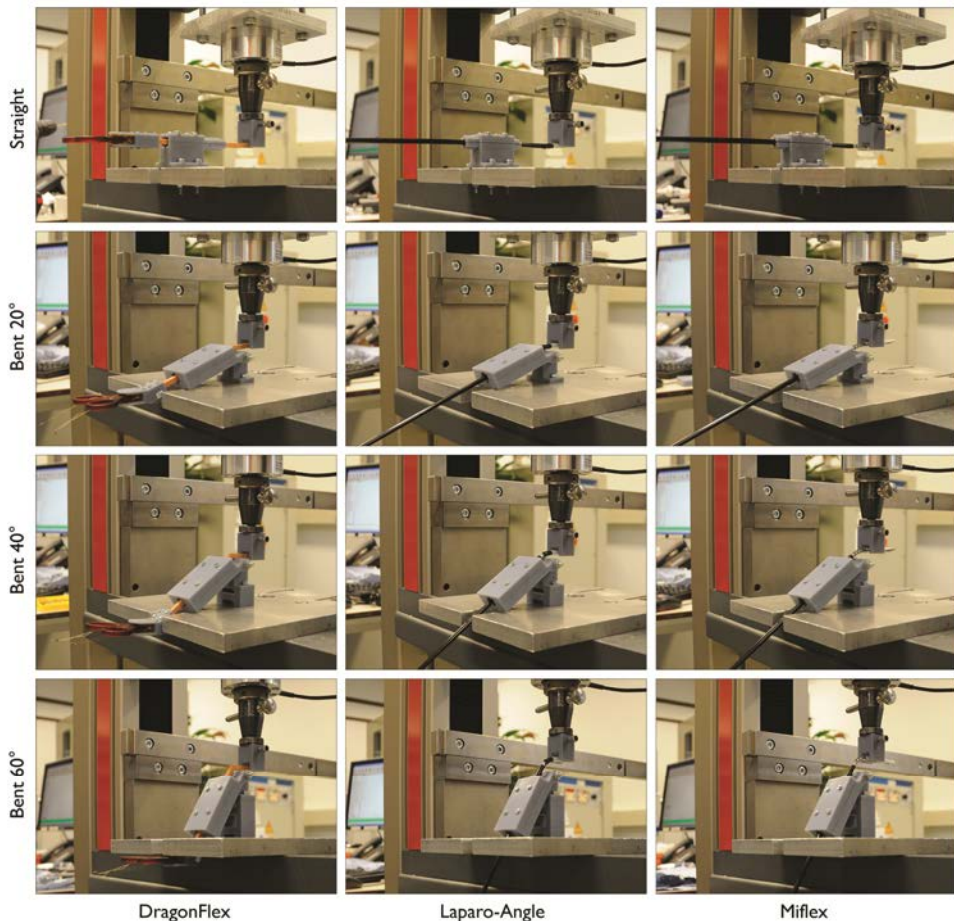


Figure 7.3 Experimental set-up showing DragonFlex, Laparo-Angle and Miflex clamped in the following bending scenarios: straight and 20°, 40°, 60° bends.

way that the free lengths of their shafts outside the clamps were minimised, so that the minor effect of the potential shaft deflection could be neglected.

The increasing vertical load was applied by a 1kN load cell. A custom-made inverted-U-shaped rapid prototyped machine head was mounted to the bottom of the load cell and allowed the instrument tips to deflect only downwards, i.e. the tips were prevented from slipping out or deflecting laterally from the measurement plane. At the same time sufficient clearance and rounded-off features were provided in the rapid prototyped piece as not to inhibit the tip's motion.

First of all, a momentary preload of 0.2N was applied to the instrument tips in all the scenarios to ensure full initial contact between the tip and the machine head. Afterwards, the vertical load was increased to 1N at a constant rate of 0.1N/s, held at its maximum for 0.2s and then dropped to zero instantaneously. The aim of this first loading and unloading trial was to determine the initial tip deflection magnitudes and the tips' neutral positions after the first loading.

The steerable constructions possess several moving components and thus mechanism friction. When unloaded, a small degree of friction can be overcome by the tip's elastic behaviour, allowing it to spring back to its straight position. However, once the frictional forces become too high, the tip's elasticity is strongly reduced and its neutral position after loading is then dependent on the amount of friction in the steerable construction. Hence, the tips' neutral positions after loading usually exhibit some degree of deflection, i.e. they are vertically lower than the initial straight positions. This can be perceived by the surgeon as a feeling of play or leeway in the tip dependent on friction.

After the first trial accounting for friction, the machine head was again brought to contact with the tip and the proper measurement trials began, where the tips deflected elastically. In total, one initial and eight subsequent measurements were performed with the same aforementioned settings for each instrument in each scenario (0°, 20°, 40°, 60°). As a result, the final tip deflections reflected the instruments' bending stiffness due to some degree of joint elasticity and, more importantly, due to any uncontrollable change in the shapes of the underactuated joint constructions. All the instruments were trialled in the same bending scenario first starting with 0°, in this order: DragonFlex, Laparo-Angle, Miflex; gradually followed by the next scenarios of 20°, 40° and 60° bends. The plots of the vertical loads [N] against the vertically downward tip deflections [mm] were acquired at a sampling rate of 20Hz.

7.3 Results

Figure 7.4 shows raw experimental data of the tip deflection magnitudes for all the instruments in all the bending scenarios. The tip deflections during the initial preload of 0.2N were not measured; hence, the deflections start at 0mm at the load of 0.2N.

Each graph shows the first tip deflection trial (red dashed) as the uppermost curve nearly in all cases. As explained, the reason for the initial deflection being the largest is that the tips were deflected from their initially straight neutral positions, which were shifted vertically lower after the first loading and unloading due to the mechanism friction. The other eight trials illustrate tips' elastic deflections and they are not graphically differentiated (black overlaying curves). The maximum tip deflection differences between the first and the second trials (Table 7.1) indicate how much the tip's neutral positions differ before and after loading.

The maximum elastic tip deflection distributions are shown as boxplots in Fig. 7.5 and do not include the initial trials. As clear from the boxplots and confirmed by the analysis of variance (ANOVA) and a post-hoc Tukey HSD test, the maximum tip deflections differ significantly ($p < 0.05$) in all the bending scenarios.

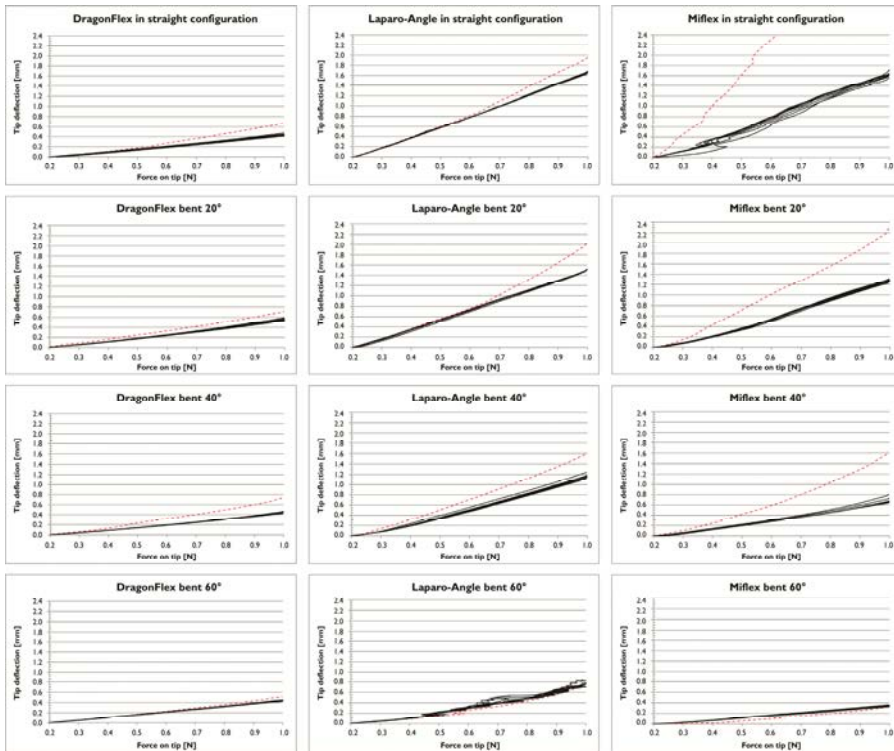


Figure 7.4 Experimental results of the tip deflection magnitudes against the force on the tip of DragonFlex, Laparo-Angle and Miflex at 0° , 20° , 40° and 60° . The red dashed line in each graph represents the first tip deflection measurement starting from the tip's initially straight position (initial tip deflection at 1N load reaches 4.23mm for Miflex in the straight configuration).

Table 7.1 Maximum tip deflection differences between the first and the second loading trials for each instrument in each scenario. The deflection difference indicates to what extent the tip's neutral positions before and after loading differ.

Maximum tip deflection [mm]	DragonFlex				Laparo-Angle				Miflex			
	0°	20°	40°	60°	0°	20°	40°	60°	0°	20°	40°	60°
Trial 1 [mm]	0.67	0.72	0.74	0.51	1.96	2.03	1.62	0.76	4.23	2.32	1.62	0.32
Trial 2 [mm]	0.48	0.59	0.47	0.45	1.68	1.51	1.24	0.76	1.71	1.31	0.80	0.36
Tip deflection difference [mm] (Trial 1 – Trial 2)	0.19	0.13	0.27	0.06	0.28	0.52	0.38	0.00	2.52	1.01	0.82	-0.04

7.4 Discussion

As seen in Figs. 7.4-7.5, the fully actuated DragonFlex prototype experiences only very little maximum tip deflections in all the bending scenarios, almost always lower than in the underactuated instruments except for the 60° bend. As a matter of fact, DragonFlex's maximum tip deflections at the 1N load remain constant at 0.44mm throughout different stages of bend, except for the 20° scenario when the deflection reaches 0.56mm. The underactuated Laparo-Angle instrument exhibits significantly higher tip deflections in all the scenarios, within the range of 1.7 to 3.8 times the tip deflections of DragonFlex. Interestingly, in the 60° scenario, the increase in Laparo-Angle's tip deflection tends to be rather noisy, probably due to the instability of the underactuated joint construction at the maximum bend. Up to the 40° scenario, the underactuated Miflex instrument shows significantly higher maximum tip deflections as well, in the range of 1.6 to 3.7 times compared to DragonFlex. In the straight configuration, underactuated Miflex exhibits a noisy behaviour when loaded and having reached 0.2mm tip deflection, possibly due to the individual joint segments shifting unexpectedly. On the other hand, in the 60° scenario, Miflex's jigsaw puzzle joint construction stiffens as the joint segments mutually

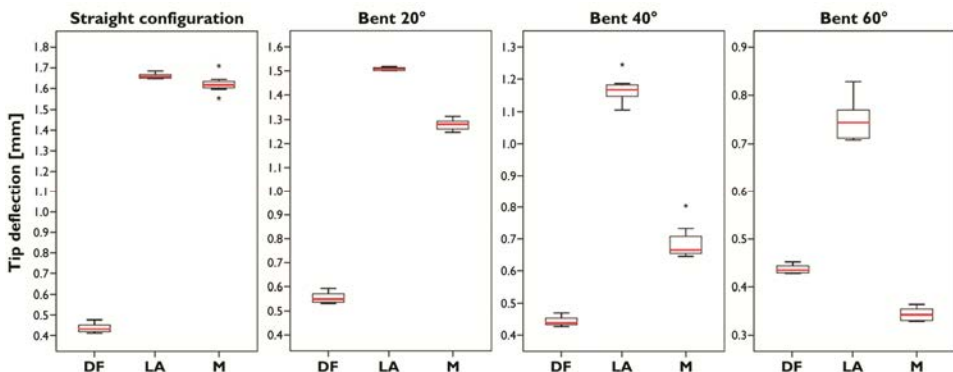


Figure 7.5 Boxplots showing the maximum elastic tip deflection magnitudes at 1N load for DragonFlex (DF), Laparo-Angle (LA) and Miflex (M) in straight configuration and bent 20°, 40° and 60° (the initial deflection values are not included in the distributions).

interlock with all the spacing eliminated; hence, Miflex's maximum tip deflection reaches merely 0.34mm, being significantly lower than DragonFlex's 0.44mm and less than a half of Laparo-Angle's 0.75mm deflection. Compared to DragonFlex's almost constantly low tip deflections, both underactuated joint constructions show a decreasing trend in the tip deflections at larger bends.

When analysing the maximum tip deflection differences in Table 7.1, one can observe that DragonFlex experiences only a very little tip deflection difference, which is slightly increased in the 40° scenario (0.27mm) and almost none in the 60° scenario (0.06mm). Since DragonFlex's steerable joint consists of only two fully actuated segments in a rolling contact, the overall mechanism friction is very low ensuring that the tip's neutral positions before and after loading are almost identical. Conversely, Laparo-Angle's long compliant construction of several flexure joints shows considerably higher tip deflection differences, in the range of 1.4 to 4 fold with respect to DragonFlex. In Laparo-Angle the maximum tip deflection difference tends to be the largest in the 20° scenario, yet, there is no difference whatsoever in the 60° scenario. Similarly, the long joint construction of Miflex of several sliding jigsaw pieces exhibits even higher maximum tip deflection differences than Laparo-Angle, being in the range of 3 to 13 fold with respect to DragonFlex. Despite being at its maximum in the 0° scenario, there is absolutely no tip deflection difference in Miflex in the 60° scenario. In both underactuated joint constructions, the large maximum tip deflection differences indicate a large gap between the tips' neutral positions before and after loading due to the considerable amount of mechanism friction and the underactuation itself. On the other hand, the absence of any tip deflection difference at the maximum bending angle of 60° is due to the fact that Laparo-Angle and Miflex were designed to bend only till 60°, unlike the 90° maximum in DragonFlex. At the 60° maximum, the neutral positions of both underactuated joint constructions are the same both before and after loading, as their tip segments mutually interface without any clearance.

Last but not least, it is relevant to note that the mutual instrument design differences did not undermine the validity of the experimental results and the evidence that a fully actuated joint construction shows significantly larger bending stiffness than an underactuated joint construction. As far as steering cables are concerned, in all the trialled instruments they are arranged approximately 2mm from the centreline. Although all these instruments use steel cables, their cable diameters slightly differ. DragonFlex uses four Ø0.3mm cables, whereas Laparo-Angle and Miflex use four or more Ø0.4-0.5mm cables, respectively. It would have been expected that the thinner cables in DragonFlex would have undermined its bending stiffness due to their lower tensile strength compared to the thicker cables. However, contrary to such reasoning, DragonFlex exhibited the lowest tip deflections, which would have been even lower had DragonFlex featured thicker cables.

7.5 Conclusions

This work provides empirical evidence that a fully actuated joint construction has a significantly larger bending stiffness than an underactuated joint construction in steerable MIS instrument tips, thus acting more reliably when being controlled by a surgeon. Tip deflection experiments also revealed that an underactuated joint construction allows for a considerably larger difference between the tip's neutral positions before and after loading, which can also be greatly eliminated by a fully actuated joint construction of fewer segments and lower friction.

Acknowledgements

The research of Filip Jelínek was performed within the framework of CTMM, the Center for Translational Molecular Medicine, project MUSIS (grant 030-202). The research of Paul W. J. Henselmans was supported by Technology Foundation STW.

References

- [1] Braga, M., Vignali, A., Gianotti, L., Zuliani, W., Radaelli, G., Gruarin, P., Dellabona, P., and Carlo, V. D., 2002, "Laparoscopic Versus Open Colorectal Surgery: A Randomized Trial on Short-Term Outcome," *Ann Surg*, 236(6), pp. 759–767.
- [2] Breedveld, P., Stassen, H. G., Meijer, D. W., and Jakimowicz, J. J., 1999, "Manipulation in laparoscopic surgery: Overview of impeding effects and supporting aids," *J Laparoendosc Adv Surg Tech A*, 9(6), pp. 469–480.
- [3] Minor, M., and Mukherjee, R., 1999, "A Mechanism for Dexterous End-Effector Placement During Minimally Invasive Surgery," *J Mech Des*, 121(4), pp. 472–479.
- [4] Velanovich, V., 2000, "Laparoscopic vs open surgery," *Surg Endosc*, 14(1), pp. 16–21.
- [5] Arrow Medical, 2012, "Bruder 5mm Ø Laparoscopic Instruments," <http://www.arrowmedical.com/sites/default/files/5MM%20LAP%20DISSECTOR,%20GRASPER,%20BIOPSY%20FORCEPS%20%26%20SCISSORS.pdf>.
- [6] Breedveld, P., Stassen, H. G., Meijer, D. W., and Stassen, L. P. S., 1999, "Theoretical background and conceptual solution for depth perception and eye-hand coordination problems in laparoscopic surgery," *Minim Invasive Ther Allied Technol*, 8(4), pp. 227–234.
- [7] Breedveld, P., 2010, "Steerable Laparoscopic Cable-Ring Forceps," *J Med Device*, 4(2), p. 027518.
- [8] Breedveld, P., Scheltes, J. S., Blom, E. M., and Verheij, J. E. I., 2005, "A new, easily miniaturized steerable endoscope," *IEEE Eng Med Biol Mag*, 24(6), pp. 40–47.
- [9] Jelínek, F., Pessers, R., and Breedveld, P., 2014, "DragonFlex Smart Steerable Laparoscopic Instrument," *J Med Device*, 8(1), p. 015001.
- [10] Jelínek, F., Arkenbout, E. A., Henselmans, P. W. J., Pessers, R., and Breedveld, P., 2014, "Classification of Joints Used in Steerable Instruments for Minimally Invasive Surgery," *J Med Device*, 8(3), p. 030914.
- [11] Catherine, J., Rotinat-Libersa, C., and Micaelli, A., 2011, "Comparative review of endoscopic devices articulations technologies developed for minimally invasive medical procedures," *Appl Bionics Biomech*, 8(2), pp. 151–171.
- [12] Cepolina, F., and Michelini, R. C., 2004, "Review of robotic fixtures for minimally invasive surgery," *Int J Med Robot*, 1(1), pp. 43–63.
- [13] Fan, C., Dodou, D., and Breedveld, P., 2013, "Review of manual control methods for handheld maneuverable instruments," *Minim Invasive Ther Allied Technol*, 22(3), pp. 127–135.
- [14] Lee, W., Chamorro, A., and Lee, W., "Surgical Instrument," Cambridge Endoscopic Devices, Inc., US Patent 8,029,531, October 4, 2011.
- [15] Danitz, D. J., and Gold, A., "Articulating Endoscopes," Novare Surgical Systems, Inc., US Patent 2010/0261964, October 14, 2010.
- [16] Marczyk, S., Pribanic, R., Farascioni, D., Taylor, E. J., and Hathaway, P., "Endoscopic Vessel Sealer and Divider Having a Flexible Articulating Shaft," Covidien LP, US Patent 2013/0274741, October 17, 2013.
- [17] Breedveld, P., and Hoeven, F. H. v. d., "Skull base surgery with multi-steerable instruments," Proc. 3rd Dutch Bio-Medical Engineering Conference, 2011.
- [18] Mueglitz, J., Kunad, G., Dautzenberg, P., Neisius, B., and Trapp, R., "Modular, Miniaturized Articulated Mechanism Symmetrically Pivotal in One Plane, for Medical Applications," Kernforschungszentrum Karlsruhe GmbH, WO Patent 94/17965, August 18, 1994.
- [19] Mueglitz, J., 1991, "Special mechanisms for robot-like systems," *Robotersysteme*, 7(4), pp. 231–237.
- [20] Madhani, A. J., and Salisbury, J. K., "Wrist mechanism for surgical instrument for performing minimally invasive surgery with enhanced dexterity and sensitivity," Intuitive Surgical, Inc., US Patent 5,797,900, August 25, 1998.
- [21] Palep, J. H., 2009, "Robotic assisted minimally invasive surgery," *J Minim Access Surg*, 5(1), pp. 1–7.

Chapter 8

Method for Minimising Rolling Joint Play in the Steerable Laparoscopic Instrument Prototype DragonFlex

Filip Jelínek, Tom Diepens, Sander Dobbenga, Geert van der Jagt, Davey Kreeft, Annemijn Smid, Rob Pessers and Paul Breedveld

Published early online in Minimally Invasive Therapy and Allied Technologies.

Abstract

Introduction | The steerable laparoscopic instrument prototype DragonFlex was recently developed with the vision of a minimalistic fully functional design, readily produced by additive manufacturing and requiring little assembly. Steering functionality is provided by rolling joints that, besides simplifying the assembly, help minimise cable fatigue and equalise force requirements on steering cables. However, the perfectly circular rolling joint design introduced some mechanism play, undermining the joint's bending stiffness. Hence, the aim of this paper is to present an innovative solution for play reduction in rolling joints.

Methods | The original play-compensating mechanism, a shaft-embedded compression spring, proved unsatisfactory for play reduction. Therefore, a new non-circular rolling joint curvature was designed with the objective to compensate for any cable slack and thus minimise the joint play. The new rolling joint design was evaluated in several tip deflection experiments and compared to the original one.

Results and Conclusions | The experimental results proved that the optimised rolling joint curvature significantly minimises play, thus being a major improvement compared to the original design. The optimised rolling joint was implemented in a new real-scale DragonFlex prototype. The presented optimisation method enables elimination of a conventionally used cable tensioning device and it is generally applicable to steerable minimally invasive instruments that use a rolling joint.

8.1 Introduction

8.1.1 Laparoscopy and Steerable Instruments

Laparoscopy is a form of minimally invasive surgery (MIS) performed in the abdomen. With MIS, as opposed to open surgery, the incisions made are small and thus lead to shorter hospital stay and recovery time of the patient. However, due to the limited site access, the traditional surgical instruments for open surgery cannot be used in MIS procedures. Therefore, specialised long and slender laparoscopic instruments have been developed [1-5]. In general, these instruments can either be fully rigid or feature a steerable tip.

Rigid instruments comprise a handle, a rigid shaft and a tip, which equips them with four degrees of freedom (DOF), i.e. axial sliding, axial rotation and pivoting in two perpendicular planes around the incision point, as annotated by nos. 1 – 4 in Fig. 8.1 [6]. As the incision acts like a fulcrum, the motion of the rigid instruments is considerably limited and so is the surgeon's approach to reaching the tissue [2, 7]. For that reason, rigid designs of laparoscopic instruments have been supplemented with a steerable tip, equipping them with two additional DOF provided by one or more joints. The steerable tip enlarges the instrument's workspace and allows the surgeon to reach behind obstacles [7, 8]. The additional steerable DOF are annotated by nos. 5 & 6 in Fig 8.1.

8.1.2 Original DragonFlex Prototype

Recently, a steerable laparoscopic instrument prototype, DragonFlex (Fig. 8.1) [6], was designed at TU Delft and made by additive manufacturing [9-13] at 5mm width from a ceramic-filled epoxy resin, which is one of the most precise and accurate materials

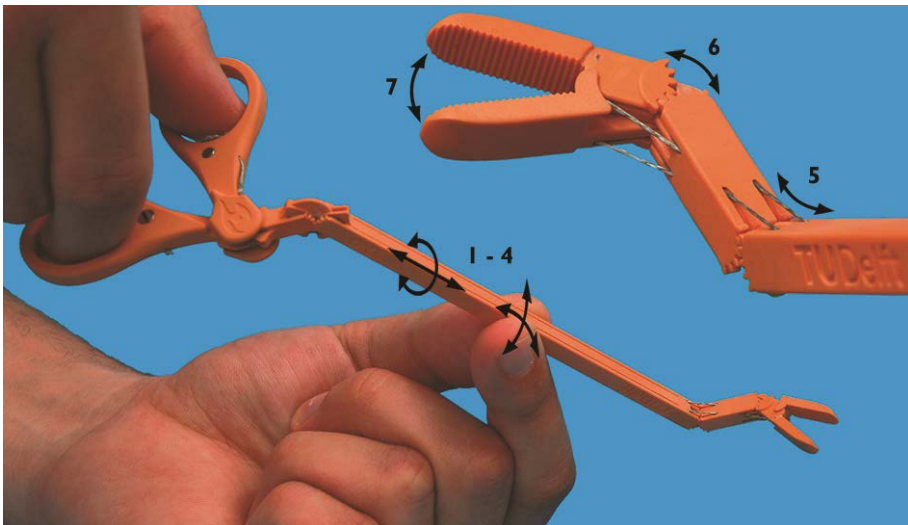


Figure 8.1 5mm wide DragonFlex prototype showing the steerable laparoscopic instrument DOF. Adopted from Jelínek et al. [6] (Courtesy of ASME).

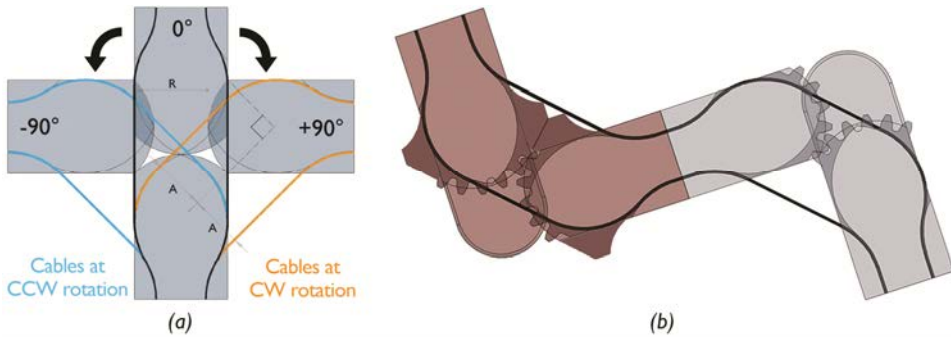


Figure 8.2 (a) Combined with the cable guiding profiles of radius R , the rolling joint equalises the cable moment arms A . (b) Section through the basic modular parallelogram construction of DragonFlex joints (bent 90°). Adopted from Jelínek et al. [6] (Courtesy of ASME).

available for stereolithography. Being the world's first additive manufactured steerable laparoscopic instrument prototype, it is composed of only seven structurally rigid components and two looped steering cables. The tip of the prototype features three fully actuated DOF provided by the theoretical minimum of only four mutually rotatable parts. For the sake of comparison, while enabling the same DOF, da Vinci's EndoWrist (Intuitive Surgical, Sunnyvale, CA, USA) features more than ten parts including miniature rivets and pulleys [6, 14-16]. DragonFlex's tip DOF include $\pm 90^\circ$ joint articulation in two perpendicular planes and grasper actuation (Fig. 8.1, no. 5, 6 & 7 respectively) with a maximum grasper opening angle of 180° .

As opposed to other state-of-the-art steerable laparoscopic instruments, DragonFlex not only minimises the number of essential structural components, but also maximises the cable bending diameter to a theoretical limit of 1.5 times the instrument width (valid for two components per rotational DOF). This was achieved by implementing specialised cable guiding profiles with a large bending radius R (Fig. 8.2(a)) reaching beyond the capabilities of embedded pulleys used for example in EndoWrist. Maximising cable bending radius theoretically leads to less cable fatigue, thus increasing the instrument's lifespan. Furthermore, DragonFlex's stacked hinge-less construction considerably simplifies the assembly, which requires only aligning of the individual components and fitting and tensioning of the steering cables as seen in the prior work.

As seen in Fig. 8.2, DragonFlex uses geared rolling joints that, besides simplifying the assembly, equalise the cable moment arms A and hence the force requirements on both steering cables. Furthermore, combined with special tight cable guidance, the rolling joints proved to limit the joint play thereby exhibiting promisingly high bending stiffness, i.e. resistance to external loading [17]. In other words, by reducing the joint play the joint deflects less from its straight configuration when subjected to a lateral load that leads to a bending moment. The rolling joints have a constant radius and describe an angle of 90° (Fig. 8.2(a)), thus providing full $\pm 90^\circ$ joint articulation.

Nevertheless, the rolling joint design in DragonFlex is still not perfect as upon careful observation in the bent state, it was discovered that the interfacing rolling joint surfaces can slightly detach from each other in radial direction. This imperfection leads to some degree of cable slack and reduces the joint's bending stiffness.

8.1.3 Objective

Generally, bending cable-driven constructions leads to a variation in the steering cable's trajectory length, while the length of the cable itself does not change [8, 18]. This introduced cable slack can lead to mechanism play, unless compensated for by a cable tensioning device. Following this general practice, the original DragonFlex design features a built-in compression spring inside the shaft (Fig. 8.3). Although this solution considerably limits the overall joint play, the small spring dimensions and its finite axial stiffness still undermine the joint's bending stiffness, making the joint slightly floppy. Furthermore, as seen in Fig. 8.3, the shaft-hole configuration due to the incorporation of the compression spring can undermine the design's sturdiness by introducing stress concentrations in the inner rod. As the compression spring does not solve the root of the cable slack problem, but merely tries to treat its symptoms while even presenting a potential downside itself, it would be better to seek for another more fundamental solution to eliminate the joint play.

8.2 Methods

8.2.1 Rolling Joint Optimisation

Rather than modifying the cable tensioning mechanism, a closer look was taken at the rolling joint design itself. It was theorised that the curvature of the rolling joint could be optimised by adding material as to fill the slightly increasing gap in between the rolling joint surfaces during bending. If this could in turn decrease the joint play to a negligible amount, the compression spring would become redundant. Thus, by adjusting the rolling joint curvature, two problems could be eliminated at once: firstly, the play in the construction and secondly, its original insufficient compensation – the compression spring. In addition to a play-free joint, this solution would lead to a simpler design and thus a faster assembly.

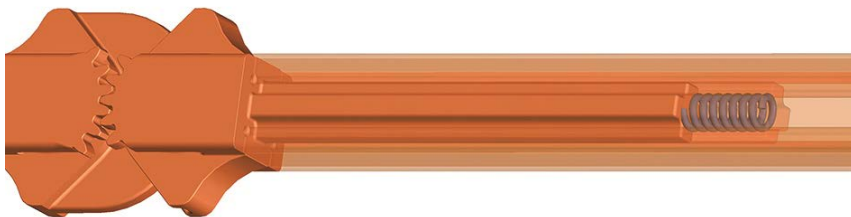


Figure 8.3 Shaft-embedded compression spring in the original DragonFlex prototype.

To optimise the rolling joint curvature, the amount of play during the bending process had to be determined. This was achieved by measuring the cable slack over various joint angles in SolidWorks. The cable slack of a single cable within one 10mm wide joint (double the original scale) was measured at 5° intervals when bent from 0° to 90°. Since DragonFlex's design is symmetrical and mirrored, as seen in Fig. 8.2(b), the total cable slack in the trajectory of a single cable (from straight to bent state) equals twice the measured value. A plot of the total cable slack of a single cable throughout rotation of the original joint design is shown in Fig. 8.4(a), annotated by no. 1.

In order to determine the optimal play-free rolling joint curvature, iteration was used. The first step in the iteration process was to add a curve approximately following the original perfectly circular rolling joint. Expecting that the optimised curvature would not differ much from the original, an arbitrary parabola $f(x_i) = A_i x_i^2$ was added to the original curve. Here A_i is a vector $[A_1, A_2, \dots, A_n]$ and variable x_i ranges within $\pm w/2$, where w is the joint's width. The resulting modified rolling joint curvature generated intermediate cable slack values plotted in Fig. 8.4(a) as no. 2 (relative to the joint width of 10mm). Next, using these intermediate slack magnitudes, the vector A_i was adjusted at 5° intervals to create zero cable slack at each value of x_i (Fig. 8.4(a), no. 3). As a result of this procedure, each element of the vector A_i is custom for each corresponding x_i value at 5° bend intervals. Using the resulting $f(x_i)$ an optimised rolling joint curve of a variable radius was designed and implemented in the new rolling joint design (Fig. 8.4(b)).

8.2.2 Experimental Set-up

With a view to evaluate the performance of the optimised rolling joint with respect to the original one, a series of tip deflection experiments was set up. Two DragonFlex prototypes, one containing the original rolling joint and one with the optimised rolling joint, were rapid prototyped at TU Delft from a resin-like Objet VeroBlue™ RGD840

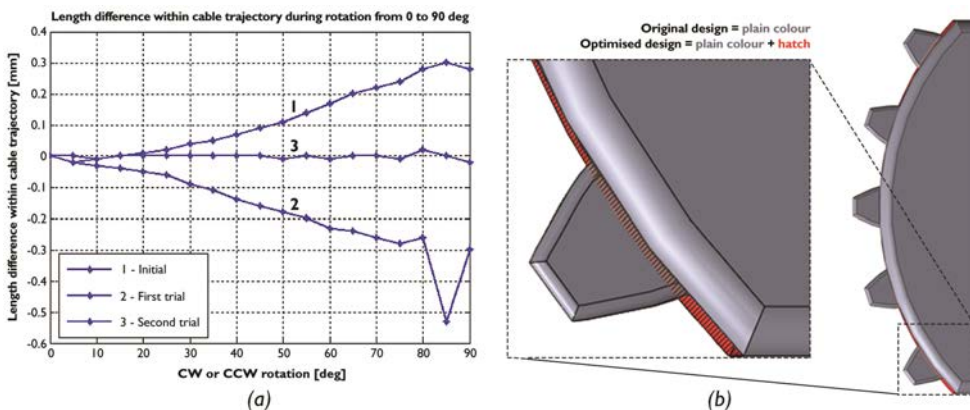


Figure 8.4 (a) Plot of cable trajectory length differences, or cable slack, during rotation and their elimination by iteration (relative to the upscaled instrument's width of 10mm). (b) The original perfectly circular rolling joint design (plain colour) overlaying the optimised rolling joint design (the added difference is marked by the darker hatched area).

material at 0.1mm voxel resolution, using Objet Eden260V™ 3D printer. Since the real-scale rolling joint exhibited only very little cable slack, the experimental prototypes were printed at twice the original dimensions for clearer performance comparison, resulting in the shaft width of 10mm. The upscaled prototype of the original design featured an embedded compression spring in the handle that was also upscaled to reflect the design of the original real-scale prototype. Afterwards, the prototypes were assembled and fitted with two \varnothing 0.45mm 7x7 steel cables, which were equally tensioned in the straight position with 1.1kg load and securely clamped in the instrument handles.

An experimental set-up was created to evaluate the deflection of the tip due to external loading. As shown in Fig. 8.5(a), the set-up consisted of a horizontal aluminium base plate mounted to the universal testing machine Zwick/Roell Z005 (TÜV Nord AG, Hanover, Germany), whereon specialised rapid prototyped handle clamps were fastened. The individual handle clamps enabled fixation at different angles and forced the upscaled DragonFlex to remain in 0°, 30°, 60° and 90° bends as to evaluate the minimisation of the play throughout the different stages of rotation. A shaft clamp of an adjustable inclination angle was attached to the base plate as well, securing DragonFlex so that it remained in the aforementioned angles and was loaded on the tip's proximal joint only. The clamp's adjustable design ensured that the tip maintained an initial horizontal at every stage of bend. Hence,

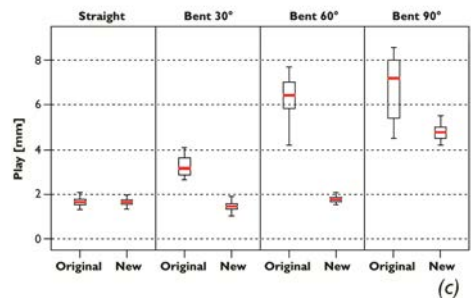
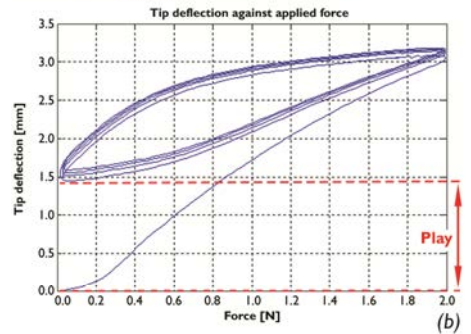
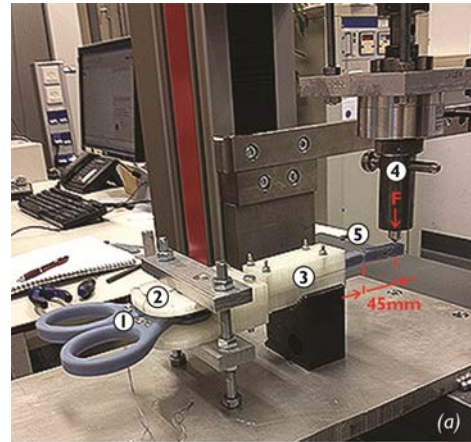


Figure 8.5 (a) Experimental set-up showing (1) the upscaled 10mm wide DragonFlex prototype fixed at 0° by (2) the handle and (3) the shaft clamps. The load F is applied by (4) the tensile tester vertically downwards and 45mm from (5) the tip's proximal joint. (b) Sample plot of raw data showing tip deflection against applied force (original upscaled prototype at 0°) clearly indicating the region of play between the joint's resting positions before and after loading. (c) Boxplots of the play magnitudes in the original and the new upscaled prototypes at 0°, 30°, 60° and 90° bends respectively.

the load was always applied vertically downwards, approximately 45mm from the proximal joint's rolling surface contact towards the distal end of the instrument tip. There was no need to test the tip's distal joint as well, since the overall design is repetitive.

Firstly, using a 1kN load cell, the original and optimised upscaled prototypes were preloaded with a force of 0.02N, ensuring proper contact with the tensile tester and the same initial conditions. The tip deflection was measured from zero after the application of the preload.

Secondly, the prototypes were loaded on their tips with a linearly increasing downward force at a rate of 0.4N/s up to a maximum of 2N. The maximum load of 2N was not motivated by any clinical application and it was chosen arbitrarily within safe limits solely for the sake of objective mutual comparison while preventing any material damage or plastic deformation of the prototypes. After reaching the maximum, the load was then brought to zero at the same rate, allowing the tip to return to its neutral position. This cycle was repeated four more times at each bending angle to ensure that no cable loosening occurred. The entire aforementioned procedure was performed for both prototypes clamped in the four different stages of bend and repeated five times altogether, ensuring validity of the findings.

Thirdly, despite the design being symmetrical, DragonFlex prototypes were flipped axially over 180° to their opposite side and the entire previous procedure was repeated, thus ensuring symmetrical behaviour. All the measurements were recorded at a sampling rate of 16.7Hz.

8.3 Results

8.3.1 Optimised Rolling Joint Evaluation

Figure 8.5(b) demonstrates a sample plot of the tip deflection due to the applied vertical load of the original upscaled prototype at the 0° scenario. At the loading point, 45mm from the rolling surface contact, the proximal joint deflects up to 3mm due to the 2N maximum load. After the load was removed, the tip returned to its neutral position still exhibiting a small deflection of 1.5mm. The shapes and magnitudes of these deflections remained mutually almost equal during the next four loading and unloading cycles, indicating that no cable loosening occurred. The 1.5mm difference between the tip's neutral positions before and after loading was regarded as the actual play in the original upscaled rolling joint mechanism.

The original and the new upscaled prototypes were evaluated based on the play values at 0°, 30°, 60° and 90° bending angles. The experimental results of both upscaled prototypes are summarised in Fig. 8.5(c) as boxplots comparing the play magnitudes.

As expected, the upscaled prototype featuring the optimised rolling joint curvature exhibits significantly lower play values ($p < 0.05$) in all the bending angles (30°-90°), compared to the original. Furthermore, the play in the new upscaled prototype is almost constant throughout rotation as would be expected from the

improved rolling joint curvature resulting in almost eliminated cable slack (Fig. 8.4(a), no. 3). Yet, this does not hold for the 90° bend, where the optimised play values differ significantly from those in the 0° - 60° bends, which is further elaborated on in the section '8.4 Discussion'.

8.3.2 Improved DragonFlex Prototype

The experimental results confirmed that the optimisation of the rolling joint geometry significantly minimises the cable slack and thus the rolling joint play. Assuming that the prototype materials were infinitely rigid with regard to the small applied forces, then the optimisation outcomes apply to the rolling joint geometry at any scale. Therefore, a new real-scale 5mm wide DragonFlex prototype was manufactured implementing these changes. The real-scale prototype, shown in Fig. 8.6(a), was made by additive manufacturing from a clear hard polymer, 3D Systems Accura® 60, printed by PROFORM AG (Marly, Switzerland) using 3D Systems Viper si2™ SLA® System at $75\pm 15\mu\text{m}$ resolution and $2.5\mu\text{m}$ layer thickness. Compared to the material of the original real-scale prototype, the ceramic-filled epoxy resin, this material is often used in the medical industry, although not biocompatible, and proved to have much larger tensile



Figure 8.6 (a) New real-scale 5mm wide DragonFlex prototype featuring (b) the optimised rolling joint curvature, no cable-tensioning spring and (c) a smart and simple bolt-and-wheel mechanism for cable clamping and easy tensioning.

strength and elongation at break, thus making it more durable and less brittle.

As resulted from the optimisation of the rolling joint curvature, the new real-scale DragonFlex prototype [19] features no cable tensioning spring as clearly seen in Fig. 8.6. Besides the play-free rolling joints enabling reliable control of the instrument's tip, Fig. 8.6(b), DragonFlex's handle has been redesigned compared to the original prototype. The cable fixation mechanism in the original prototype was a special bolt press fitted into the handle (Fig. 8.1). However, it was later discovered that the ceramic-filled epoxy resin suffers from creep, thus gradually enabling bolt loosening and undermining its cable fastening capabilities. For that reason the new real-scale DragonFlex prototype features a bolt-and-wheel mechanism, Fig. 8.6(c), that does not rely on the material's ability to retain its initial shape. Furthermore, it was observed that, similarly to the structural material of the original real-scale prototype, the originally used ultra-high-molecular-weight polyethylene Dyneema cable [6] also suffers from creep, thus requiring re-tensioning after some time. Therefore, the new real-scale prototype was fitted with \emptyset 0.2mm steel cables, having much better creep properties than Dyneema.

8.4 Discussion

The experimental evaluation of the upscaled prototypes confirms the expected rolling joint behaviour both before and after implementing the design changes. As a result of the increasing cable slack values in the original rolling joint design (Fig. 8.4(a), no. 1), the joint play was also expected to increase in magnitude with the increasing bending angle, which was confirmed by the experimental data (Fig. 8.5(c)). More specifically, the original prototype exhibits increasing play (more than three times its initial value) as the bending angle increases from 0° to 60° . Clearly, neither the original perfectly circular rolling joint curvature nor the embedded compression spring of limited stiffness and dimensions fully compensated for the cable slack.

In contrast, the play in the new spring-less upscaled prototype retains approximately its initial value during rotation, showing that the optimisation efforts were successful. However, it should be noted that in the 0° state both the upscaled tips already exhibited a play of almost 2mm, even though they were supposedly perfectly tensioned and play-free. A reasonable cause for this initial play, which was still minor with respect to the upscaled prototype dimensions, could be minor manufacturing inaccuracies or a slight cable extension. Nonetheless, these factors did not have any detrimental effect on the overall joint behaviour or the mutual comparison of the prototypes' performance.

In the 90° bend both upscaled prototypes showed larger play magnitudes and distributions as compared to the other bends. As seen in Fig. 8.2, at the 90° bend the two rolling joint curves touch each other only at their very extremes making the mechanism play much more sensitive to inaccuracies in the rapid prototyping process, possibly introducing non-zero gear clearances. Even though the play values exhibit a significant

drop from the original to the optimised joint curvature at the 90° bend (Fig. 8.5(c)), the steering angle of the new real-scale DragonFlex prototype (Fig. 8.6) was limited to $\pm 80^\circ$ in the interest of avoiding the instability at the former extremes. When looking at the state-of-the-art steerable MIS instruments [17, 20, 21], the steering angle usually spans within $\pm 60^\circ$ as in the case of Autonomy Laparo-Angle (Cambridge Endo, Framingham, MA, USA) or Miflex (DEAM, Amsterdam, The Netherlands) [7] and even reaches $\pm 80^\circ$ in SILS Hand (Covidien, Mansfield, MA, USA) [22] and 90° in half a DOF (articulation in a single plane and direction) in r2 DRIVE (Tuebingen Scientific, Tuebingen, Germany) [23]. Thus, the $\pm 80^\circ$ steering angle in the new DragonFlex prototype should not pose any restriction.

Maximum opening angles of the currently available laparoscopic graspers, whether rigid or steerable, range within 60°-90° [16, 24]. The $\pm 80^\circ$ steering angle in the new DragonFlex prototype enables the maximum grasper opening angle of 160°, which makes it superior to the state of the art. However, rather than aiming to maximise the steering and opening angles, a research question that remains unanswered in the literature on steerable instruments is what angle magnitudes are actually needed for which procedures or operations. This represents an important topic for further research and design of the steerable MIS instrumentation as a whole.

Last but not least, even though the polymeric material of the new DragonFlex prototype has very good mechanical properties and appears to be a step closer to a clinical application, its printing resolution is less than a half compared to the ceramic-filled epoxy resin. Although hardly distinguishable by the naked eye, the implications can be severe, especially to very tight tolerances and movable components. As the additive manufacturing technology is still in its infancy, there remains to be a trade-off between material properties and geometrical accuracy. Similarly, the biocompatible materials still tend to be mechanically inferior to their non-medically approved counterparts. However, due to the rapid developments in this field of manufacturing, fine medical instrumentation providing smart mechanical functionality and simple or no assembly is becoming much closer to reality potentially leading to more affordable and readily available technological solutions important within the context of present and future economic situation of healthcare worldwide [25].

8.5 Conclusions

This paper presents an optimisation procedure involving mathematical iteration for minimising play in rolling joints by critical adjustments already in the design phase. As illustrated on the example of the steerable laparoscopic instrument prototype DragonFlex, rather than using conventional methods for play reduction, the approach involved optimisation of the rolling joint curvature. As a result, the curvature optimisation proved to be successful in minimising the joint play as shown experimentally, thereby eliminating the need for a cable tensioning mechanism as such. This method is generally applicable to play minimisation in rolling joint constructions of

minimally invasive instruments and it was implemented in a new spring-less real-scale DragonFlex prototype.

Acknowledgements

This research was performed within the framework of CTMM, the Center for Translational Molecular Medicine, project MUSIS (grant 030-202). The authors would like to thank the Dutch Organisation for Applied Scientific Research (TNO) for their collaboration. Many thanks to David Jager and Menno Lageweg from TU Delft's fine mechanical workshop DEMO for their support.

References

- [1] Braga, M., Vignali, A., Gianotti, L., Zuliani, W., Radaelli, G., Gruarin, P., Dellabona, P., and Carlo, V. D., 2002, "Laparoscopic Versus Open Colorectal Surgery: A Randomized Trial on Short-Term Outcome," *Ann Surg*, 236(6), pp. 759–767.
- [2] Breedveld, P., Stassen, H. G., Meijer, D. W., and Jakimowicz, J. J., 1999, "Manipulation in laparoscopic surgery: Overview of impeding effects and supporting aids," *J Laparoendosc Adv Surg Tech A*, 9(6), pp. 469-480.
- [3] Khorijestani, S. M., Najarian, S., Simforoosh, N., and Farkoush, S. H., 2010, "Design and Modeling of a Novel Flexible Surgical Instrument Applicable in Minimally Invasive Surgery," *Int J Nat Eng Sci*, 4(1), pp. 53-60.
- [4] Minor, M., and Mukherjee, R., 1999, "A Mechanism for Dexterous End-Effector Placement During Minimally Invasive Surgery," *J Mech Des*, 121(4), pp. 472-479.
- [5] Velanovich, V., 2000, "Laparoscopic vs open surgery," *Surg Endosc*, 14(1), pp. 16-21.
- [6] Jelínek, F., Pessers, R., and Breedveld, P., 2014, "DragonFlex Smart Steerable Laparoscopic Instrument," *J Med Device*, 8(1), p. 015001.
- [7] Breedveld, P., 2010, "Steerable Laparoscopic Cable-Ring Forceps," *J Med Device*, 4(2), p. 027518.
- [8] Breedveld, P., Scheltes, J. S., Blom, E. M., and Verheij, J. E. I., 2005, "A new, easily miniaturized steerable endoscope," *IEEE Eng Med Biol Mag*, 24(6), pp. 40-47.
- [9] Janssen, R., 2011, "3D Printing Now With Ceramics Too," TNO Time, TNO, Delft, pp. 18-19.
- [10] Kruf, W., Vorst, B. v. d., Maalderink, H., and Kamperman, N., 2006, "Design for Rapid Manufacturing functional SLS parts," *Intelligent Production Machines and Systems*, D.T. Pham, E. E. Eldukhri, and A. J. Soroka, eds., Elsevier, Oxford, pp. 389-394.
- [11] Kruth, J. P., Leu, M. C., and Nakagawa, T., 1998, "Progress in Additive Manufacturing and Rapid Prototyping," *CIRP Ann - Manuf Technol*, 47(2), pp. 525-540.
- [12] Taylor, C. S., Cherkas, P., Hampton, H., Frantzen, J. J., Shah, B. O., Tiffany, W. B., Nanis, L., Booker, P., Salahieh, A., and Hansen, R., "Spatial forming - a three dimensional printing process," *Proc. IEEE MEMS*, 1995, p. 203.
- [13] Yan, X., and Gu, P., 1996, "A review of rapid prototyping technologies and systems," *Comput Aided Des*, 28(4), pp. 307-318.
- [14] Cepolina, F., and Michelini, R. C., 2004, "Review of robotic fixtures for minimally invasive surgery," *Int J Med Robot*, 1(1), pp. 43-63.
- [15] Palep, J. H., 2009, "Robotic assisted minimally invasive surgery," *J Minim Access Surg*, 5(1), pp. 1-7.
- [16] Intuitive Surgical, 2013, "EndoWrist - Instrument and Accessory Catalog," http://www.intuitivesurgical.com/products/871145_Instrument_Accessory_%20Catalog.pdf.
- [17] Jelínek, F., Gerboni, G., Henselmans, P. W. J., Pessers, R., and Breedveld, P., 2014, "Attaining high bending stiffness by full actuation in steerable minimally invasive surgical instruments," *Minim Invasive Ther Allied Technol*, in press.
- [18] Breedveld, P., and Hirose, S., 2004, "Design of Steerable Endoscopes to Improve the Visual Perception of Depth During Laparoscopic Surgery," *J Mech Des*, 126(1), pp. 2-5.
- [19] van Dijk, T., 2014, "Printing Plastic," Delft Outlook, TU Delft, Delft, July 2014, p. 13.
- [20] Fan, C., Dodou, D., and Breedveld, P., 2013, "Review of manual control methods for handheld maneuverable instruments," *Minim Invasive Ther Allied Technol*, 22(3), pp. 127-135.
- [21] Jelínek, F., Arkenbout, E. A., Henselmans, P. W. J., Pessers, R., and Breedveld, P., 2015, "Classification of Joints Used in Steerable Instruments for Minimally Invasive Surgery—A Review of the State of the Art," *J Med Device*, 9(1), p. 010801.
- [22] Covidien, 2010, "SILS™ Articulating Hand Instruments," <http://surgical.covidien.com/imageserver.aspx/sils-articulating-hand-instruments-brochure.pdf?contentID=38919&contenttype=application/pdf>.
- [23] Mettler, L., Clevin, L., Ternamian, A., Puntambekar, S., Schollmeyer, T., and Alkatout, I., 2013, "The past, present and future of minimally invasive endoscopy in gynecology: A review and speculative outlook," *Minim Invasive Ther Allied Technol*, 22(4), pp. 210-226.
- [24] Aesculap, 2010, "Laparoscopic Instruments - Product Catalog," http://www.aesculapusa.com/assets/base/doc/DOC465_REV_F_Laparoscopic_Catalog.pdf.
- [25] Arezzo, A., 2014, "The past, the present, and the future of minimally invasive therapy in laparoscopic surgery: A review and speculative outlook," *Minim Invasive Ther Allied Technol*, 23(5), pp. 253-260.

Chapter 9

Discussion

9.1 Envisioned Steerable Opto-Mechanical Biopsy Harvester

The aim of this thesis was to provide a scientific framework behind the development of an envisioned steerable minimally invasive opto-mechanical biopsy harvester, whose ultimate design is outlined in the following pages. The harvester would serve as a resection and a validation tool for the newly emerging optical biopsy technology based on the differential pathlength spectroscopy (DPS).

9.1.1 Biopsy Harvester Design

In the beginning of the design process, *Chapter 2* clarified that the currently available minimally invasive instruments featuring a hollow channel and a tissue manipulator for both the optical and the mechanical biopsies are very limited. For that reason, a novel spring-loaded biopsy harvester was devised and presented in *Chapter 3*. As pointed out in the Introduction (*Chapter 1*), this experimental design of the opto-mechanical biopsy harvester was devised with a great consideration of its final usage and made almost at real scale, thus making the step to the final design easier. As clear from the reasoning throughout the first part of this thesis (*Chapters 1-4*), the main feature of the biopsy harvester, besides the actual harvesting, is to house a fibre optic cable serving for the optical biopsy via DPS. As explained, the radical tumour resection has to be performed controllably, accurately and ideally without tumour perforation. This can only be achieved if the resected tissue volume closely matches the one that was optically analysed.

The fibre optic cable is a \varnothing 2mm bundle of glass fibres and it is capable of optically analysing the tissue with its entire cross-section, while the visible light signal can penetrate up to a few hundreds of micrometres into tissue. The current crown-cutter that would fit in a \varnothing 5mm instrument and encompass a \varnothing 2mm fibre optic cable is made of \varnothing 4.3x0.15mm steel tube and when collapsed inwards, each tooth is angled 20° from the vertical. This means that the analysed cylindrical \varnothing 2mm tissue volume fitting within the conical biopsy volume can be up to 1-1.5mm deep, while considering the fibre polishing angle of 15° . Since the actual analysed tissue volume should not exceed a couple of hundred micrometres in depth, the mechanically extracted biopsy should safely contain the analysed tissue volume, while not extending too much beyond it. Nevertheless, since the mechanical biopsy is essentially a pointy cone surpassing the depth of the optical biopsy, one might wonder how to ensure that a possible tumour below the maximum depth of the optical biopsy is not perforated. Naturally, the current biopsy harvester's design cannot prevent such a probability, however, a prior use of the near-infrared (NIR) fluorescence with a greater penetration depth than DPS should warn against taking the biopsy at such a hazardous spot. Yet, as explained in *Chapter 1*, such operation would rely on NIR fluorescence's ability of depth perception and discrimination of various depth levels, which remain to be investigated or further developed.

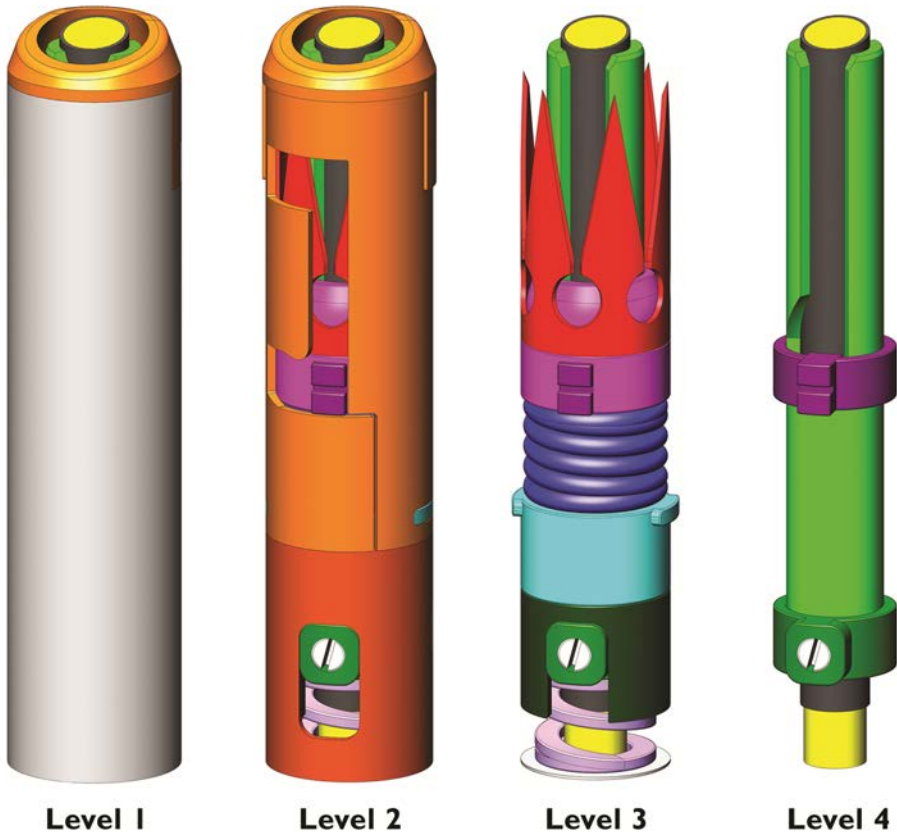


Figure 9.1 Decomposition of the final envisioned biopsy harvester design in four levels.

After the 2mm inner diameter and the 5mm outer diameter limits, the aforementioned crown-cutter geometry presents the next checkpoint in dimensioning the final biopsy harvester's design. As clear from the arrangement of the components in the biopsy harvester (*Chapter 3*), the crown-cutter's closing angle and the resulting axial travel determine the length of the compression spring actuating the cutter and hence the length of the biopsy harvester overall. The experimental biopsy harvester design provided some fine-tuning with regard to the spring force ensuring proper collapsibility and operation of the crown-cutter. This resulted in the biopsy harvester's length of 30mm. Nevertheless, since the biopsy harvester proved to work as planned already with the original custom-made spring design, the adjustability feature was no longer needed. Hence, with regard to the crown-cutter's dimensions and axial travel, the final biopsy harvester's design, presented in Fig. 9.1, was shortened to 20mm, being in the range of short laparoscopic graspers.

The biopsy harvester's outer diameter was decreased from 6mm to the more clinically acceptable 5mm by decreasing the thickness of its robust 0.75mm thick outer shell. Even though the 1mm drop in diameter may go unnoticed in the eyes of a common observer, a more visible design change is in fact apparent already on the outside, as demonstrated in Fig. 9.1 (Level 1). The biopsy harvester's outer shell was completely enclosed along its length, sealing off the inner mechanism from the outer environment. This was done in order to prevent any potential entanglement of the surrounding tissue in the working mechanism and to help maintain inner sterility to an extent. Hence the outer shell is now composed of two layers (Levels 1 & 2).

The initial requirements for the biopsy harvester's design (Chapters 1 & 3) stated a removability feature that would enable containing each biopsy sample in a separate container suitable for storage, transport and further pathological analysis, if needed. The experimental design presented in Chapter 3 did not provide such a functionality, yet. However, a further step was taken in the final design towards enabling this. For that reason, the shell's inner layer (Level 2, light & dark brown) is composed of two concentric tubes interconnected with a bayonet connector (Fig. 9.2). The disposable part of the biopsy harvester (Level 2, light brown) would house the factory preloaded crown-cutter and one half of the cutter actuation mechanism in either mounted or demounted state. The permanent part of the biopsy harvester (Level 2, dark brown), connected to the steerable construction, would feature the second half of the cutter actuation mechanism, while housing and protecting the fibre optic cable. A complete description of the harvester's inner working mechanism can be found in the Appendix.

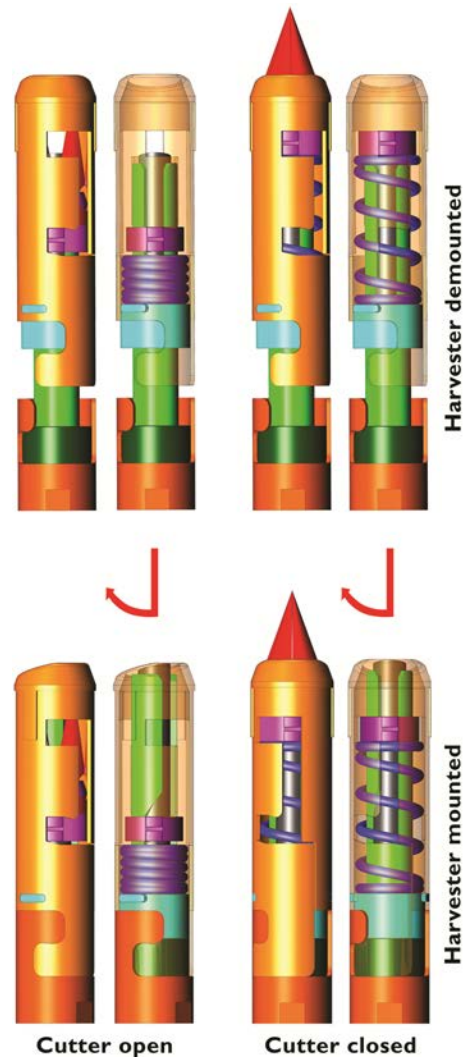


Figure 9.2 Method of mounting the disposable part of the biopsy harvester to the permanent part by means of a bayonet connector (transparency and hidden features for the clarity of component alignment).

With reference to Figs. 9.1-9.2, when mounting the disposable part onto the permanent part, the inner components of the disposable part would slide over the long inner sleeve (Level 4, light green) containing the fibre optic cable (Level 4, yellow). Once slid on completely, the disposable part would be turned axially clockwise with respect to the permanent part and secured by means of a single robust bayonet connector. On the other hand, once biopsy is taken and the crown-cutter is in its closed state, the disposable part of the biopsy harvester would have to be turned anticlockwise in order to demount it from the permanent part, hence serving as a container for sample transport. This could have only been made possible by extending the J-shaped slot by a horizontal opening at its tip allowing space for the short-pinned sleeve (Level 4, violet), whose axial rotation is restricted by the slot in the long inner sleeve (Level 4, light green).

9.1.2 Joint Construction Design

Chapter 5 provides an overview of all the mechanical joint constructions used in or potentially applicable to the steerable minimally invasive surgical (MIS) instruments. The review was performed with the focus on the joints' capabilities of preventing axial spin, as well as transverse and axial split; their capacity for featuring an internal lumen; the possibility of miniaturisation and the overall design simplicity. Bearing all these factors in mind, the primary goal within the presented endeavours is ensuring reliable controllability of the joint construction with the vision of performing an accurate biopsy. All these considerations led to the development of a geared fully actuated rolling joint design (*Chapters 6-8*) with a special cable guidance for the maximisation of the cable bending radius and the equalisation of the force requirements on the steering cables. The promising potential and the implications of such a joint construction were demonstrated in DragonFlex prototype by its simplicity (*Chapter 6*) and high bending stiffness (*Chapter 7 & 8*).

As elaborated on throughout this thesis, precise and accurate biopsy targeting can only be enabled if resistance to external forces can be maintained. The factors eliciting the external forces on the envisioned biopsy harvester would include influence from the tissue or the overall surgical environment, as well as the impact of the biopsy harvester's actuation and spring action. *Chapter 7* demonstrates that a high bending stiffness of a joint construction can be achieved through full actuation provided by the developed rolling joint, as opposed to underactuation. The presented mutual performance comparison was done with DragonFlex's fully actuated rolling joint and the underactuated joint constructions of the currently available steerable MIS instruments. Even though the evaluated joint constructions featured some minor design differences, mostly in favour of the state of the art, DragonFlex's rolling joint still proved much stiffer when bent. The follow-up design optimisation (*Chapter 8*) is specific to this particular rolling joint, due to the special cable guidance (*Chapter 6*). However, the general procedure could be modified to other rolling joint designs, thus removing any residual play and achieving total bending stiffness in theory.

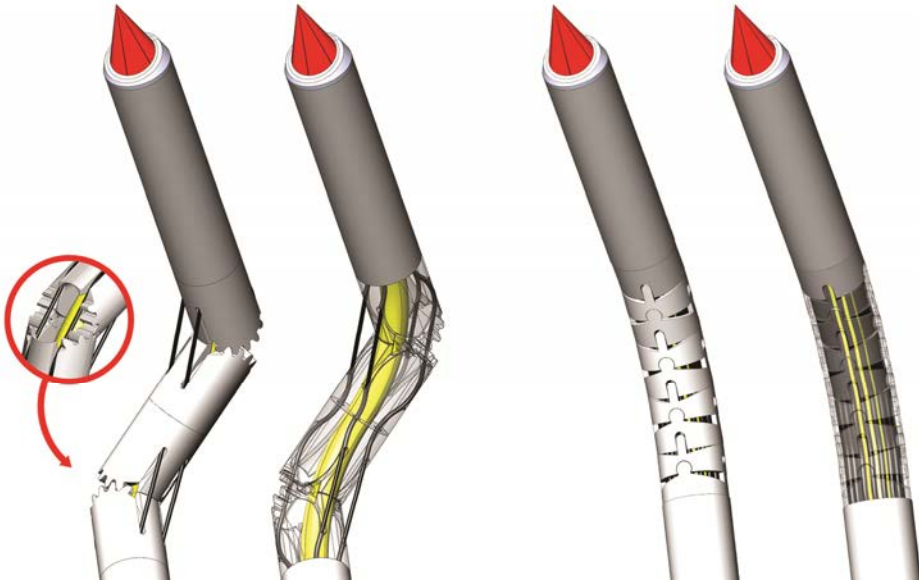


Figure 9.3 Feasible steerable joint constructions: the additive manufactured rolling joint construction and the laser cut joint construction. Joints are actuated by steering cables (black).

Due to the aforementioned qualities, the rolling joint design was modified further in order to serve as a stiff and reliable articulation medium for aligning the biopsy harvester with the targeted tissue, leading to the design presented in Fig. 9.3, left. The first most obvious step with respect to the original design involved transforming the rolling joint's 5mm wide square cross-section into a \varnothing 5mm circular cross-section, which involved downscaling the overall geometry by almost 15%. The next step involved incorporating a \varnothing 2mm hollow channel for the fibre optic cable inside the previously solid geometry of the rolling joint. Since each rolling joint features only two elements, thus delivering one rotational DOF, the minimum allowed bending radius of the fibre optic cable presented the most crucial design checkpoint. According to the manufacturer, the minimum bending radius of a \varnothing 2mm DPS fibre optic cable is 70mm when stored long-term. However, since long-term storage in the bent state is not the case here, a feasibility test was performed by DEAM (Amsterdam, The Netherlands) who fitted the \varnothing 2mm fibre optic cable into their steerable laser cut joint construction used in Miflex instrument. Although not estimating the very minimum bending radius for steering, the feasibility test has shown that the joint construction's bending radius of 13mm did not have any detrimental effect on the fibre optic cable's integrity. Hence, setting the bending radius to 13mm, the geared rolling joint can be steered by two \varnothing 0.3mm cables up to $\pm 57^\circ$ bending angle, which is comparable to the common range of $\pm 60^\circ$ in the state of the art as discussed in *Chapter 8*. However, the hollowing out of the rolling joint results in removing its main centrally-positioned load-bearing rolling surface (Fig. 9.3, inset). Of course, the joint can still function as the rolling motion is also provided by the gears whose pitch angle follows the rolling joint curvature. However,

potential tooth jamming or even breakage could occur if not manufactured accurately and precisely enough, or if made of an inferior material as explained in *Chapter 6*.

Considering the limited possibilities of the state-of-the-art manufacturing processes, an alternative solution to the additive manufactured rolling joint could be either its machinable modification, or the laser cut joint construction (Fig. 9.3, right) as used in DEAM's Miflex. However, as explained in *Chapter 7*, Miflex's joint construction is underactuated and thus susceptible to an uncontrollable change in shape and bending angle to an extent, when loaded externally. However, as it was shown, a reliable controllability could be achieved by implementing the full actuation principle. As indicated in *Chapter 6* this was achieved in a similar joint construction in TU Delft's fully actuated Multi-Flex prototype, where each two-DOF joint section has four steering cables soldered or spot welded in. Hence, since the individual elements in the laser cut joint construction are rigid, then one rotational DOF provided by two such elements can be fully actuated by two cables. Miflex's laser cut joint construction consists of eight one-DOF joints that can provide a bending angle of $\pm 60^\circ$ in total. If fully actuated, these eight joints would require sixteen steering cables arranged circumferentially just below the outer shell and their diameter could be up to twice the diameter of the steering cables in the rolling joint construction. The increased diameter might represent a benefit in the end, however, as *Chapter 7* illustrates the actuation of each steering element is the most crucial factor for delivering high bending stiffness.

Whether using DragonFlex's rolling joint or Miflex's laser cut joint construction in the end, a sealing would be a necessity in both cases in order to prevent any potential tissue entanglement. While fitting a shrink tube over the laser cut joint construction is relatively effortless from the design point of view, in case of the rolling joint this might present a difficulty due to the sticking-out cables and local bending. On a different note, while the laser cut joint construction could provide even larger bending radius ($>13\text{mm}$) and bending angle ($>60^\circ$) for the fibre optic cable by adding more joint elements, its bending stiffness remains to be evaluated when implementing full actuation. On the other hand, the rolling joint could only provide potentially larger bending radius if the joint elements were considerably lengthened, which would in turn put the cable moment arms out of balance as elaborated on in *Chapter 6*. In addition, the bending angle of the rolling joint is related to the fibre optic cable's bending radius more closely than in the laser cut joint construction, since only two joint elements are used for one rotational DOF as opposed to multiple joint elements. Hence, there seems to be a trade-off between the large bending radius/angle, provided by the laser cut joint construction, and high bending stiffness, provided by the rolling joint. Lastly, it remains to be investigated which joint could be controlled with greater ease, while providing more optimal route to the targeted tissue. The rolling joint construction would require an independent actuation of its two rolling joints while enabling a formation of a double bend to an extent, whereas the laser cut joint construction could be controlled as a whole and possibly more intuitively. The ultimate decision and preference would

depend on the exact final clinical application and use, the needed workspace and the required bending angles.

9.1.3 Steerable Opto-Mechanical Biopsy Harvester Prototype

To satisfy the line of reasoning throughout this thesis as well as the researcher's and the reader's curiosity, a steerable opto-mechanical biopsy harvester prototype was manufactured at real-scale via conventional machining and additive manufacturing. On top of the design presented in 9.1.1, the final prototype shown in Fig. 9.4 features a rolling joint construction as suggested in 9.1.2. Nevertheless, for the sake of design simplicity, sturdiness, manufacturability and assembly, the rolling joint segment neighbouring the biopsy harvester was split into two sections. The first peripheral section contains a pair of the actual geared rolling joint surfaces, designed to be in one piece with the permanent tube of the biopsy harvester's outer shell. The second central section features the core of the rolling joint segment, incorporating the curved cable channels and a central lumen for the fibre optic cable. Due to its complex geometry, this



Figure 9.4 Final manufactured steerable opto-mechanical biopsy harvester prototype.

central section was made by additive manufacturing, just as DragonFlex prototype discussed in *Chapters 6-8*. The additive manufactured central section fits tightly into the machined peripheral section and it is fixed in place by two press fitted pins and the joint's steering cables. The steering cables run through the curved holes of the central section and loop through an inner partition between the peripheral section and the permanent tube of the outer shell, where they are pressed on from the distal side by a rear compression spring (Fig. 9.1, Level 3, light violet) and a washer. The rest of the rolling joint construction would be simply additive manufactured.

9.1.4 Envisioned Instrument Usage

As outlined in the Introduction (*Chapter 1*), the envisioned use of the steerable opto-mechanical biopsy harvester would be radical tumour resection performed firstly by rough tumour localisation through the NIR fluorescence and multispectral imaging; then

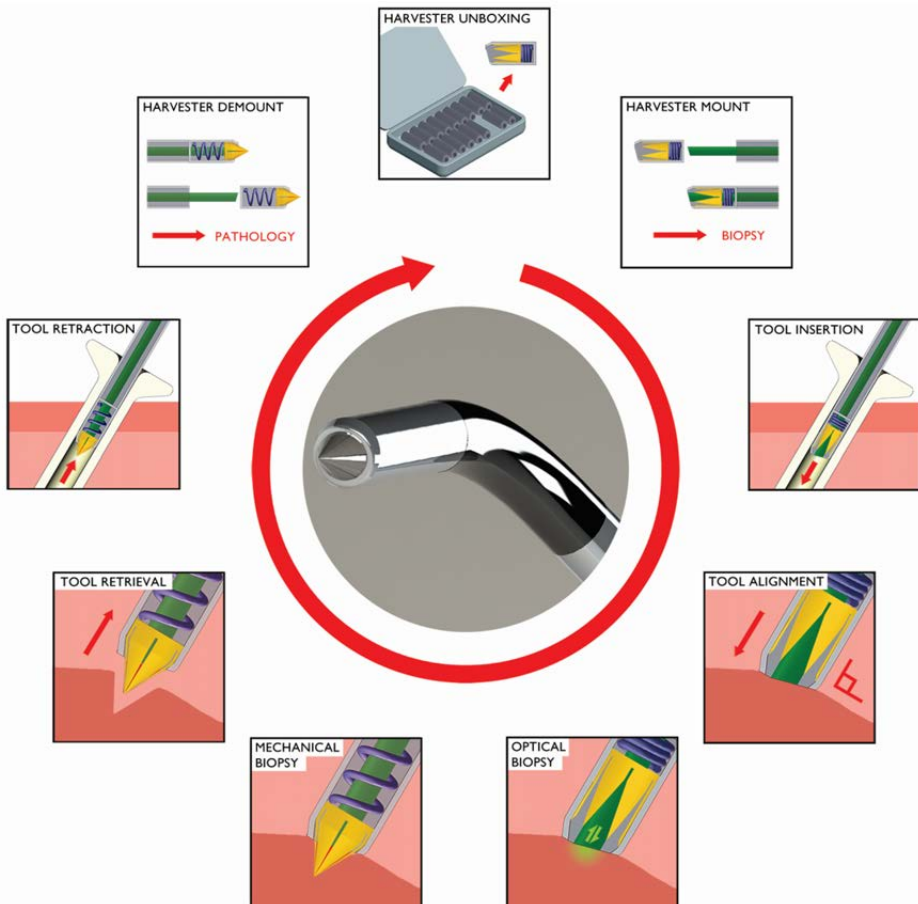


Figure 9.5 Envisioned usage of the biopsy harvester taking into consideration the feature of removability and thus suitability for single use (colour coding differs from previous figures for better contrast against tissue).

by precise tumour localisation via the DPS and finally by the actual tissue resection. The envisioned clinical usage is explained by the scheme in Fig. 9.5.

A single-use removable part of the biopsy harvester would be stored preloaded in large numbers in a storage box. One of these disposable parts would be unpacked and mounted on top of the biopsy harvester's permanent part (demonstrated in detail in Fig. 9.2) sitting on top of the instrument's steerable shaft. The instrument would be then inserted into the body, most probably the abdominal cavity, through a trocar. Based on rough tumour localisation, the biopsy harvester would approach the approximate location of the tumour and would be aligned by means of the steerable construction ensuring proper fibre-tissue contact. This contact would be verified by means of an endoscope visualising the entire procedure as well as the real-time DPS readout. Of course, the DPS would have to be capable of distinguishing between the carbon-dioxide atmosphere in the abdominal cavity and the healthy or the supposedly highly oxygenated tumorous tissue. Once the optical biopsy confirms a tumorous tissue, the mechanical biopsy could be performed *in situ* and in a matter of seconds. Right after the tissue resection, the biopsy harvester tip would be retrieved from the site and the entire instrument would be retracted from the body. Once outside, the disposable part of the biopsy harvester would be demounted from the instrument, thus enabling storage of each biopsy sample in an individual container. Alternatively, the instrument might be kept in the body, while retracting only the fibre optic cable and using the instrument's lumen as a suction channel for the biopsy sample. Such use would then enable taking another biopsy without having to retrieve the entire tool, yet the reloading of the crown-cutter would have to be provided by an extra functionality, if feasible at such a small scale. The biopsy sample, whether retrieved by suction or stored in the disposable part of the biopsy harvester, could be then sent to pathology for further analysis.

With regard to the pathology, an alternative use of the steerable opto-mechanical biopsy harvester would be as a validation device for other emerging optical biopsy technologies that use the fibreoptics as a signal carrier. Such a small and accurate validation tool would be especially useful in the research practice, where the experimentation is most easily and affordably performed on mice and other small animals. As illustrated in Fig. 9.6, the experimental biopsy harvester prototype (*Chapter 3*) was successfully used during *in vivo* experiments at Erasmus University Medical Center (Rotterdam, The Netherlands) on a mouse liver in conjunction with the fibre optic cable for the DPS measurements. It should be noted that the experiments could not have been performed with other available instruments, such as a biopsy punch. Similar applications might even enable possible open surgery modification of the biopsy harvester, the upscaling of which could be done with ease if needed.

Whether its MIS or open surgery embodiment, the biopsy harvester could find use in the field of forensics as well, for example as an end effector for a robotic instrument, such as Virtopsy robot developed by Institute of Forensic Medicine Zurich (University of Zurich, Switzerland) in collaboration with ACMIT (Wiener Neustadt, Austria), hence enabling retrieval of small tissue samples and body fluids from cadavers.



Figure 9.6 *In vivo* trials on a mouse liver with the experimental biopsy harvester prototype housing a DPS fibre optic cable, showing its potential as a validation device for other optical biopsy technologies.

On a different note, the biopsy harvester might even return the favour to the sea world, where the inspiration for the crown-cutter's design was taken from, and find use as a sampling device for research or investigation purposes in hard to reach, long and thin crevices and even deep sea spaces where the use of robotics or tele-manipulators would be essential. Same applies to any other potentially hazardous research or industrial application, such as taking geological, even radioactive, samples whether on planet Earth or even during exploration of planetary bodies in near space.

9.2 Design Aspects and Issues for Further Consideration

9.2.1 Design and Manufacturing

The discussion so far presented the envisioned design and usage of the steerable opto-mechanical biopsy harvester as a result of a step-by-step elaboration throughout the chapters of this thesis. Yet, several other design, manufacturing and usage issues would have to be considered before delivering a clinically applicable instrument.

First and foremost, for a reliable optical analysis of the targeted tissue, it is vital that the polished surface of the fibre optic cable is perfectly aligned with the surface of

the biopsy harvester's cap. More specifically, in order to ensure complete fibre-tissue contact, the fibre optic cable would have to be prevented from detaching and creating a gap during the optical biopsy or, on the contrary, from impeding the blood flow by protruding from the biopsy harvester. In order to prevent the fibre optic cable from sliding in and out, it would have to be fixed inside the permanent part of the biopsy harvester, ideally by means that would enable its removal or replacement once required. Similarly, the coplanar alignment of the fibre-cap interface could be disrupted by joint steering and especially during shaft's axial rotation when the fibre could twist independently from the joint construction. For these reasons and the need for the inner mechanism actuation via the fibre optic cable, the setscrew was implemented in the current embodiment, supposedly solving all these issues at once.

Secondly, it should be noted that both the experimental and the final steerable biopsy harvester prototypes are on the verge of manufacturing possibilities nowadays. The experimental biopsy harvester already had several miniature components that depend on tight manufacturing tolerances and mutually perfect interfacing. The slight increase in the number of components in the final biopsy harvester prototype may eventually result in a lengthy assembly of the final instrument, possibly making the envisioned design uneconomical for the eventual mass production. Yet, before reaching any preliminary conclusions, the aspect of assembly would have to be investigated in an objective manner.

When it comes to further research, the rolling joint manufacture and its implications should be discussed in brief. Even though mechanically simple, the rolling joint design has certain geometrical features as elaborated on in *Chapter 6* due to which the most suitable method by which it could be easily and economically materialised is additive manufacturing. *Chapters 6 & 8* discuss the manufacturing limitations and the most immediate potential of this technology in more detail, especially with respect to several aspects of the medical device design. However, the bottom line is that there are certain paradoxical limits to this process, since even with the best materials nowadays, it is difficult to combine sufficient precision and accuracy with ideal material properties due to the layer building nature of these processes. It is also important to mention that while certain promising materials exist, such as very strong additive manufactured ceramics, it is of great importance for the medical device development that such materials are modified towards biocompatibility. While several biocompatible materials exist and are widely used, they are usually of inferior mechanical properties, such as brittle plastics, or they are manufactured at a low resolution requiring post processing, such as metals. Taking all these factors into consideration, it has to be noted that unless their ideal balance is determined and reached soon, the actual onset of mass additive manufacturing of steerable MIS devices, such as DragonFlex, lies further in the future. On the other hand, as shown in *Chapters 7 & 8*, the additive manufacturing or the more affordable rapid prototyping can be readily used for the design and convenient immediate manufacture of experimental set-ups, provided that the material properties and the printing accuracy suffice. Once, however, the full potential of additive

manufacturing is seized, one can only speculate what its true implications could be. While staying focused on the medical instrument manufacture, one could logically expect a demise of manufacturing facilities as such. The reason being that designers could simply supply all the virtual medically approved tool designs directly to the hospitals, which, in possession of additive manufacturing machines, would readily print all their equipment in-house. Naturally, this notion could be easily extrapolated to almost any industry and product, even food, which is closer to reality than one might expect, as any additive manufacturing specialist, such as TNO in Eindhoven, could readily verify.

Last but not least, having discussed the individual design and manufacturing limitations of both the biopsy harvester and the rolling joint construction, it is important to devote a few down-to-earth thoughts specifically to the control of the final instrument, despite not being the focus of this thesis. In a design embodiment where the biopsy harvester would sit on top of the laser cut joint construction mounted to a shaft of an instrument just like DEAM's Miflex, the steering of the joint construction could be eventually provided by a two-DOF joystick with a single pivoting point and the harvester actuation could be performed by a trigger. However, the joint construction of two one-DOF rolling joints could not be combined with a joystick & trigger operated handle with such an ease. As clear from *Chapter 6* the rolling joint construction in the tip would require a mirrored design in the handle. The easiest design scenario would then be to place the actual handgrip behind the rolling joint construction, resulting in a wrist-controlled design just as in Cambridge Endo's Laparo-Angle. Alternatively, one might desire a thumb-controlled interface as in DEAM's Miflex, which would have to combine and incorporate two one-DOF rolling joints of displaced axes of rotation in an easily and intuitively controllable joystick, the design of which would have to be investigated in the future. However, if the handle kept its original scissor-shaped design, then the critical question would be how to combine joint steering with the biopsy harvester actuation. In other words, the focus for further investigation would be implementing another trigger or lever in an existing construction of two levers, while operating them easily and intuitively together.

9.2.2 Usage

Similarly to the design and manufacturing, there are some other practical issues to be considered with regard to the final instrument usage. When it comes to the actual size and volume of the sampled tissue, the small biopsy harvester geometry may be beneficial as far as small tumours are concerned or when used on small organs and tissues that are difficult to reach, as in the case of a mouse liver. Nevertheless, the small dimensions of the biopsy harvester and the crown-cutter could be limiting for the radical tumour resection of larger tumours as their perforation would have to be prevented.

Aside from the resected tissue volume, the targeted tissue type presents another issue. The biopsy harvester's evaluation was provided in free space and on a

chicken liver *in vitro* fulfilling the initial goal (Chapter 3), then on a gelatine (Chapter 4) and on a mouse liver *in vivo*. However, depending on the final application, further evaluation on other tissues could be needed. Several other animal tissues were experimented on *in vitro* at the Utrecht University's Equine Clinic. As demonstrated in Fig. 9.7, the biopsy harvester was capable of sampling a veal kidney almost perfectly; only one sample was not resected entirely (close to the centre of Fig. 9.7) due to the oxidisation of the tissue when experimented on *in vitro* for a longer period. The oxidisation had even more detrimental effect on a veal spleen that formed a thick crust, while being very compliant below the surface, thereby making the experimental biopsy harvester unusable on such an abnormal tissue. The biopsy harvester was also trialled on a horse's brain, which however flowed out due to its high water content. This indicates that the crown-cutter is not watertight despite the tight mutual fit of its teeth as shown in Chapter 3. Furthermore, tougher tissues might need a stiffer spring or potentially some changes to the crown-cutter design itself.

With regard to the optimisation issue, the 6-teeth crown-cutter proved to be the most optimal with respect to minimising tissue deformation, penetration forces and enabling proper tooth collapsibility and thus full enclosure of the resected biopsy volume (Chapter 4). Nevertheless, Chapter 3 explained that the 6-teeth crown-cutter sampled approximately one third of the maximum theoretically extracted biopsy volume. While measuring the mass of the resected tissue samples with micro scale it was noticed that the liver tissue started to lose mass quickly and readily through water evaporation right after the biopsy was taken. Together with the likely possibility that

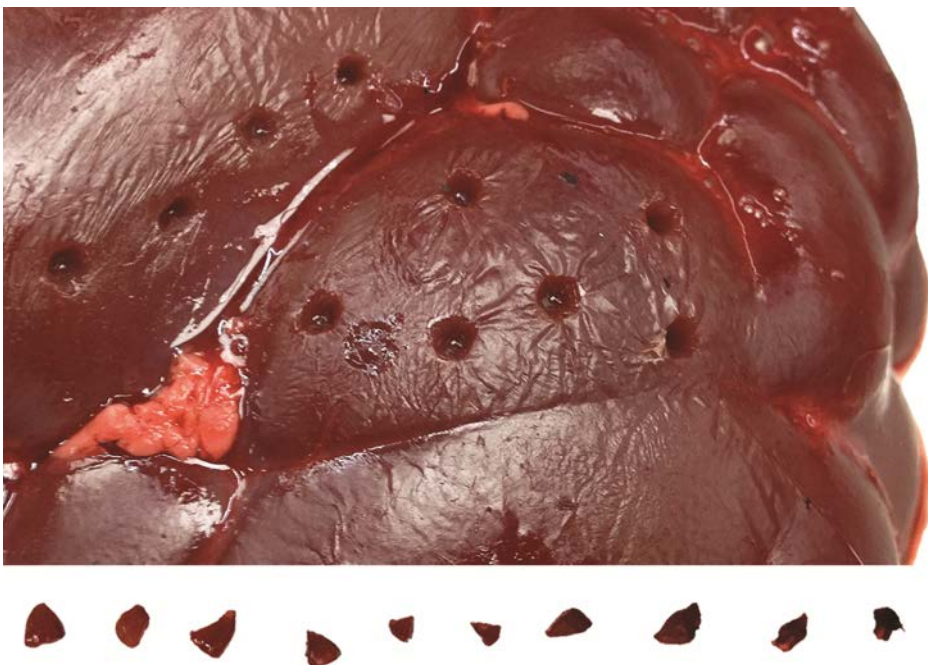


Figure 9.7 *In vitro* trials with the experimental biopsy harvester prototype on veal kidney.

the liver tissue of higher water content has flown out as soon as the biopsy was retrieved, the water evaporation could have accounted for a considerable loss of mass and hence more pessimistic estimate regarding the biopsy harvester's resecting and retrieving capabilities. Nevertheless, even though the water loss should not have presented any negative impact on the harvester's accuracy and reliability, further crown-cutter optimisation efforts could be undertaken in the future.

For the sake of biopsy volume maximisation and efficient resection of other tissue types, other geometrical aspects of the crown-cutter could be investigated and possibly optimised. As suggested in *Chapter 4* open features could be introduced to the crown-cutter teeth decreasing the cutter-tissue contact area, however, these would have to be designed with care in order to prevent any eventual release of the retrieved biopsy. Similarly, tissue penetration could be further eased by using a cutter of smaller wall thickness, while possibly introducing the bevel not only to the very tips of the teeth, but also along their entire cutting edges. Making the cutter as thin and as sharp as possible was attempted already from the very beginning, however, manufacturing limits started to pose a problem. The crown-cutter tube of 0.15mm wall thickness already presented the thinnest acquirable design available on the market for the given tube diameter, which was at the same time thick enough to prevent any tooth deformation during use. Since, the crown-cutter was manufactured by electric discharge machining (EDM) for the sake of mutual design accuracy of its teeth, achieving a uniform and continuous bevel along their entire edges would be impossible as explained in *Chapter 4*. Due to the miniscule and relatively fragile geometry of the teeth, their sharpening would also be almost unachievable by other manufacturing methods, or at least not in an accurately controlled and repeatable fashion for the purpose of mutual performance comparison.

The last part of the discussion deals with possible limitations of the biopsy harvester after having taken a tissue biopsy. Once retrieving the sampled tissue from the disposable part of the biopsy harvester, this would have to be done from the rear, at the location of the bayonet connector, while avoiding the risk of getting pricked by the closed crown-cutter. For that reason a blunt protective cap would have to be designed and put on the closed biopsy harvester as soon as it is retracted from the body. Assuming the envisioned usage in Fig. 9.5, it would be more economical if the multitude of disposable biopsy harvester tips were re-sterilised for the next use. The issue of re-sterilisation could be a little cumbersome, especially for the permanent part of the biopsy harvester, since body fluids can enter in between the harvester's cap and the fibre optic cable. On the contrary, the disposable part would be hollow and flushable when demounted, thereby making it easier to re-sterilise. Nevertheless, the re-sterilisation would only stand to reason, if the biopsy harvester's spring could be manually loaded afterwards either by hand or using a specialised tool interfacing with the grooves in the short-pinned sleeve (Fig. 9.1, Level 4, violet).

9.3 Conclusions

The motivation for this thesis stems from the recent developments in the field of optical biopsy (*Chapter 1*). The objective to develop a MIS tool for radical tumour resection of a flat superficial tissue of intra-abdominal organs, while utilising the benefits of the optical biopsy, was fulfilled by presenting a design and evaluation of a steerable minimally invasive opto-mechanical biopsy harvester.

The design of the harvesting component was initiated by reviewing the state-of-the-art MIS instruments potentially capable of performing the optical and mechanical biopsies (*Chapter 2*). The vast scope of the discussed MIS devices showed that with relevant design modifications these devices can easily house a fibre optic cable and thus provide the optical biopsy functionality. Nevertheless, the MIS devices intended specially for the optical and the mechanical biopsies represented only a modest category. Moreover, they were revealed to favour the use of a biopsy forceps, thus being limited to the sampling of a protruding tissue, rather than of a flat superficial tissue.

The lack of suitable concepts and devices for the purpose of this work motivated the development of the experimental bio-inspired spring-loaded biopsy harvester (*Chapter 3*). The \emptyset 6mm prototype proved to work successfully in terms of mechanical functionality, i.e. its preloading, locking and actuation mechanism. Inspired by the sea urchin's chewing organ, Aristotle's lantern, the embedded crown-shaped cutting tool enables rapid tissue incision and enclosure in only 0.8ms, which were demonstrated *in vitro* on a piece of chicken liver.

The fine-tuning of the biopsy harvester's design was performed in an optimisation study of the crown-cutter (*Chapter 4*), where its tooth quantity and bevel type were varied while studying their effect on tissue deformation, penetration forces and tooth collapsibility. In general, it was found that a crown-cutter with a higher number of teeth causes a significantly greater maximum tissue deformation and induces a slightly higher force when penetrating the tissue. On the other hand, the bevel's effect was found to be of negligible importance. Together with tooth collapsibility calculations it was concluded that a 6-teeth crown-cutter of an arbitrary bevel is the most optimal.

The thesis then continues with a review of the mechanical joint constructions used in the steerable MIS instruments (*Chapter 5*) with the aim to devise a stiff and reliable articulation for a proper execution of the biopsy. Several categories and subcategories of joint types were identified based on their geometrical configuration (planar, perpendicular, revolved), the means of establishing the rotational motion (rolling, sliding, the combination of rolling and sliding, bending) and the phenomenon or feature used for transferring the rotational motion (friction, teeth, belts, curved features, hinges). The most preferred joint types were identified as the sliding hinged joints, the sliding curved revolved joints and the bending joint category overall. Yet, it was recognised and that novel, superior joint configurations can be generated by combining several fundamental categories together.

With regard to the new insights and the initial design requirements, a promisingly stiff and simple rolling joint design was devised and demonstrated in the resulting DragonFlex prototype (*Chapter 6*). In addition to tip steering in $\pm 90^\circ$ and grasper opening angle of 180° , DragonFlex's tip contains only four parts, driven and bound by two cables. Two orthogonal planar rolling joints feature an innovative cable guidance maximising the cable lifespan and equalising the length of and forces on both cables throughout the joint rotation. The stacked instrument construction enables control of seven DOF by only seven structural instrument components. Finally, DragonFlex concept sheds a new light on the possibilities of additive manufacture of the surgical instruments, allowing for a feature-packed design, simple assembly, suitability for a disposable use and even potential MRI compatibility.

DragonFlex's rolling joint design was then evaluated empirically in terms of its bending stiffness (*Chapter 7*). The study compared its fully actuated joint design with two other underactuated joint constructions implemented in the state-of-the-art MIS instrument tips. Not only did the fully actuated rolling joint prove significantly stiffer, thus acting more reliably when controlled by a surgeon, but the tip deflection experiments revealed that a fully actuated joint construction can greatly eliminate a large difference between the tip's neutral positions before and after loading allowed by the underactuated joint constructions.

The penultimate section (*Chapter 8*) deals with the optimisation of DragonFlex's rolling joint curvature thus achieving further increase in the bending stiffness. The curvature optimisation not only proved to be successful in minimising the joint play as shown experimentally, but also eliminated the need for a cable tensioning mechanism as such. This method is generally applicable to play minimisation in rolling joint constructions of minimally invasive instruments and it was implemented in a new spring-less real-scale DragonFlex prototype.

The final optimised designs of the biopsy harvester, its crown-cutter and DragonFlex's rolling joint were brought together in the last section (*Chapter 9*) presenting the final envisioned design as well as the real-scale $\emptyset 5\text{mm}$ machined prototype of the steerable opto-mechanical biopsy harvester. Besides taking a critical look at the individual design features and the overall manufacturability, the aspect of the clinical use is discussed with regard to the harvester's permanent and disposable parts.

Appendix



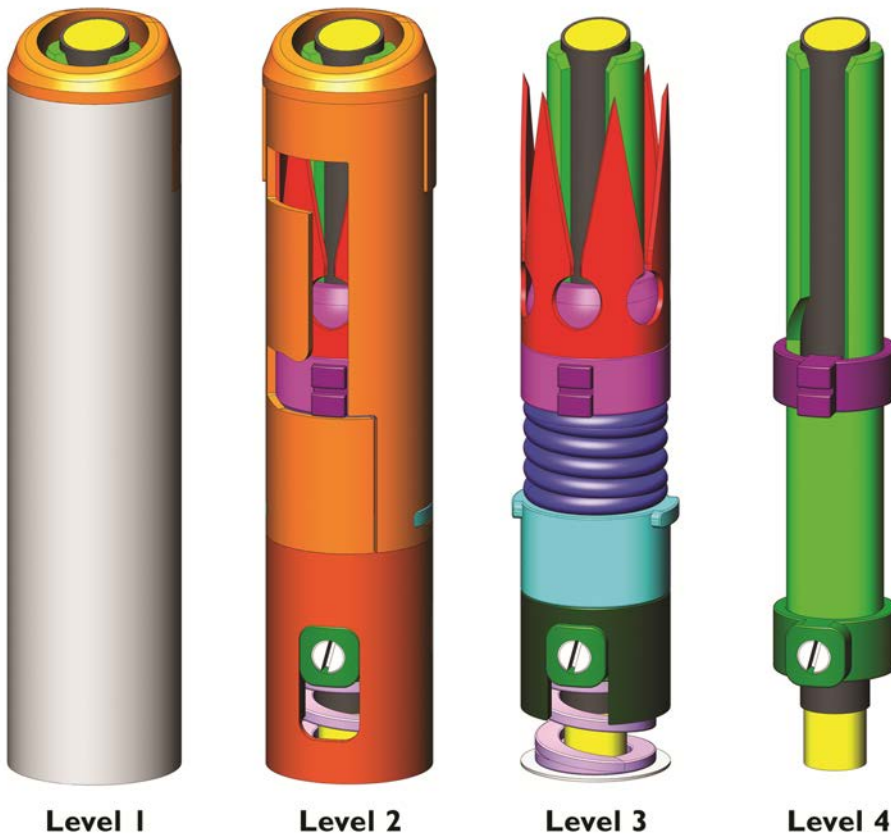


Figure A.1 Decomposition of the final envisioned biopsy harvester design in four levels.

For a curious reader, the following paragraphs describe the individual components of the envisioned opto-mechanical biopsy harvester and their functioning in detail with reference to Fig. A.1.

The outermost torsion-stiff layer (Level 1, light grey) is formed of a 0.1mm thick tube serving the sealing and protective functions as well as mutually aligning the inner components. Due to this all-encompassing layer, the preloading of the inner mechanism would have to be performed before sliding the outermost layer over the inner layer.

The cap on the harvester's tip (Levels 1 & 2, light brown, top) was originally connected to the outer shell by means of a thread, which was the main reason for the shell's increased wall thickness. Nevertheless, for the sake of easier manufacture and assembly, the cap and the shell's inner layer were designed as a single piece, hence removing the need for the thread.

The shell's inner layer (Level 2, light & dark brown) is made of a much thicker 0.25mm tube and features the J-shaped slot from the original design (*Chapter 3*) for cutter preloading and locking. The light brown tube represents a removable, or disposable, part of the harvester and contains the following components in either

mounted or demounted state (Levels 3 & 4): the crown-cutter (red), the sleeve for accommodating the crown-cutter (purple), the short-pinned sleeve for preloading, locking and actuation (violet), the crown-cutter's compression spring (dark blue) and the end ring enclosing the removable part (light blue). Due to the thin cuts in the light brown removable tube running on both sides from the bottom of the J-shaped slots downwards, the end ring would click inside the tube upon slightly deflecting the two tube halves laterally outwards. The end ring would also serve an alignment function when mounting the removable tube onto the permanent tube.

The permanent tube (Level 2, dark brown) would house a short-pinned sleeve (Level 4, green) for the actuation of the cutter, sliding inside a spacer sleeve (Level 3, dark green) and the vertical slot of the permanent tube. In the experimental biopsy harvester design, this short-pinned sleeve did not actually feature a short pin, but two round protrusions reaching out from the harvester's tubular geometry. The protrusions were drilled through, so that the sleeve could have been easily and symmetrically operated from the outside by means of two Bowden cables. However, the actuation had to be brought inside the final harvester's geometry for the purposes of minimally invasive use and the enclosed design of the outer shell.

As explained in *Chapter 3*, the actuation would involve translating the pulling motion of the green sleeve to the rotational motion of another short-pinned sleeve (Level 4, violet). This functionality is provided by an angled slot in the long inner sleeve (Level 4, light green) meshing with the inner pins of the short-pinned sleeve (violet). This long inner sleeve (light green) is fused by means of a metal glue to the short-pinned sleeve (green) or they can even be made as a single component. The long inner sleeve would also serve a protective and housing functions for the central fibre optic cable (Level 4, yellow). Due to the high tensile strength of glass, the fibre optic cable will be used to actuate the inner mechanism of the biopsy harvester by pulling the green sleeves backwards. The pulling motion will be transferred from the fibre optic cable to the green sleeves by a single M1.2 slotted setscrew running through the threaded hole in the short-pinned sleeve to the fibre's protective sleeve (Level 4, dark grey), which in turn will be glued over the fibre.

The last component of the biopsy harvester's assembly is a rear compression spring (Level 3, light violet), which would return the green fibre-actuated sleeves to the original position after being pulled back on for the cutter actuation. The rear compression spring would sit on a steerable joint construction and it would ideally consist of a coil of a rectangular cross-section, thereby increasing its axial stiffness. The importance of the spring's enhanced axial stiffness lies in its ability to sufficiently pull on the fibre optic cable running all the way from the biopsy harvester, through the steerable construction and the shaft up to the instrument's handle, where the fibre would be actuated by means of a trigger.

Acknowledgements



I would like to express my deepest gratitude to my nearest and dearest – my parents, my girlfriend Martina and my sister Dominika – for their love, support and patience with me during all these years I spent abroad, not to mention their help with the design of this thesis. Of course, besides other family members, I would also like to thank my grandma Paula for some of her genes without which all this writing would have been a lot more difficult.

My great thanks goes to my supervisors Jenny and Paul for their guidance, support and for giving me the opportunity to pursue my goals within such a creative academic atmosphere in the first place. Furthermore, I would like to thank Paul for all the time spent brainstorming and designing together, for the insightful feedback to every word I ever wrote and for all the beautiful photographs spread around this thesis.

Similarly, I would like to thank my project partners and advisors Dick and Jules for providing their help and sharing their expertise within the fields of optical biopsy and steerable laparoscopic instruments. At the same time my gratitude goes to the staff of TU Delft's fine mechanical workshop DEMO including Aad, Menno and the gifted instrument maker David, who never said no to a challenging manufacturing assignment. I would like to thank the PME technicians Harry and Patrick as well for their help and support during all my experiments and to the people from TNO for their collaboration.

Naturally, my great thanks goes to my friends and colleagues Aimée, Annetje, Arjan, Arjo, Awaz, Chunman, Dennis, Ewout, Gerwin, Giada, Hélène, John, Kirsten, Linda, Nick, Paul, Tim and all the others for all the interesting and inspiring talks, their help and support. My special thanks goes to Chunman for being a great friend and for showing me around in the beginning of my PhD, as well as for our interesting collaboration on the Endo-PaC project. At the same time I would like to thank Aimée, Awaz, Ewout and Paul for their collaboration on several articles and for their generous help with the Dutch translations in this thesis. I would also like to thank Arjo for his professional help with several DragonFlex prototype photographs in this thesis.

Likewise, I would like to thank my friends and former students Alice, Annemijn, Bart, Daan, Davey, Geert, Jeffrey, Johan, Rob, Sander and Tom for their valuable contribution to this thesis. Of course, my special thanks goes to my friend and squash mate Rob whose inspiring Master's project gave rise to DragonFlex prototype and laid ground to the steerability part of this thesis.

Last but not least, I would like to thank the ever-helpful BMechE secretaries Anouk, Dineke, Diones, Nancy and Sabrina for all the little big things they do for all the staff members every day. To conclude my Dutch experience I would like to give my great thanks to my former landlords and eternal friends Olga and Nol for their hospitality and to the fate that brought me to them via Olga's mother Emília and my grandpa Vojto.

All this would not have been possible without all the prior experience, preparation, education and training during the years spent in England during both my childhood and the University times. For all this time I am eternally grateful to my not so distant family Chinko and Marianka who always warmly welcomed me in London and once again thanks to my grandma Paula for bringing us all together.

Furthermore, my great thanks goes to my UK mentors and supervisors from the Department of Engineering at the University of Hull – Dr Dobson, Prof Fagan and Dr Itskevich – for their supervision, support and encouragement to pursue a PhD after my UK studies. Of course, I am very grateful for the friendship and the fun times spent together with my University mates Anwar, Dean, Dima, Imran, Raghu, Rich and Sam while playing squash, working out or going out into the murky Yorkshire nights. Lastly, I would like to thank Balázs for bringing me to the postgraduate fair in Manchester where I found out about this not-really-English-sounding university – TU Delft.

Finally, I would like to thank Gernot, Nik and Wolfgang for taking the interest in my work and myself, giving me the opportunity to join their ACMIT team and do what I like while being with my family on a daily basis once again after a very long time.

Curriculum Vitae



3 February 1988

Born in Bratislava, Slovakia.

2002 – 2004

Gymnasium Jur Hronec in Bratislava, Slovakia.

2004 – 2006

International Baccalaureate at Gymnasium Jur Hronec in Bratislava, Slovakia.

2006 – 2010

MEng in Mechanical and Medical Engineering (with honours) at the University of Hull, England, United Kingdom. Bachelor's thesis on studying the impact of various boundary conditions on strain distribution across human juvenile pelvis using finite element analysis. Master's thesis concerned with the development of a novel component fixation for total knee arthroplasty in cooperation with Smith & Nephew York.

2010 – 2014

PhD candidate at the BioMechanical Engineering department at Delft University of Technology. PhD thesis dealing with the development of a steerable minimally invasive biopsy instrument tip enabling optical and mechanical biopsy for safe and accurate real-time tumorous tissue detection and resection.

2014 – Present

Researcher at Austrian Center for Medical Innovation and Technology, Wiener Neustadt.



Publications



Journal Articles

Jelínek F., Arkenbout E. A., Sakes A., Breedveld P. Minimally invasive surgical instruments with an accessory channel capable of integrating fibre-optic cable for optical biopsy: A review of the state of the art. *Proc Inst Mech Eng H*. 2014; 228(8): 843-53.

Jelínek F., Smit G., Breedveld P. Bioinspired Spring-Loaded Biopsy Harvester—Experimental Prototype Design and Feasibility Tests. *J Med Device*. 2014; 8(1): 015002.

Jelínek F., Goderie J., van Rixel A., Stam D., Zenhorst J., Breedveld P. Bioinspired Crown-Cutter—The Impact of Tooth Quantity and Bevel Type on Tissue Deformation, Penetration Forces, and Tooth Collapsibility. *J Med Device*. 2014; 8(4): 041009.

Jelínek F., Arkenbout E. A., Henselmans P. W. J., Pessers R., Breedveld P. Classification of Joints Used in Steerable Instruments for Minimally Invasive Surgery: A Review of the State of the Art. *J Med Device*. 2015; 9(1): 010801.

Jelínek F., Pessers R., Breedveld P. DragonFlex Smart Steerable Laparoscopic Instrument. *J Med Device*. 2014; 8(1): 015001.

Jelínek F., Gerboni G., Henselmans P. W. J., Pessers R., Breedveld P. Attaining high bending stiffness by full actuation in steerable minimally invasive surgical instruments. *Minim Invasive Ther Allied Technol*. 2014; in press.

Jelínek F., Diepens T., Dobbenga S., van der Jagt G., Kreeft D., Smid A., Pessers R., Breedveld P. Method for minimising rolling joint play in steerable laparoscopic instrument prototype DragonFlex. *Minim Invasive Ther Allied Technol*. 2014; in press.

Arkenbout E. A., Henselmans P. W. J., Jelínek F., Breedveld P. A state of the art review and categorization of multi-branched instruments for NOTES and SILS. *Surg Endosc*. 2014; in press.

Fan C., Jelínek F., Dodou D., Breedveld P. Control Devices and Steering Strategies in Pathway Surgery. *J Surg Res*. 2014; in press.

Sakes A., Arkenbout E. A., Jelínek F., van der Kolk J. H., Breedveld P. Design of an Endovascular Flexible Instrument for the Surgical Treatment of Equine Cushing's Disease. Submitted

Conference Articles

Jelínek F., Pessers R., Breedveld P. DragonFlex – Smart Steerable Laparoscopic Instrument. *J Med Device*. 2013; 7(2): 020911.

Jelínek F., Breedveld P. Bio-Inspired Spring-Loaded Biopsy Harvester. *J Med Device*. 2013; 7(2): 020912.

Jelínek F., Arkenbout E. A., Henselmans P. W. J., Pessers R., Breedveld P. Classification of Joints Used in Steerable Instruments for Minimally Invasive Surgery. *J Med Device*. 2014; 8(3): 030914.



